Universitat Autònoma de Barcelona

Dental Care Process Characterization. Spectroscopic Methods for a Robust Determination of Remineralization and Dental Sensitivity

Olga Kotkowska

Universitat Autònoma de Barcelona

Dental Care Process Characterization. Spectroscopic Methods for a Robust Determination of Remineralization and Dental Sensitivity

Olga Kotkowska

Doctoral Thesis

Doctoral Studies in Chemistry

Supervisor:

Manuel Valiente

Department of Chemistry

Faculty of Science

2015

Universitat Autònoma de Barcelona

Report submitted to aspire for the Doctor Degree by:

Olga Kotkowska

Supervisors' approval:

Prof. Manuel Valiente

Bellaterra, 25/11/2015

Nauce też trzeba się przyglądać, zwykle odkrywa to co już dawno wiadomo...

Pani Zielarka z „Rancza”

Pracę dedykuję Rodzicom,

w podziękowaniu za ustawiczne wsparcie

The work presented in this doctoral thesis has been done in collaboration with other research groups and scientific centers to whom the author of this work is especially grateful for their cooperation and guidance:

	***A novel methodology for the evaluation of the dentinal tubuli obliteration*** In collaboration with Dr Rubén Cárdenes Universitat Pompeu Fabra, Barcelona, Spain
  	***A novel HSI approach for the evaluation of the efficacy of the remineralising treatment*** Measurements were performed at Sapienza University di Roma, Roma, Italy In collaboration with Dr Juan Rosas Universitat Autonónoma de Barcelona Dr Maike Windbergs and Branko Vukosavljevic Universität des Saarlandes, Saarbrücken, Germany
 	***Study of the remineralised human dental tissues by the Synchrotron Infrared Spectroscopic Ellipsometry: optical constants determination*** Measurements were performed at BESSY II and ISAS, Berlin, Germany In collaboration with Dr Hinrichs Karsten Leibniz-Institut für Analytische Wissenschaften – ISAS, Berlin, Germany Dr Ulrich Schade BESSYII, Helmholtz Zentrum Berlin, Germany
 	***Application of FTIR Spectroscopy for the dental tissue characterization: a curve fitting approach*** Measurements were performed at SOLEIL, Paris, France and ALBA, Cerdanyola del Vallés, Spain In collaboration with Dr Christophe Sandt French Synchrotron National Facility, Paris, France

The author would like to also thank his Director Manuel Valiente for the possibility of forming a part of his research group.

A part form the scientific investigation the author of this thesis performed multiple researches for the private companies that finalized with the creation of the new toothpaste that is currently available on the market:

Lacer S.A, Barcelona, Spain

Colgate – Palmolive S.A , New York, USA

Studies presented in this doctoral dissertation resulted in three scientific papers that were sent to journals enlisted below:

Kotkowska O, Cardenés R, Ricra E, Muroc J, Valiente M. "A novel method for the evaluation of the dentinal tubuli obliteration" send to Journal of Dental Research

Kotkowska O., Rosas Portugal J., Vukosavljevic B., Windbergs M., Lubreras F, Serranti S, Bonifazi G, Valiente M. " Application of Hyperspectral Imaging and Raman Spectroscopy for the characterisation of the remineralised dental tissue " send to Dental Materials

Kotkowska O, Karsten H., Schade U., López Mesas M., Valiente M. "Application of IR synchrotron ellipsometry for the characterisation of dental specimens: a reference sample evaluation" send Journal of Dental Research

Contents

Summary

treated. A novel, scientific tools for the evaluation of the efficacy of products targeting the hypersensitivity or caries creation were proposed. Moreover, experiments implementing FTIR spectroscopy as well as synchrotron techniques for the dental tissue investigation were performed.

In order to design a proper sealing material and to investigate its efficacy, the porosity of the dentine has to be determined. In the present dissertation a novel methodology for the evaluation of the efficacy of the hypersensitivity treatment has been developed. It is presented in the first part of the work and is based on the dentin disc model methodology. Specimens treated with a desensitizing agent were observed under Scanning Electron Microscope (SEM) and the resulting images were analyzed by the MATLAB automatic segmentation algorithm developed to calculate the number and area of the open tubuli. The present method is a suitable scientific tool that will allow scientists and private companies the *in vivo* monitoring and assistance on the development of new remineralising agents. The comparison of three commercial toothpastes presented in this work showed a successful application of the developed methodology and proved it to be suitable for that kind of comparative studies.

The proceeding parts of the presented dissertation were focused on the problem of the demineralization and opposite-remineralisation processes of teeth.

In the second part of presented PhD thesis a novel approach implementing the Hyper Spectral Imaging (HSI) technique for the evaluation of the efficacy of the remineralising treatment is presented. Hyper Spectral Imaging (HSI) with two types of NIR cameras (161 and 256 channels) and confocal Raman microscopy (CRM) as a complementary technique were applied for analysis of teeth before and after application of different remineralizing agents. Obtained results were carefully analyzed and compared by the implementation of a MATLAB routine that used the correlation coefficient and MCR data analysis in order to obtain necessary information from the acquired spectra of dental samples. Taking into consideration the simplicity of the presented method it can be a powerful tool to obtain basic information about the performed treatment. In the process of the evaluation of a new dental product, this kind of information can lead to the decision whether to continue the development of the product or to proceed with another, more promising approach.

In the third part of the presented dissertation the Infrared Spectroscopic Ellipsometry (IRSE) and synchrotron ellipsometry is proposed for the determination of the optical constants of human dental tissues. Human teeth were treated with the remineralising agent and analyzed with the synchrotron IR ellipsometer. Furtherly, a series of experiments and simulations were performed in order to obtain the most suitable reference sample for the interpretation of the obtained synchrotron data.

In the last – fourth part, structural changes in the human enamel and dentin induced by the remineralization process were investigated. The spectra from various points proceeding from different locations of the tooth were compared and studied by the FTIR technique. Obtained data were interpreted applying Principal Component Analysis (PCA) and curve-fitting procedures. Obtained results were compared to the reference hydroxyl and fluorapatite powders and scientific literature.

Resumen

En la presente disertación han sido tratados el problema de la hipersensibilidad dental y los procesos remin/demin. También han sido desarrolladas nuevas herramientas científicas para la evaluación de la eficacia de los productos dirigidos a la hipresensibilidad y a la prevención de la creación de caries dentales. Además, se han diseñado y llevado a cabo varios experimentos para investigar el estado del tejido dental mediante espectroscopia FTIR sin y con la fuente de sincrotrón.

Con el objetivo de desarrollar el material oclusivo adecuado y determinar su eficacia; la porosidad de la dentina debe ser determinada. En la presente tesis doctoral ha sido desarrollada una nueva metodología para la evaluación de la eficacia del tratamiento de la hipersensibilidad dental. Este estudio se ha presentado en la primera parte del trabajo y se basa en la metodología de los discos dentinarios (*dentin disc model*). Los especímenes tratados con los agentes desensibilizantes han sido observados mediante la Espectroscopia Electrónica de Barrido (SEM). Las imágenes obtenidas han sido analizadas por un algoritmo automático de segmentación, desarrollado para ser usado mediante el software de MATLAB, el cual calcula el número y el área de los túbulos abiertos. Dicho método es una herramienta adecuada para que tanto científicos, como compañías privadas puedan llevar a cabo la supervisión y asistencia de los procesos remineralizantes de los tejidos dentales, o bien para el desarrollo de los nuevos productos focalizados en el problema de la hipersensibilidad dental.

Las siguientes partes de la disertación se han enfocado en el problema de los procesos desmineralizantes del tejido dental.

En la segunda parte de la tesis doctoral se presenta la implementación de una nueva técnica, la de *Hyper Spectral Imaging* (HSI) para la evaluación de la eficacia del tratamiento remineralizante. Para el análisis de los dientes humanos antes y después de la remineralización, se ha utilizado principalmente el *Hyper Spectral Imaging* que implementa dos tipos de cámaras de Infrarrojo Cercano (NIR) (161 y 256 canales); y como método complementario la Microscopía Confocal de Raman (CRM). Los resultados obtenidos han sido detalladamente analizados mediante una rutina de MATLAB desarrollada especialmente para analizar ese tipo de imágenes. El coeficiente de correlación y la técnica de MCR (*Multivariate Curve Resolution*) han sido utilizados para recabar la información necesaria de los espectros adquiridos. Gracias a su simplicidad, el método puede convertirse en una poderosa herramienta para obtener información sobre los efectos del tratamiento remineralizante aplicado sobre el tejido dental. Durante el proceso de evaluación del nuevo producto dental, ese tipo de información puede ayudar a decidir si el producto es eficaz y compararlo con otros agentes del mismo tipo.

En la tercera parte de la presente tesis doctoral la Elipsometría de Infrarrojo (IRSE) y la Elipsometría con la radiación de Sincrotrón han sido escogidos para la determinación de las constantes ópticas del tejido dental humano. Los especímenes dentales han sido tratados con el producto remineralizante y analizados mediante la Elipsometría IR con la radiación de Sincrotrón. Posteriormente, una serie de experimentos y simulaciones han sido llevados a cabo para obtener una muestra de referencia adecuada para la interpretación de los datos obtenidos en el sincrotrón.

En la última parte, se han estudiado los cambios de la estructura del esmalte humano y de la dentina producidos por el proceso de la remineralización. Los espectros de varios puntos de los

especímenes dentales han sido comparados mediante la técnica FTIR (*Fourier Transform Infrared Spectroscopy*). Los datos obtenidos han sido interpretados aplicando el Análisis de Componentes Principales (PCA) y la deconvolución de los espectros (*curve-fitting*). Los resultados han sido comparados con las muestras de referencia de hidroxiapatita, fluorapatita y las consideradas en la bibliografía científica.

.

Glossary

RGB image- Red Green Blue scale image
β-TCP – Beta Tricalcium Phosphate
ACP - Amorphous Calcium Phosphates
CPP-ACP - Casein Phosphopeptide-Amorphous Calcium Phosphate nanocomplexes
CPP-ACFP - Casein Phosphopeptide containing a sequence Ser-Ser-Ser-Glu-Glu
HSI – Hyper Spectral Imaging
nHAP – nano Hydroxyapatite
HA/HAP – Hydroxyapatite
FA/ FAP – Fluorapatite
NIR – Near Infrared
NMTD- remineralizing agent, mixture of ion exchange resins
DEJ - Dentin Enamel Junction
OTC - over-the-counter
SEM - Scanning Electron Microscopy
AFM - Atomic Force Microscopy
XPS - X-Ray Photoelectron Spectroscopy
SIMS - Secondary Ion Mass Spectrometry
TEM - Transmission Electron Microscopy
IR - Infrared
FTIR - Fourier Transform Infrared
CI - Crystallinity Index
MWIR – Medium Infrared or Mid-wave Infrared
FIR - Far Infrared
PCA - Principal Component Analysis
MVA - multivariate analysis
MIA - multivariate image analysis
PLS- Partial Least Squares
MCR- Multivariate Curve Resolution
MCR-ALS – Multivariate Curve Resolution Alternating Least Squares
CRM - Confocal Raman Microscopy
IRSE - Infrared Spectroscopic Ellipsometry
MCR (*Multiplicative Scatter Correction*)
SNV (*Standard Normal Variate*)

Introduction

1. *Dental tissues*

Teeth are anatomical hard structures rooted in the maxillae bones. They play the principal function in the digestion process by participating in the mechanical fragmentation of the food. Moreover they participate in the oral communication acting as a resonance box that allows producing sounds but above all teeth are important for the simple esthetical reasons (15). Being a crucial part of the human body and health it causes an increase in the importance of dental health in modern society. Recently the market is trying to fulfill the necessity to look after the dental health by the constant development of the new methodologies and dental products (16).

2. *Tooth structure*

Tooth can be divided into three parts: crown, neck and root. Crown is the part that is covered by the enamel and is the visible part of the tooth, whereas the root is covered with cementum and is inserted in the dental alveoli located in the jaw. Neck is the junction between the root and the crown and is located close to the gingiva. On the Figure 1 the transversal cut through the tooth is presented where all the mentioned parts can be distinguished. The most outer part of the teeth is the enamel, underneath can be found dentine and in the center, the pulp cavity with all the nerves and blood vessels.

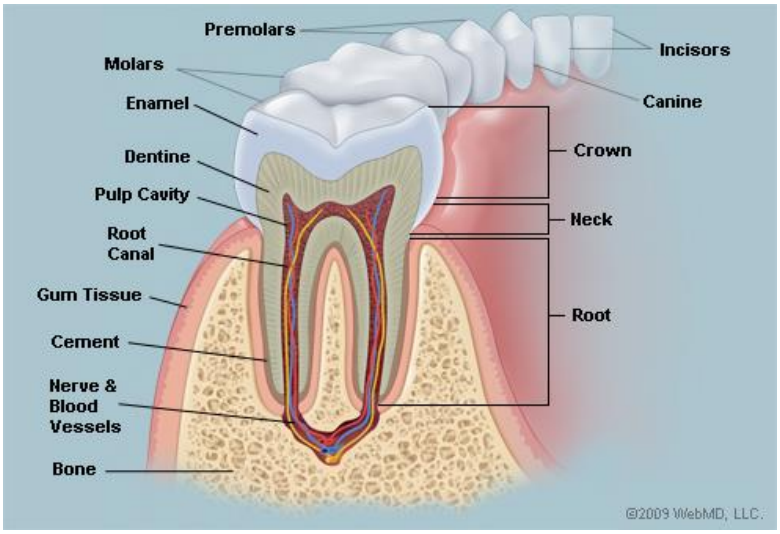

Figure 1. Tooth structure (transversal cut)

2.1. Tooth enamel

2.1.1. Enamel histology

Enamel is built by the carbonated hydroxyapatite nanocrystals that are grouped in clusters called prisms or rods. They are glued by interrods which are also hydoxyapatite crystallites but oriented in the different direction. The rods are approximately 1-2 nm thick and 1 mm long where the last value also corresponds to the thickness of the enamel. Rods begin in the interjunction dentine-enamel and spread perpendicular to it through the entire length of the enamel (17). On the Figure 2 the organised structure of carbonated hydroxyapatite crystals is presented.

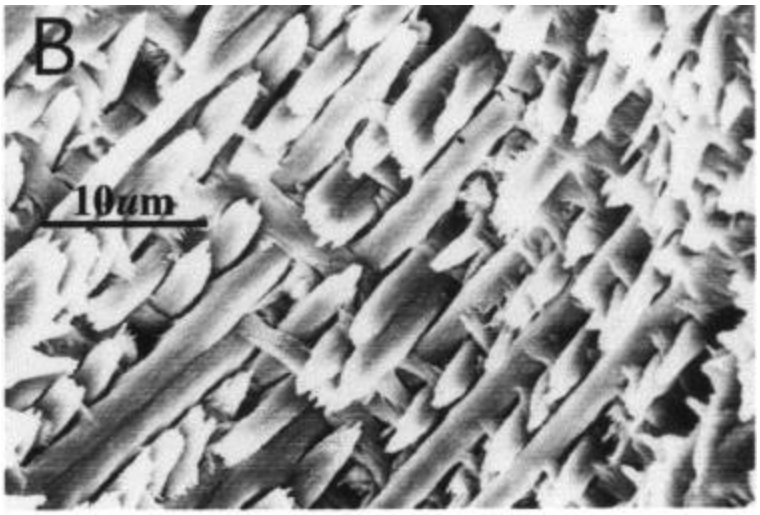

Figure 2. The organisation of dental enamel. SEM image of the acid – etched enamel where organised enamel rods (prisms) can be seen (18).

2.1.2. Chemical composition of enamel

Mature enamel is in 96% of weight made of hydroxyapatite (HA), 1% of protein and 3% of water (17). It has a very high mineral density what can be easily demonstrated by comparing its density (2,85-3,00 g/cm^3) to the density of the pure HA monolith (3,08 g/cm^3) (19).

From the crystallographic point of view, hydroxyapatite has a hexagonal structure with space group $P6_3/m$. One unit cell contains 10 Ca^{2+}, 6 PO_4^{3-} and 2 OH^- ions. Phosphate ions form hexagonal channels. Along those channels OH^- ions are located; each ion is surrounded by three calcium ions. Two Ca^{2+} triangles are shifted by 60˚ (17). The shift in the hydroxyapatite structure, as well as the entire structure, is presented on the Figure 3.

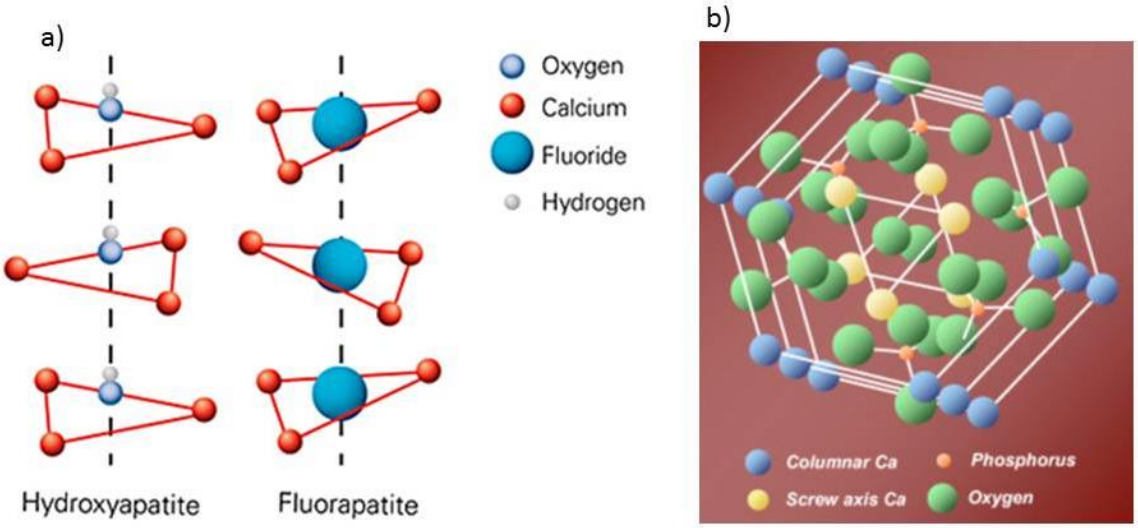

Figure 3. a) Hydroxyapatite and Fluorapatite structure b) Crystallographical structure of hydroxyapatite

In the crystallographic structure some common substituents can be encountered. As a lattice component, the phosphate or hydroxyl groups can be substituted by the CO_3^{2-} ion. Biological apatites normally contain 2-3% of carbonate ions incorporated into the structure (17).

Another common substitution is the incorporation of the fluoride ion into the crystal lattice. During the creation of the dentine and enamel, fluoride replaces calcium and creates fluorapatite (FA) - a different type of apatite that, from the crystallographic point of view, differs from hydroxyapatite only in the substitution of the ion OH^- by the F^-. To this structural change, FA can attribute its increased stability that results, for example, in better resistance to the acid attacks than HA presents (20). Fluorapatite was one of the first apatites which structure was revealed and described in the scientific literature (21).

During the mineralisation some other elements in minor or trace quantity are also incorporated into the structure (Table 1 and 2). The concentration of those elements may influence the general stability of the structure as well as the resistance of the apatite against acid attacks. The distribution of the elements varies depending on the teeth zone (17).

Table 1. Major and minor elements of the enamel (17)

Element	Average concentration (dry weight %)
Ca	36.6
P	17.7
CO_3	3.2
Na	0.67
Mg	0.35
Cl	0.35
K	0.04

Table 2. Trace elements in the enamel (17)

Element	Mean concentration (µg/g, dry weight)
Zn	179
Sr	156
Si	136
F	120
S	59
Al	51
Fe	33

2.1.3. Morphogenesis of the enamel

Enamel starts to grow from the dentine-enamel junction (DEJ). After the nucleation, the created crystals start to elongate perpendicularly to the junction (*c-axis*) and form the above mentioned rods (prisms). Crystals are created in the ameloblast- a protein cell that produces protein matrix responsible for the development of the enamel. Enamel is formed in three phases: secretion, transition and maturation (17).

Growth of the crystals is possible due to the unceasing supply of calcium produced by the calcium pump. When the local concentration of the calcium is very high it precipitates in forms of calcium phosphate. When it happens close to the ameloblasts the amelogenins are segregated. Those proteins (amelogenins) control the morphology, size and orientation of the growing crystal. One ameloblast produces one ribbon – like crystal where the amelogenins are assembled in the spherical structure (*nanosphere*) around it. In that moment the secretion is finished.

Transition phase begins when the ameloblast cell shrinks and the proteins are degraded by certain enzymes. In the secretion phase, the content of the protein reaches 20-30%, when the crystal enters into the maturation stage this percentage drops dramatically to 1% of weight (17). This decrease is attributed to the fact that in the last stage the enamel grows in thickness and width and is almost completely covered with the mineral. During this complex process the enamel is being transformed from the cellular tissue into a mineralised tissue (17). The above described process is illustrated in the Figure 4.

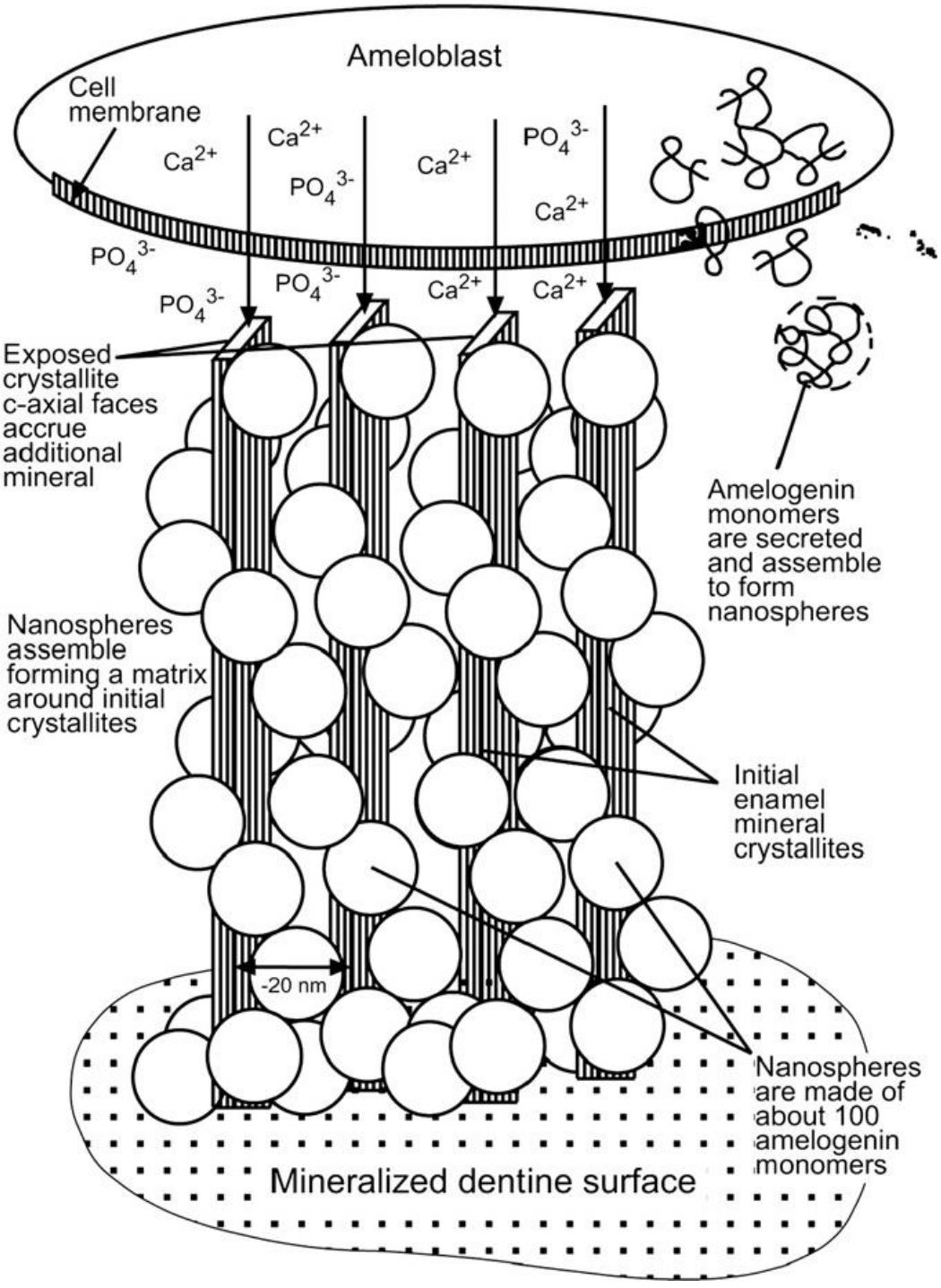

Figure 4. Rod (prism) like crystal formation controled by the amelogenins (17).

2.1.4. Proteins role in the mineralisation of enamel

Protein extracellular matrix located in the ameloblasts is responsible for the production and further mineralisation of the enamel. Almost 80% of the proteins that form the

matrix are amelogenins. As a continuation, the role of amelogenins as well as non-amelogenins in the mineralization process is explained.

Amelogenin plays a very important role in the enamel creation. The self-assembled nanospheres influence the orientation of the growing hydroxypaptite crystals during the biomineralization process of the enamel (22). The amelogenin establish the orientation of the alignment of apatite crystals what results in the "ribbon-like" form of the structure (22) (23). In general, it is believed that amelogenin on a developing stage of the enamel, is a key protein that delivers the calcium and phosphate ions that are further transferred from the protein into the growing crystal (24).

According to the literature (25), (26), (27), (28), (18), (29) enamel mineralization depends in 90% on the presence of amelogenins but there are other proteins that can alter the remineralization process such as enamelins, tuftelins, ameloblastins and proteases.

Enamelin is a glycoprotein that represents only 5% of extracellular matrix; nonetheless it happens to be essential in the enamel formation (25). Its lack proved to cause a disorder during the amelogenesis (6). After proteolithic a cleavage, enamelin is cut into six pieces, among all of them enamelin 32kDa occurred to be the most stable one and it has the strongest affinity towards the hydroxyapatite (25). The enamelin supports the nucleation of hydroxyapatite together with amelogenin (27). Basing on the literature knowledge, enamelin itself will not alter the biomineralization of enamel, only in presence of amelogenin the difference can be noticed, thus those two proteins interact with each other. It is believed that enamelin regulates the amelogenin assembly and the further process of nucleation and hydroxyapatite crystals formation (28).

Tuftelin is believed to play an essential role in the hydroxyapatite nucleation too (18), (29). Basing on its characteristics, anionic character and localization in the newly secreted matrix enamel, it is postulated to contribute highly in the biomineralization of enamel (29). Paine et al. discovered proteins that interact with tuftelin (TIP). Among them the 39 kDa TIP molecule was selected as the protein that contributes in linking the ameloblasts with the enamel surface (29).

The presence and connections between some of the crucial proteins for the enamel development are illustrated in the Figure 5.

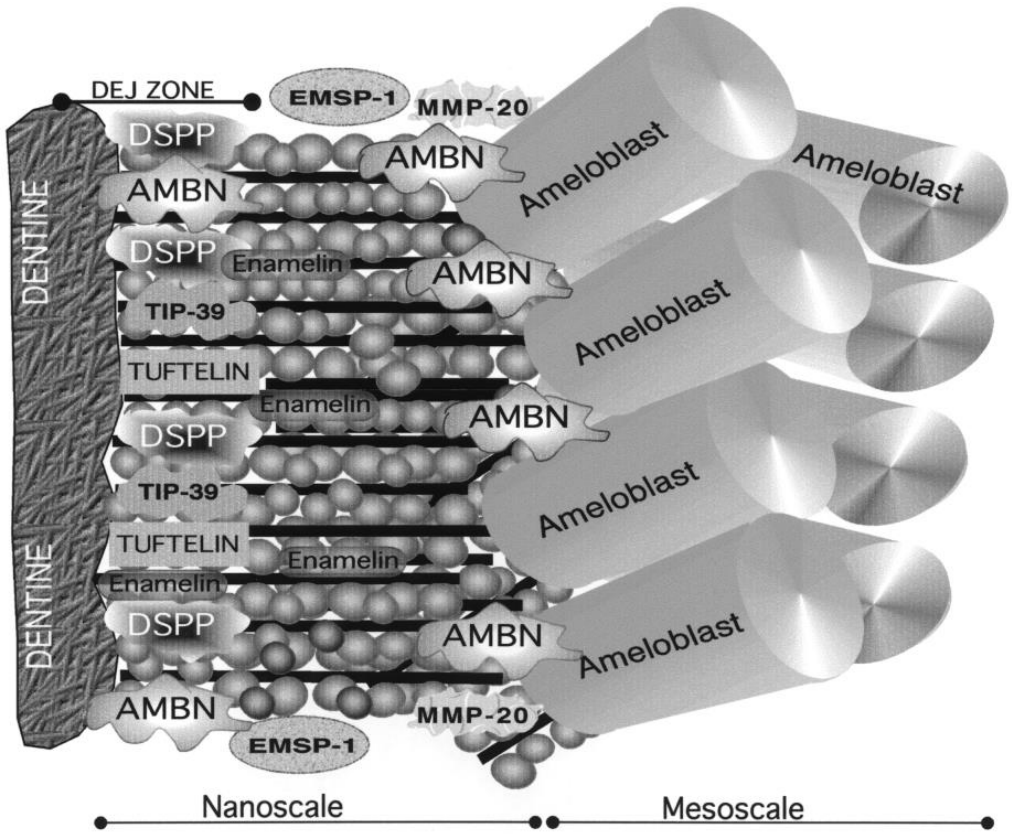

Figure 5. Creation of the enamel at the DEJ (dentin enamel junction) with the participation of proteins. Ameloblasts express the proteins crucial for the creation of the enamel (18). Proteins segregated by theameloblasts: DSPP- dentine sialophosphoprotein,, TIP-39, tuftlein, enamelin, AMBN- amelogenin; EMSP-1- Enamel matrix serine proteinase 1; MMP-20- Matrix metalloproteinase-20; TIP-20 - tuberoinfundibular peptide of 39 residues.

2.2. Dentin

2.2.1. Histology and chemical composition of dentin

The internal tooth part, beneath the enamel layer is formed by the dentin. This dental tissue has a calcified form filled with tubules that are the reminiscences of the odontoblast location during the dentin formation (*dentinogenesis*). In the adult tooth, the resting cell bodies are accumulated at the inner edge of the dentin where they form the boundary with the pulp chamber (30), (31).

Dentin is constituted in 50 % wt of mineral (mostly hydroxyapatite), 40% wt organic phase and 10% wt of fluids. The composition of dentin is similar to the composition of bone. The organic phase in 98% wt refers to collagen type I fibers that form the network which builds the dentin matrix (31).

The calcified content of the dentin is mostly hydroxyapatite and is located between the collagen fibers (intrafibrillar) or attached to it (extrafibrillar). The morphology of the mineral is mostly plate-like and cylindrical (20-5 nm big). Proteins such as glycoproteins and proteoglycans on the other hand, cover the collagen fibrils. The most crucial components for the dentin functioning are phosphoproteins responsible of inducing the mineral nucleation and binding to the calcium phosphates (31). Unlike the enamel,

dentin is able to repair itself due to the presence of the previously mentioned proteins, but most of all, thanks to the odontoblasts that can be stimulated in order to form more tissue (30).

2.2.2. Dentin morphology

Depending on the stage of formation, three types of dentin can be found: primary, secondary and tertiary. The first one is produced during the formation of the tooth and constitutes the major part of its mass. When the root is formed the secondary dentin is produced by the odontoblast cells which are deposited on the pulpal part of the primary dentin. As a result of some external stimuli such as caries creation, application of restorative products or some trauma, tertiary dentin can be formed (32).

2.2.2.1. Dentinal tubules

One of the main characteristics of the dentin is its permeability; the entire material is filled with dentinal tubules. Those structures resemble an inverted cone with the diameter from 0,5-0,9 µm at the DEJ (dentin enamel junction) increasing to 2-3 µm near the pulp (33). Since the tubule diameter is bigger close to the chamber comparing to the DEJ region the permeability of dentin increases exponentially in the direction of the deeper parts of the tooth (34) (Figure 6).

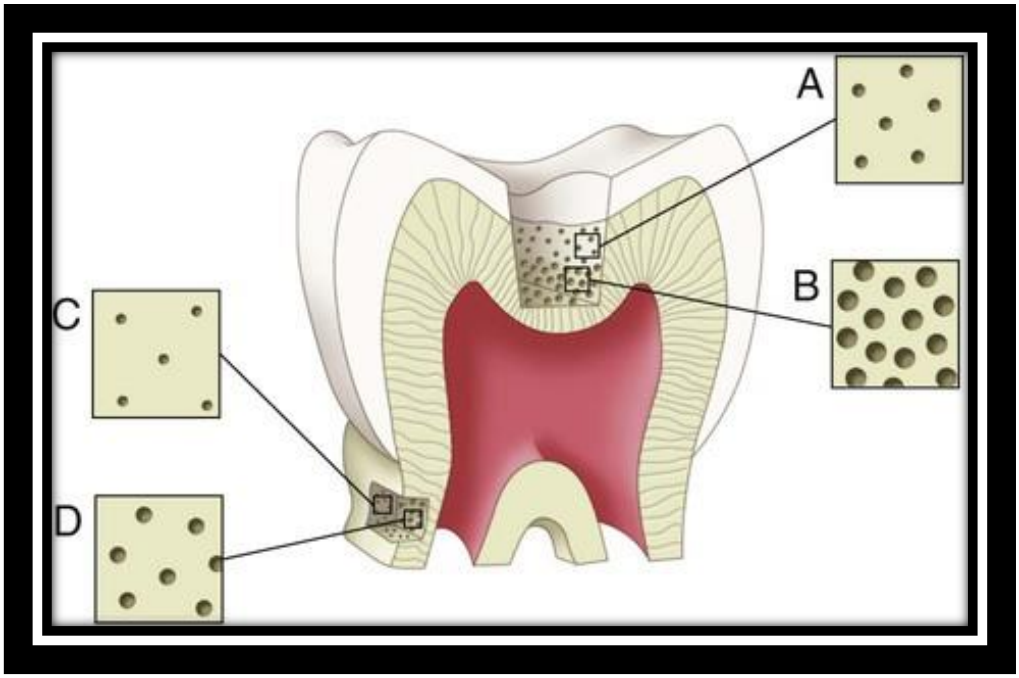

Figure 6. Distribution of the dentinal tubules. Tubules close to the DEJ are smaller and the density of tubules is also smaller. Going deeper into the dentine, density and the size of the tubules increases.

The longitude of the tubules normally oscillates from 3 to 3,5mm and has an S - like shape. They are densely packed throughout the entire dentin. It is calculated that in the outer dentin there are 15 000 tubules/mm^2, whereas in the central part increases to 25 000/mm^2 and up to 55 000/mm^2 close to the pulp chamber region (32).
Dentinal tubules are filled with the fluid responsible of transmitting the sensations, such as pain, to the pulp chamber where the nerves are located. The permeability of dentin is one of the main causes of the hypersensitivity of teeth (Figure 7).

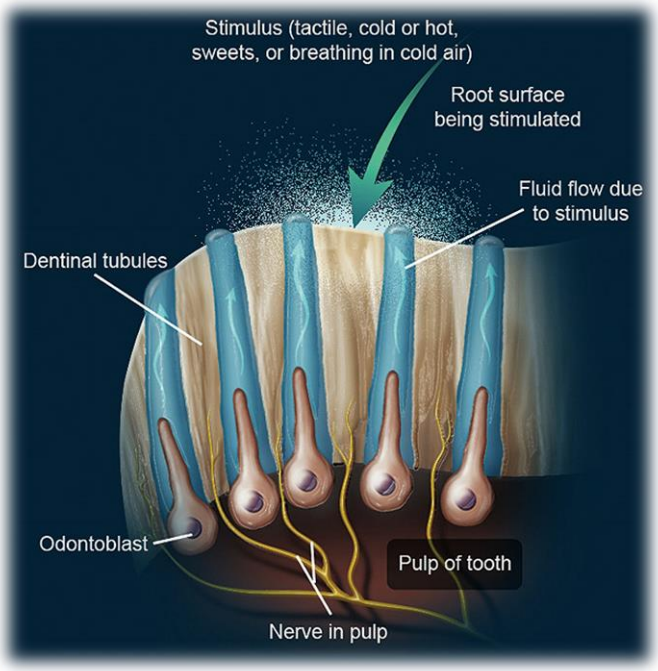

Figure 7. Cross-section of the dental tubules filled with the fluid that transmits the stimuli.

3. Dentinogenesis

The essential role in the dentin formation plays the odontoblast cells. Firstly they form the predentin that works as a base for the dentin formation. All along the dentinogenesis, odontoblasts perform the secretion and synthesis of the dentin constituents. They are organised in a columnar shape and the dental tubules are the reminiscence of its activity during the dentinogenesis. Once the process is finalised and the dentin is created odontoblasts move to the inner edge of the dentin where they are stored in order to produce the tertiary dentin when it is necessary. The number of odontoblast in teeth diminishes with age as the pulp gradually retracts (32).
The dentinogenesis occurs in two different phases: formation of the predentin and the subsequent mineralisation. At first *preodontoblasts* are created in the *basement membrane*. Afterwards cells undercome polarisation in order to be dentinogenically active. After this step, the predentin starts its formation (Figure 8). Simultaneously, the

basement membrane diminishes in order to be replaced by the new created *predentin* (32).

The next step is the creation of the nonmineralised *mantle dentin* and the formation of the type I collagen that create a dense network of fibres. The subsequent mineralisation process begins in the matrix vesicles located in the *mantle dentin*. Once the initial crystals are formed the mineralisation of the tissue begins (32).

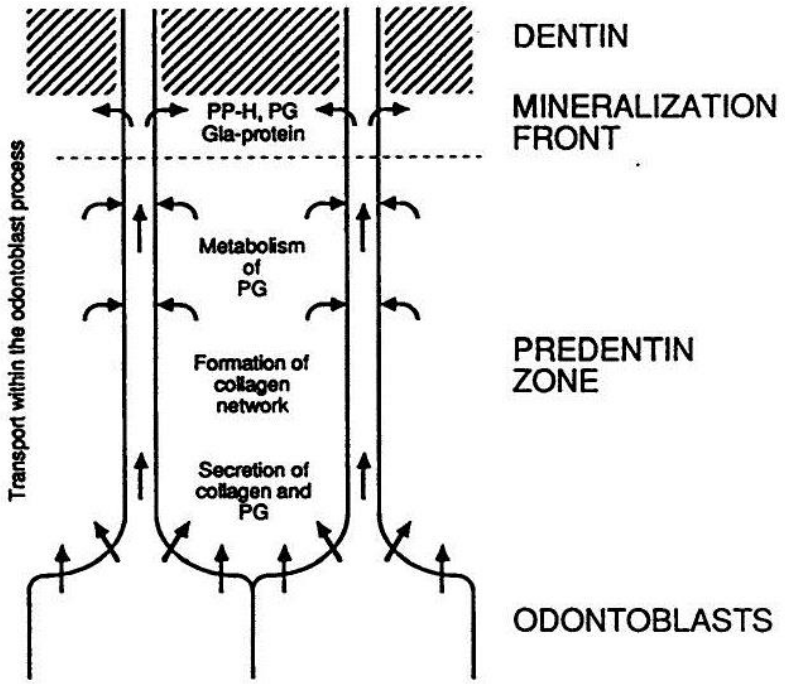

Figure 8. Predentin region in dentinogenesis (32). Odontoblasts segregate collagen and proteoglycan (PG) that form extracellular predentin. Proteins such as phosphorylated phosphoprotein (PP-H) and Gla- protein are transported by the odontoblasts into the mineralisation front in order to implement the mineralisation process.

4. Demineralization of the teeth

Dental caries are defined as a localised destruction of the hard tissue caused by the acids produced during the bacterial activity in the buccal plaque. The process begins in the bacterial biofilm by the fermentation of the carbohydrates (present due the ingestion of food) and starts to be visible on the hard tissue. Dental caries are the most common reason of the oral pain and the tooth loss (7).

The origin of the dental caries is the imbalance in the pH of the mouth caused by the acid formation proceeding from the bacterial plaque. Biofilm is a natural and indispensable part of the buccal environment. It is responsible of the protection against the desiccation and resistance to antimicrobial agents. However, when this microenvironment is out of balance the endogenous bacteria *Streptococcus mutans*, *Streptococcus sobrinus and Lactobacillus* produce too much acid causing the drop of the pH what results in the demineralization of teeth (7). As a consequence the apatite is dissolved and the subsequent reaction takes place:

$$Ca_{10}(PO_4)_6(OH)_2 + 8H^+ \rightarrow 10Ca^{2+} + 6(HPO_4)^{2-} + 2H_2O \quad (Eq.1)$$

Caries can normally be differentiated on the enamel as white spots that are basically small areas that undercame the demineralization. If the described process is not stopped, the created cavity can enlarge, finally reaching the pulp and the nerve endings, perceived by the organism as pain (Figure 9). Untreated dental caries can lead even to the necrosis of the pulp and the necessity of the piece extraction (8).

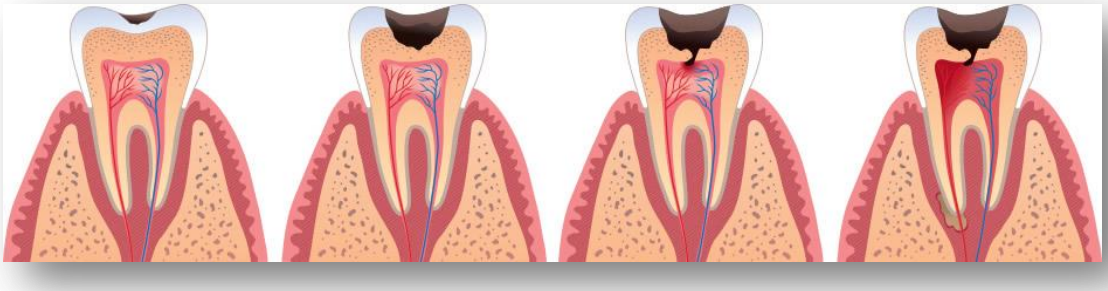

Figure 9. Scheme of the dental caries propagation

There are a wide number of risk factors that favor the dental caries creation and development (7):

- Inadequate salivary flow and composition
- Elevate number of bacteria
- Insufficient supply of fluoride ions
- Gingival recession
- Genetic factors
- Poor oral hygiene
- Poor dietary habits

5. Remineralization of teeth

The process of demineralisation and remineralisation takes place constantly during the day in the oral cavity. The balance between those two processes stops, reverse or maintains the progress of caries disease. Remineralisation process prevails frequently, especially thanks to the saliva which acts as a pH buffer (35). The crucial function play the proteins, such as glycoproteins, that are adsorbed on the tooth surface where they form a pellicle layer and additionally the phosphoproteins which regulate calcium activity. Mentioned pellicle protects enamel from mineral loss especially when acidic conditions are introduced being able to reverse the demineralization process (Eq.2) (36).

$$Ca_{10}(PO_4)_6(OH)_2 + 8H^+ \leftrightarrow 10Ca^{2+} + 6(HPO_4)^{2-} + 2H_2O \quad (Eq.2)$$

5.1. Prevention and treatment of dental caries

Without any doubt the most popular agent used for enhancing the teeth remineralization process nowadays is fluoride. Beside the antibacterial properties at low concentrations, fluoride stops the demineralization and favours the opposite-remineralizing process on the tooth surface. At higher concentrations it creates a calcium fluoride layer that protects the enamel from the formation of caries (11), (12). It reacts with hydroxyapatite ($K_{ps} \sim 10^{-40}$) and forms fluorapatite ($K_{ps} \sim 10^{-55}$) which is less soluble. Described processes, is represented by the chemical equation:

$$Ca_{10}(PO_4)_6(OH)_2 + 2F^- \rightarrow Ca_{10}(PO_4)_6(F)_2 + 2(OH)^- \quad \text{(Eq.3)}$$

Attin et al (12) evaluated the influence of fluoridation on the hardness of enamel. Teeth treated with bleaching agent and without subsequent fluoridation showed significantly higher hardness loss than fluoridated samples. Similar conclusion was made by Gladwell et al. (37) but in their studies fluoride ion was directly added to the bleaching gel. As a result a significant reduction in lesion depth was recorded. Generally it is claimed that presence of fluoride at level of 1 ppm increases enamel remineralization (11), (38).

Apart from fluoride, a wide number of agents with different chemical approaches designed for teeth restoration has been evaluated (Table 3). One of them are tricalcium phosphate (TCP) (11), (39), unstabilized calcium, phosphate and fluoride salts (11), (40), amorphous calcium phosphates (ACP) (11), (41)) casein phosphopeptide-amorphous calcium phosphate nanocomplexes (CPP-ACP) (11), (42), (36). Also agents very common in the modern society designed to avoid the hypersensibilty of teeth (NovaMin™ (11), Pronamel™ (43) , especially as a result of a bleaching treatment, can be classified as remineralizing products. All those methods a part from the remineralising characteristics have also desensitizing properties. Since they act as sealants of open tubuli, they prevent the inter-tubular liquid movement that would cause the stimulation of the nerve and result in the reaction that patient would recognize as pain (11), (43).

Tricalcium phosphate is a compound that can be found in human bones and teeth. It can be found in two different forms: alpha and beta. The β-TCP is insoluble in aqueous medium and plays an important role as a precursor of hydroxyapatite formation. Crystalline β-TCP is created to provide bio-available calcium or fluoride (11).). One of the biggest problems that can be found nowadays in dental materials technologies on the delivery of calcium and fluoride using TCP particles is the formation of calcium-phosphate (calcium fluoride) complexes that diminish the bio-available calcium and fluoride. The solution of this problem is the application of a low concentration of TCP or the addition of titanium dioxide or other metal oxides which limits the interactions between calcium and phosphate. Particles can be also coated with surfactants, polymers or carboxylic acids that prevent interactions between fluoride and calcium (11). Karlinsey et al. (39) modificated TCP with sodium lauryl sulfate (SLS) with the purpose of

avoiding the formation of calcium fluoride in dental products. In general, products containing this agent or its modifications in its formulation are focused on the supply of biologically available calcium in order to enhance the remineralization (11).

Similar problems can be found with Enamelon ™, which has the precipitation of salts before reaching the enamel surface. It brings into play the unstabilized calcium, phosphate ions together with sodium fluoride, although in a toothpaste tube those components are separated. During the application, soluble calcium and phosphate are delivered together with fluoride ions into the enamel surface (11). Regardless the co-precipitation problems, clinical trials performed by Papas et al. proved the significant efficacy of fluoride dentifrice at enhancing tooth remineralization in radiation patients (40).

A similar approach towards the remineralisation process presents amorphous calcium phosphates (ACP). It is a novel technology that delivers calcium and phosphate salt when ACP is dissolved in human saliva. Remineralizing ions are released separately. The big disadvantage of ACP agent is that under physiological temperatures and pH 7.4 it hybridizes and forms octacalcium phosphate to subsequently form a surface apatite. Unfortunately such properties prevent from penetration of calcium and fluoride into the subsurface, thus from remineralization of enamel subsurface lesions (11). As a result, only desensitizing effect of the product application can be expected because no remineralizing activity could be associated. Skrtic et al (41) created ACP hybrids with silica and zirconia that cause retardation of ACP transformation into hydroxyapatite form (HAP). During low temperature synthesis of ACP tetraethoxysilane and zirconyl chloride were introduced. As a result, slower formation of ACP hydroxyapatite form was observed. Presumably silicon and zircon particles are adsorbed on nucleation and growth sites of hydroxyapatite and stop HAP formation.

The problem of the simultaneous precipitation was solved by the invention of casein phosphopeptide-amorphous calcium phosphate nanocomplexes (CPP-ACP). Phosphoproteins are derived from bovine milk and combined with nanoparticles of amorphous calcium phosphate. Beside the ability to remineralize tooth, CPP-ACP was proved to have anti cariogenic properties (44). That is why it is recently being incorporated in many food and dental products (Recaldent ™) as a tool against caries (42). CPP-ACP nano-complexes are pH responsive. The amount of calcium and phosphate bounded by CPP grows when pH increases. It begins with pH 5 and stops at pH 9 to reach the level when the CPP bounds the amount of ions that are equivalent to its weight. When the pH drops the ions are liberated. Most of the products that apply this technology are active in pH 4 to 7 and are the most effective in 5.5 (11). In general CPP-ACP controls the spontaneous precipitation of calcium phosphate which is very hard to obtain in agents that use other forms of calcium. Moreover, protein technology allows achieving subsurface remineralization, since CPP maintain high concentration gradient of calcium and phosphate ions that migrates into the subsurface lesions (11). Calcium and phosphate CPP-ACP complexes can include fluoride ions and be able to

control its levels in the dental plaque. This formulation contributes in both processes: remineralization and control of the bacteria plaque. Another complex that is able to bind calcium, phosphate as well as fluoride is CPP-ACFP (casein phosphopeptide amorphous calcium fluoride phosphate). This substance is based on the casein phosphopeptide containing a sequence Ser-Ser-Ser-Glu-Glu. CPP has a remineralizing ability of enamel subsurface lesion at pH values in the range of 4.5 to 7 with the best effect at pH 5,5. At pH below this value CPP-ACFP is known to have better remineralizing proprieties than CPP-ACP. The main product of CPP-ACFP formation is fluoroapatite that is more resistant to acid conditions than hydroxypaptite (11).

Regarding tooth hypersensibility symptom, potassium nitrate is the compound that is mostly applied in order to overcome this problem. Since it cannot remineralize tooth by itself it is normally used in combination with other compounds in order to achieve this aim. Recently a very popular one on the market is Pronamel^{TM} – the main component of a Sensodyne^{TM} dentifrice. The product is enriched with fluoride ions in order to enhance the remineralization process (43). The main goal is to avoid the dental erosion by the deposition of calcium fluoride on the enamel. Another commercial agent for the remineralization/hypersensitivity treatment is NovaMin ^{TM} which consists of bioactive glass (calcium sodium phosphosilicate) as an alternative for the standard abrasive silica. Again this component is combined with fluoride in order to obtain the remineralized surface of the enamel (11).

As it has been explained previously, two effective methods to enhance the remineralization of teeth can be found in the market: fluoride application or simultaneous delivery of calcium, phosphate and fluoride ions into the enamel surface. The last one brings a lot of problems due to the co-precipitation of calcium and fluoride before reaching the enamel or because of the inadequate formation that prevents the remineralization of the subsurface of the enamel.

5.2. NMTD

As explained in chapter 5.1, the remineralization process obtained from the nowadays commercial products is not 100% effective that is why novel systems are still investigated by the scientists. One of the recently researched approaches are ion exchangers.

The controlled exchange of ions is a consistent and reversible transfer between ions that are immobilized in a solid or liquid matrix and the ions that are present in the solution. The efficacy of the process depends on the equilibrium between the solid and the liquid faze and on the velocity of the transfer. Normally, the ion exchangers are classified into 3 groups depending on the ion charge exchanged. We can distinguish between cationic, anionic and bifunctional exchangers Ion exchangers are applied in many industrial areas such as water treatment (45), analytical separations (46), pharmacy and medicine (47).

When it comes to dental materials, normally polymeric resins are used as ion exchangers (48). These synthetic materials that are insoluble in water, have spherical forms of about 0,3-1,2 mm diameter, although they can also be applied in powder form (49) From the chemical point of view, ion exchanging resins are hydrocarbon chains with polar groups (acidic or basic) incorporated in the polymer chain (acrylic, styrenic etc.). The functional group of the resin can be ionized or exchanged by the ion that is eliminated from the solution. The previously explained exchange can only happen between ions of the same charge: cations for cations and anions for anions. The most commonly used cationic groups (that interact with cations) are phosphate, sulfate or carboxylic groups. Anionic resins (that interact with anions) are most of the times amines. A important advantage of the described resins is that the process of the ion exchange is reversible; it means that they can recover its previous exchanging capacity with a very simple treatment with a regenerative solution (15).

Grup de Tècniques de Separació (GTS) from the UAB have recently developed a unique bioactive composite (NMTD) (39) based on a controlled release of ions that allow us to obtain dental product (based on ion exchanger technology) with a very efficient remineralising properties. Developed material allows delivering simultaneously calcium, phosphate and fluoride ions to the surface of the teeth in order to trigger the remineralization process by the formation of fluorapatite. In general, most of the remineralising products available on the market avoid the simultaneous incorporation of calcium and fluoride ions due to the calcium fluoride precipitation (CaF_2 k_{ps} ~10^{-10}). The control over the release of those ions prevents from the co-precipitation and facilitates the formation of the fluorapatite remineralising layer. By different combinations of various types of ion exchanging resins or nanoparticles, the NMTD material can be applied in different dental materials as toothpastes or chewing gums with the objective of engaging the remineralization process. In the present work, it was applied on the surface of the teeth in order to enhance the remineralization.

Table 3. The most commonly used agents designed for enhancing the remineralisation of teeth

Rem. agent	Advantages	Disadvantages	Approach	Commercial Product	Ref.
Fluoride	Antibacterial, reacts with hydroxyapatite and forms fluorapatite which is less soluble than hydroxyapatite, desensitizing agent,	In high concentrations it can be toxic especially during early childhood, can cause dental fluorosis, stomach ailments, acute toxicity, skin rashes (perioral dermatitis), and impairment in glucose metabolism	Teeth treated with bleaching agent and without fluoridation show significantly higher hardness loss and reduction on lesion depth than fluoridated samples	Almost all of the toothpastes contain fluoride in its composition	**(50)**, **(51)**, **(52)**, **(53)**, **(54)**
β-TCP	Supplies bio-available calcium or fluoride	Formation of calcium-phosphate (calcium fluoride) complexes that diminish the bio-available calcium and fluoride	Low concentrated TCP, TCP + TiO_2 or other metal oxides, coating particles of TCP with surfactants, polymers or carboxylic acids what limits interactions between calcium and phosphate	Clinpro™ 5000, Vanish™	**(9)**, **(39)**,
ACP	Delivers calcium and phosphate salt when ACP is dissolved in human saliva; remineralizing ions are released separately, achieves the desensitizing effect	Under physiological temperatures and pH 7.4 it hybridizes and forms octacalcium phosphate to subsequently form a surface apatite what prevents from penetration of calcium and fluoride into the subsurface	Created ACP hybrids with silica and zirconia that cause retardation of ACP transformation into hydroxyapatite form (HAP). Presumably Si and Zr are adsorbed on nucleation and growth sites of hydroxyapatite and stop HAP formation. Another solution is the separation of the components in the toothpaste tube in order to deliver soluble calcium and phosphate separately to the enamel surface	Arm& Hammer® Enamel Care™, Enamelon ™	**(9)**, **(41)**, **(56)**
CPP-ACP	Remineralizing and anti - cariogenic properties, controls the spontaneous precipitation of calcium phosphate, allows achieving subsurface remineralization by maintaining high concentration gradient of calcium and phosphate ions that		The amount of calcium and phosphate bounded by CPP grows when pH increases. It begins with pH 5 and stops at pH 9 to reach the level when the CPP bounds the amount of ions that are equivalent to its weight. When the pH drops the ions are liberated. Most of the products that apply this technology are active in pH 4 to 7 and are the most effective in 5.5	Recaldent®	**(44)**, **(9)**, **(42)**

	migrates into the subsurface lesions, can include fluoride			
CPP-ACFP	Remineralizing ability of enamel subsurface lesions, the main product of CPP-ACFP formation is fluoroapatite that is more resistant to acid conditions than hydroxypaptite	The pH values in the range of 4.5 to 7 with the best effect at pH 5,5. At pH below this value CPP-ACFP is known to have better remineralizing proprieties than CPP-ACP	Recaldent ®	**(9)**
Bio glass/ Nova-Min®	Bioactive glass (calcium sodium phosphosilicate) as an alternative for the standard abrasive silica, combined with the fluoride, reduces hypersensitivity	Precipitation of hydroxycarbonateapatite on the teeth surface and therefore the occlusion of dental tubules, when fluoride is added also fluorapatite is deposited	Sensodyne® Repair and Protect, Sensodyne® Complete Protection	**(57)**, **(58)**
Arg-$CaCO_3$	Physically seals dentin tubules with a plug that contains arginine, calcium carbonate, and phosphate, reduces hypersensitivity	Calcium carbonate with arginine let the positively charged amino acid binds the negatively charged dentin what facilitates the attraction of calcium ions to form a sealing layer	Colgate® Sensitive Pro-Relief™	**(59)**, **(60)**, **(61)**, **(62)**, **(63)**,
n-HAP	nHAP has a strong affinity to the tooth and can easily be adsorbed on the enamel surface what helps to promote remineralization, reduces hypersensitivity	The action of nanoparticles is the deposition on the enamel surface in such a way that it seals the exposed dentinal tubules forming a wash-resistant protective layer helping to decrease the dentin sensitivity	BioRepair® and BioRepair® Sensitive, ApaCare®, Desensin® Dentaid,	**(64)**, **(65)**, **(66)**

6. Hypersensitivity of teeth

Teeth hypersensitivity is a common clinical problem in modern society. Its symptoms are short and sharp pain that comes from the exposed dentin as a result of a susceptibility to thermal, chemical, osmotic or dehydrating factors (1).This disease affects a wide range of adult population, 25-30 %, women are more eager to suffer from hypersensitivity, especially at age 30-40. Also young patients present high prevalence due to teeth erosion. Older patients on the other hand tend to suffer from hypersensitivity as a result of a periodontal disease and its treatments (66). In this case, the prevalence of hypersensitivity is 72.5-98% (67). Such high prevalence indicates that hypersensitivity of teeth is an important issue and should be treated in order to prevent or eliminate the pain.

The principal cause of the hypersensitivity of teeth are exposed dentin tubules often associated to the gingival recession that leaves the cementum exposed to eroding or abrasive factors. Brannstorm's hydrodynamic theory of pain explains the mechanism as a change in the fluid flow in dentine tubules as a result of external stimuli such as changes in the temperature or osmotic parameters. Mentioned factors stimulate the bar receptor and depolarize the nerve. Since there is a relationship between the amounts of the fluid flow in the tubules and the charge produced in the nerve fibers, the uncontrolled movement of the fluid such as inward flow cause by its expansion with the temperature, leading to pressure changes across the dentin perceptible by patient as pain (Figure 10) (1), (68) (69).

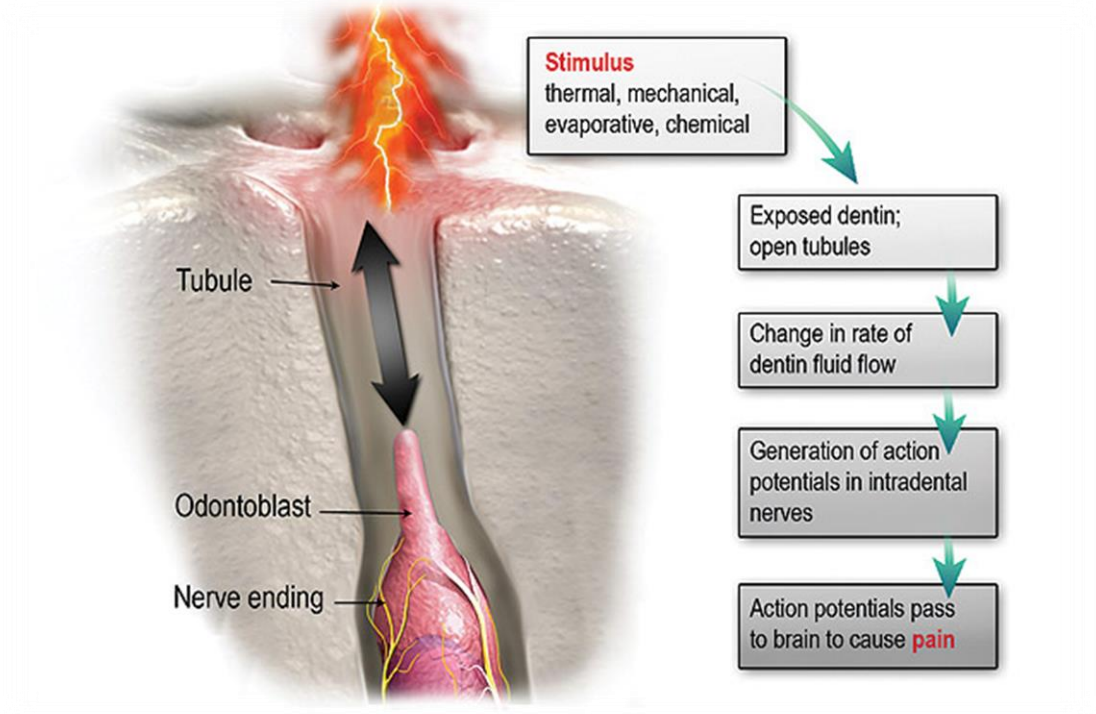

Figure 10. Scheme of the mechanism that causes the hypersensitivity of teeth. An external stimuli affects the nerves located on the odontoblast at the end of the dentinal tubuli. This stimulus affects the flow of the dentin fluid what changes the charge of the nerve endings and results in pain reception

The hypersensitivity of teeth can be remarkably reduced by the sealing of dentinal tubules or by preventing the nerves depolarization. The second approach is currently reached by potassium containing compounds like potassium nitrate (Crest® Sensitivity Protection Fluoride Toothpaste, Orajel® Sensitive Pain Relieving Toothpaste for Adults, Colgate® Sensitive Maximum Strength Toothpaste and Protect® Sensitive Teeth Gel Toothpaste). This compound penetrates into the tubules and reaches the nerve, than the potassium ions increase the contraction on the extracellular fluid around the nerves causing its depolarization and the elimination of pain (1) (67) (68) (70).
The occlusion of dental tubules, apart from the surgery intervention or laser etching (2), can be also reached by the over-the-counter (OTC) products. Most of them are salts that can precipitate inside the tubules resulting in its occlusion: stannous fluoride (Gel Kam® Pro-Dentx®, and OMNI product lines of stannous fluoride) (3), oxalate (Protect Dentin Block and Sensodyne Sealant) (71), strontium chloride (Sensodyne® Rapid Relief) (67) (5) (6), sodium fluoride (4) or ferric oxalate (Sensodyne Sealant) (72). Another type of occlusion can be caused by the precipitation and coagulation of proteins and amino acids inside the tubules. That process can be accompanied by the sealing of the tubules with methyl methacrylate (1), (Gluma Desensitiser ® All Bond DS Desensitizer, Microprime and ConfiDental). Similarly, calcium carbonate with 8% of arginine (Colgate®) let the positively charged amino acid binds the negatively charged dentin what facilitates the attraction of calcium ions to form a sealing layer (5) (73) (74) (75) (76). A different approach for hypersensitivity treatment is the bioactive glass (NovaMin®,developed by NovaMin Technology Inc., Alachua, FL, USA based on the original 45S5 Bioglass® US Biomaterials Corp.,Jacksonville, FL, USA). This technology enhances remineralisation of teeth by the precipitation of hydroxyapatite on the teeth surface and therefore the occlusion of dental tubules (6).

7. Characterization of dental tissues

In order to characterize the tooth surface a wide numbers of methodologies have been applied. Among them the most popular one is SEM (*Scanning Electron Microscopy*) which allows the study of the teeth surface structure (13). Environmental SEM found a special application in the teeth study, since no pretreatment of sample, such as gold coating, is necessary (77), (78), (79), (80), (81). With this method most of the times a surface of the enamel is under observation. Morphology changes on the teeth enamel, before and after various treatments, such as bleaching or remineralization, are able to be described and compared thanks to this methodology (78) (79) . Another common application is dentinal tubuli observation. The size, shape and obliteration of tubuli is studied in order to see the influence of the applied treatment or to characterize the dentine (82).

Another commonly used method is AFM (*Atomic Force Microscopy*) for topography and growth mechanisms studies (13), (83), (84), (85) (86), (87) (88). As well as SEM, the AFM microscopy is mostly used to study the surface of the teeth and its changes such as erosion or deterioration as a result of the bleaching treatment (84), (85) (86) or fluoride application as a remineralising treatment (87) . AFM was also used to determine particle arrangement, packing, and size distribution (83).

XPS (*X-Ray Photoelectron Spectroscopy)* on the other hand is used in order to obtain the chemical composition of the teeth (13), (89), (90) . It can be applied to observe the changes of the chemical composition after the treatment was applied (90). It was also used in order to study the changes that occurred when the orthodontic brackets are applied (89).

SIMS (*Secondary Ion Mass Spectrometry*) is used to determine the concentration gradients of building elements such as F, Cl, Na, Mg or K (91), (92), (93), (94). The comparison of the results of various treatments or investigation of dental tissue affected by some sickness (such as hyperfluorosis (92)) allows studying its influence on the content of the building elements.

TEM (*Transmission Electron Microscopy*) that gives information about crystalline properties (95), (81), allows the observation of the micro-structure of the teeth and close investigation of the crystalline structure. It also facilitates investigation of the intratubular section of the teeth and the nature of the occluding material depending on the applied treatment. With the electron diffraction more detailed information about the nature of the crystalline structured can be derived (81).

Another test that provides important information about the characteristics of the sample is micro-hardness measurement. That experiment allows investigating the influence of the various deteriorating agents (eg. acid beverages) or dental treatments (bleaching or remineralization) on the hardness of the enamel or dentine. It allows detecting the degree of erosion in teeth and by such to assess the influence of the applied treatment (96).

IR/FTIR (*Infrared/ Fourier Transform Infrared*) technique delivers very valuable information about the chemical structure of the dental tissues (97), (90), (98), (99). The careful analysis of the spectra proceeding from the teeth allows observing the nature of the sample and its changes depending on the applied treatment or the stress agent. It allows examining inorganic and organic materials of the sample and has been successfully applied for the quantitative analysis of the mineralized composition and the determination of the physical properties of the dental tissue (98). Moreover it was also applied in order to determine the CI (crystallinity index) of the teeth that informs about the percentage of the crystalline material in the sample (97).

7.1. Protocols for the estimation of the teeth porosity

As it was previously explained in the paragraph 6 the principal cause of teeth hypersensitivity is exposed dentin tubules and the main approach to reduce the problem is the sealing of dentinal tubules. In order to design a proper sealing material and to investigate its efficacy the porosity of the dentine has to be determined. Table 4 summarise all methods commonly used in order to evaluate the porosity of teeth.

According to Table 4, methods used for the evaluation of dental porosity can be divided into two groups: perfusion analysis and image analysis. From the perfusion methods, water permeability method stands out. In order to perform the measurement, dentine is cut into discs of a specific thickness and area and mounted into a perfusion system. Subsequently, a water reservoir is placed at a determined height over the samples in order to control the pressure on the samples. The bigger the number of open tubules, bigger amount of water is collected. Thanks to this method the comparison of the same sample before and after the treatment is possible. On the other hand the preparation of the sample is crucial and when is not performed properly can lead into false results.

Other two perfusion methods are *Silver nitrate intrusion* and *Mercury intrusion*; both consist in the implemention of the desired element (mercury or silver nitrate) into the tubules of the dentine. In the first method, teeth are submerged in a silver nitrate solution and after the photoreduction of samples, elemental silver is deposited inside the tubules. Afterwards, teeth are cut longitudinally and the obtained sections are observed in an optic microscope. In the second technique, the tooth is cut into cubes and mercury is introduced into the tubules by applying high pressure. The volume of introduced mercury, density variations and applied pressure are calculated. From the calculations, the size distribution of pores is obtained. The big disadvantage of both methods is that blank samples are not the treated samples. Consequently, they do not allow observing the changes in porosity in the same sample what introduce another variable into the experiment.

Among the image analysis method SEM or AFM are applied in order to estimate the occlusion of the dentinal tubuli. In both methods images obtained by SEM or AFM are analyzed manually, or by applying a scientific software in order to obtain the number and/or total surface of the open tubuli. With the Co-site digital microscopy samples are cut into discs and several images of its surface are acquired automatically with a microscope at different positions, so each picture is adjacent to each other (co-site). Images are processed and analyzed with the software in order to obtain the number of tubules and its area.

All of the presented methods are simple to perform, although they are dependent from the operator. In general, to be able to perform the before mention measurement a highly qualified and skilled technician is needed. Moreover, when SEM is used the dehydration of biological sample is a big disadvantage whereas for the AFM the crucial moment is the proper preparation of the sample. Comparing to perfusion methods

image analysis allows observing the changes in the obliteration of the dentinal tubuli in the real time what is a big advantage of a method and highly minimizes the number of variables in the measurements. Due to above mentioned advantages of the image analysis this methodology was implemented in present work for the evaluation of the dentinal tubuli obliteration.

7.1. SEM image analysis

Proper determination of the dentinal porosity is of great importance not only in the determination of the obliteration efficacy in the desensitizing treatments but also in the restorative dentistry. Restorative adhesive materials (like resins) penetrate the inter- and intra-tubular dentin in order to attach the material into the cavity walls (82). Because of that, the porosity measurements found a great interest in the oral investigations. The most commonly used and applied is the image analysis of the SEM microphotographs. The big disadvantage of this method, as it was previously mentioned in the paragraph 7.1, is its dependence from the operator's personal judgment.

There are a wide number of techniques useful for the determination of the number, density and surface of the dentinal tubules from the SEM images. Normally the parameters are evaluated by the direct observation of the microphotographs at different magnifications ranging from 1000-5000 × (82).

More traditional techniques implemented projection of the SEM images on a white picture where the contour of the tubules where drawn on the picture (105), (108) or with graphic tablet connected to the computer (114). Another method consisted on the manual coloration of the tubule orifice where subsequently the colored area was measured and counted by the image analyzer (115). Ahmed et al. applied ImagePro Plus® for Windows in order to mark the dentinal tubuli and to further analyze its area and number (116). Most of those studies due to high dependence on the operator skills and judgment gave the qualitative indication rather than reliable quantitative information (82).

The most modern and up to date approach was proposed by Ciocca et al (82) that presented an automatic method for the quantification and analysis of dentinal tubuli. This method minimized the influence of the operator on the analysis results. The software applied in the study implemented MATLAB and the Image Processing Toolbox. The entire procedure was divided into two steps. In the first one, routine named CONTOURS extracted the contours of the tubules and removed the noise, equalize the contrast etc. according to the first image. The second one ANALYSIS, read the obtained countered image and calculated the area (in square pixels) of the tubuli. The main disadvantage of the presented approach is that it was not applied in the samples treated with some remineralising product. It means that it can be easily and successfully applied on the acid etched dentin samples but will probably generate problems with the detection of open tubuli when implemented in the treated sample. It reduces highly its application in the scientific investigation.

To the best of my knowledge, until now there is no other methodology or software for the SEM image analysis developed in order to quantitatively and qualitatively analyze dentin tubules.

Table 4. Analytical methods for the remineralisation/desensitization assessment evaluation

Method	Porosity estimation	Advantages	Disadvantages	Reference
		Perfusion analysis		
Water permeability	Measurement of the volume of water that can flow through a section of dentine in a determined period of time under a determined pressure	Good simulation of the hypersensitivity of teeth from the clinical point of view (according to the hydrodynamic theory (96)).	1. Only the obliteration due to the mineral that remains stuck in the tubule walls can be evaluated, since the rest of material will be eluted by water. 2. Sample preparation is critical, since any variation of the thickness will lead to an error.	(101)
Silver nitrate intrusion	The measurement of the length at which silver has been deposited in the dentinal tubuli is correlated directly with porosity.	Methodology is simple and cheap, since the required equipment is quite common and affordable.	Does not allow observing the changes in porosity in the same sample, since the cut and silver staining of the sample are obviously not reversible steps. Methodology cannot be applied for studies that require comparing changes before and after a treatment.	(102)
Mercury intrusion porosimetry	Porosity is estimated by measuring mass changes that take place when a high density fluid (elemental mercury) is deposited inside the tubular pores.	Minimizes the influence of the operator due to its high automatization	1. Working with toxic element (mercury) 2. Samples cannot be reutilised, therefore the method is unable to compare samples before and after the treatment	(103)
		Image analysis		
Tubular opening visual estimation (SEM)	Calculating the number of open and closed tubules, in dentinal surface images	1. Methodology is simple and cheap, since the required equipment is quite common and affordable. 2. Real time observation	1. Strongly operator dependant 2. Time consuming 3. Implements the vacuum conditions that can destroy the sample	(82) (104) (105) (106) (107) (108) (109) (110) (111) (112)
Tubular opening visual estimation (AFM)	Calculating the number of open and closed tubules, in dentinal surface images	1. Does not implement vacuum conditions 2. Real time observation 3. Methodology is simple and cheap, since the required equipment is quite common	1. Preparation of the sample is crucial since the method requires flat surfaces 2. Sample that is not flat can give false results that are hard to detect	(113)

		and affordable		
Co-site optical digital microscopy	The use of a motorized microscope with computer image analysis are combined	1. Covers most of the surface in a short period of time 2. Works under biological conditions 3. Fully automatized procedure – operator independent	1. Preparation of the sample is crucial since the method requires flat surfaces 2. Sample that is not flat can give false results that are hard to detect	(113)

Objectives of the PhD thesis

In previous introduction, two most common dental diseases: hypersensitivity of teeth and caries creation have been highlighted. The objective of the present studies is to propose new approaches for the evaluation of the efficacy of the restorative treatments. Furthermore, an influence of the mentioned treatments on the dental tissue micro-structure is to be studied.

To investigate the porosity of dentin tissue, a novel methodology has been developed by applying disc model technique and observation of the dentin tubuli under the Scanning Electron Miscroscope (SEM). This will include specifically developed MATLAB software to determine the evolution of dentinal tubuli. This technique aims to be a reliable scientific tool to investigate the efficacy of obliteration products.

A Hyperspectral-Near Infrared Imaging (NIR HSI) technique is proposed as an effective and fast way to observe the influence of a remineralising treatment on dental enamel. The methodology consists of image acquisition, processing and multivariate data treatment. Confocal Raman Microscopy will be applied to check the reliability of the obtained results. Influence of the fluoride concentration, presence of protein application and contact time under this treatment are to be studied by the implementation of the optimized NIR-HSI method.

In order to evaluate the influence of the fluoride-based remineralising treatment on the teeth micro-structure a synchrotron Infrared Ellipsometry is to be applied. Since the success of synchrotron measurements and subsequent data treatment depends on the adequate reference sample selection, a series of experiments and simulations are to be designed in order to choose a suitable reference sample.

Further investigation of the teeth structural changes are to be performed with the FTIR spectroscopy. A detailed study of the various points of the targeted tooth under the remineralisng treatment will provide key information on the influence of the related treatment on the dental tissue. Deconvolution approach is to be used in order to investigate the structure of teeth and Principal Component Analysis is to be implemented to compare various regions of the tooth and to reveal the spectral differences.

A part from the scientific objectives of the developed research lines a multidisciplinary collaborative work with various research groups is planned in order to ensure the appropriate development of the main objectives.

Methodology

8. Scanning Electron Microscopy

Scanning Electron Microscopy (SEM) is commonly applied in the characterization of the surface of a given material at high magnifications. In this method, interaction of the electrons with the material's surface is represented on the digital image. It is considered a very powerful method that allows producing 3D images on a high resolution and observing with details studied material (15).

First step is the acceleration of the electrons by the electric gun; the flux of generated electrons hits the sample thanks to the high vacuum conditions created at the experimental chamber. Subsequently, they are reflected from the sample and gathered on the detector. The final image is the representation of the electrons interactions with the elements of the sample. The principal parts of the equipment are represented at the Figure 11.

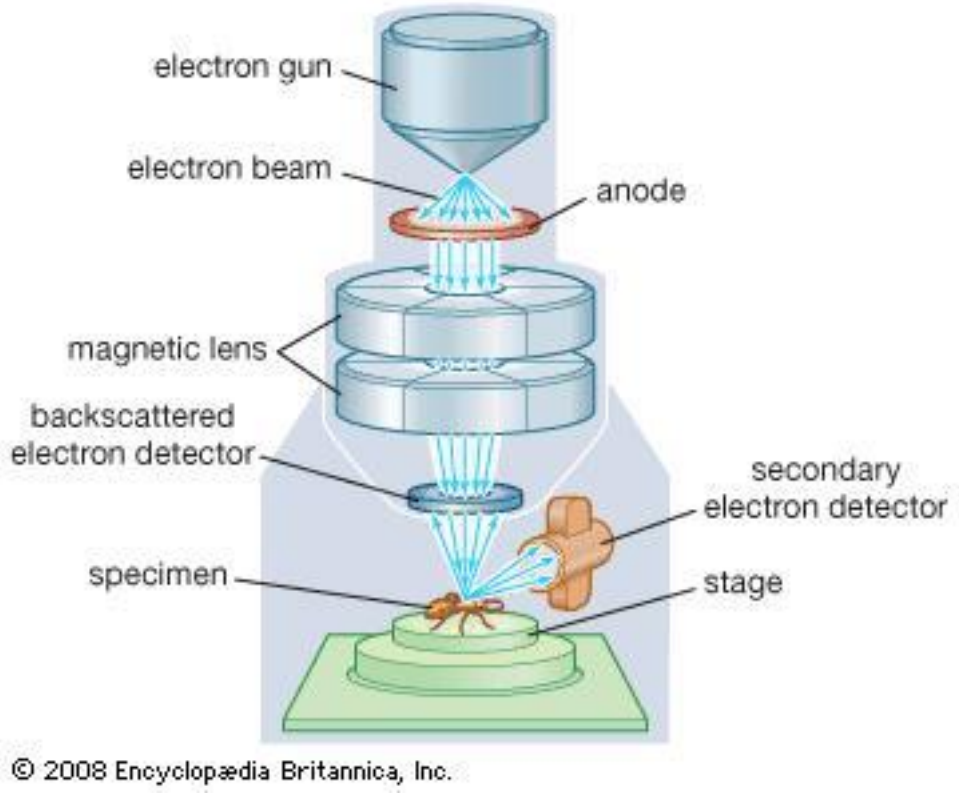

Figure 11. SEM set up

Formerly, in order to observe a sample with SEM, the sample had to have a conductive surface. In the case of having a nonconductive material, the sample was covered with a thin layer of a conductive material (silver or gold) for its observation. Nowadays, thanks to the advancements in the scientific technology it is possible to work with sample under a low conductivity configuration without the necessity of the metallization pretreatment.

Due the charge compensation systems in new SEM instruments, electrons accumulated on the surface of the sample are eliminated by a gentle flux of nitrogen that prevent from over- charging (117).

In presented work SEM was applied in order to determine the characteristics of the denitn surface. Images of the dentinal tubuli before and after the remineralising treatments were obtained and analyzed by the self-developed analytical software that allowed the evaluation of the efficacy of the treatment. The new generation SEM with charge compensation system allowed observing the changes of the studied sample without the necessity of metallization (Figure 12).

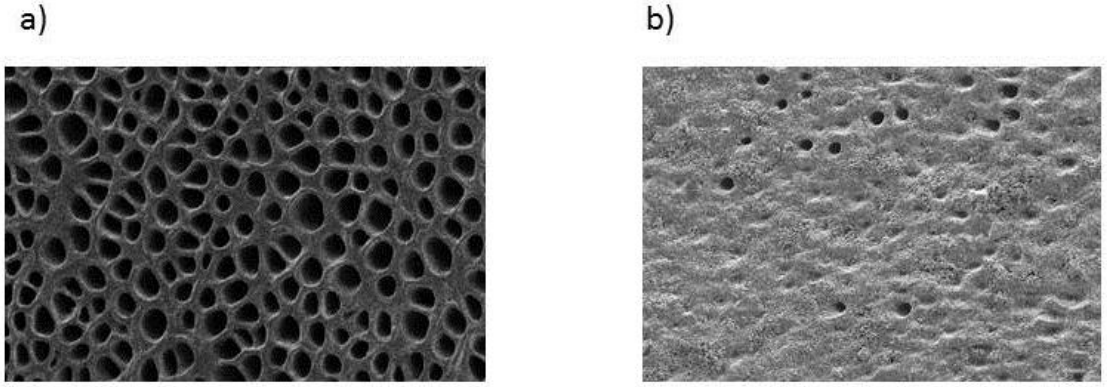

Figure 12. SEM images of dentinal tubuli a) before and b) after the remineralizing treatment

9. Raman spectroscopy

Raman spectroscopy is a technique that delivers information about the structure and composition of the studied material within a very short time and with high resolution. Through this method, vibrational and rotational modes of the law frequency are detected. Light proceeding from the laser (visible, IR or ultraviolet range) is inelastically dispersed on the sample surface. As a result of this process, changes in the characteristic frequency of the analyzed material (independent from the frequency of the incident light) are obtained (118).

When photons with energy higher than the energetic difference between two vibrational (or rotational) levels of the molecule collide with it, most of the energy goes through, but a small part of it gets dispersed. It is caused by the photon with the exact amount of energy necessary to provoke the transition of the molecule into a higher energy level (*not permitted)* that is abandoned by the molecule at once, in order to come back to the *permitted* level of energy by the emission of a photon. The frequency of the emission received back is equivalent to the difference of the energy between those two occupied levels.

If the result of the interaction between the photon and the molecule is the same frequency than the incident photon, we speak about an elastic collision. Molecule comes back to the same energetic state as before the collision and the emitted photon has the same energy as the incident one – Rayleigh dispersion is (Figure 13)

On the other hand, when the dispersed photon has different frequency than the incident one, the inelastic collision takes place and two phenomena can occur: molecule absorbs the energy and the emitted photon has smaller energy than the incident one (Stokes scattering or red shift) or the molecule loses energy and the emitted photon has higher energy than the incident one (anti-Stokes scattering or blue shift).

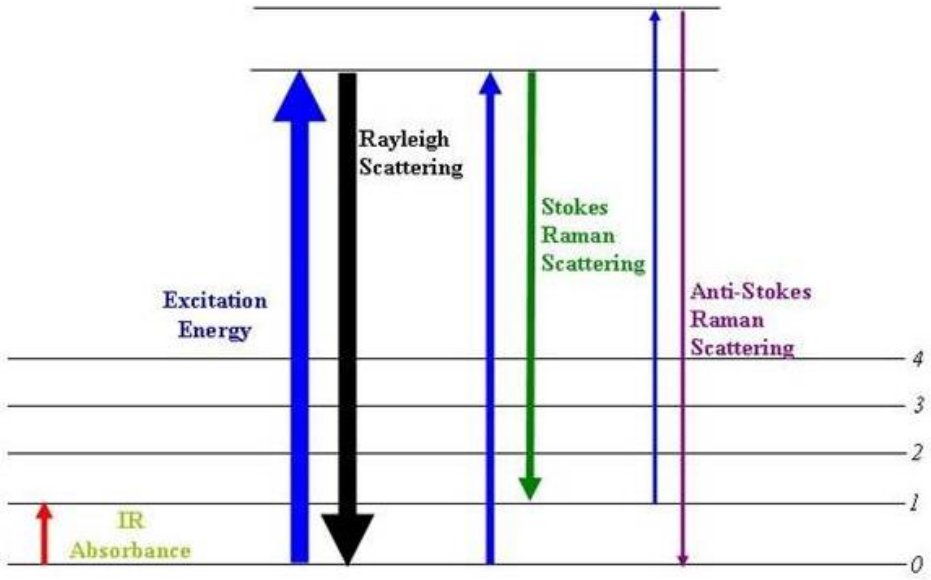

Figure 13. Illustration of a Raman Scattering

Raman is a non-destructive method where sample is analyzed directly and without any surface pretreatment. In present study Confocal Raman technique was used in order to detect and distinguish fluorapatite from the hydroxyapatite on the enamel surface treated with various remineralising products.

In the confocal technique, the resolution and contrast is increased thanks to the pinhole (confocal detector aperture) that is introduced into the instrumentation and that eliminates the light that is not focused properly. The out of focus light is rejected improving the resolution and reducing the background signal (Figure 14). In difference with the traditional Raman where only few spectra are acquired at one experimental point with confocal Raman the entire Raman spectrum is collected at each point. With this methodology a depth profile or a 3D image of the sample can be obtained.

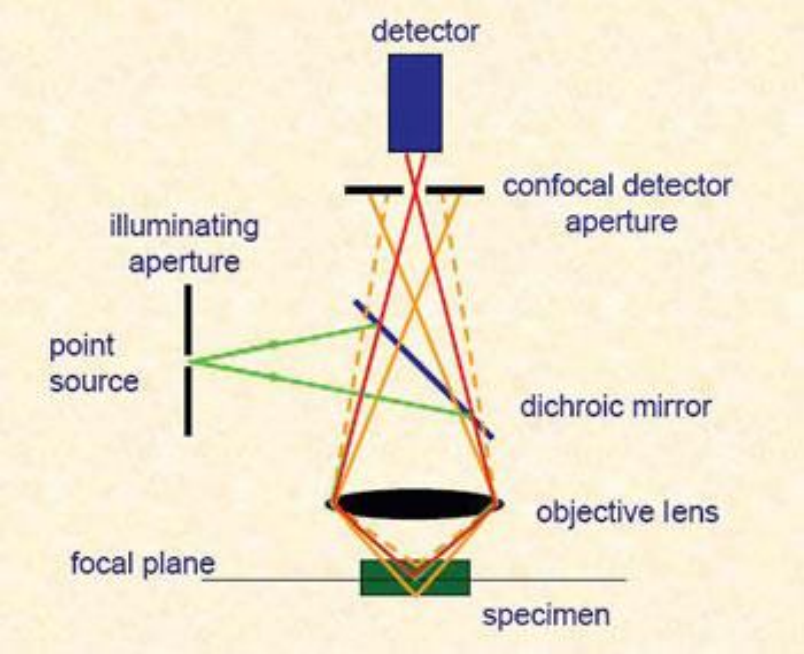

Figure 14. Confocal microscopy principles

Experiments performed in previous studies with the traditional Raman instrumentation on the curved enamel surface did not allow the study due to the changes of the enamel topography (15). With the instrumentation used in the present study, small maps (1000x1000µm) on dental samples were acquired and both FA and HA were distinguished in the cluster analysis of the spectra.

10. Synchrotron Techniques

Synchrotron is an accelerator able to maintain a closed orbit of the circulating particles. Synchrotrons are successors of cyclotrons in which the constant flow of the particles accelerated by the electric field is curved by a magnetic field. In cyclotrons both, electric and magnetic fields, have constant intensity whereas in synchrotrons applied fields are not constant (119).

Nowadays there are around 70 synchrotron facilities around the world where researchers from various fields meet in order to perform scientific experiments. Synchrotron methods have been applied in biology, chemistry, physics, material science, cultural heritage and many more branches of science (120). In this PhD project, IR synchrotron ellipsometry (section 11.3) was used in order to determine the micro-structure of dental tissues (120).

There are two kinds of manipulations that can be performed in this type of accelerators: particles can collide with each other or can maintain the same direction of the movement. In the first case there are two beams of particles accelerated in opposite directions in order to cause its collision and to study the resulting products. In the second type, only one beam is accelerated with constant energy and with a curved

trajectory. As a result synchrotron radiation with vide range of energy (from IR to X Rays) is emitted (121).

The intensity of synchrotron radiation is much higher than in case of traditional sources of electromagnetic wave. Another advantage is its high brilliance. In other words, synchrotron beam can be focused into a very small area and as a consequence obtain very high intensity. Synchrotron radiation brilliance is million times superior to the traditional sources of energy. It is also tunable; it means that from the entire beam an adequate and concrete wave range can be extracted. Due to the characteristics of the applied radiation, IR microscopic or ellipsometric measurements have a very high spatial resolution and a high signal to noise ratio.

Synchrotron accelerators have various constants components present in each facility (Figure 15) (15):

- ✓ Source of particles
- ✓ Auxiliary accelerators: particles are injected in the linear accelerator (Linac) and are directed into a Booster- an accelerator where they get the final energy before being injected into the Storage Ring
- ✓ Radiofrequency cavities (RF): cavities where oscillating voltage is applied in order to accelerate the particles and maintain them in parts (packages) of the same velocity and frequency
- ✓ Magnetic elements: magnets with poles oriented perpendicularly to the particles orbit. It is responsible for focalization and bending the beam trajectory.
- ✓ Beamlines: a certain range of wavelength is extracted from the main beam and directed to the experimental beamlines. A linear cavity transports the radiation into a specific instrumentation that adapts the beam into the necessities of the applied methodology. Normally optic and experimental cabin together with the work station form each beamline. In case of IR beamline the instrumentation consists of a series of mirrors, monochromators and the IR microscope (ellipsometer).

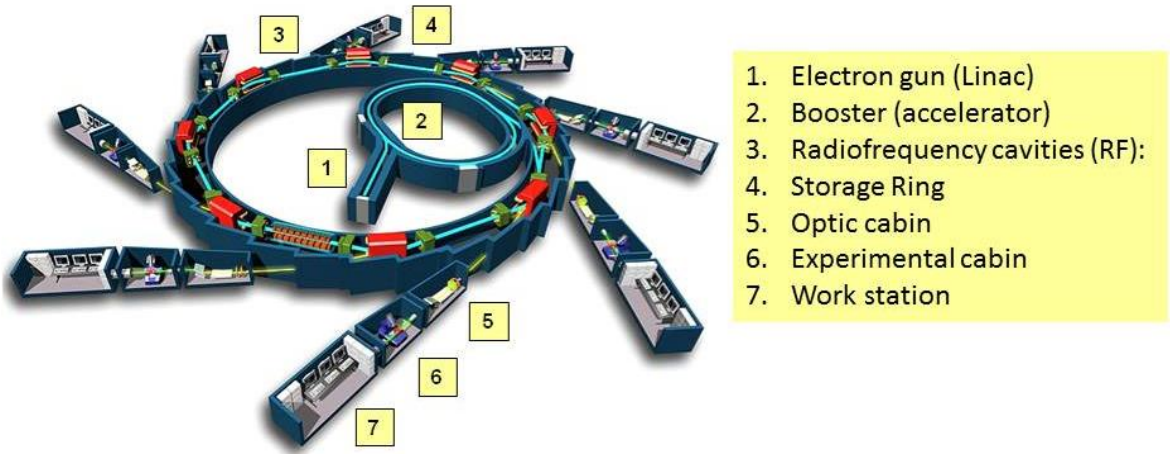

Figure 15. Scheme of the synchrotron accelerator

11. IR spectroscopy

Infrared spectroscopy (IR) implies the infrared range of the electromagnetic wave. It includes three regions depending on the energy: near, medium and far infrared. The far infrared (FIR) (10 - 400 cm^{-1}), located next to the microwaves, has the lowest energy from all IR waves and is mostly applied in the rotational spectroscopy (Raman). Medium-infrared, or mid-wave infrared (MWIR) (400-4000 cm^{-1}) is used to study the fundamental vibrations of the molecules whereas near-infrared (NIR) (4000-14000 cm^{-1}) can excite overtones or harmonic vibrations (122).

IR technique is based on vibrations of atoms that build the molecule. It is performed by interaction the IR wave with a sample and observing which part of the spectral radiation is absorbed at particular energy. The peak that appears at the IR spectrum represents the vibration of a molecule and has a specific frequency. In order to see the vibration in the IR light, an electric dipole moment of the molecule has to undecome a change. As a matter of fact, the process of the IR determination can be treated as a change in the dipole moments associated with vibrations and rotations of the molecule. Common movements of the molecule that result in such a change are stretchings and bendings of the molecular bond that result in a change of the bond length or bond angle (Figure 16).

Stretching can be symmetrical (in phase) and asymmetrical (out of phase) (123). The symmetrical stretchings of a molecule are inactive in the IR measurement (such as CO_2) since no change in the dipole moment is produced during its vibration.

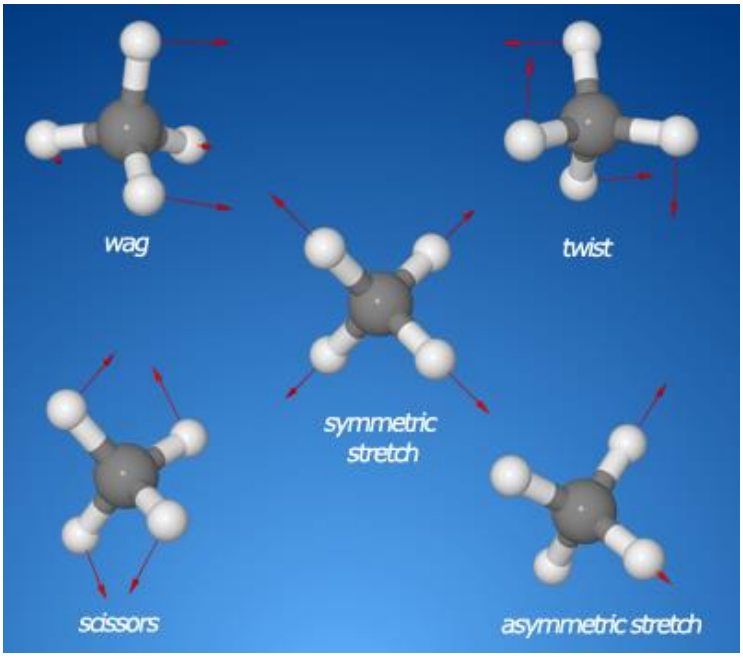

Figure 16. Common vibrations of the molecule as a result of the interaction of the IR wave with the sample (presented on the methane molecule) Image courtesy of Prof Przemyslaw Maslak

11.1. FTIR Spectroscopy

The invention of the FTIR (Fourier Transformed IR) caused a significant advance in the development of the IR instrumentation (123). This type of equipment implements an interferometer that applies a well-known mathematical operation: Fourier transformation. FTIR significantly improved the quality of the spectra and shortened the time of the measurements (123).

In the FTIR spectrometer, the electromagnetic wave has to pass through the interferometer to the sample before reaching a detector. The signal is amplified and the high frequencies are eliminated by a filter, subsequently the data is converted to the digital form and analyzed by the application of Fourier transformation (123).

The most common interferometer used in FTIR is a Michelson interferometer (Figure 17) (123). It is made of two perpendicularly placed mirrors; one of them is fixed whereas the second one moves back and forth. Light that goes through a beamspliter is separated: one part is reflected by the fixed mirror whereas the second one by the moving mirror. As a result, when they finally meet again in the spliter, retardation is generated since the paths that traveled both of the beams are not equal. When the modulated beam passes through a sample, an interferogram is created that further undercomes Fourier transformation.

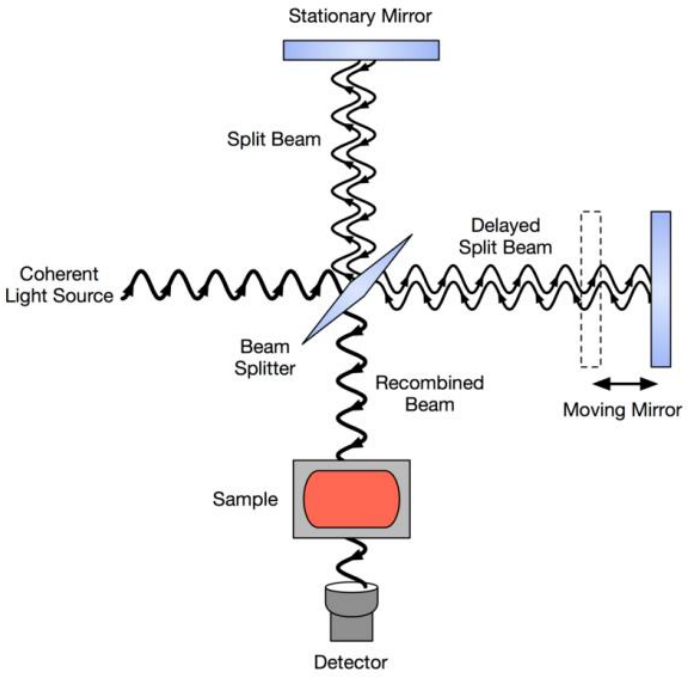

Figure 17. Scheme of Michelson interferometer

Another important part of the FTIR instrumentation is the source of light. The commonly applied sources in spectrometers are Globar (silicon carbide rod) or Nernst (ceramic

rode). In FIR the high pressure mercury lamp is applied whereas for the NIR measurements tungsten-halogen lamps are common.
When it comes to detectors, there are two options available: the commonly used DTGS (deuterium tryglycine sulfate) or the more sensitive MCT (mercury cadmium telluride) however, in the second case a cooling with liquid nitrogen is necessary. Germanium or Indium-Antimony detectors are applied in FIR at liquid helium temperature. For NIR, lead sulfide photoconductors are used.
IR spectroscopy is commonly applied in organic chemistry in order to identify organic compounds. It also found application in characterizing polymers and biological materials such as peptides, lipids, proteins, biomembranes, animal tissues or cells (123). IR/FTIR method deliver valuable information about the chemical structure of the dental tissues (97), (90), (98), (99). The careful analysis of the spectra proceeding from the teeth allows observing the nature of the sample and its changes depending on the applied treatment or the stress agent. It examines inorganic and organic materials of the sample and has been successfully applied for the quantitative analysis of the mineralized composition and the determination of the physical properties of the dental tissue (98).
In present work FTIR was applied to investigate structural changes in the human enamel and dentin induced by the remineralization process. Spectroscopic results were based on the deconvolution of the phosphate band. The spectra from various points proceeding from different locations of the tooth were compared and studied applying Principal Component Analysis (PCA) and curve-fitting procedure.

11.2. IR ellipsometry

The principles of the ellipsometry have been established at the beginning of XX century; however it was not considered a reliable scientific instrument in that time. The situation changed thanks to the development of the computer technology in 1990s that allowed the automatization of the instrumentation and data analysis. After that, ellipsometry became a high precision optical characterization technique and is commonly applied in science and industry until present moment (124) .
In ellipsometry, an optical characterization of the material is performed through the reflection or transmission of light. It measures changes in the polarization as a consequence of the reflection or transmission of the light on the measured sample. Very often polarized light adopts an elliptical shape as a result of the reflection and to this fact ellipsometry owes its name (124).
During the ellipsometric measurement two values are extracted: amplitude ratio (Ψ) and phase (Δ) differences between two light waves p- and s- polarized (Figure 18). As a result a ρ value is obtained:

$$\rho = \frac{r_p}{r_s} = \tan\Psi \cdot e^{i\Delta} \quad \text{(Eq.4)}$$

Where:

r_s – complex reflection coefficient of the s – polarized wave

r_p - complex reflection coefficient of the p – polarized wave

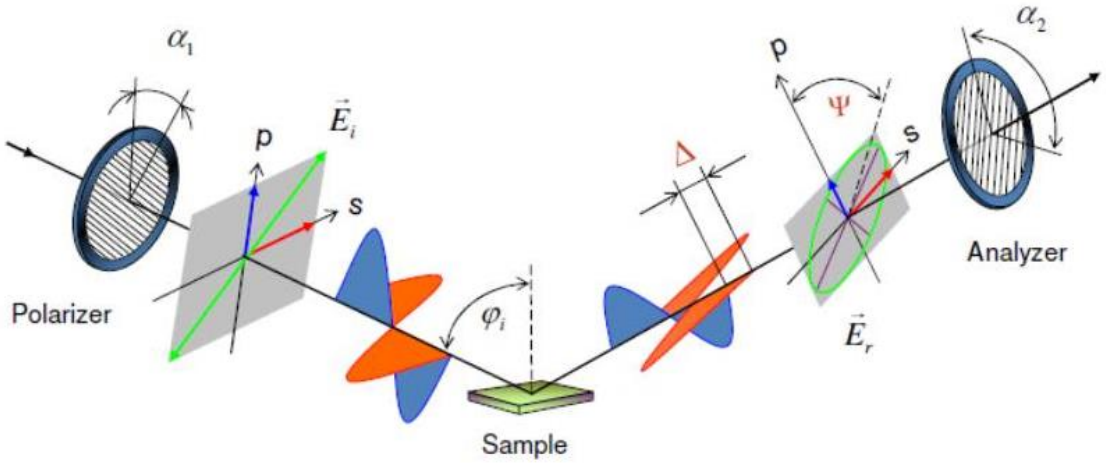

Figure 18. Experimental set-up of ellipsometer. Image courtesy of Dr Ulrich Schade (BESSY, HZB Helmholtz Zentrum Berlin)

Ellipsometric measurement is applied in ultraviolet, visible and infrared region. Depending on the wave length used in the experimental set up, different information about the studied material can be extracted (Figure 19).

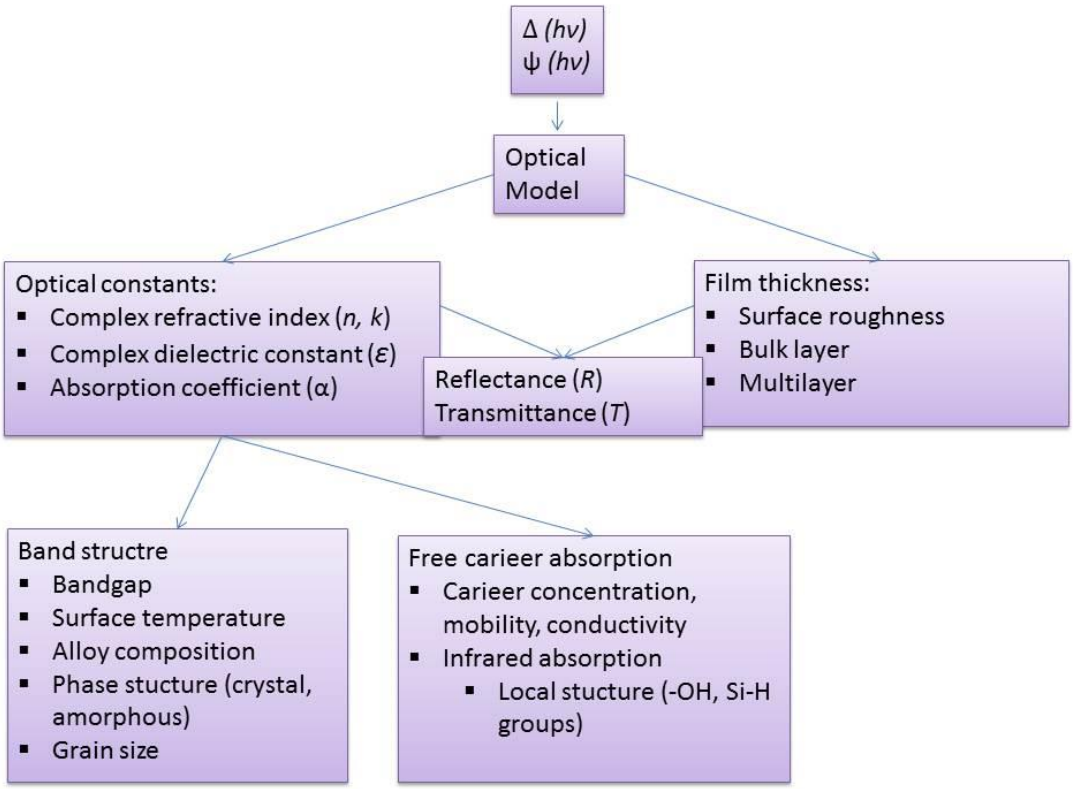

Figure 19. Physical proprieties derived from ellipsometric measurement (124)

The interpretation of the ellipsometric data is very difficult from the raw values (Ψ , Δ). A construction of the adequate optical model is necessary in order to obtain valuable information. Once the model is applied, the physical properties such as optical constants or film thickness can be derived and from the obtained data the reflectance and transmittance can be calculated (124).

A very critical part of the ellipsometric measurement is the selection of an adequate incidence angle in order to obtain the highest sensitivity. Normally the 70-80˚ angle is chosen for the semi-conductive materials, such as teeth samples. Measurement performed at normal incidence angle in ellipsometry cannot be performed because the p- and s- polarizations cannot be distinguished. Other limitation of the method is the surface characteristics. It has to be very flat and smooth in order to avoid the scattering that diminishes the intensity of the reflected light (124). Advantages and disadvantages of the method are sum up in Table 5.

Table 5. Advantages and disadvantages of the spectroscopic ellipsometry (124)

Advantages	**High precision (thickness sensitivity ~0,1Å)**
	Nondestructive
	Fast
	Wide application area
	Obtaining many physical characteristics (optical constants, thickness, etc)
	Possible real-time monitoring
Disadvantages	Optical model is needed (indirect characterization)
	Complicated data analysis
	Low spatial resolution (several mm)
	Difficulty in characterization of low absorption coefficient (α<100 cm^{-1})
	Surface have to be flat and smooth (well polished)

Ellipsometric method is applied in various branches of science and industry. The most common are thin-film growth, real-time monitoring of oxidation or etching processes (124) (125), (126). In the characterization of biological materials, ellipsometry is applied in bioadsorption measurements (layer thickness, surface mass density), biosensors (monitoring the biomolecular reactions), materials research (nano and chemical structure), structural analysis (photonic structures) and diagnostics (monitoring of the layer formation) (125). In Table 6 some of the applications of the spectroscopic ellipsometry and the general characteristics of the method have been sum up.

Table 6. Sum up of the characteristics of the spectroscopic ellipsometry (124)

Measurement probe	**Light**
Measured value	Amplitude ratio (Ψ), phase difference (Δ) between p- and s-polarised waves
Measured region	IR, UV-Vis
Application	
Semiconductors	Substrates, thin films, gate dielectrics, lithography films
Chemistry	Polymer films, self-assembled monolayers, proteins, DNA
Display	TFT films, transparent conductive oxides, organic LED
Optical coating	High and low dielectrics for anti-reflection coating
Data storage	Phase change media for CD and DVD, magneto-optic layers
Real-time monitoring	Chemical vapor deposition, etching, oxidation, thermal annealing, liquid phase processing
General restrictions	High surface roughness
	Oblique incidence angle

11.3. Synchrotron IR ellipsometry

Ellipsometric studies are getting popular nowadays especially in composition, thickness or roughness determination of organic films and multilayers (126). When determined properties are changing along the probed material the polarization degree is affected and a very sophisticated model is required in order to process the obtained data. For applying a reasonably defined angle, the spot size of the probed sample has to be limited; sometimes it has to be set close to the diffraction limit. It means that IR ellipsometry is limited by the degree of the light brightness. With the purpose to improve it, the synchrotron storage rings have been applied due its superior brillance (126).

Nowadays, there are three instruments that apply the IR synchrotron radiation to ellipsometry studies: NSLS in Brookhaven (New York), ANKA in Karlsruhe (Germany) and IRIS at BESSY II in Berlin (Germany). The last one, constructed as a micro-focus mapping ellipsometer, was applied in present work. The experimental set-up, presented in Figure 20, allows to scan an area of 50x50mm, has a spectral range of 2,5-30µm (4000-333 cm-1) (126) and lateral resolution below 1 mm^2 whereas the traditional ellipsometers are of around 50 mm^2 (127).

The sensitivity improves enormously thanks to the brilliance that is of twice the magnitude than in the Globar source instrumentation. Its first commissioning was performed in 2003 and since than it has been applied in many investigations but mainly in the thin films area (126).

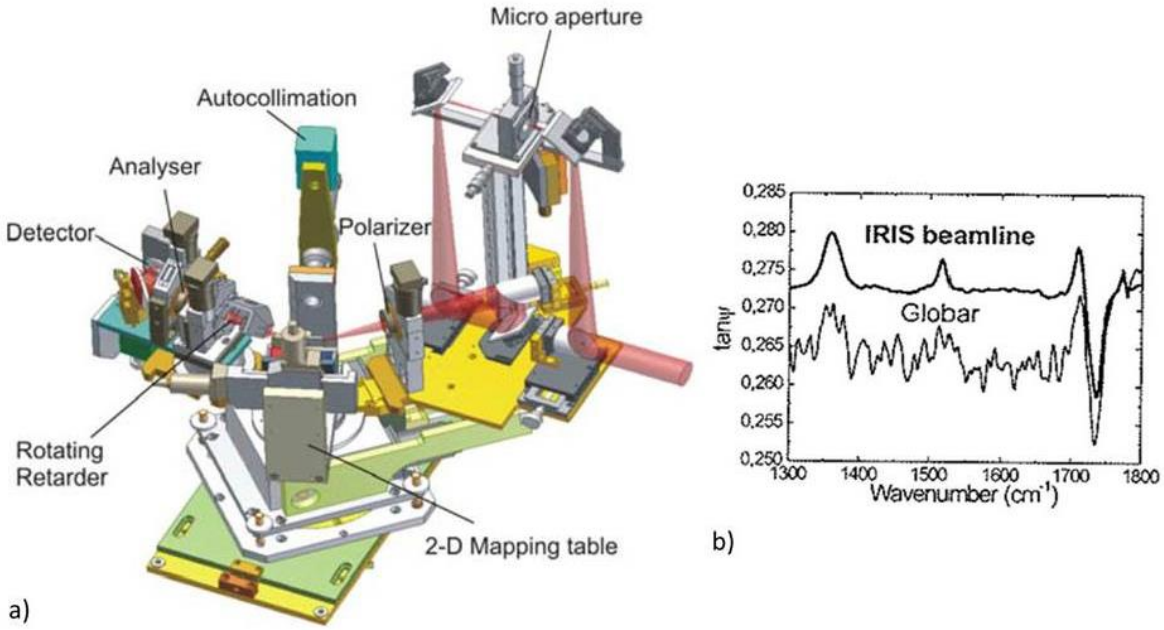

Figure 20. a) Experimental set up of the IRIS BESSY II instrumentation b) spectra of the polyamide film on silicon acquired on IRIS beamline and by standard Globar source (126).

11.4. NIR Spectroscopy

NIR started to be applied as an analytical method in 1950s but it gained its popularity in 1970s. General development of the electronics, optics and computational methodologies improved the acquirement and processing of the NIR data and as a consequence took part in the expansion of the method in scientific and industrial world (128).

With NIR spectroscopy, solid and liquid samples can be analyzed. It requires no pretreatment; measurement is quick and provides information about chemical aspects of the sample. Since bond vibrations can alter other characteristic bands in the crystal structure, the physical properties (density, viscosity, particle size) of a sample can also be determined (128).

NIR works mainly in range 780-2500 nm where overtones and fundamental vibrations are located. The intensity of the NIR band is conditioned by the change in the dipole moment and the anharmonicity of the bond. The most active bands in the NIR measurements contain typically hydrogen atom (C-H, N-H, O-H, S-H etc). On the other hand, bands with equal or similar atoms are absent or have a very weak intensity (C-C, C-Cl, C=O etc) (128).

NIR Spectrometers have similar configuration to those applied in other spectral regions. The instrument can cover the entire range (whole spectrum spectrometers) or only a certain range of the spectrum (discrete spectrometer). The commonly used detectors can be semiconductors (PbS, InGaAs), diode arrays or planes (CCD) in the multi-channel detectors. Last types of multi-channel detector allow the acquisition of spectra at different points of the sample and at the same time to determine its shape, this data

combination allowed the development of NIR-imaging spectroscopy. With this method a three dimensional image that is a function of spatial composition and the radiation wavelength is obtained (128).
Very often, NIR spectroscopy data requires chemometric methods in order to extract the needed information. Multivariate analysis techniques are the most commonly applied in NIR data treatments. It relates the analytical variables to the properties (such as concentration) by grouping similar characteristic together and establishing classification methods for the qualitative and quantitative analysis (128).
Since NIR spectroscopy is fast, easy to perform and can be applied in a wide variety of samples without pretreatment, it has a multiple application in science and industry. It is commonly used in agricultural food, pharmaceutical, environmental, petrochemical and clinical sector (128). In the present work, it was proposed for the first time together with the Hyper Spectral Imaging method as a tool for the control of the process of remineralization of human dental tissue. Teeth samples were acquired with the NIR spectrometer and further obtained images were analyzed applying multivariate analysis techniques.

12. Hyper Spectral Imaging

HSI was designed and applied at first in cartography, although very quickly it started to gain popularity also in chemical analysis (129). Till now, this technique is a very popular method for the image analysis and is commonly applied in many branches of science, especially in development and control of drugs (130).
In HSI technique a full spectrum of the applied range (in case of this work NIR range) is acquired for each point (pixel) of the sample by the spectrometer in combination with the digital camera (Figure 21). Resulting data is organized in the *hyperspectral cube*, a three dimensional set of data with two spatial dimensions (x and y axis of an image) and one spectral (wavelengths). This kind of a very compact image gives plenty of information where multivariate analysis is necessary to implement, in order to extract wanted information.

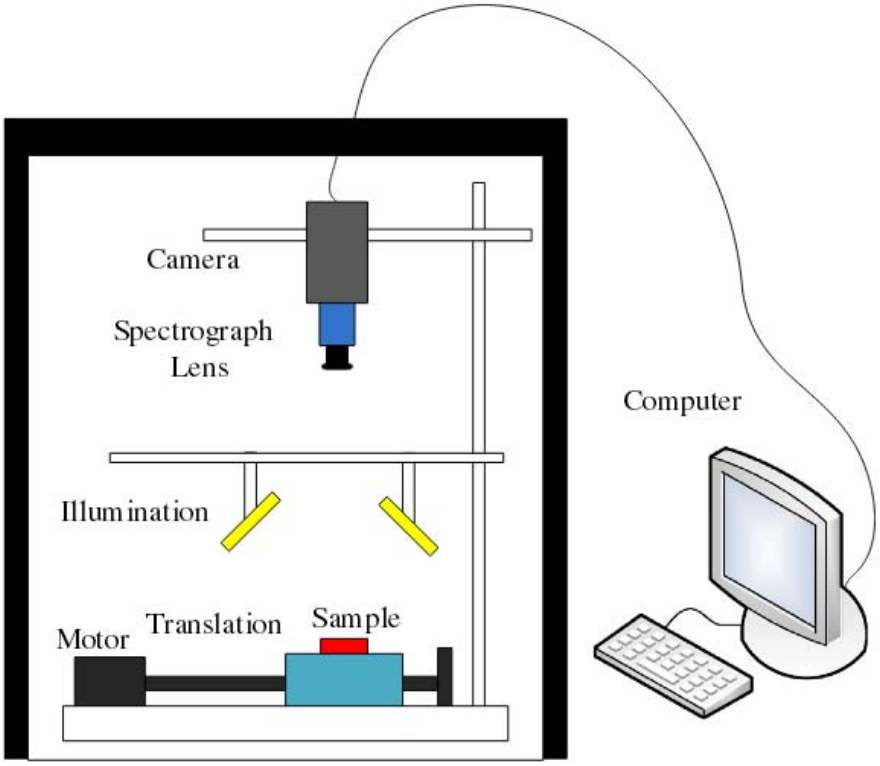

Figure 21. Scheme of a typical HSI instrumentation (131)

Before the multivariate data analysis is implemented, a simple pretreatment of the initial data is performed. All acquired information can be represented as a set of bidimensional matrixes that need to be unfolded (separated) in order to analyze all the information from the initial set of data (a cube) (Figure 22). Since the acquired spectra are the sums of components of the sample's pure spectra, D matrix can be decomposed to concentrations, C, and spectra matrix, S, with its residuals, E:

$$D = C \cdot S^T + E$$

D matrix has three dimensions: x and y, which are spatial dimensions (represented on the picture as a position of the pixel) and the third - the spectral one (all measured wavelengths). Matrix C is composed of two dimensions: to every point a concentration of the component is assigned. It shows the distribution of the given signal on the image, it can be represented for all wavelengths. S^T matrix contains the measured data (absorbance, transmittance etc) for each wavelength. E matrix is a residual error (131).

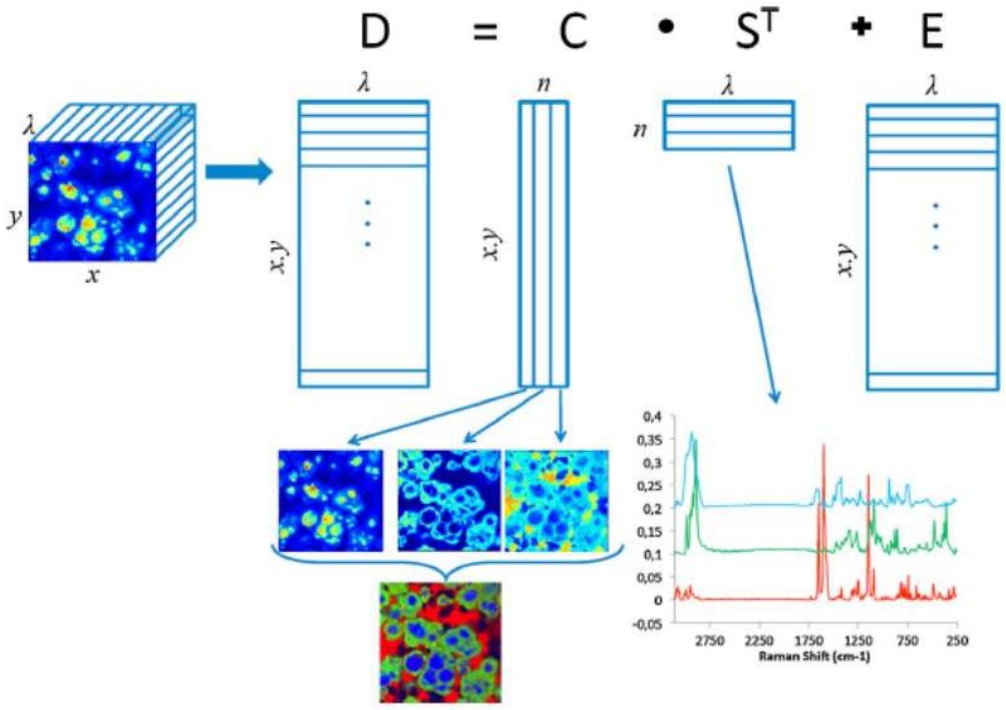

Figure 22. Unfolding of the hyperspectral cube data set (132)

12.1. HSI Data Treatment

At the beginning of the HSI development, images were analyzed as a RGB (red-green-blue) images, gray scale images or histograms. The following application of the MVA (multivariate analysis) and especially MIA (multivariate image analysis) allowed a better exploration of the data and the extraction of detailed information from the studied sample.

Exists a wide number of approaches for the data treatment when HSI methods are implemented (133). Among them, PCA (134), (135), (136), (137), PLS-DA (138), (139) or PLS (Partial least squares) (140) are the most popular one. In the present study, the correlation coefficient and MCR-ALS (Multivariate Curve Resolution Alternating Least Squares) (141) were used in order to obtain necessary information from the acquired spectra of dental samples. Both methods are useful tools to find similarities between two spectra; correlation coefficient allows a qualitative comparison of parameters (133) whereas with MCR both qualitative and quantitative analysis can be performed (141). In this work both methods were applied in order to differentiate fluorapatite and hydroxyapatite species on the human enamel.

12.1.1. Correlation Coefficient

In case of correlation coefficient, spectra obtained in the measurement is compared to spectra of pure components. As a result, a correlation (degree of similarity) map that

represents the distribution of those components can be constructed. The correlation coefficient is calculated from the subsequent equation:

$$corrcoef = \frac{\sum_\lambda x_{mn\lambda} y_\lambda}{\sqrt{\sum_\lambda x_{mn\lambda}^2 \sum_\lambda y_\lambda^2}} \quad \text{(Eq.5)}$$

where, for each wavelength, $x_{mn\lambda}$ is the spectrum for the *mn*-th pixel and y_λ the pure spectral profile for one analyte. Similarity is the greatest when corrcoef = 1 and it means that two spectra are identical (142), (143).

12.1.2. MCR-ALS (Multivariate Curve Resolution Alternating Least Squares)

MCR-ALS is a popular method for the identification of multi-component mixtures. The advantage of this method is that a great variety of data sets can be analyzed by its decomposition into a bilinear model. Moreover, multiple analyzes can be performed simultaneously on many matrices (144).

MCR-ALS method is often applied when the pure spectra of the constituents are not known (145). The algorithm (141) consists in the decomposition of the spectral matrix ***X*** (MN x λ) in two matrices, ***C*** (MN x F), which contains the concentration profiles, and $\boldsymbol{S^T}$ (F x λ), which contains the spectral profiles for each F constituent.

$$X = CS^T + E$$

Being E (MN x λ) the residual matrix related to experimental error. MCR-ALS works by iteratively optimizing the matrices C and S^T with the help of constraints based on chemical knowledge or on mathematical features of the data (145).

ALS algorithm calculates possible concentration C and pure spectra S^T by fitting it in the D matrix. It is performed for the concrete number of components for the estimated initial C and S^T (evaluated by Evolving Factor Analysis or SIMPLISMA). The model is finished when in two calculative cycles difference in standard deviations of the residuals calculated and experimental ALS are less than 0,1%. The value can be modified by the user depending on the optimization stage desired (144).

MCR-ALS is applied in spectroscopic, electrochemical, composition experiments where a big variety of aspects such chromatographic elution, spectroscopic images, environmental data, industrial processes or chemical reactions can be studied (145).

A NOVEL METHODOLOGY FOR THE EVALUATION OF THE DENTINAL TUBULI OBLITERATION

Summary of the study

Objectives

A methodology based on the dentin disc model was evaluated. Specimens treated with a desensitizing agent were observed under Scanning Electron Microscope (SEM) and the resulting images were analyzed by an automatic segmentation algorithm developed to calculate the number and area of the open tubuli. The dependence from the operator, error of the algorithm, experimental error, the influence of focus adjustment during SEM measurements and vacuum conditions of the presented method has been evaluated. The determination of the region of interest was established by analyzing images that covered the entire surface of teeth. Subsequently, the representative number of pictures was calculated and discussed. Once the method was optimized a comparison of three different commercial tooth pastes targeting the hypersensitivity of teeth was carried out. The experimental error of the study was calculated.

Methodology

The tooth paste applied in the optimization part of the study was a commercial product of Sensodyne® Protect and RepairTM with the Bioglass® NovaMin™ technology. Daily cyclical applications of the demineralization solution and remineralising tooth paste were performed during 5 days. Specimens were observed with SEM after the demineralizing process and for the second time after toothpaste applications. Resulting images were analyzed by automatic segmentation algorithm applying the Matlab routine especially developed for the study. The number and area occupied by open tubules were detected by the automatic algorithm (Figure 23) and statistically analysed. For the second part of the experiment three commercial toothpastes, namely, Sensitive Pro-Relief™ *Colgate*® with the Pro-Argin Technology, Repair and Protect™ *Sensodyne*® with NovaMin™ Technology and Desensin™ *Dentaid*® with nanoparticles of hydroxyapatite, were applied in the study to test the performance of the evaluated methodology.

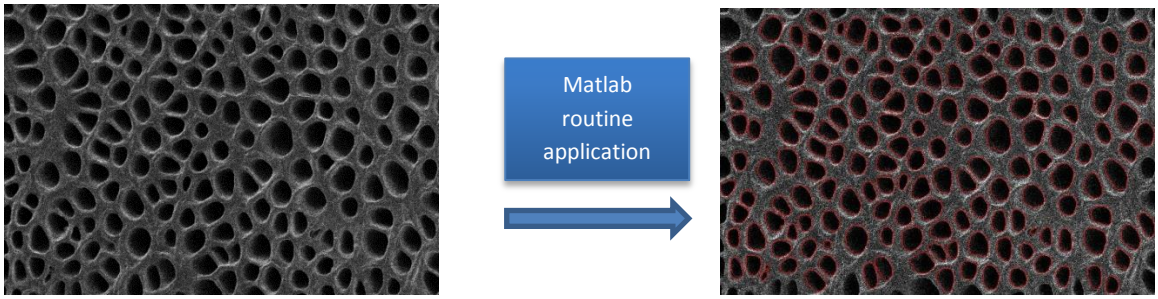

Figure 23. Illustration of one image analyzed by the automatic segmentation algorithm

Results

Very low values of the standard deviation for both: detected number of tubules (0,54) as well as the calculated percentage area of open tubules (0,16%) indicated that the performance of the routine on the designed digital simulations was correct. The calculated experimental error of the performance of the developed MATLAB routine (0,04%/sample) was also low when pictures after the demineralization process were concerned. On the other hand, slightly higher errors for the pictures after the application of the remineralising treatment (0,06% / sample) occurred mostly due to impurities detected over the surface of the dentin.

It is also remarkable, that the presented method is independent from the operator since the standard deviations for the detected area for three independent technicians were significantly low before the treatment (0,13%) as well as after the application of the tooth paste (0,11%).

The described studies have demonstrated that the average number and area of open tubules is bigger for the central zone of the teeth, indicating that developed routine performs better in that zone.

Furthermore, such studies demonstrate that once the sample is immersed into a microscope vacuum chamber for approximately two hours, the conditions of the environment does not change the number or the detected area of tubules. Therefore, the developed routine is also independent from the focus adjustment.

As a result of the comparative study after 3 and 5 days treatment the n-HAP based product of Dentaid ® revealed to be stable in the studied range of time obtaining 93,3% of the final average obliteration. On the other hand, the Sensitive Pro-Relief™ tooth paste that contains arginine revealed much smaller average obliteration after 3 days (71,2%) comparing to 5 days (95,5%). A completely different phenomenon was observed for the Sensodyne® Repair and Protect™ tooth paste. The obliteration dropped from the 84,5% to 70,7%.

Conclusions

The present method becomes a suitable scientific tool that will allow scientists and private companies the *in vivo* monitoring and assist on the development of new remineralising agents. The method also facilitates the comparison of different occluding methods and the evaluation of its efficacy.

Introduction

Remineralisation is a natural reconstructive process of a tooth that aims rebuilding the damaged surface in order to prevent creation of caries. It is based on the deposition of calcium and phosphate ions assisted by fluoride on the enamel what results in the creation of the new hydroxyapatite crystals on the area affected by the deminaralising process (9) (10). The crucial role plays the saliva that delivers all necessary ions, behaves as a natural buffer and controls the equilibrium between the demineralization and remineralization (9). When the equilibrium is not maintained the demineralization starts to dominate and the process of caries creation is triggered. The problem of caries is the most relevant dental disease worldwide. It is the main cause of pain and tooth loss (35). That is why there is a constant demand for the new remineralising methodologies in order to prevent or to diminish the creation of caries.

Since the introduction of the fluoride based remineralising methods (50) (146) (147) (148) the prevalence of dental caries disease dropped significantly (10). This method is the most common, although it is limited by the adequate concentration levels of calcium and phosphate ions and its delivery to the surface of the teeth. Recently, other remineralising approaches have been considered (9). Among them, the most popular ones are a casein phosphopeptide stabilized amorphous calcium phosphate technology (CPP-ACP, RecaldentTM) (9) (149) (150), unstabilized amorphous calcium phosphate (ACP, Enamelon TM) (9) (151) (55), bioactive glass containing calcium sodium phosphosilicate (NovaMin®, Sensodyne®) (152) (153) and calcium carbonate supported by arginine technology (Arg- $CaCO_3$, Sensitive Pro-Relief™ Colgate®) (154) (155) (156) (60) (61) (62) . All those methods, a part from the remineralising, have also desensitizing properties. Since they act as open tubuli sealants, such methods prevent the inter-tubular liquid from movements that would cause the stimulation of the nerve and result in the reaction that patient would recognize as pain.

Such huge demand for the development of remineralising or desensitizing methodologies also creates a necessity for new analytical methods to test the performance evaluation. In order to determine the mechanism or the effectiveness of remineralizing/desensitizing agents, having a suitable approach to evaluate the dentine porosity is crucial.

Several different methodologies had been studied (Table 4) so far. In general, all of the available methods can be classified in two main categories: the ones based on the perfusion and intrusion analysis; and those based on the image analysis. Both apply a dentin disc model technology that is a commonly applied method for dentin morphology and characteristics evaluation. It also allows to qualitatively and quantitatively studying the obliteration capacity of various dental products (105) (114) (106) (107) (108) (109) (82) (110) (115) (111). Perfusion methods are based on the measurement of the ability

of a fluid to penetrate the dentine tubuli. On the other hand, image analysis implements optical methodologies in order to obtain pictures of the tooth surface that are further analyzed for the number and/or area of the open tubuli.

The implementation of SEM techniques requires from skilled technician the ability to distinguish the open tubuli from the closed one. Further, the detected tubules are counted and its contours are determined in order to measure the area of open tubules. The manual method becomes strongly operator dependent and time consuming (110) (114) (109) (105) (108) (115) A step forward was made when computerized systems for the image analysis were developed. Most of them implemented software such as MATLAB, OPTIMAS, IMAGIC-5, LUCIA (82) in order to analyze SEM images. However, those methods also implemented the technician judgment as the basic step in the data analysis. So far, these types of tools were tested only on the clean, demineralized or etched dentinal surface.

At this point, it is important to highlight that implementation of the SEM microscope requires the vacuum conditions that can negatively affect teeth samples. High vacuum creates cracks and fissures on the surface of teeth sample that can make the observation of the specimen impossible.

On the other hand, the AFM (Atomic Force Microscopy) microscope methodology does not require the vacuum conditions. Such fact, allows eliminating the problem of the negative influence of the fast elimination of water on experimental samples. Although, this method requires a flat sample to properly observe the teeth surface what makes the study of the treated sample more difficult due to the presence of the impurities on the surface of the specimen. Moreover, the interpretation of the image, especially the tubuli orifice, is more challenging comparing to SEM images, where a skilled technician can easily classify the content of the tubuli.

In this section, a robust, universal and automatic methodology for the determination of dental products obliteration capacity is being presented. Such methodology is based on the dentin disc model (107) (106) (111) where specimens treated with remineralising/desensitizing agent are observed under Scanning Electron Microscope and the resulting images are analyzed by the automatic segmentation algorithm developed in order to calculate the number and area of the open tubuli.

Experimental section

13. Methodology

13.1. Specimen preparation

Bovine teeth were extracted and carefully selected in order to obtain specimens lacking any defects like cementoenamel defects that could possibly affect results of the study. After the extraction, specimens were stored in the 0,05% Chloramine-T solution that besides its antibacterial properties also prevents the precipitation of ions.

Subsequently, the teeth were immobilized in a Triplex Cold ® polymer and perpendicularly cut in order to obtain discs of 5 to 10 mm thickness. Each tooth was cut into two discs of equal thickness and the resulting surface was subsequently subjected into further treatment.

In case of the comparative study of 3 different commercial toothpastes discs contained 5 different specimens and each one was implemented for only one corresponding tooth paste application (Figure 24).

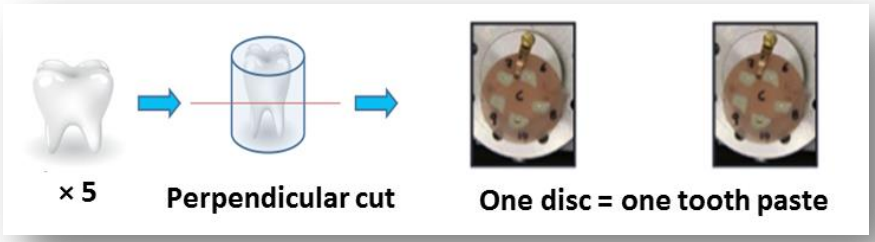

Figure 24. Preparation of specimens: 5 teeth were immobilized in the polymer, subsequently teeth were cut perpendicularly. Resulting discs contained 5 specimens that were further demineralized. On one disc only one, corresponding toothpaste was applied in order to evaluate its performance.

13.2. Treatment performance

Demineralization of the teeth, in order to create cariogenic-like lesion, was performed by its submersion in the demineralizing solution (0,1 M lactic acid/0,2% polyacrylic acid/50% saturated hydroxyapatite solution at pH 5) for 72 hours. Described process is carried out as a preliminary treatment of the dental surface in order to activate it and accelerate the process of remineralization/demineralization (157) (158).

Daily cyclical applications of the demineralization solution were performed during 5 days. Treatments with the tooth paste/artificial saliva and demineralizing solution were alternatively applied. Tooth paste was applied in 1 minutes periods with an electric tootbrush (Vitality Oral-B®) of a controlled velocity of oscillations (7600 osc/min). The replecement tooth brush heads were always used with only one tooth paste in order to

avoid cross-contaminations. The demineralizing solution was used in 3 hours periods. The process was originally designed by Ten Cate and Duijsters. It simulates tooth brushing exposure,the subsequent remineralisation through the generated pellicle and daily acid challenges from the bacterial plaque. The process was designed in order to simulate real changes in the mouth cavity (159). Below, the employed treatment is ilustrated in Figure 25.

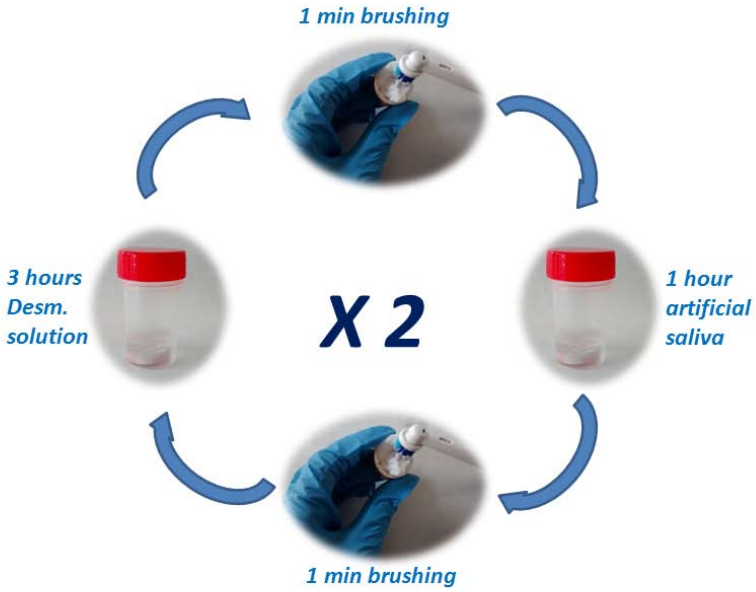

Figure 25. Scheme of a daily treatment in the durability study. On the discs with immobilized specimens corresponding toothpastes were applied, specimens were brushed carefully with electric toothbrush during one minute. Afterwards discs were submerged in the solution of the artificial saliva for 1 hour. Subsequently another application was performed but this time it was followed with the submersion in the demineralizing solution for 3 hours. The above described cycle was repeated. Specimens were stored overnight at room temperature in the solution of artificial saliva.

Evaluated toothpastes that were stored under controlled humidity environment and room temperature were previously dissolved in 3 drops of artificial saliva and applied on the surface of the specimens. Dilution was performed right before each application of the toothpaste. Specimens were stored in artificial saliva between daily treatments. During the weekend, they were stored in the refrigerator under a relative humidity of 100%, also in artificial saliva.

13.3. Control group

Since the goal of the present study is to detect changes in the teeth surface at various stages of the experiment and taking into consideration the big variance in the homogeneity between different teeth, pictures acquired after the demineralisation process were considered as a control group (160).

13.4. Evaluated toothpastes

Tooth pastes implemented in the study are Sensitive Pro-Relief™ *Colgate®* with the Pro-Argin Technology, Repair and Protect™ *Sensodyne®* with NovaMin® Technology and Desensin™ *Dentaid®* with nanoparticles of hydroxyapatite (Table 7).

Table 7. Comparison of three studied commercial toothpastes with different approaches to enhance the tubuli obliteration

Tooth paste	***Obliterating component***	***Obliteration enhancement***	***Reference***
Sensitive Pro-Relief™ Colgate® *(Pro-Argin Technology)*	*arginine-calcium carbonate (Arg-CaCO3)*	Positively charged arginine is attracted to dentine surface together with $CaCO_3$. It adheres to fiber networks and deeply infiltrate into dentinal surface. In this manner, the compound agglomerate generates an alkaline environment that allows the phosphate and calcium ions to precipitate and seal dentinal tubuli.	*(58) (59) (60) (61) (62) (161)*
Repair and Protect™ Sensodyne® (with NovaMin®)	*bioactive glass – calcium sodium phosphosilicate (NovaMin®)*	The mechanism starts with the exchanges of Na^+ by H^+ or H_3O^+ at the same time that Ca^{2+} and PO_4^{3-} are released. As a pH increases and induces the precipitation of ions and formation of hydroxyapatite crystals. At the end, a homogeneous layer that covers dentine surfaces and blocks dentinal tubuli.	*(56) (153) (161)*
Desensin™ Dentaid®(with nanoparticles of hydroxyapatite)	*n-HAP (nano-hydroxyapatite)*	The action of nanoparticles is the deposition on the dentin surface in such a way that it seals the exposed dentinal tubuli forming a wash-resistant protective layer helping to decrease the dentin sensitivity.	*(63) (64) (65)*

13.5. Scanning Electron Microscope (SEM) observations

SEM analyses were performed on MERLIN FE-SEM, ZEISS with the detector EDS Oxford LINCA X-Max and EBSD analisys Oxford Nordlys II, resolution of 0,8nm at 15kV and 1,4nm at 1kV, the current of the probe from 4pA to 100nA and voltage of the acceleration form 0,2 to 30 kV.

As a first preparation step before the observation, specimens were carefully brushed with artificial saliva with a toothbrush in order to eliminate any spare material that could possibly prevent the observation of the surface under SEM.

Described procedure of the preparation of specimens was previously studied and optimized in order to minimalize the deterioration of the sample that results in the creation of fissures on the dental surface. Those fissures can be provoked by the constant changes in the humidity of the sample, as a result of the experimental procedure, which includes immersion of samples 3 times into the vacuum conditions. The creation of fissures destroys the sample and invalidates it from the study. Employment of the discs of thickness below 5-10 mm leads to even stronger degradation of the specimen and makes the observation of the obliteration impossible. To avoid such threats 5-10 mm thickness discs were prepared for this study.

Moreover, a sequence of the vacuum drying process before SEM observation was developed in order to avoid the destruction of the specimens. Before each observation, firstly, all specimens were held for 4 min in a vacuum pump of 101 mbar, subsequently they were transferred into the preliminary vacuum chamber until reaching approx. $8 \cdot 10^{-3}$ mbar in order to introduce the samples into the main chamber of approximately $4\ 10^{-4}$ mbar. Through this process, drying is performed in 3 steps what allows diminishing the creation of cracks and fissures on the surface of the specimens.

Samples were visualized by SEM with minimal handling of the specimens, after assuring that the surface of the specimen has not overcame any procedure that could intervene in the result. Samples were introduced into the microscope without previous metallization, under a controlled humidity and at room temperature. Determinations by SEM were performed two times: After the demineralization process and after 5 days of the remineralising treatment.

Images were always acquired at the same conditions: focal distance 3,5-5 mm and voltage of 1kV.

13.5.1. Analysis of the entire surface of the teeth

In order to acquire the entire surface of the teeth, an automatic routine was developed and implemented. Once the adequate parameters (focal distance 3,5-5 mm and voltage of 1kV) were adjusted, the length and the width of the resulting image was measured (for magnification 3000: 100µm x 67,4 µm). Subsequently those parameters were introduced into the SEM software in order to move the sample holder always in the same dimensions (100µm in longitudinal movements and 67,4 µm in vertical). In such a way, the entire surface of the teeth could be recorded and furtherly analyzed.

13.6. Image analysis

The automatic segmentation of the cavities is carried out as follows. For normalization purposes, the input image is normalized between 0 and 255 in grayscale values. We will refer to this normalized image as I(x). To avoid biasing the results, the regions of the images containing text information in black frames were automatically excluded, and saturated image values are shifted to values corresponding to the closest image minimum, prior to the normalization. In the following step, the noise of the image was partially filtered by using a Gaussian kernel of 8 pixels size. Then, an automatic threshold (R) is computationally obtained to separate the holes from the rest of the image points, such as the points belonging to holes can be expressed as:

$$H = \{x \backslash in\ I(x) \mid I(x) < R\} \quad \text{(Eq.6)}$$

The threshold value R, is obtained from first order statistics of the images. This is justified observing that the histogram of the images present similar shapes, which differ in their mean, m(I), and standard deviation, std(I), values. Assuming a linear dependence of the threshold R with these values:

$$R = a^* \text{std}(I) + b^* m(I) + c, \quad \text{(Eq.7)}$$

the optimal values of the parameters a, b and c are obtained by using a least squares analysis from a set of training set images where the threshold R was manually set by expert observers. The optimal values found were: a = 0.75, b = - 0.75 and c = 15.
The obtained segmentation was afterwards processed to avoid false detections. First, a cleaning step was performed (removing isolated pixels), and then, the holes that occupy areas below a minimum and above a maximum pre-defined size were removed (if existing). In our images the holes are normally bigger than 20 pixels and smaller than 5*10^3 pixels, any hole below and above that range were eliminated to avoid including it in the final result. Since holes touching the image borders change their shape, what most of the times result in the false detection, were also removed. Finally, the contours obtained are smoothed by morphological operations. As a result, the percentage of points occupied by the holes as well as their total size were computed.

13.7. Statistical and Data Analysis

Xlstat (Addinsoft, New York, USA), SigmaPlot 13 (Systat, San Jose, USA), Ene 3.0 (GlaxoSmithKline, Brentford, Great Britain) software were employed for data analysis purposes. Outliers were determined applying Grubbs Test within a confidence interval of 95%. In order to evaluate difference in the variance of various sample groups the ANOVA test was implemented. The differences between the series of results of various

categories were compared using t- Test along with Tukey's Test (HSD) and Dunet's test within a confidence interval of 95%.

14. Results and Discussion

14.1. Determination of the magnification properties of the image

In order to evaluate the adequate parameters of the pictures acquired in the entire study the optimization of the magnification was performed (82). Three magnifications were considered: 1000, 3000 and 5000. 10 points of interest were recorded applying the same parameters (focal distance 3,8 mm and voltage of 1kV, constant contrast and brightness) where only the magnification was changed. The study was performed with samples after the demineralization process.

The resulting images were analyzed with the developed routine, further images were analyzed by the skilled SEM technician and the errors committed by the software were corrected. The resulting number and the percentage of the picture occupied by the open tubules before and after the intervention of the technician were compared.

Images performed at the magnification 1000 were discarded due to the poor resolution capabilities. Since the surface of the teeth is not completely flat and can get bent by the vacuum conditions, the resulting SEM image may consist of some parts of the picture that are well focused whereas other parts stay out of focus. That phenomenon makes the unfocused parts inadequate for the software application. Even for the skilled technician, it is extremely difficult to decide whether the observed tubules are open or closed (Figure 26).

The error analysis revealed significantly better performance for a 3000x magnification (0,62% for the number of detected tubules; 2,93 % for the area occupied by open tubules) than in case of a 5000x magnification (4,56% for the number of detected tubules; 5,12 % for the area occupied by open tubules). With higher magnification the detected area of tubuli is bigger and the possible error is consequently higher. Furthermore, taking into consideration that analysis performed at the smaller magnification requires less time than bigger magnification it was decided to proceed with the rest of the experiment applying a 3000x magnification.

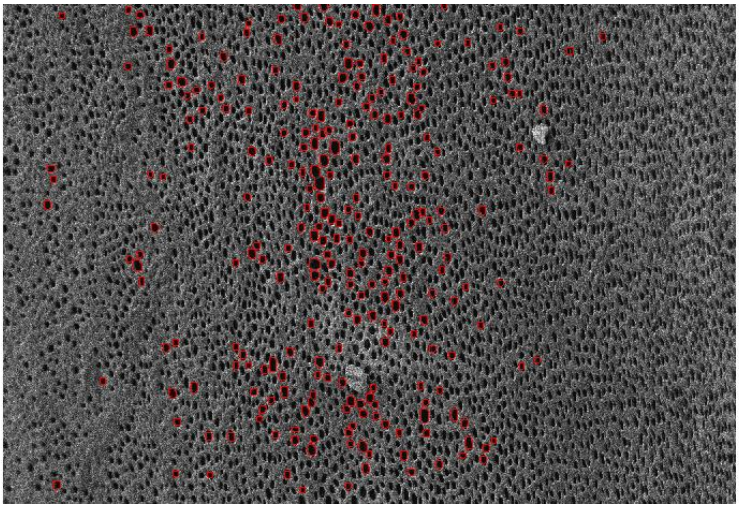

Figure 26. Example of a picture analyzed by the software at 1000x magnification. Some tubules were not detected because of the surface characteristics.

14.2. Analysis of the entire surface of the teeth

14.2.1. Determination of the zone of interest

A perpendicularly cut teeth represents a surface that is not homogenous. It could be observed that there is a big difference in the number, distribution and shape of the dental tubule depending on the zone of the teeth from which it proceeds. In order to characterise those tendencies of the dentine, images from the entire surface of the teeth from 3 different specimens after the demineralisation process, where carefully analyzed. The surface of the teeth was divided into two zones: zone 1 that is located in the center of the teeth and is composed of two parts that are surrounding the pulp chamber and zone 2 that is located on the opposite sides of zone 1 (Figure 27). Further, the number of tubules, the number of pictures with tubules presenting the orifice cut perpendicularly, the area occupied by the tubules (mm^2) and the percentage of pictures with orifice cut longitudinally and the shape of the tubules in 2 zones were studied (Table 8).

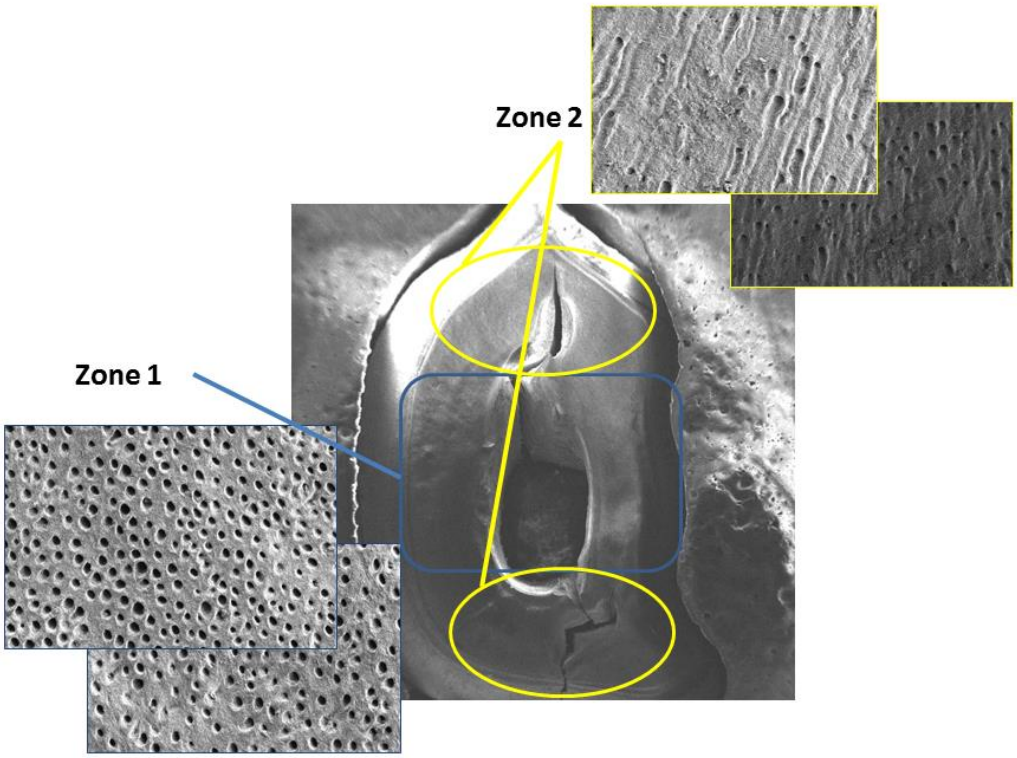

Figure 27. Two different zones that can be distinguished in a perpendicularly cut surface of a teeth: zone 1 – where tubules are cut perpendicularly and zone 2 – longitudinal.

Table 8. Characteristics of zone 1 and 2 as a result of analyzed teeth.

Characteristics	Zone	Tooth 1	Tooth 2	Tooth 3
Av. number of tubules	1	172	83	188
	2	100	47	157
Av. area occupied by tubules [%]	1	7,01	3,64	8,00
	2	3,67	1,66	6,24
Surface occupied by tubules [mm^2]	1	0,3441	0,1084	0,2873
	2	0,0607	0,0075	0,1086
Number of images with tubules cut perpendicularly	1	733	445	536
	2	247	68	260
Number of images with tubules cut longitudinal	1	42	37	31
	2	230	107	252

As a result of the performed experiment, it could be concluded that both, the average number of tubules and the average percentage area of tubules is much higher in zone 1 in case of all of the analyzed teeth (Figure 28). As a result, a surface covered with the open tubules is bigger for the zone 1 comparing to zone 2. Number of photos that contained tubules cut perpendicularly represents the number of images suitable for the study since only a well exposed open and round tubule allows a reliable observation of its further obliteration. In this type of surface, dental tubules can be properly examined and compared when treated with various remineralising products. Since the obliteration

is easy to observe, the number of tubules or its obliteration degree can be examined and detected by the developed software. Again, for the zone 1, this number is much higher than for the zone 2. On the other hand, the number of images with the tubules cut longitudinally, rises for the zone 2 in all of the cases. This type of tubule's cut invalids the picture from the study since it makes the observation of the inside of the tubule impossible for the technician and what is more, the tubule cannot be detected properly by the software.

To define such issues, the Test ANOVA within a confidence interval of 95% showed that there are significant statistical differences between the zone 1 and 2 in case of all of the studied teeth (*Supplemental Material 1*).

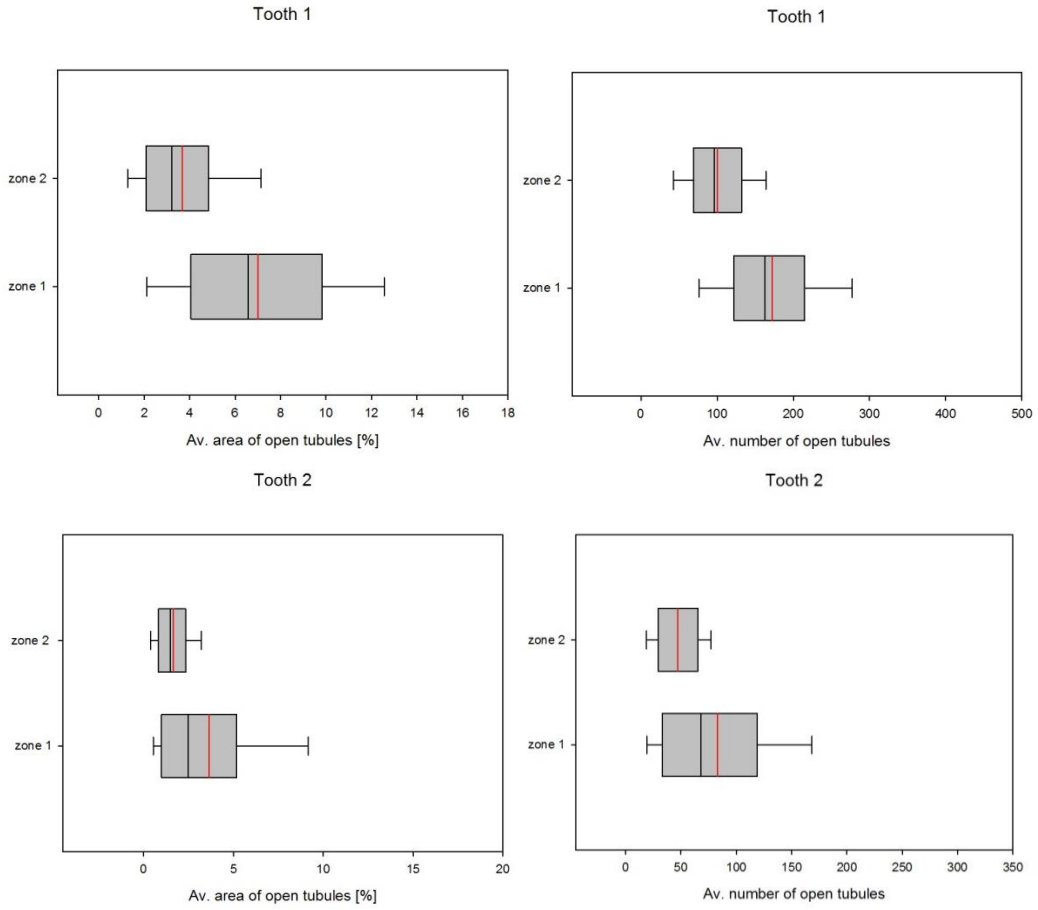

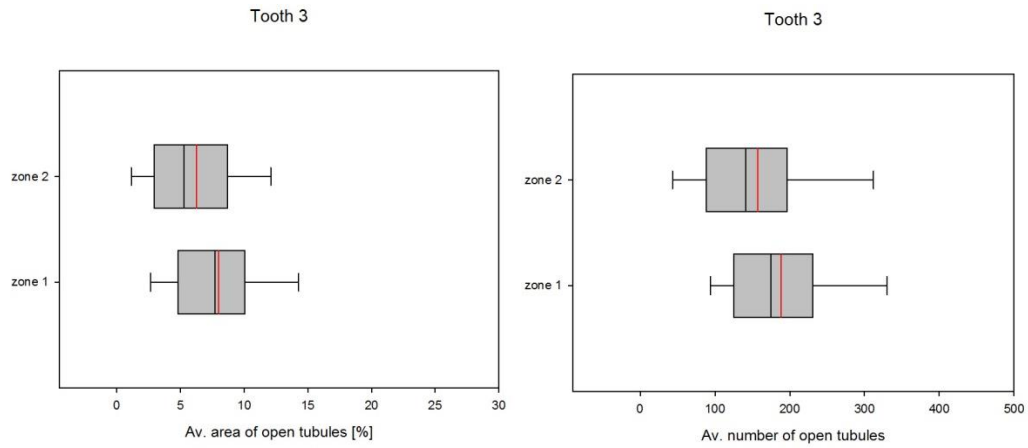

Figure 28. The statistical characteristics of all of the studied populations of three specimens. In black the median, in red average values were marked. Whiskers show the highest and the lowest values. Outliers were excluded from the presented sample distributions.

Having in mind the described phenomena, it is advisable to always work in the zone 1, when the teeth is cut perpendicularly. Such zone allows the proper observation of the tubules and potential changes provoked by various treatments. Therefore, only pictures acquired in that zone of the specimens were further considered and analyzed.

14.3. Error determination

14.3.1. Sensitivity of the automatic segmentation algorithm under different illumination conditions

To verify the applicability of the automatic segmentation algorithm under different illumination conditions, a numerical experiment in digitally simulated images was performed. These images were created starting from the reference simulation shown in Figure 29A, that represents a typical distribution of the holes in a SEM image, as the ones analyzed here, and will constitute the reference in this experiment.

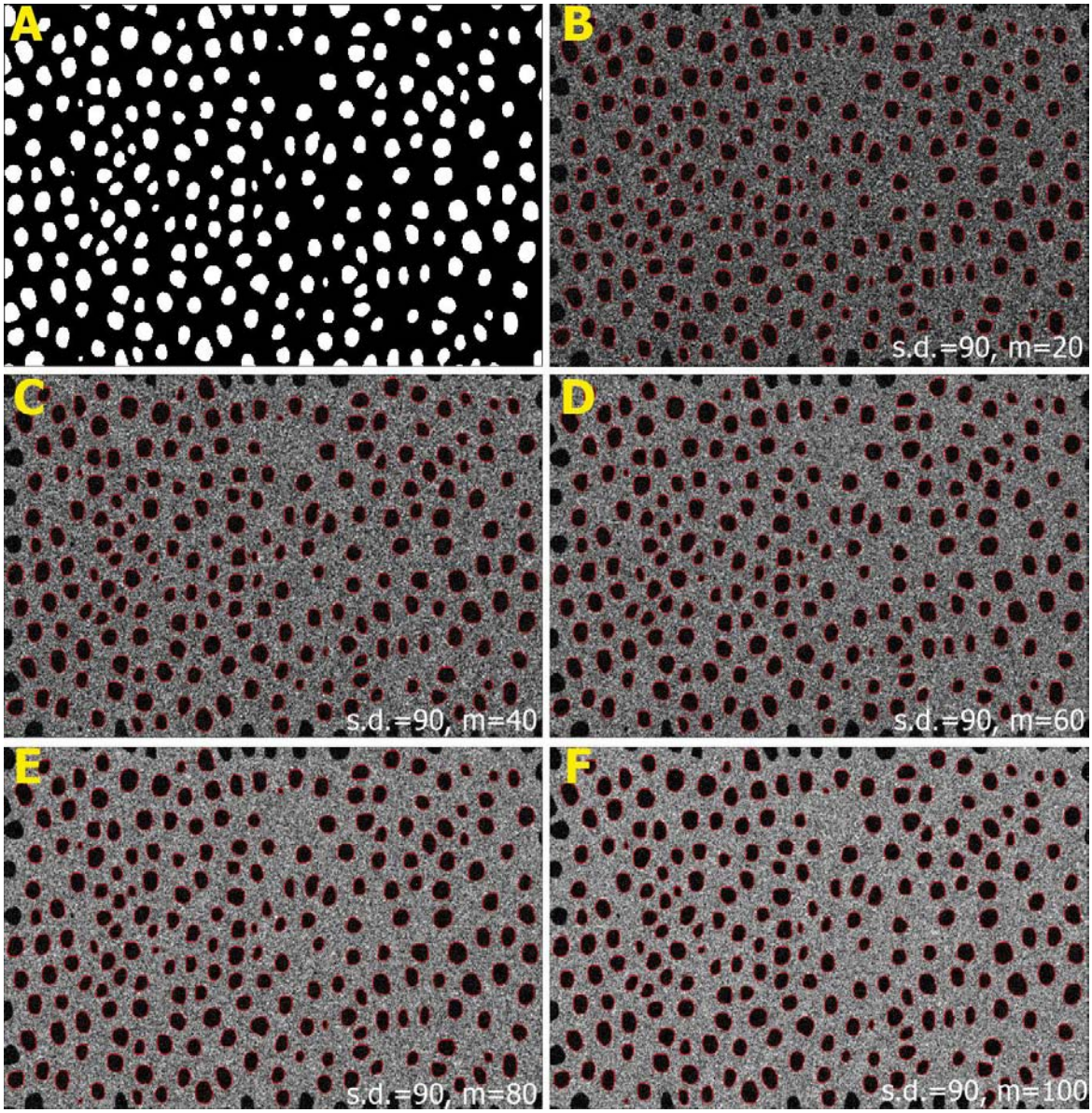

Figure 29. The segmentation results for the digitally generated images. A: reference, B-F digitally generated images varying the illuminations with Gaussian distributed grayscale ranges with standard deviation = 90 and means from 20-100.

In total, there are 237 holes with a total occupied surface of 22.31 %. From this reference image, we generated a total of 11x9 digitally simulated images representations, mimicking the characteristics of the images obtained in the SEM. To this end, the image values of the holes were generated using a Gaussian distribution centered at zero with a small standard deviation of 4 (in a normalized gray scale of 0 - 255). For the gray values of the rest of the image, a Gaussian distribution was also used but using 11 different standard deviations (from 50 to 150) and 9 different means (from 20 to 100) to account for a wide range of illuminations. The values of the standard deviation and the means used also correspond to the normalized grayscale range 0 - 255. Finally, Gaussian noise was introduced to obtain more realistic image results. A set of generated images can be seen in Figure 29 B-F.

The 99 generated images were then processed with the automatic segmentation algorithm, obtaining in average, a value of area occupied of 20.80 % (+/- 0.16 %) and number of holes detected of 201.9 (+/- 0.54). The values of area occupied and number of detected holes obtained for all the images are shown in Figure 30A and B respectively and the threshold values obtained by the algorithm are shown in Figure 30C. The segmentation results are overlaid in red for several image images the Figure 29Figure 29 B-F.

The differences obtained are clearly defined due to the detection of holes in the border of the image. The results obtained were very consistent all along the processed images as shown by the values presented in Figure 30 and the segmentations in Figure 29, and the low standard deviations obtained for the occupied area (0.16 %) and number of holes detected (0.54).

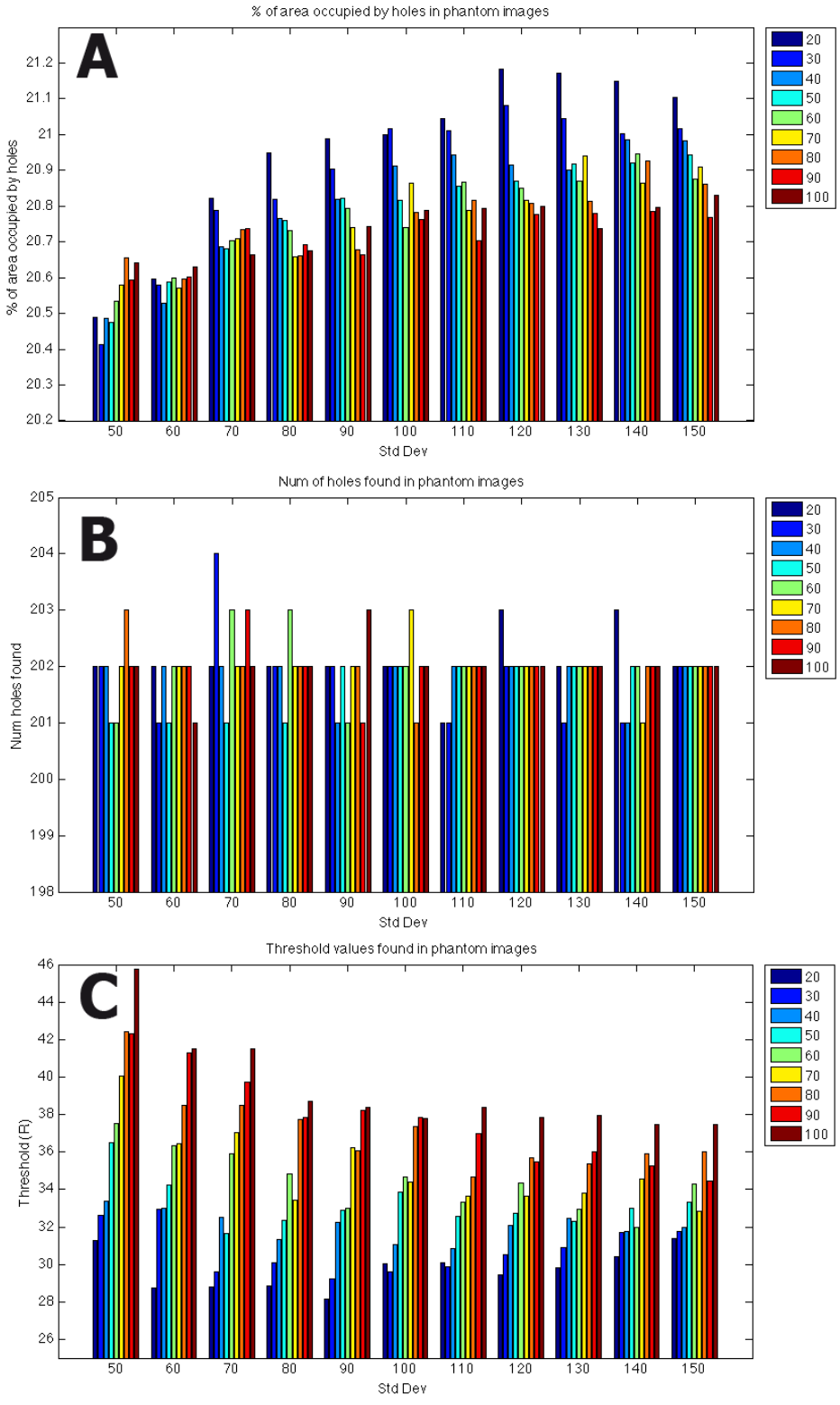

Figure 30. A: Values of area occupied B: number of detected holes C: threshold values obtained for all the generated images. The standard deviation. and mean values characteristic of the different illuminations of the generated images are represented in the horizontal axis (50 - 150) and as colors (20-100) respectively.

14.4. Study of the experimental error of the method and the dependence from the operator

In order to evaluate the error of the method and to study the dependence from the operator, 120 images were randomly chosen from zone 1 of 3 different specimens before and after the treatment. The images were analyzed by 3 skilled SEM technicians. Thereafter, the 120 images were loaded into the developed software routine. The resulting percentage area and the number of open tubules were calculated by the software. The determination performed by Matlab was controlled by 3 technicians separately in order to manually correct the errors committed by the software. Further, the automatically computed data was compared with the semi-automatic results. In the second type of the analysis, open tubuli was first detected by the automatic segmentation algorithm and the result was subsequently supervised by the skilled SEM technician. All possible errors made by the software were corrected. The resulting percentage errors were calculated:

$$E = \left(\frac{|X - X_{Corr}|}{X_{Corr}}\right) \times 100\% \quad \text{(Eq.8)}$$

X- number or percentage area occupied by the open tubules calculated by the software- the automatically computed analysis

X_{Corr}- number or percentage area occupied by the open tubules calculated with the intervention of the technician – the semi- automatic analysis

14.4.1. Experimental error of the method

The automatically computed analysis showed an average number of 165,55 and 11,18% of the surface area occupied by the open tubules after the demineralization process. Whereas the semi- automatic analysis varied in 0,35 % of the average value from the computed one, when the number of open tubules was concerned and 1,13 % for the area occupied by the tubules that were not occluded (Table 9, Table 10, Table 11). The difference in the number of tubules and percentage area of open tubules in the confidence interval 95% was not significant for neither of the technicians (*Supplemental Material 2*).

The comparison of two types of analysis after the remineralizing treatment revealed an average number of open tubules of 75,55 and percentage area of 2,56 % for the automatically computed analysis. The resulting average values of the semi- automatic analysis varied from the automatically computed in 1,62 % (number of open tubules) and 3,71 % (area of open tubules) (Table 9,Table 10,Table 11). The analysis of the entire set of data showed no statistical differences in the confidence interval 95% for neither of the technicians (*Supplemental Material 2*).

In general, the analysis performed without the intervention of the technician, counted slightly higher number as well as the percentage area of open tubules. Almost all of the

deficiencies were located in the experimental areas were some impurities, like small particles proceeding from the rest of the dentine or from the applied treatment, could be detected (Figure 31).

a)

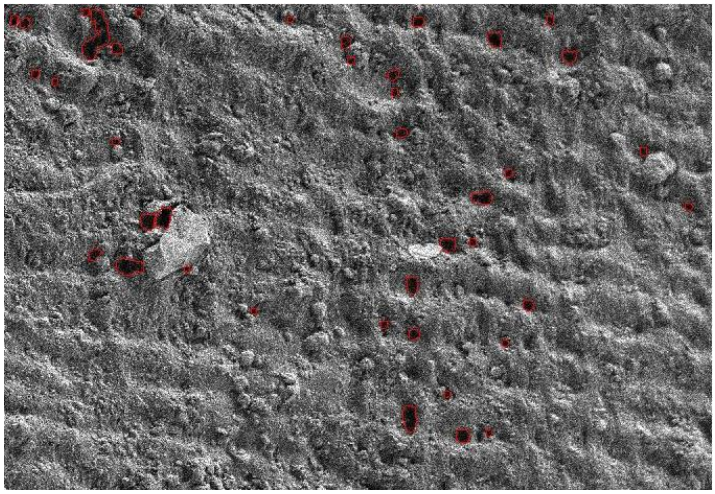

b)

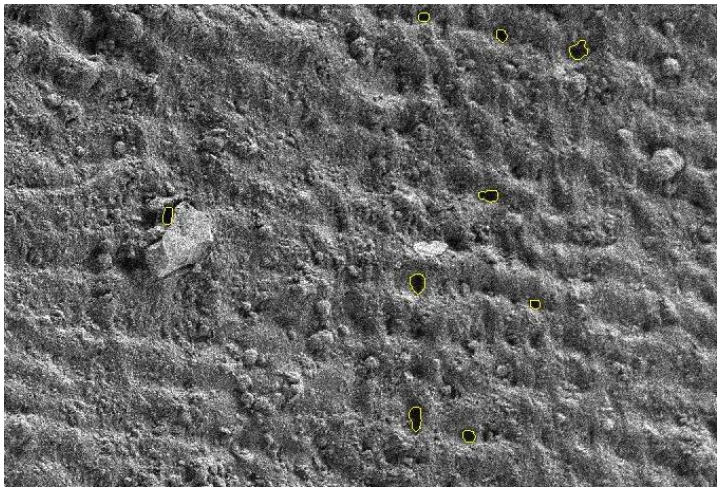

Figure 31. a) Example of a picture with small impurities what results in a wrong detection of the tubules by the software b) the same picture corrected by the operator

The average error calculated for one sample for the number of tubules and area before the remineralising treatment was of 0,01% and 0,02 % respectively. Whereas after the treatment the error were of 0,03% and 0,06% (Table 11).

Table 9. Comparison of the automatically computed and semi-automatic analysis when the number of open tubules is concerned

	Av.nr of open tubules detected after the demineralisation					
	Technician 1	Technician 2	Technician 3	St dev	Average	Average error [%]
	165,55	165,55	165,55		165,55	
X corr	165,08	165,07	164,75	0,2	164,97	0,35
	Av.nr of open tubules detected after the remineralisation					
X	75,55	75,55	75,55		75,55	
X corr	74,92	74,85	73,27	0,9	74,34	1,62

Table 10 Comparison of the automatically computed and semi-automatic analysis when the percentage of the area of open tubules is concerned

	Av.area of open tubules detected after the demineralization [%]					
	Technician 1	Technician 2	Technician 3	St dev	Average	Average error [%]
X	11,18	11,18	11,18		11,18	
X corr	11,07	11,10	11,00	0,1	11,06	1,13
	Av.area of open tubules detected after the remineralisation[%]					
X	2,56	2,56	2,56		2,56	
X corr	2,52	2,51	2,38	0,1	2,47	3,71

Table 11.Percentage errors of the software after the demineralisation and the remineralizing treatment calculated by 3 independent skilled SEM technicians.

	Error after the demineralisation [%]				
	Technician 1	Technician 2	Technician 3	Average	Av. Error/sample
number of tubules	0,28	0,29	0,49	0,35	0,01
Area [%]	1,00	0,74	1,64	1,13	0,02
	Error after the remineralizing treatment[%]				
number of tubules	0,85	0,94	3,12	1,63	0,03
Area [%]	1,56	2,00	7,78	3,78	0,06

14.5. Dependence from the operator

Statistical analysis performed on the data obtained from the semi-automatic analysis proceeding from 3 different technicians showed no significant statistical differences between the groups within the confidence interval of 95% (*Supplemental Material 2*).
Overall, the standard deviations were very small in all considered cases (Table 9, Table 10). For the number of tubules calculated after the demineralization, the difference was of 0,2 and after the remineralising treatment of 0,9. Whereas for the percentage area of open the resulting standard deviations were of 0,1 in both cases.
Analyzed data had the same characteristics for all three technicians (*Supplemental material 3*). The unique differences that could be encountered concern leptokurtic kurtosis results of the area of open tubules after the demineralization treatment for the

technician 3. In general, all data showed positive asymmetry. The visual description of the data is shown in Figure 32.

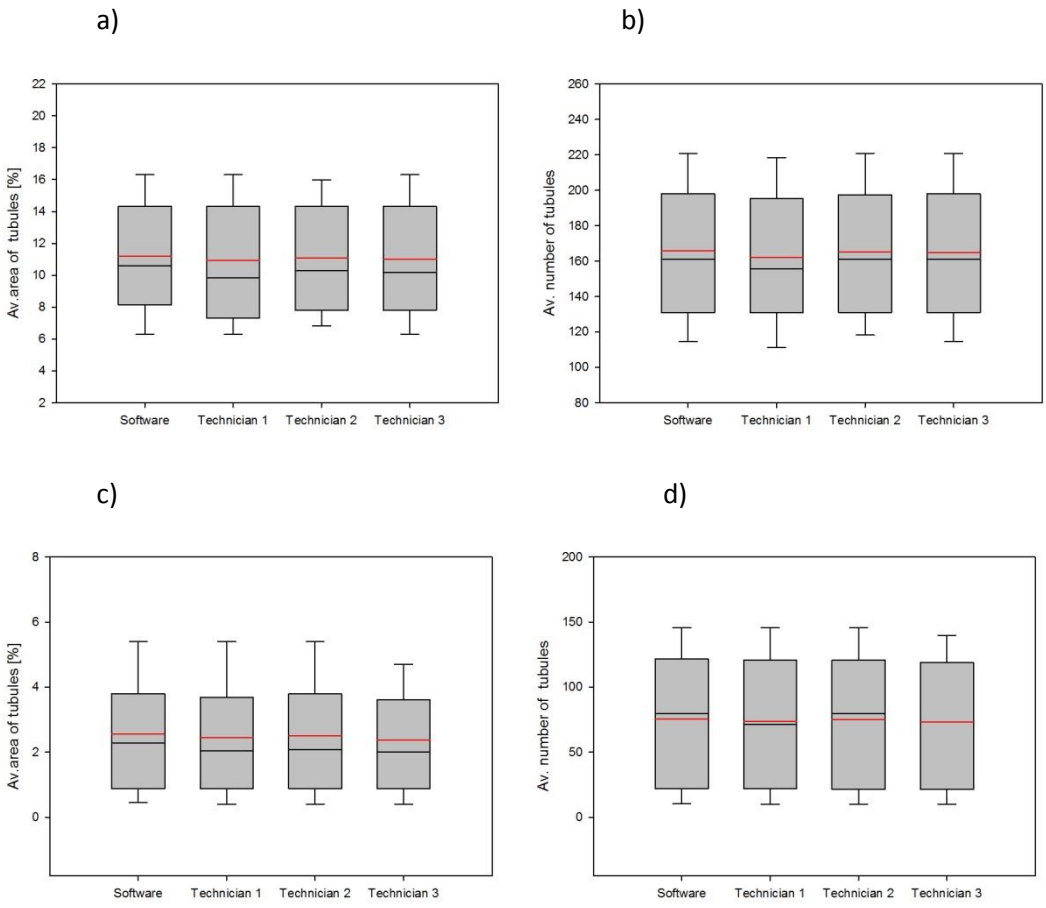

Figure 32. Resulting representation of the analysed data a) area of open tubules after the demineralising treatment b) number of open tubules after the demineralising treatment c) area of open tubules after the remineralising treatment d) number of open tubules after the remineralising treatment. In black the median, in red average values were marked. Whiskers show the highest and the lowest values. Outliers were excluded from the presented sample distributions.

14.6. Influence of the focus adjustment

To evaluate the influence of the focus adjustment on the software performance, 9 images of the same experimental point of the sample were acquired. All conditions (Mag: 3000, Volt:1kV, contrast and brightness) beside the focus were constant. Small adjustments in the focus adjustment were performed. Since the adjustments were not changing the focal distance, the detected changes were only visual, this is why, unfortunately, none numerical value could be assigned to those adjustments.

Subsequently images were analyzed by the developed software and the resulting number and the percentage of the image occupied by the tubule cavities were compared.

The standard deviation of the number of detected tubuli was of 7,35 and the surface of only 0,86. The result would suggest that changes in the focus influence more the number of the detected tubules than the detected area. Besides, out of focus images

involve a smaller number of open tubuli. The obtained results would suggest that some of the cavities are not interpreted as open. Although it applies only to smaller cavities, since the standard deviation of the percentage of the area occupied by the open tubules is very low and the area of the better defined tubules stays unchanged.

14.7. Influence of the vacuum conditions on the measurements performance

In order to check the influence of the experimental conditions on the samples, a study of the influence of the vacuum on the performed measurements was implemented in the study. Three teeth samples were demineralised and further under came the usual gradual vacuum drying (explained in point 13.5). One experimental point from the zone 1 of the teeth was measured every 10 minutes, during 1 hour and 50 minutes (the approximate working time necessary to acquire a total area of the zone 1 of a tooth) for all three samples. During the experiment the voltage, contrast and brightness values stayed fixed for all of the samples. The chosen area of the picture was compared for all resulting images of the experimental point. The percentage area occupied by the open tubules was analyzed and compared for all three samples (Figure 33).

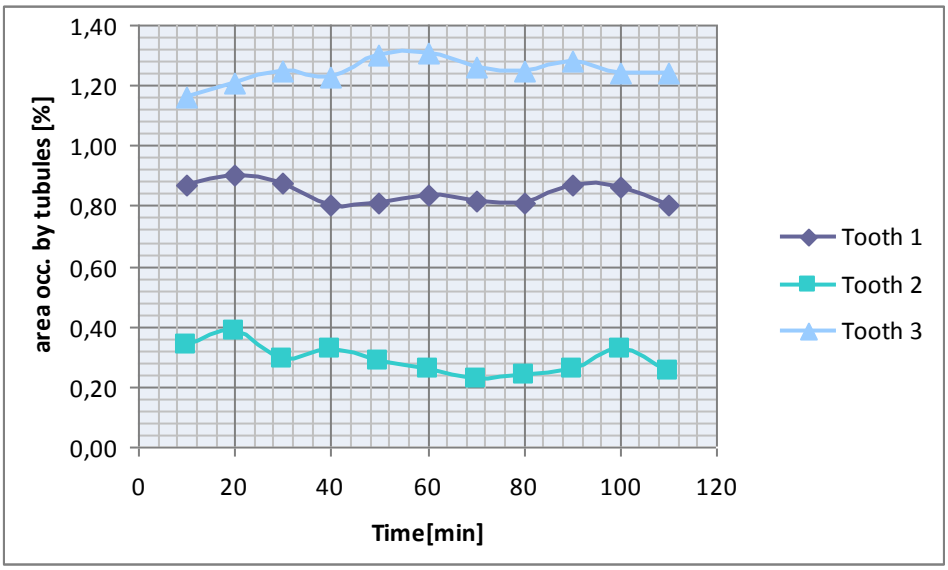

Figure 33. Influence of the vacuum conditions on the performed measurements. Comparison of the percentage area occupied by open tubules measured for the same experimental point during 1 hour and 50 min for 3 different samples.

As it could be observed from the resulting data, the percentage area was constant (SD = 0.04 -0.05). Since the area measured by the software did not change during the experimental time, it could be concluded that the vacuum conditions do not have an important influence on the presented result. The observed slight differences between the results for the same experimental point could proceed from the small differences in the focus adjustment, what has been considered and included in the error of the software (14.3.1).

However, the performed experiment represents only the influence of the vacuum conditions that could be measured from the moment the sample is introduced into the SEM chamber. In general, it could be observed that all samples were affected by the vacuum conditions. It can be confirmed by the shape of the cavities that samples become more elliptical when introduced into the chamber. There are also some parts of the tooth that are squeezed together as a result of the vacuum performance. These phenomena can be observed especially well for the samples after the remineralising treatment application (since they are submerged twice into the vacuum). In such case, sometimes, entire zones of the teeth are distracted. This kind of problem eliminates the specimen from the study and force the operator to repeat the experiment. Unfortunately, described phenomena cannot be measured since no data about the previous state of the sample can be obtained.

14.8. Sample size determination

In order to evaluate the number of pictures representative for the teeth at each stage of the treatment, the sample size have been calculated with the Ene 3.0 software within the confidence interval of 95% and 1% of error. Analyzed pictures represent the percentage area of open tubules proceeding from the zones 1 of the three different teeth. Results for all of the analyzed samples are presented in the Table 12.

Table 12. Sample size determination after the demineralisation and remineralisation process.

Area of open tubules detected after the demineralisation			
	Teeth nr 1	Teeth nr 2	Teeth nr 3
number of images	300	412	350
error	1%	1%	1%
st.dev	4,51	6,17	1,58
sample size	62	108	10
Area of open tubules detected after the remineralisation			
number of images	80	131	135
error	1%	1%	1%
st.dev	1,53	2,46	0,84
sample size	9	20	3

As a result, in order to cover the entire variability of the calculated area occupied by the open tubules, the highest encountered sample size should be taken into consideration. Therefore, to represent the area occupied by open tubules, approximately 110 pictures should be taken after the demineralisation treatment, while 20 should be employed for the samples previously treated with the remineralising paste.

14.9. Comparison of the obliterating capacity of three tooth pastes after 3 days of treatment

After the demineralization process 15 specimens under came a treatment with three studied tooth pastes during 3 days consecutively, following the protocol described in point 13.2. Subsequently samples were observed in SEM and 110 pictures of each specimen were analyzed by the developed Matlab routine (13.6). Results for all specimens treated with its' respective tooth pastes are presented in Table 13, Table 14 and Table 15.

Table 13. Results obtained for specimens treated with Sensitive Pro-Relief™ Colgate® for 3 days consecutively.

	Sensitive Pro-Relief™				
	Tooth 1	Tooth 2	Tooth 3	Tooth 4	Tooth 5
Av % of tubuli before	16,3	20,8	11,0	21,6	18,2
Av % of tubuli after	4,6	5,8	3,8	5,0	5,6
Av % of obliterated area	71,8	71,9	65,8	77,0	69,3
Av. nr of tubules before	149,0	141,7	115,2	135,5	165,6
Av. nr of tubules after	105,9	138,9	85,6	83,4	133,2
Av nr of obliterated tubuli	28,9	2,0	25,6	38,4	19,6
Total area before [μm^2]	121150,6	154936,2	81729,6	160992,4	133787,9
Total area after [μm^2]	34157,3	43322,6	27936,8	37058,1	41114,2
% of open tubules	28,2	28,0	34,2	23,0	30,7
% of obliteration	71,8	72,0	65,8	77,0	69,3

Table 14. Results obtained for specimens treated with Repair and Protect™ Sensodyne® for 3 days consecutively.

	Repair and Protect™				
	Tooth 1	Tooth 2	Tooth 3	Tooth 4	Tooth 5
Av % of tubuli before	8,4	5,7	24,4	14,7	16,4
Av % of tubuli after	1,9	0,8	4,8	1,1	2,2
Av % of obliterated area	76,8	86,6	80,4	92,5	86,4
Av. nr of tubules before	199,9	106,3	164,9	160,1	160,5
Av. nr of tubules after	61,9	25,7	94,1	35,3	47,7
Av nr of obliterated tubuli	69,0	75,8	42,9	78,0	70,3
Total area before [μm^2]	62447,5	42079,3	181165,9	108654,7	120790,2
Total area after [μm^2]	14472,2	5650,4	35485,7	8168,9	16417,5
% of open tubules	23,2	13,4	19,6	7,5	13,6
% of obliteration	76,8	86,6	80,4	92,5	86,4

Table 15. Results obtained for specimens treated with Desensin™ Dentaid® for 3 days consecutively.

	Desensin™				
	Tooth 1	Tooth 2	Tooth 3	Tooth 4	Tooth 5
Av % of tubuli before	5,0	16,1	9,3	17,7	18,4
Av % of tubuli after	0,7	1,0	0,4	2,0	0,8
Av. nr of tubules before	72,6	162,8	124,4	196,6	214,0
Av. nr of tubules after	18,2	29,7	20,9	77,0	37,5
Av nr of obliterated tubuli	74,9	81,8	83,2	60,8	82,5
Total area before [μm^2]	37406,0	120000,8	69046,9	131544,7	136623,1
Total area after [μm^2]	5227,9	7140,6	2750,6	14586,2	5637,7
% of open tubules	14,0	6,0	4,0	11,1	4,1
% of obliteration	86,0	94,0	96,0	88,9	95,9

As a result of a 3-days treatment, the most effective toothpaste in achieving obliteration occurred to be the n-HAP technology tooth paste (92,2% +/- 4,5) (Table 16). It is followed by NovaMin® (84,5% +/- 6,1) , whereas the worst result was obtained for the Sensitive Pro-Relief™ (71,2% +/- 4,1). In order to calculate the final total obliteration capacity achieved by studied toothpastes the tubuli area from all five specimens of the corresponding treatment were summed in order to obtain the total surface occupied by open tubuli. The same mathematical operation was performed with data obtained after the treatment. As a result, (Figure 34) the best obliterating capacity was obtained for Desensin that reached (92,9%) of obliteration, followed by Repair and Protect (84,4%) and also in this case the last one was Sensitive Pro-Relief (71,9 %). The obliterating capacity was calculated by adding together the surface of all analyzed teeth and comparing the resulting total surfaces before and after the remineralization.

Table 16. The average obliteration capacity derived from 15 analyzed specimens during 3 days treatment.

	Sensitive Pro-Relief™	Repair and Protect™	Desensin™
Av. Percentage of obliteration[%]	71,2	84,5	92,2
Standard deviation	4,1	6,1	4,5

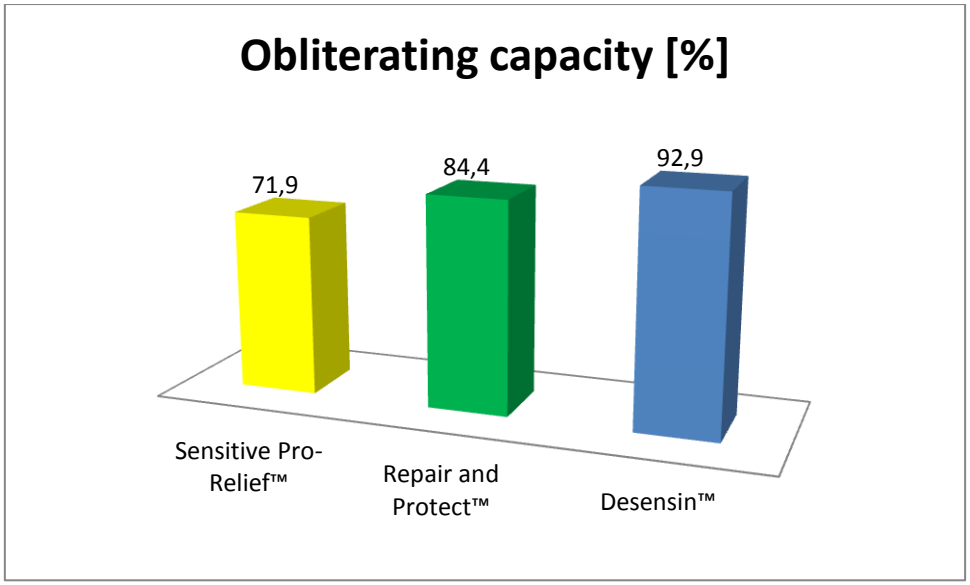

Figure 34. Comparison of the final obliterating capacity for three analyzed toothpastes after 3 days of treatment

14.10. Comparison of the obliterating capacity of three tooth pastes after 5 days of treatment

The same procedure previously described in paragraph 14.9 was repeated on 15 new bovine specimens. Results obtained for the corresponding treatment are shown in Table 17, and Table 19.

Table 17. Results obtained for specimens treated with Sensitive Pro-Relief™ Colgate® for 5 days consecutively.

	Sensitive Pro-Relief™				
	Teeth 1	Teeth 2	Teeth 3	Teeth 4	Teeth 5
Av % of tubuli before	16,4	9,8	11,0	5,1	10,8
Av % of tubuli after	1,2	1,2	0,2	0,3	0,8
Av % of obliterated area	92,6	87,5	98,0	93,2	93,0
Av. nr of tubules before	200,3	142,0	148,9	101,6	141,9
Av. nr of tubules after	37,6	38,3	10,5	16,8	29,7
Av nr of obliterated tubuli	81,2	73,0	93,0	83,4	79,1
Total area before [um]	121095,0	1046875,0	81504,2	37870,0	80431,1
Total area after [um]	8996,8	9035,5	1371,1	2272,4	5392,4
% of open tubules	7,4	0,9	1,7	6,0	6,7
% of obliteration	92,6	99,1	98,3	94,0	93,3

Table 18. Results obtained for specimens treated with Repair and Protect™ Sensodyne® for 5 days consecutively.

	Repair and Protect™				
	Teeth 1	Teeth 2	Teeth 3	Teeth 4	Teeth 5
Av % of tubuli before	12,2	12,8	9,2	11,8	3,6
Av % of tubuli after	4,5	4,8	2,0	3,1	0,9
Av % of obliterated area	63,5	62,3	78,0	73,4	75,6
Av. nr of tubules before	181,3	169,0	161,3	158,5	88,9
Av. nr of tubules after	100,1	101,2	75,7	89,4	32,2
Av nr of obliterated tubuli	44,8	40,1	53,1	43,6	63,8
Total area before [um]	90876,0	94968,1	68437,6	87564,5	26524,1
Total area after [um]	32906,8	35467,7	15037,2	23315,4	6459,6
% of open tubules	36,2	37,3	22,0	26,6	24,4
% of obliteration	63,8	62,7	78,0	73,4	75,6

Table 19. Results obtained for specimens treated with Desensin™ Dentaid® for 5 days consecutively.

	Desensin™				
	Teeth 1	Teeth 2	Teeth 3	Teeth 4	Teeth 5
Av % of tubuli before	17,9	17,5	10,8	9,8	11,2
Av % of tubuli after	1,4	3,4	0,4	0,5	0,7
Av % of obliterated area	92,2	80,6	96,0	94,8	93,3
Av. nr of tubules before	197,1	159,9	199,5	156,5	149,4
Av. nr of tubules after	55,2	94,2	12,9	8,5	9,1
Av nr of obliterated tubuli	72,0	41,1	93,5	94,6	93,9
Total area before [um]	131945,5	128897,8	80434,9	72609,8	82949,4
Total area after [um]	10277,1	24961,0	2119,3	3601,0	5537,6
% of open tubules	7,8	19,4	2,6	5,0	6,7
% of obliteration	92,2	80,6	97,4	95,0	93,3

After 5 – day treatment, the highest average obliteration percentage was achieved by the Sensitive Pro-Relief™ tooth paste (95,5% +/- 3,0) followed by the Desensin™ (93,3% +/- 6,5) (Table 20). The worst average obliteration was calculated for the Repair and Protect™ (70,7% +/- 7,0). When it comes to a final total obliteration 98,0 %, 90,6 % and 69,3 % were calculated for the Colgate®, Dentaid® and Sensodyne® tooth pastes respectively (Figure 35). Comparing the final obliterations after 5- day treatment to the results after 3 days treatment, the NovaMin® (Repair and Protect™) based product reviled a huge drop in the obliterating capacity from 84,4% (3 days) to 69,3% (5 days). Whereas the Sensitive Pro-Relief™ obliteration raised from 71,9% to 98%. When it comes to n-HAP based tooth paste a slight drop was observed (from 92,9 to 90,6%).

Table 20. The average obliteration capacity derived from 15 analyzed specimens during 5 days treatment.

	Sensitive Pro-Relief™	Repair and Protect™	Desensin™
Av. Percentage of obliteration[%]	95,5	70,7	93,3
Standard deviation	3,0	7,0	6,5

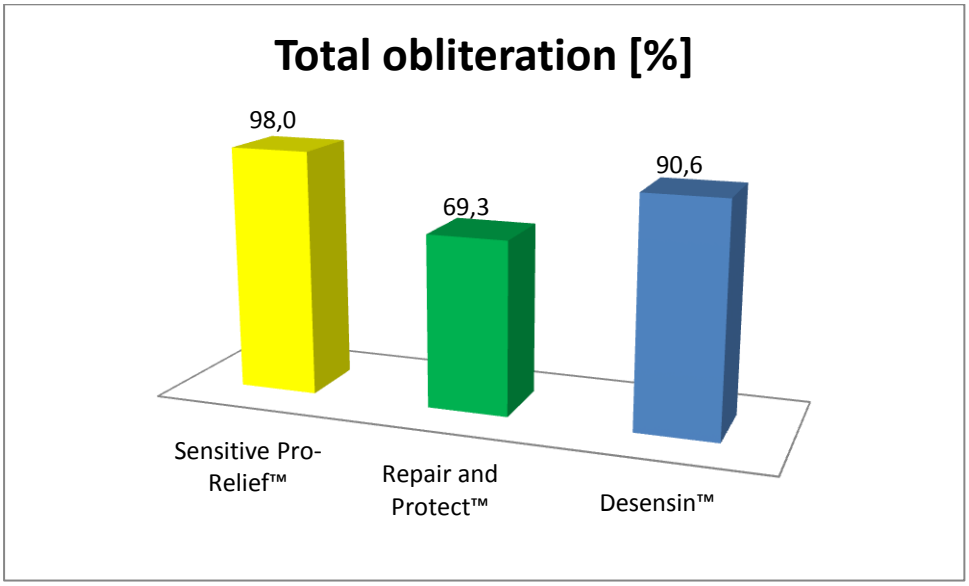

Figure 35. Comparison of the final obliterating capacity for three analyzed toothpastes after 5 days of treatment

14.11. Experimental error of the applied Matlab routine

Results derived from all the analyzed specimens during the experiment were further used in order to calculate the experimental error of the automatic segmentation algorithm. In total, 3300 images (110 images each specimen) resulting from the 3 days treatment and the same number from the 5 day treatment, were used in order to calculate the experimental error in both cases: before and after the remineralising treatment (Table 21, Table 22, Table 23 and Table 24).

Table 21. Experimental error of the automatic segmentation algorithm for the area of detected open tubuli of samples treated during 3 days with the corresponding treatments.

Area of open tubuli			
Tooth paste		Av. error after dem. [%]	Av. error after rem. [%]
Sensitive Pro-Relief™	Tooth 1	0,07	13,06
	Tooth 2	0,24	3,58
	Tooth 3	0,17	1,24
	Tooth 4	0,67	1,50
	Tooth 5	0,97	0,00
Repair and Protect™	Tooth 1	0,75	1,26
	Tooth 2	0,32	0,00
	Tooth 3	0,74	0,43
	Tooth 4	0,18	1,60
	Tooth 5	0,20	0,00
Desensin™	Tooth 1	1,20	0,00
	Tooth 2	0,04	0,46
	Tooth 3	0,36	3,28
	Tooth 4	0,14	0,04
	Tooth 5	0,15	3,04
Average [%]		0,41	1,97
St.dev.		0,36	3,31

Table 22. Experimental error of the automatic segmentation algorithm for the number of detected open tubuli of samples treated during 3 days with the corresponding treatments.

Nr.of open tubuli			
Tooth paste		Av. error after dem. [%]	Av. error after rem. [%]
Sensitive Pro-Relief™	Tooth 1	0,03	10,92
	Tooth 2	0,37	2,76
	Tooth 3	0,22	1,13
	Tooth 4	1,47	0,86
	Tooth 5	0,50	0,00
Repair and Protect™	Tooth 1	0,37	0,64
	Tooth 2	0,15	0,00
	Tooth 3	1,38	0,52
	Tooth 4	0,22	1,01
	Tooth 5	0,10	0,00
Desensin™	Tooth 1	1,35	0,00
	Tooth 2	0,02	3,13
	Tooth 3	0,35	2,59
	Tooth 4	0,00	0,35
	Tooth 5	0,77	0,78
Average [%]		0,49	1,65
St.dev.		0,52	2,77

Table 23. Experimental error of the automatic segmentation algorithm for the area of detected open tubuli of samples treated during 5 days with the corresponding treatments.

		Area of open tubuli	
		Av. error after dem. [%]	Av. error after rem. [%]
Sensitive Pro-Relief™	Tooth 1	0,00	5,62
	Tooth 2	0,00	0,70
	Tooth 3	0,14	5,75
	Tooth 4	0,38	8,59
	Tooth 5	0,09	0,67
Repair and Protect™	Tooth 1	0,61	0,99
	Tooth 2	0,28	8,21
	Tooth 3	0,08	1,74
	Tooth 4	0,33	1,66
	Tooth 5	0,38	0,62
Desensin™	Tooth 1	0,00	0,89
	Tooth 2	2,13	8,63
	Tooth 3	0,84	0,21
	Tooth 4	0,39	1,57
	Tooth 5	0,74	0,23
Average [%]		0,43	3,07
S.d		0,54	3,27

Table 24. Experimental error of the automatic segmentation algorithm for the number of detected open tubuli of samples treated during 5 days with the corresponding treatments.

		Nr.of open tubuli	
		Av. error after dem. [%]	Av. error after rem. [%]
Sensitive Pro-Relief™	Tooth 1	0,00	2,10
	Tooth 2	0,00	0,33
	Tooth 3	0,05	3,19
	Tooth 4	0,10	1,98
	Tooth 5	0,01	1,94
Repair and Protect™	Tooth 1	0,80	0,74
	Tooth 2	0,12	0,15
	Tooth 3	0,02	0,32
	Tooth 4	0,14	0,00
	Tooth 5	0,04	0,62
Desensin™	Tooth 1	0,00	0,41
	Tooth 2	1,69	9,51
	Tooth 3	0,49	0,07
	Tooth 4	0,02	0,00
	Tooth 5	0,25	0,10
Average [%]		0,25	1,43
S.d		0,46	2,44

After 3 as well as 5 days treatment, the calculated error was higher after the remineralising treatment than after the demineralization procedure. In case of 3 days experiment, an error of 1,97 % was observed, comparedto 0,41% before the applied treatment when the area of the open tubuli was considered. The figures rise when the treatment was prolonged to 5 days (0,43 and 3,07% before and after the treatment respectively). On the other hand, when the number of not obliterated tubuli is analyzed, the error was of 0,49% ; 1,65% for the 3 days and 0,25%; 1,43% for the 5 days treatment.

15. Discussion

In the presented study, a methodology based on the dentin disc model was developed and optimized. The entire set of experiments was performed in order to develop a suitable routine that would allow studying the mechanism of the tubule obliteration and to compare the efficacy of various dental products. In comparison to Ciocca et al. (82), the method was also applied on the dentin surface treated with commercial toothpaste in order to see the performance for samples that undergo a remineralising /desensitizing treatment.

Once the proper magnification for the image analyses was selected (3000 X), the error of the automatic segmentation was evaluated. Very low values of the standard deviation for both: detected number of tubules (0,54) as well as the calculated percentage area of open tubules (0,16%), indicated that the performance of the routine on the designed images was correct and almost all of the present orifices, were detected. The resulting differences come mostly from the tubules that were detected at the edge of the image, since that number varied depending from the analyzed generated photos. On the other hand, the calculated experimental error of the performance of the developed MATLAB routine (0,01% per sample for number of tubules; 0,02% per sample for the area of tubules) was also low when pictures after the demineralization process were concerned. Slightly higher errors were found after the application of the remineralising treatment (0,03% per sample for number of tubules; 0,06% per sample for the area of tubules) occurred mostly due to impurities detected on the surface of the dentin. Those impurities proceed from the applied toothpaste and are impossible to eliminate. The results obtained by the automatic algorithms were corrected by technicians to perform the comparison, although these corrections consist only on the elimination of the impurity zone. It is worth highlighting that difference between the automatic and semi – automatic analysis are not statistically significant within a confidence interval of 95% for both types of obtained pictures, after the demineralizing and remineralising treatment. Consequently, the presented method can be implemented on the edged/demineralised dentin surfaces almost without any intervention from the technician. Meanwhile, the study performed on the samples treated with the agent that has capacity to occlude dental tubules should be supervised by the skilled SEM technician. Although, the analysis

performed by the developed routine facilitates the identification of the zone of impurities or other erroneous detection performed.

The present method is independent from the operator since the standard deviations for the detected area for three independent technicians were very low before and after the treatment (0,1%). Furthermore, there were no significant differences between the technicians within the interval of 95%. Therefore, the automatic method reduces the variability that comes from the human operator and guarantees the correct identification of the detected open tubules.

A very important conclusion that should be extracted from the performed measurements is the careful selection of the ROI when the analysis of open dentinal tubules is performed. A perpendicular cut of teeth can be clearly divided into two type of dentin surface: zone 1 where tubules are cut perpendicularly and are well exposed for its further observation and zone 2 where tubules are cut longitudinal what makes the observation of the orifice impossible. It has been clearly demonstrated that the average number and area of open tubules is bigger for the zone 1 respect to zone 2, due to the distribution of the dentinal tubuli in the tooth (what has been explained in section **Error! eference source not found.** page **Error! Bookmark not defined.**). It indicates that developed routine performs better on the zone 1. As a result, in order to properly perform the study and obtain images with dentinal tubules that can be easily observed, to evaluate the content of the orifice and calculate its area, the analyst should always perform the acquisition of images on the central (zone 1) of the tooth.

In order to represent the variability of the zone 1 it has been calculated that approximately 110 pictures should be taken. It means, that in order to study changes in the characteristics derived from the developed routine of the examined dentinal surface, 110 pictures after the demineralization should be compared with the same number of pictures after the occluding treatment performance. In such a way, the comparison of the number of open tubules and area occupied by open tubules will facilitate the necessary information about the applied treatment and enable the comparison between various occluding methods.

On the other hand, the limiting point of the present method that would be the influence of the vacuum on the tubules area contour should be considered. We have demonstrated, that once the sample is immersed into a vacuum chamber of the Scanning Electron Microscope during approximately two hours, the conditions of the environment does not change the number or the detected area of tubules. Although the most impacting factor, which is the influence of the first immersion at the vacuum conditions could not be measured, since the dimensions of the orifice could not be measured without the vacuum conditions. However, during the performed study it could be observed that some parts of the teeth undercame destruction due to the dehydration provoked by the vacuum. When the distracted part is also the studied region of interest, the sample has to be eliminated from the study and repeated. In order to avoid the influence of the severe vacuum conditions on the study, the new FEG-SEM technology,

where experiments are performed in low vacuum conditions (162), could be implemented.

Taking into consideration all above mentioned points, as well as the fact that the developed routine is also independent from the focus adjustment; the present method appears to be a robust approach in order to characterize quantitatively and qualitatively the dentinal surface. For demonstrative purposes, it was applied in order to study the mechanism of the occlusion of three remineralising/desentitizing treatments as well as to compare their efficacy.

The average percentage as well as a number of open tubules before the treatment in case of all analyzed specimens (30 tooth samples) varies a lot between samples (Table 25). It resembles very well a big variance between teeth in general. Even a very careful selection of specimens does not allow obtaining samples of exactly the same characteristics. Although, the method makes the problem of the variability in the tubules density and distribution irrelevant, since the observation of the same region of interest of the same samples before and after the treatment, concentrates on the final obliteration of the specimens.

Table 25. Average area and number of open tubules detected after the demineralisation process for all 30 specimens analyzed in the study.

	Average [%]	St.dev
Av % of tubuli before	13,13	5,2
Av. nr of tubules before	154,17	34,3

It is also interesting to notice, that the main information about the efficacy of the obliteration, is delivered by the calculation of the area of open tubuli rather than by the number of detected tubuli. In fact, the last value sometimes can deliver confusing results as in case of Tooth 2 treated with the Sensitive Pro-Relief™ tooth paste (Table 13). Clearly, the resulting average number of obliterated tubuli is smaller than for the rest of the samples. The source of the confusion comes from the fact that the number of tubules does not deliver entire information about the nature of the surface, since the dimensions and density of the tubuli orifice varies depending on its location (163). What is more, its dimensions also vary among different teeth. Since it is hard to control the homogeneity of the characteristics of teeth specimens, the obliteration capacity should be evaluated rather by the calculation of the area of the obliterated tubuli than by its number, which should be taken into consideration as additional, supporting information.

Comparing results obtained for each toothpaste (

Figure 36) after 3 and 5 days treatment the n-HAP based product of Dentaid ® revealed to be stable in the studied range of time. The average obliteration capacity varied from 92,2% +/- 4,5 to 93,3% +/- 6,5. It could suggest that the product reached its maximum occlusion capacity of tubuli that did not change when the treatment was prolonged. On the other hand, the Sensitive Pro-Relief™ tooth paste that contains arginine revealed

much smaller average obliteration after 3 days (71,2% +/- 4,1) comparing to 5 days (95,5% +/- 4,1). In this case, the highest obliteration was reached later than in case of Desensin® product, although the final obliteration, taking into consideration the standard deviations values, had reached an almost complete obliteration of the dentinal tubuli. A different phenomenon was observed for the Sensodyne® Repair and Protect™ toothpaste. The obliteration dropped from the 84,5 +/- 6,1 to 70,7 +/- 7,0 . Probably, the sealing of the tubuli was washed away during the prolonged treatment or the final obliteration capacity contributing to the oscillation between the calculated numbers. Although comparing the final results with two other studied tooth paste, Sensodyne® product appears to be less efficient in enhancing as well as in maintaining the obliteration of the dental tubuli. Nevertheless, all of presented conclusions apply to the studied conditions and period of time. In order to confirm the assumptions derived from the performed study a more prolonged treatment with bigger number of samples should be performed.

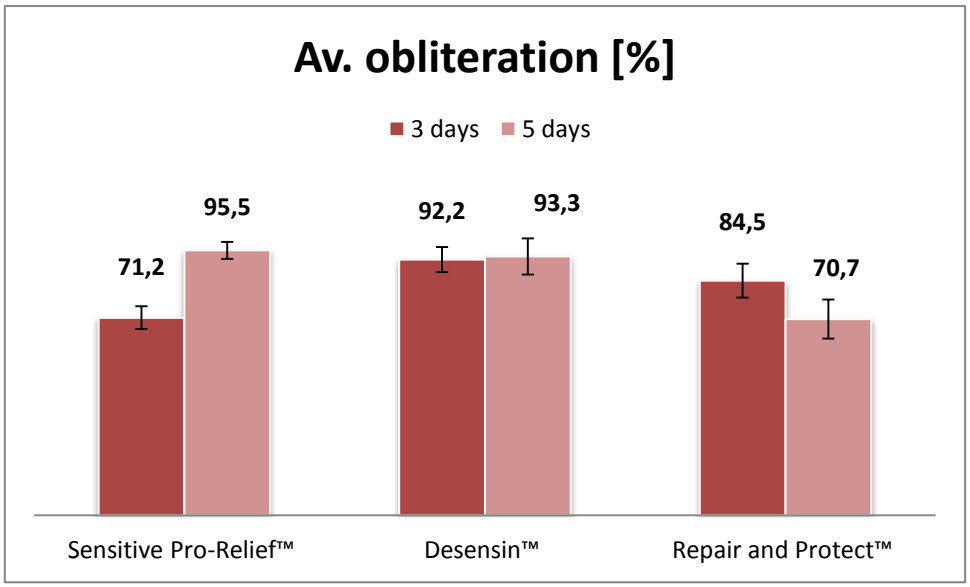

Figure 36. Comparison of average obliteration enhanced by all three studied products during 3 and 5 days treatment.

The analysis of the error resulting from the experiments performed after 3 and 5 days of treatment revealed, that in both cases, the error from the images acquired after the demineralizing treatment is smaller than for the images after the application of tooth pastes. The automatic segmentation algorithm has a very low error values before the treatment performance mostly because of the absence of impurities. The surface of the teeth after the demineralization process is usually clean what makes the detection and interpretation of the images easier than in case of the samples previously treated with the remineralising agent. Applications of any toothpastes a part form sealing the tubules, leaves the rest of the treatment on the surface of the specimen. Sometimes, the shade of the impurities can be detected by the automatic routine as a darker spot on the

image, and when its shape is close to round one, it can be classified as an unsealed obliteration. Since the presence of the impurities is independent from the treatment, and impossible to avoid, the analysis performed on the treated samples should be always supervised by the skilled SEM technician. Meanwhile, the specimens that under came only the desmineralisiation process do not need such intervention.

The prolonged treatment accumulates more impurities on the surface of the sample what is causing the misleading detection by the developed routine. In this sense, an increase of the error of the automatic segmentation algorithm after the 5 days of the treatment was observed.

It is worth mentioning that the error derived from the analysis of the number of tubuli is smaller than the error of the area of the open tubuli. Such fact would suggest that the automatic segmentation algorithm is not detecting a wrong presence of the tubules but is instead detecting additional shape that is generated by the shade of the impurities that normally have bigger area than the dentinal tubuli. As a result, the percentage of the detected area increases whereas the number of detected tubuli varies less from the corrected value.

Nevertheless, it should be highlighted that the calculated error that remains in the range of 0,41-0,43 % after the demineralization process and 1,97-3,07% after the remineralising treatment represent a very low number and very good detection of the open dentinal tubuli at the same time. The number of pictures analyzed in both cases is of 1650, what makes the error negligible, taking into consideration such a big sampling. Consequently, the presented method can be considered as a reliable tool for the detection of the open dentinal tubuli and comparison of various obliterating treatments.

16. Conclusions

As a result of the performed study, the following conclusions can be presented:

1. A robust method for the dentin characterization has been developed and optimized.
2. An automatic segmentation algorithm for the data analysis has been applied and optimized.
3. The method is operator independent; it can be implemented on the edged/demineralised dentin surfaces almost without any intervention from the technician.
4. Developed routine facilitates the observation and characterization of the dentin surface treated with the occluding agent.
5. The method is independent from the focus adjustment or influence of the vacuum conditions during the performed observation.
6. The proper way to establish the ROI of the method has been evaluated.
7. The sample size number of the studied ROI was evaluated.
8. The obliterating capacity of three different commercial toothpastes were studied and compared.

9. The experimental error of the automatic segmentation algorithm resulting from the performed study represented a very low number and very good detection of the open dentinal tubuli at the same time.

A NOVEL HSI APPROACH FOR THE EVALUATION OF THE EFFICACY OF THE REMINERALISING TREATMENT

Summary of the study

The problem of demineralization has been occupying the interest of many dentists and scientists, since it is the most common reason of dental caries creation. Various agents with different chemical approach designed for teeth restoration have been evaluated and are still being developed. However, there still exists some controversy concerning the remineralisation efficacy of recently developed chemical approaches. Therefore, it is crucial to understand the role of fluoride concentration on the remineralisation efficacy or the influence of novel approaches including the use of protein applications and the durability of such treatments, which will be focus of the present study. In this context, suitable analytical techniques for evaluation of teeth remineralization are urgently needed.

In the presented study, a novel complementary analytical approach, based on Hyper Spectral Imaging (HSI) with two types of NIR cameras (161 and 256 channels) and confocal Raman microscopy (CRM) was applied for analysis of teeth before and after application of different remineralizing agents. As a result, the novel NIR HSI MCR method that allows differentiating remineralised tissue from the demineralized was developed, facilitating the comparison of the efficacy of various remineralizing treatments and characterization of the enamel surface that undercame the remineralization process. Additionally, it also shows the distribution of the deposited fluorapatite on the tooth surface. As an example, Raman measurements confirmed the creation of fluorapatite in case of samples treated with Sensodyne as well as mixture III.

Obtained results were carefully analyzed and compared by the implementation of a Matlab routine that applies the correlation coefficient or MCR multivariate data analysis to obtain necessary information from the acquired spectra of dental samples. The resulting correlation of various samples with the pure hydroxyapatite and fluorapatite crystals was evaluated and discussed. Obtained results were compared with the characterization performed with Raman Spectroscopy.

In overall, the study of the influence of the fluoride on the remineralisation process showed clear differences in samples treated with mixtures of different concentration of that ion. However, the application of the protein occurred not to improve the process of remineralisation.

Introduction

The mineral composition of dentine and enamel is a mixture of compounds. The primary one is hydroxyapatite that is a crystalline calcium phosphate. Among others are carbonated apatites and fluoroapatites. The remineralization process is assisted by fluoride and bases on calcium and phosphate delivery into cavities remaining after the process of demineralization (11).

The problem of demineralization has been occupying the interest of many dentists and scientists, since it is the most common reason of dental caries creation. Table 1 depicts an overview of different approaches, which are nowadays used for teeth restoration.

Without any doubt, the most popular agent that enhances the remineralization is fluoride. Besides its antibacterial properties at low concentrations, fluoride stops the demineralization and favours the opposite-remineralizing process on the tooth surface. At higher concentrations, it creates the calcium fluoride layer that protects the enamel from the formation of caries (11), (12). It reacts with hydroxyapatite and forms fluorapatite, which is less soluble. The chemical equations describing the aforementioned processes are as depicted below:

$$\text{Demineralization: } Ca_{10}(PO_4)_6(OH)_2 + 8H^+ \rightarrow 10Ca^{2+} + 6(HPO_4)^{2-} + 2H_2O$$

$$\text{Remineralization: } Ca_{10}(PO_4)_6(OH)_2 + 2F^- \rightarrow Ca_{10}(PO_4)_6(F)_2 + 2(OH)^-$$

Generally, it is accepted that presence of fluoride at level of 1 ppm increases enamel remineraliaztion (11), (38).

Among the differenT existing technologies that guarantee the appropriate concentration of fluoride for enhancing a remineralization process, the GTS research group recently developed a unique dental product. Based on a bioactive composite (NMTD, an ion exchanger formulation) (48)**,** the product provides a controlled release of ions with very efficient remineralizing properties. The mentioned exchange is a consistent and reversible transfer between ions that are immobilized in a solid or liquid matrix and the ions that are present in the solution. The efficacy of the process depends on the equilibrium between the solid and the liquid phase and on the transfer kinetics. Generally, the ion exchangers are classified into 3 groups by the charge of ions that are exchanged, namely cationic, anionic and bifuncional exchangers (164). Ion exchangers have found application in many industrial areas such as water treatment (165), (166), analytical separations (167), pharmaceutics (168) and medicine (169). In dental materials, normally, polymeric resins are used as the ion exchangers (48).

Remineralization is also regulated by the presence of glycoproteins in human saliva which play a very important role in the tooth remineralization process. Such glycoproteins are absorbed on the tooth surface where they form a pellicle layer and

phosphoproteins which regulate calcium activity. The pellicle protects enamel from mineral loss especially in acidic conditions (36).

The more predominant enamel proteins are amelogenins (90%). Apart from that, ameloblatins, enamelins and tuftelins can be distinguished (24). Amelogenins importance on the hydroxypaptite development (22) (23) (24) and structure (170) was subject of interest for many scientists. Chemical conditions that have particular influence on the activity of the protein have been carefully studied (23) (171) (172) (173) (174) .

Amelogenin plays a very important role in the enamel creation. The self-assembled nanospheres influence the orientation of the growing hydroxypaptite crystals during the biomineralization process of the enamel. J. Moradian-Oldak et al. proved that this protein accelerates the nucleation of hydroxyapatite (22). Amelogenin becomes a key component on establishing the orientation of the alignment of apatite crystals what results in the appropriate "ribbon-like" form of the structure (22), (23). In general, it is believed that amelogenin on a developing stage of the enamel formation, is a key protein that delivers the calcium and phosphate ions or amorphous units that are present on its surface. Those components are then transferred from the protein into the growing crystal (24).

In order to characterize the tooth surface, a variety of methodologies has been applied so far (section 7). Among them, the most popular one is *Scanning Electron Microscopy* (SEM) that allows studying the teeth surface structure. Environmental SEM found a special application on the teeth study, since no pretreatment of a sample, such as gold coating is necessary. Other methods commonly applied for the characterization of dental tissue are presented in Table 26.

Table 26. Methods applied for the dental tissue characterisation

Method	Application	References
***Scanning Electron Microscopy* (SEM)**	studying the surface structure of the teeth	(13), (77), (78), (79), (80), (81)
***Atomic Force Microscopy* (AFM)**	topography and growth mechanisms studies	(13), (83), (84), (85) (86), (87), (88)
***X-Ray Photoelectron Spectroscopy* (XPS)**	chemical composition	(13), (89), (90)
***Secondary Ion Mass Spectrometry* (SIMS)**	distribution of elements	(91), (92) , (93), (94)
***Transmission Electron Microscopy* (TEM)**	information about crystalline properties	(95), (81)
micro-hardness measurements	changes in the micro-hardness of the dental tissue	(14)
***Fourier Transform Infrared* FTIR**	chemical structure , inorganic and organic composition	(97), (90), (98), (99)
Raman	chemical composition of the surface,	(80), (175), (176)

In the present study, two techniques were implemented to characterize teeth samples treated with various remineralising treatments: HSI and *Confocal Raman Microscopy* (CRM). Hyperspectral Imaging (HSI) also known as a Chemical Imaging (CI) combines the advantages of the digital image with the spectroscopic techniques to extract the numerical information from a sample. As a result, spatial and spectral data is obtained, what allows to characterize various parameters such as concentration or distribution of different components in solid, semi solid and powdered samples (133), (177). Such characteristics transform NIR-HIS technique into a suitable tool for surface analysis. Since it allows obtaining qualitative and quantitative information (e.g. chemical composition) it is commonly applied in pharmaceutical research(135) , (140), (178), (179), (180).

However, the generated spectral data by such technique must be processed. There are a large number of approaches for the spectral data processing (133). Among them *Principal Component Analysis* (PCA) (134), (135), (136), (137), *Partial least squares (*PLS) (140) or *Partial least squares discriminant analysis* (PLS-DA) (138), (139) are the most popular ones. In the present study, the correlation coefficient and Multivariate *Curve Resolution* (MCR) (141) were used in order to obtain the necessary information from the acquired images of dental samples. Correlation coefficient encounters the similarity degree between sample and the pure reference spectra. As a result, a correlation map that gives the qualitative information about the contents and its distribution in the sample can be constructed (133). MCR on the other hand unfolds the spectral matrix in order to obtain the concentration profiles of the sample. With this method, both qualitative and quantitative analysis can be performed (141)

The aim of this study is to present a novel material that enhances the remineralization of teeth by simultaneous delivery of calcium, phosphate and fluoride ions without its previous precipitation and with the creation of a fine fluorapatite layer on the tooth surface as a result of the applied treatment. The influence of the amelogenin application, prolongation of the treatment and daily monitoring of a sample remineralization on the efficacy of the remineralising process of the enamel was also studied. In comparison, the same study was performed with commercially available toothpastes. Further, the data acquired by HSI and CRM were compared. The resulting HSI data was verified and confronted with the measurement performed with the Raman spectrometer.

Near-IR was already applied in dental studies mostly for the detection of dental caries (181) (182) (183). R.C.Lee et al. (184) studied the influence of remineralization on the water loss of dental tissue. In the above mentioned works, spectra were acquired only at certain wavelengths; authors did not analyze the entire near-IR range. In present work, a *NIR HSI* together with multivariate analysis techniques were applied in order to obtain images of remineralised human teeth. Such combination allows evaluating the efficacy of the remineralizing treatment. Taking into consideration the simplicity of the method, it can be a powerful tool to obtain basic information about the performed treatment. In the process of the evaluation of a new dental product, this kind of information can

facilitate the decision whether to continue the development of the product or to proceed with another, more promising approach.

Experimental Section

17. Materials and Methods

17.1. Instrumentation

Teeth were cut longitudinally using the diamond saw Southbay Technology Inc., USA. The concentration of the remineralising agent was analyzed by ICP-MS Thermo Elemental X Series 2, USA and Fluoride Ion Selective Electrode Thermo Fisher Scientific Inc.

Two types of NIR HSI set-ups were employed and described in Figure 37, while their specifications are enlisted in Table 27.

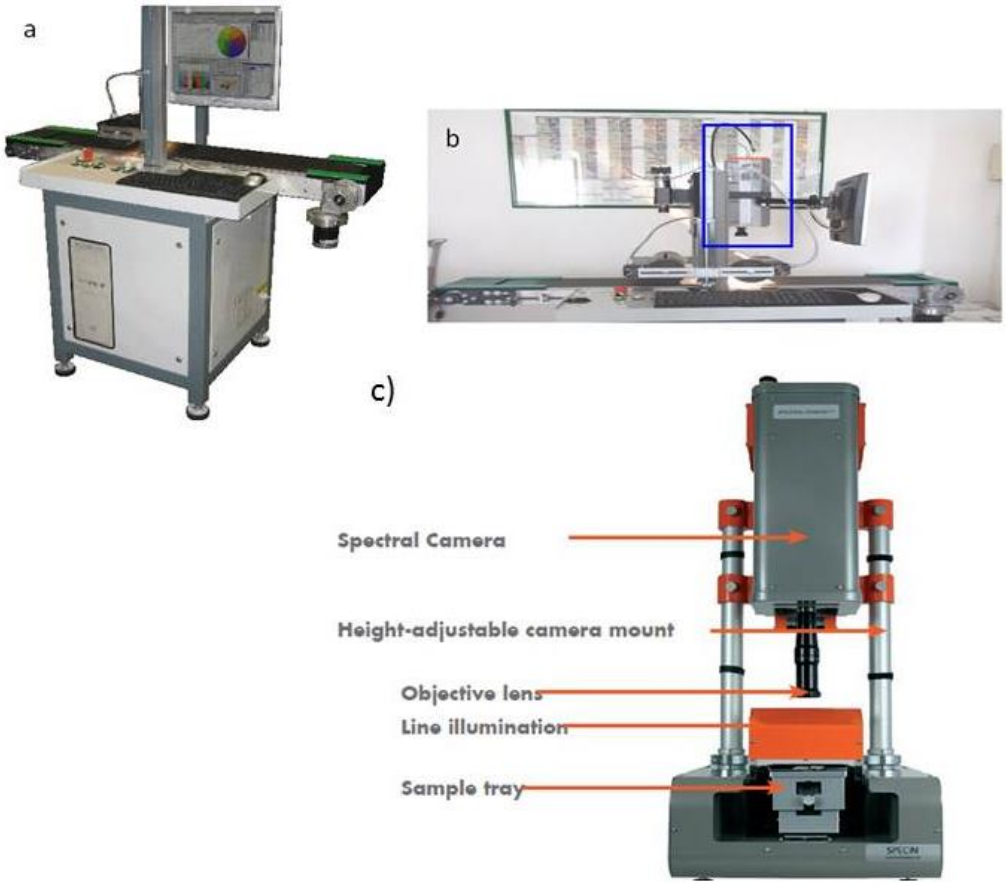

Figure 37. a) Conveyor belt and PC unit b) spectral camera of the 121 channel NIR HSI set-up c) SisuChema Hyperspectral Scanner set-up with 256 channels

Table 27. Comparison of two cameras applied in the study

Characteristics of the camera	Camera	
	ImSpector™ N17E	SisuChema Hyperspectral Scanner
Producer	Specim Ltd., Finland	
Wavelengths measured	121 channels	256 channels
Spectral resolution [sampling /pixel]	7	6,3
Spatial resolution [pixel/line]	320	
Distance conveyor belt-detector [cm]	32	28
Wavelength range [nm]	1000-1700	1000-2500
Spot radius [µm]	<15 µm	
Acquisition/preprocessing software	Spectral Scanner™ v.2.3 (DV srl, Italy)	ChemaDAQ™

17.2. Confocal Raman microscopy (CRM)

Confocal Raman microscopy measurements were performed using a WITec alpha 300R$^+$ microscope (WITec GmbH, Ulm, Germany). The excitation source was a diode laser with a wavelength of 532 nm, adjusted to the power of 20 mW before the objective. Enamel spectra were obtained using a 50x long distance objective (Epiplan Neofluar, Zeiss, Germany) with a numerical aperture of 0.55. The signal was detected by ACCD camera after passing a 50 µm confocal pinhole. The spectrometer was equipped with a 600 lines/mm grating. The Raman spectra in large area scan mode were recorded with 0.5 s integration time, and in single spectra mode with 0.1 s and 10 accumulations. Step size of the large area scans was 10 µm. All spectra were background subtracted, normalized and converted into false color images using WITec Project Plus software (WITec GmbH, Ulm, Germany).

17.3. Optical profilometry

The structured surface of teeth necessitates optical profilometry analysis prior to Raman mapping. Optical profilometry analysis was performed using a True surface® analyzer combined with the WITec 300R$^+$ confocal Raman microscope. An area of 1000 x 1000 µm^2 of a tooth was topographically resolved with the same step size, which was subsequently used for Raman data acquisition (10 µm). The integration time was 0.1 s and the sampling rate was 100 Hz.

17.4. Amelogenin Preparation

Purified recombinant porcine amelogenin full-length rP172 was prepared as described previously (185). The rP172 protein consists of 172 amino acids and is an analogue to

the full-length native porcine P173, but lacking the N-terminal methionine and phosphate group Ser16. The proteins were expressed in Escherichia coli strain BL21-codon plus and purified by ammonium sulfate precipitation and reverse-phase high performance liquid chromatography (Water Alliance, USA, Grace fenil, 250*4 mm, Vydac C18, 250*4.6mm, 5µm).

17.5. NMTD (Remineralizing Agent) Preparation (48)

Three different types of remineralising mixtures that varied in the ratio of calcium, phosphates and fluoride were prepared. The mass ratio is presented in Table 28

Table 28. Mixtures applied during the study. The concentration is presented in the mass ratio of atoms of calcium, phosphate and fluoride.

	Ca	P	F
Mixture I	2	3	1
Mixture II	2	3	3
Mixture III	2	3	6

Apart from above mentioned ions all resins contained of 2% of Zn for anti-bactericide purposes (186).
In order to confirm the concentration of prepared mixtures the ICP-MS analyze was performed for calcium, phosphor and zinc content. Fluoride concentration was measured by ISE (Ion Selective Electrode). The comparison of the theoretical load and the measured one are presented in Table 29. Remineralising mixtures were prepared taking into consideration the experimental loadings.

Table 29. Theoretical and experimental loading of loaded resins

Element	Theoretical load [g/mmol]	ICP/ISE load [g/mmol]
P	3	2,73
Ca	3	2,97
Zn	3	3,09
F	3	3,56

17.6. Specimen Preparation for the NIR measurements

A scheme of the specimen preparation is illustrated in
Figure 38. 30 recently extracted human teeth free from caries were chosen and cut into 3 or 4 pieces by a diamond saw. All parts were at first etched with 1M HCl for 30 seconds to simulate the early stage caries creation. Two out of three parts of each tooth was treated with NMTD (remineralizing agent) with or without the protein. Each treatment was repeated for 10 samples, as it is illustrated in Table 30. The third part of the sample was used as a blank, it means that it was not treated with the agents and during the

time of the application, it was placed in the saliva solution at 37°C. The procedure was as it follows (30): approximately 0.5 g of the remineralizing agent was mixed with few drops of artificial saliva (KCl 0,625 g/l; $CaCl_2 \cdot 2H_2O$ 0,166 g/l, K_2HPO_4 0,804 g/l; pH 6,8 ± 0,4) in order to obtain the optimal consistence for its further application on the enamel surface. In case of amelogenin application, the NMTD was mixed with the solution of amelogenin in artificial saliva. The concentration of the amelogenin was 40 µg/ml and the pH was of 6,8 ± 0,4 (187). The coating was changed every 12 hours and the treatment lasted 4 days. The NMTD agent was renewed by carefully washing the specimens with artificial saliva and applying a fresh portion of NMTD. During the time of the experiment, samples were placed in the incubator in order to maintain it in the natural temperature of the mouth (37°C). Once the treatment was finished, the samples were stored under a relative humidity of 100% in a 0,5% chloramine –T solution in the refrigerator.

Together with those studies addressed to test the effect of different concentrations of NMTD and the presence of the protein, the influence of the duration of the treatments was studied. In order to do that, the above-described procedure was performed in the same way for 8 and 12 days on 10 specimens treated with mixture I.

The daily monitoring of the treatment was performed by making the applications of the above-mentioned mixtures and acquiring the spectral data each day after two applications. For each treatment, five teeth were used. After 3 days of consecutive applications samples were stored in the refrigerator in a 0,5% chloramine –T solution and measured again after 7 days.

As reference samples, two commercially available toothpastes were applied: Sensodyne® Repair and Protect with the NovaMin® technology and SensiLacer® from Lacer. The application procedure was the same as for the remineralising NMTD product (4 days treatment changed every 12 hours). The total number of studied teeth was of 10 samples for each toothpaste.

Table 30. Treatments performed during the study. Samples were divided into 3 groups were the applied mixture was changing. Each group was analyzed with 10 replicates.

Group 1	Group 2	Group 3
Blank	Blank	Blank
I mixture	II mixture	III mixture
I Mixture + protein	II Mixture + protein	III Mixture + protein

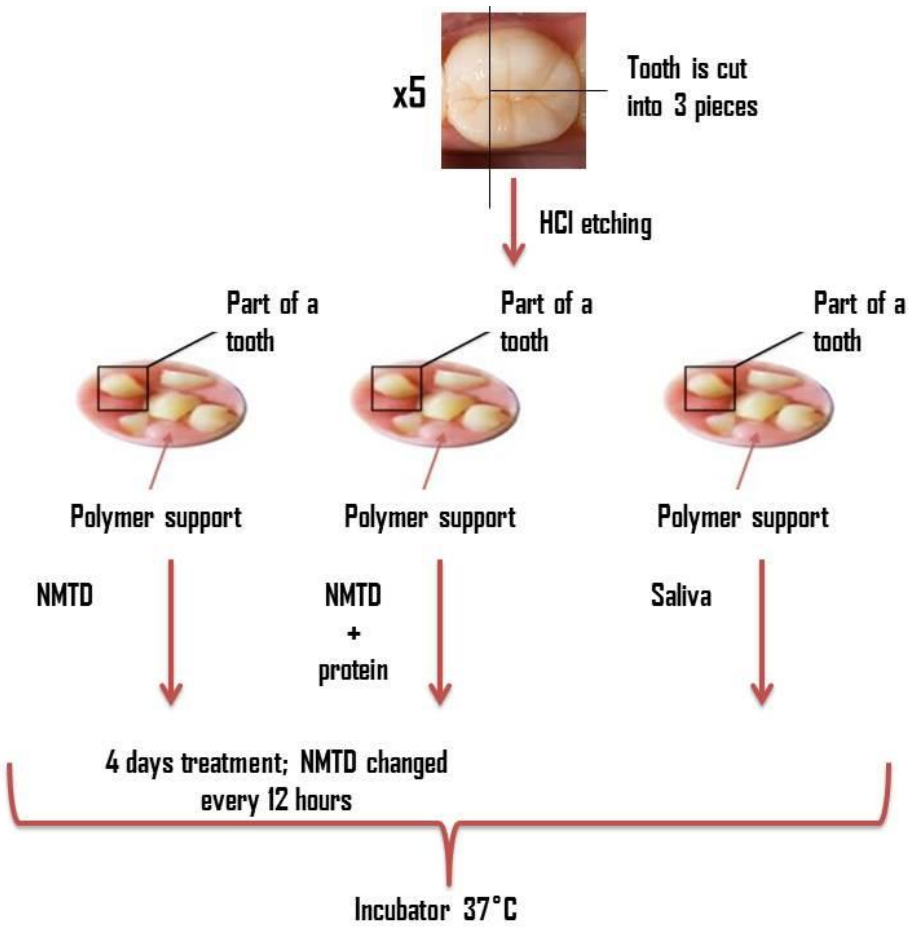

Figure 38. Scheme of the specimens' treatment

17.7. Specimen Preparation for Raman measurements

Daily monitoring of the remineralising treatments was performed with Sensodyne and mixture III applications. A human tooth free from caries was cut in two sections by a diamond saw. All parts were at first etched with 1M HCl for 30 seconds to simulate the early stage caries creation. Further, the treatment was performed as previously described in paragraph 17.6. Three experimental spots of the analyzed samples were measured before etching, after etching with the acid, and after each day of the daily treatment routine (after two remineralizing applications). Treatment was performed for four subsequent days.

17.8. Software

Correlation coefficients and histograms were computed by using custom developed m-files in Matlab 7.1 (The Matworks, Massachusetts). Spectral treatments were applied by using PLS-Toolbox 6.0 (Eigenvector Research, Wenatchee, WA, USA). Hyperspectral images were also analyzed with MCR-ALS (141).

17.9. Data processing

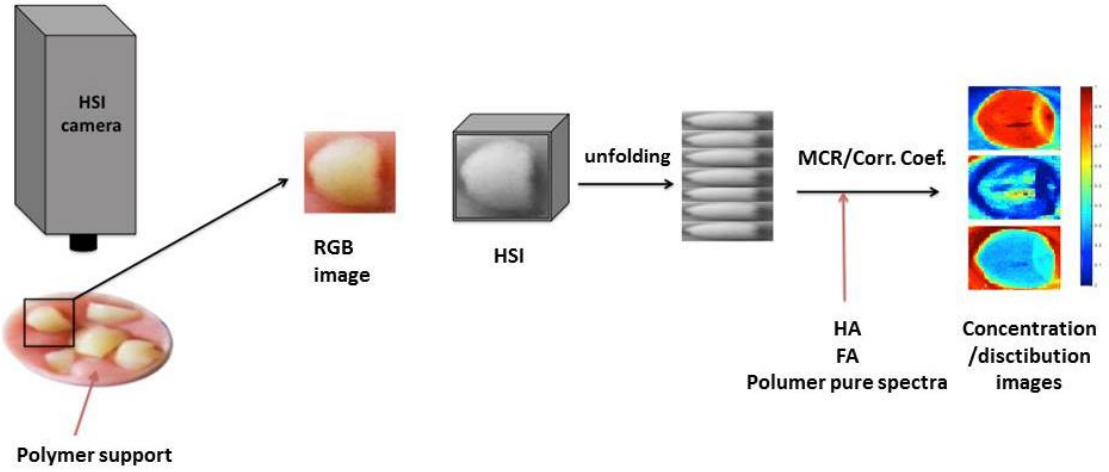

Figure 39. Scheme of the presented method for the evaluation of the remineralisation treatment efficacy

Figure 39 illustrates the experimental procedure applied in presented study. Teeth sample of various treatments were acquired with the HSI NIR camera. Prior to application of any spectral treatment or algorithm to extract the needed information, the three way data array (M x N x λ) was unfolded into a two-dimensional matrix. Most of the available treatments and algorithms have been developed for two-dimensional data – where M and N represent spatial dimensions and λ denotes spectral information. Two different spectral treatments were used: standard normal variate (SNV) and Savitzky–Golay smoothing with and 11 points window and fitting to a second-order polynomial. These treatments were followed by application of correlation coefficient and MCR method in order to assess the best approach to extract information from HSI of samples.

In the case of correlation coefficient, spectra obtained in the measurement were compared to the one of the pure components of hydroxyapatite and fluorapatite. As a result, a correlation map that represented the distribution of those components was constructed. The correlation coefficient was calculated from the subsequent equation:

$$corrcoef = \frac{\sum_\lambda x_{mn\lambda} y_\lambda}{\sqrt{\sum_\lambda x_{mn\lambda}^2 \sum_\lambda y_\lambda^2}} \quad \text{(Eq.5)}$$

where, for each wavelength, $x_{mn\lambda}$ is the spectrum for the *mn*-th pixel and y_λ the pure spectral profile for one analyte. Similarity is the greatest for two identical spectra, i.e. with corrcoef = 1 (142), (143).

The other parameter employed in the present study is based on the MCR-ALS (141) algorithm consists in the decomposition of spectral matrix ***X*** (MN x λ) in two matrices, ***C*** (MN x F), which contains the concentration profiles, and $\boldsymbol{S}^T$ (F x λ), which contains the spectral profiles for each F constituent.

$$X = CS^T + E$$

Being E (MN x λ) the residual matrix related to experimental error. MCR-ALS works by iteratively optimizing the matrices C and S^T with the help of constraints based on chemical knowledge or on mathematical features of the data (188).

17.10. Statistical analysis

Basic statistical data were evaluated and compared using statistical software (Microsoft Excel 2007). Xlstat (Addinsoft) and SigmaPlot 13 (Systat) software were also employed for data analysis purposes. Outliers were determined applying Grubbs Test within a confidence interval of 95%. In order to evaluate the difference in the variance of various sample groups the ANOVA test was implemented. The differences between the series of results of various categories were compared using t- Test along with Tukey's Test (HSD) and Dunet's test within a confidence interval of 95%.

18. Results

18.1. Spectral differences between FA and HA implementing 2 cameras (121 and 256 channels)

Comparing the absorbance spectra of HA and FA pure powders acquired by two cameras of 121 and 256 channels (

), a peak at 1420 nm for the HA was clearly identified with both cameras. This peak is related to -OH groups (189) and is not observed in the FA spectrum, probably due to influence of the F ion. When the second derivative is applied (Figure 40 b and c), in mentioned region, a negative peak with the following positive peak is observed. The lack of such signature for the FA sample could allow the differentiation of the two apatite species. Another spectral difference useful for differentiation can be observed in the second derivative at 1360 nm. There is a negative peak for the FA and positive for the HA sample with the 121 channels camera. Interestingly, there is a lack of this peak in the 256 channels camera instead a positive peak more intense in case of HA and less intense for the FA sample appears.

Another spectral region where differences could be found is located around 2130 nm for the 256 camera. A negative peak for the FA and much less intense one for HA could be differentiated. In the second derivative it results in the presence of the negative peak for the FA and the lack of it in the HA signature. The same situation was encountered around 1955 nm where a positive peak for the FA and the absence of such one for HA was observed.

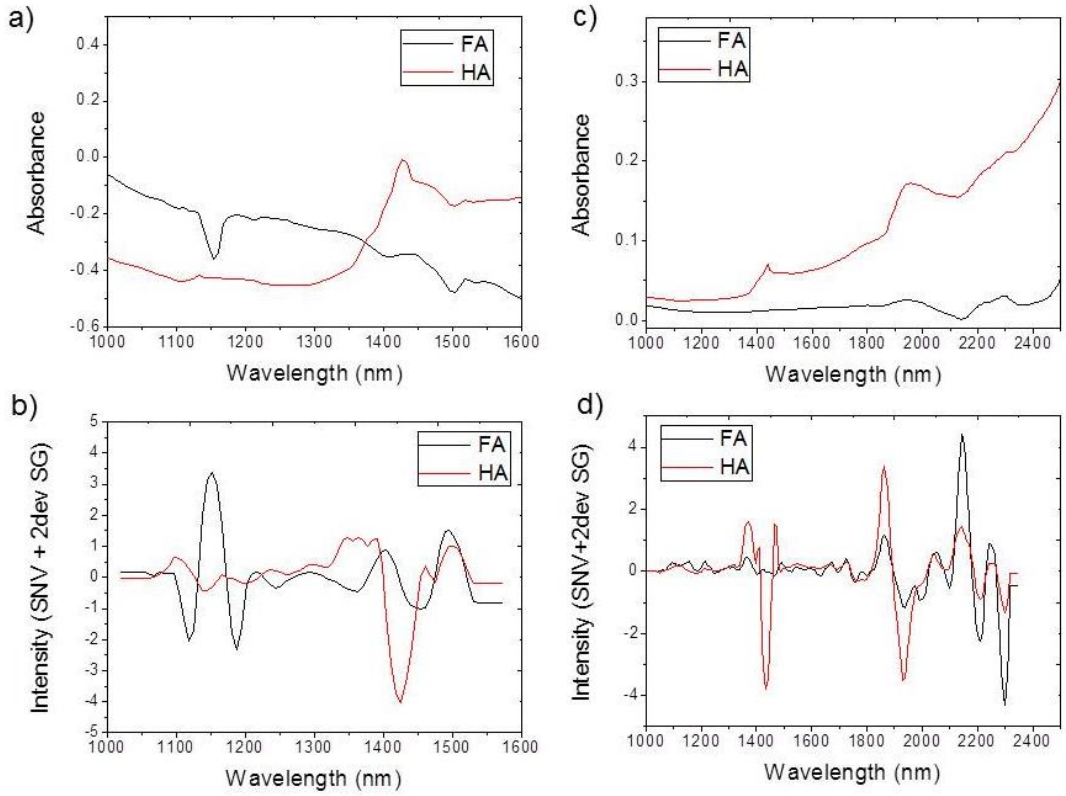

Figure 40. Absorbance hydroyapatite and flouroapatite pure spectra and its SNV with second derivative (Savitzky – Goley) mode with two NIR cameras with 121 (a and b) and 256 channels (c and d).

As observed, the 256 channels camera can deliver more information in comparison to the 121 channels camera. Due to the wider wave range (942 to 2542 nm) and higher resolution we can obtain more information from the 256 channels camera. Moreover, in the 121 camera some peaks are overlaid whereas in the 256 channels camera those peaks are better resolved (region 1400-1500 nm), what facilitates the differentiation of the two species. It explains the differences in the results obtained for both cameras and presented in the following results sections.

18.2. Results obtained for the samples treated with commercial products

18.2.1. Application of the correlation coefficient method and the comparison between two cameras (121 and 256 channels)

An increase in the number of pixels correlated with HA was observed for the treated samples comparing to the blank samples (
Figure 41). The observed tendency is the same for data acquired with both cameras although for the camera with 256 channels the correlation with HA for all samples were moved to lower values. It means that the correlation with hydroxyapatite where the highest number of pixels were classified is of 0,5-0,55 for all of the samples (reference sample and treated samples) in the camera with 121 channels. In the case of the 256 channels camera, the peak for blank sample is moved to 0,35-0,4 whereas for the treated samples it is located between 0,4-0,45 correlation (Table 28). In both cases,

when comparing the different commercial toothpaste, Sensodyne is the one that leads to the strongest increase in HA correlated pixels.

Table 31. Position of the maximum peak for the samples treated with commercial toothpastes and blank sample acquired with the camera with 121 and 256 channels.

	121 channels			256 channels		
	Blank	Lacer	Sensodyne	Blank	Lacer	Sensodyne
Position max. peak	**0,5-0,55**	**0,5-0,55**	**0,55-0,6**	**0,35-0,4**	**0,4-0,45**	**0,4-0,45**

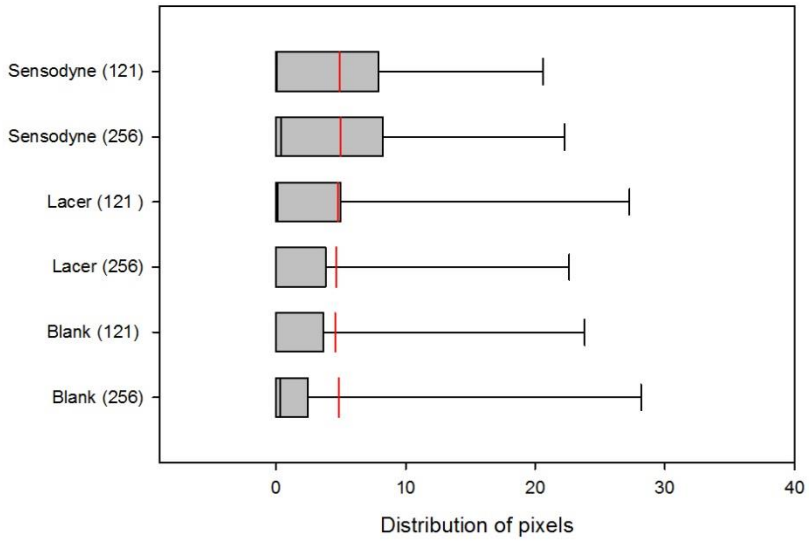

Figure 41. Distribution of pixels obtained for samples treated with commercial products compared with the blank samples and acquired with both 161 and 256 channel camera.

The remineralised zones can be observed also in the hyperspectral images (
Figure 72). Samples that were only treated with acid resemble a homogeneous distribution of HA among the observed teeth, whereas in treated samples pixels correlated with HA are concentrated in zones what could indicate a possible influence of the applied treatment.

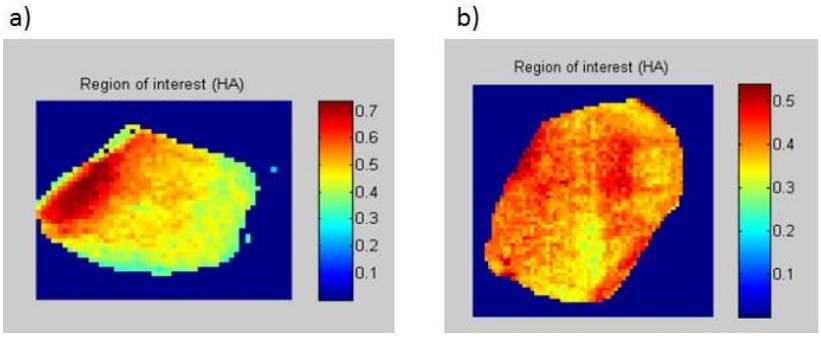

Figure 42. a) Teeth treated with the commercial toothpaste with a zone of pixels highly correlated with HA b) tooth only etched where the correlation with HA is distributed homogenously images acquired with the camera of 256 channels

The results of the correlation with the FA showed no differences between blank and treated samples. There was almost no correlation with the FA detected applying this method.

18.2.2. Application of the MCR method

An increase in the concentration of FA comparing to blank samples has been detected with the simultaneous drop in the concentration of HA (Table 32) when the MCR analyses was applied for the acquired samples treated with the commercial toothpastes. The highest concentration was registered for the Sensodyne toothpaste. At the HSI images observed changes are visible in form of small areas where an increase in the concentration of fluorapatite (decrease in the concentration of HA) could be differentiated (Figure 43).

Table 32. Average concentrations of HA and FA for samples treated with commercial toothpastes and blank sample

	Concentration of HA			**Concentration of FA**		
	Sensodyne	Lacer	Blank	Sensodyne	Lacer	Blank
Average	92,2%	93,3%	95,1%	7,8%	6,7%	4,9%
SD	0,02	0,03	0,01	0,02	0,03	0,01

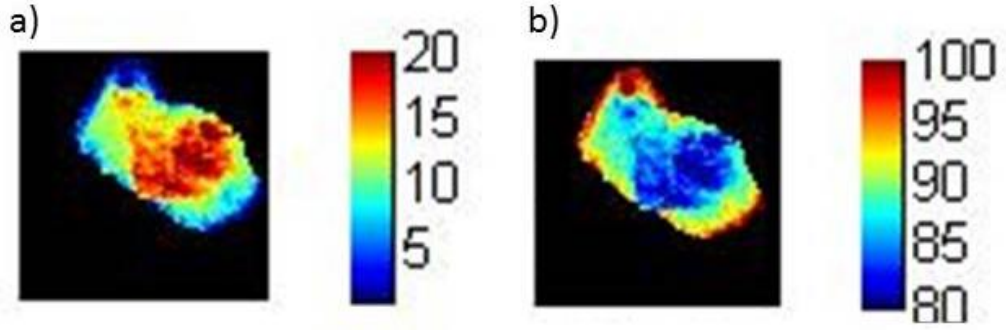

Figure 43 Example of a tooth treated with the remineralising agent (Sensodyne) where an area of the increased concentration of FA (a) with the simultaneous decrease of the HA concentration (b) in that region could be observed.

In Figure 44 five samples treated with Sensodyne paste are illustrated, most of them were detected as increasing content of HA, although the concentration of detected FA pixels can go up to 20%.

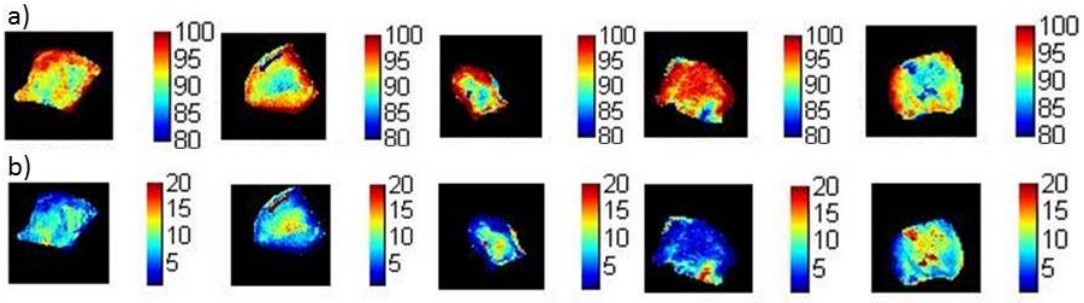

Figure 44 Example of the images ilustrating concentration levels of a) HA and b) FA calculated by MCR method for five sample treated with the Sensodyne product.

18.3. Influence of the fluoride concentration

18.3.1. Application of the correlation coefficient method and the comparison between two cameras (121 and 256 channels)

The comparison of the distribution of pixels correlated with HA for all three mixtures with growing concentration of the fluoride applying the camera of 121 channels reveals the mixture II to have more correlation with the poor HA than the rest of samples. However, it could not be confirmed by the camera with 256 channels where mixture III showed the highest correlation and mixture II the lowest. What is more again for the 256 channels camera the peak of the maximum correlation is moved to the smaller values (Table 33).

There is a clear difference between samples treated with the remineralising treatment when compared with the blank samples. The distribution of the pixels correlated with the HA gets wider when the treatment is applied (

Figure 45), although there were no significant differences between groups when ANOVA test within a confidence interval of 95% was implemented.

Table 33. Position of the maximum peak for the samples treated with mixtures with growing concentration of fluoride acquired with the camera with 161 and 256 channels.

	MI 161	MII 161	MIII 161	MI 256	MII 256	MIII 256
Position max. peak	**0,55-0,6**	**0,55-0,6**	**0,55-0,6**	**0,45-0,5**	**0,45-0,5**	**0,4-0,45**

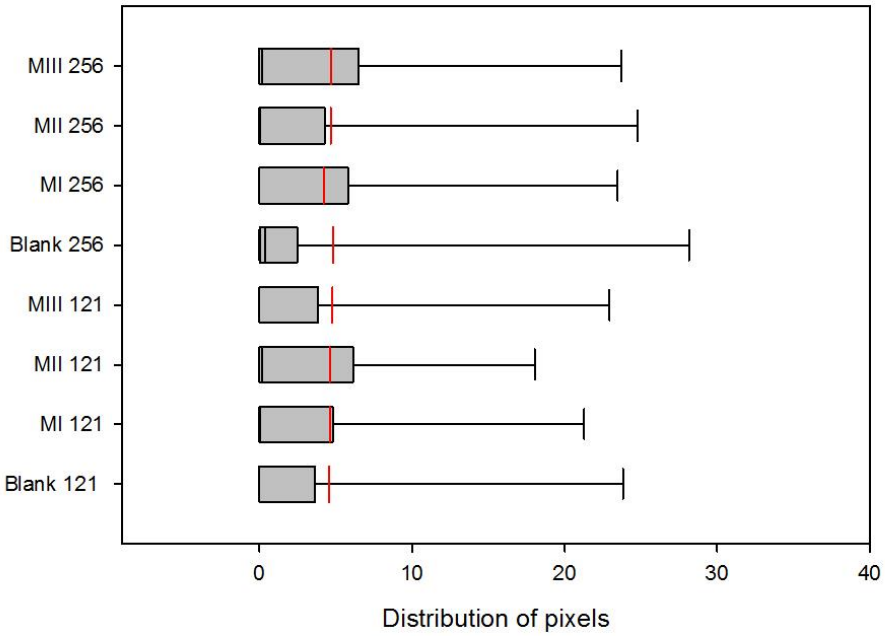

Figure 45. Distribution of pixels obtained for samples treated with mixtures with growing concentration of fluoride acquired with both 161 and 256 channel camera.

18.3.2. Application of the MCR method

The comparison of the concentrations of HA for all the samples treated with the remineralising product with the growing concentration of the fluoride revealed mixture II to have reached the highest concentrations of the FA (16,1%) (Table 34, Figure 46). Comparing to the blank samples only in case of mixture III the concentration of FA did not increase.

Table 34. Concentrations levels of HA and FA for samples treated with remineralising mixtures of the growing concentration of fluoride.

	Concentration of HA				**Concentration of FA**			
	Blank	MI	MII	MIII	Blank	MI	MII	MIII
Average	95,1%	92,7%	83,9%	95,4%	4,9%	7,3%	16,1%	4,6%
SD	0,01	0,03	0,05	0,01	0,01	0,03	0,05	0,01

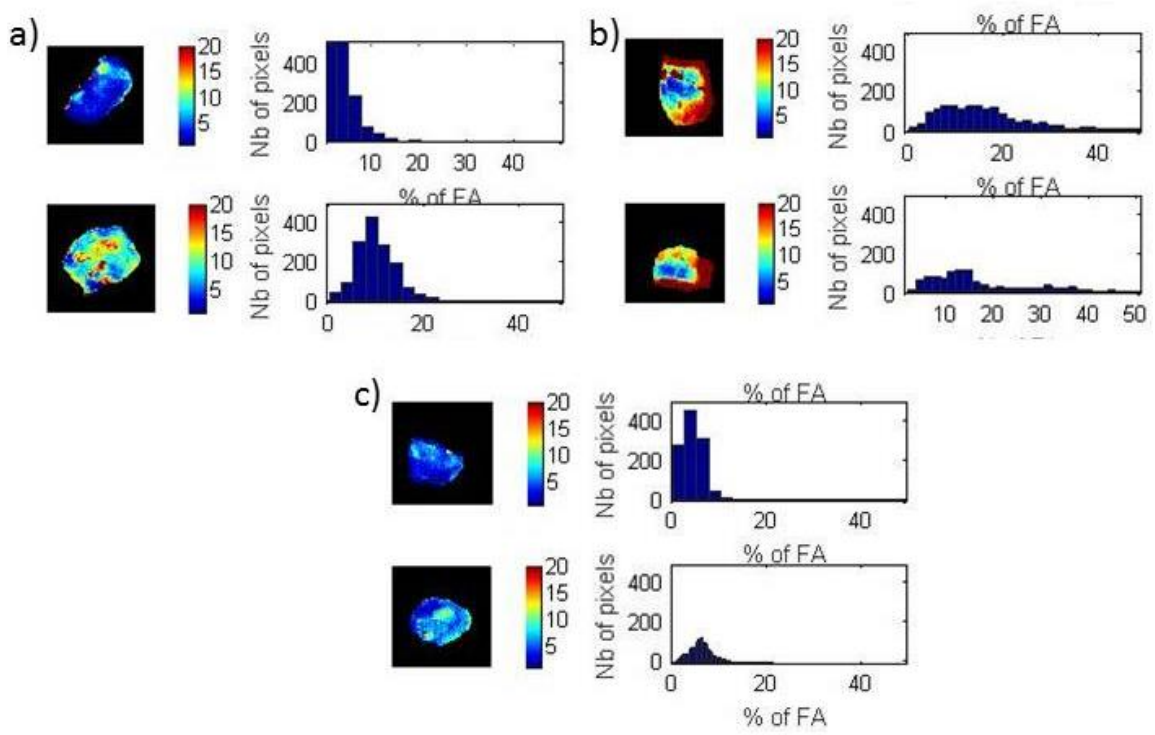

Figure 46. Example of the images with its respective histograms of the FA concentration calculated by MCR method for samples treated with a) Mixture I b) Mixture II c) Mixture III

The distribution of the data is the widest for mixture II (
Figure 47) comparing to the rest of the samples but still remains with the leptokurtic kurtosis as the rest of the analyzed data. Comparing the resulting data with the ones obtained for the correlation method, exactly the same observations were encountered for the camera with 121 channels.

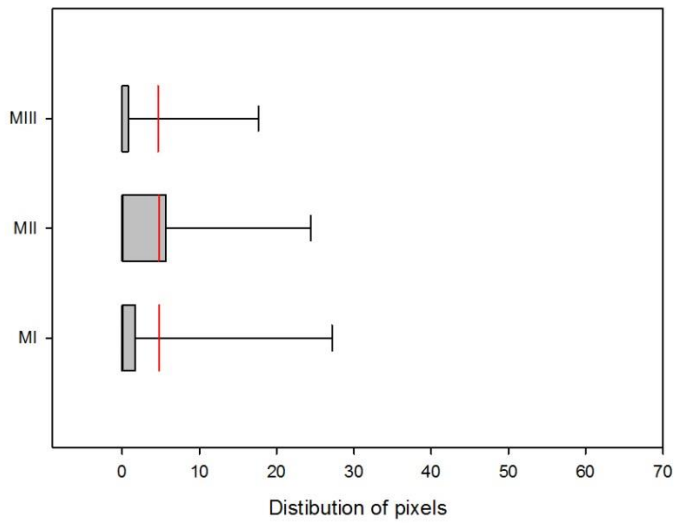

Figure 47. . Distribution of pixels obtained for samples treated with remineralising mixtures of the growing concentration of fluoride.

Wide range of the obtained data for the Mixture II can cause an overestimation of the obtained average for this mixture. An example of histograms obtained for the

concentrations of FA detected for various samples treated with mixture (Figure 48), shows that the average of the obtained data does not reflect well the general influence of the performed remineralisation when compared to other treatments, although, there are no outliers detected by Test of Grubbs in the confidence interval of 95%. Presented data should be first carefully analyzed with the obtained images and histograms rather than with the average derived from of all samples. After doing so, it was observed that mixture number II is more effective in the fluorapatite creation than mixture I, although the observed difference is not as big as 8,8% as it suggests the average value consideration. Moreover, the mixture III is the less efficient in enhancing remineralization.

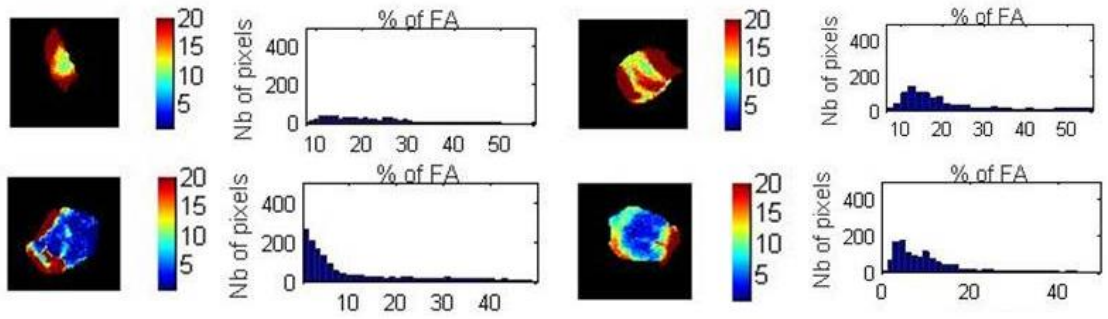

Figure 48. Representative samples with histograms of FA distribution obtained for four different samples treated with Mixture II.

Comparing the developed remineralising mixture to the commercial samples the concentrations of the detected FA are much higher (4,6- 16,1 % and 6,7-7,8% respectively). The increment of FA is localized in zones where the increment of the fluoride concentration is correlated with the drop in the concentration of the HA (Figure 49).

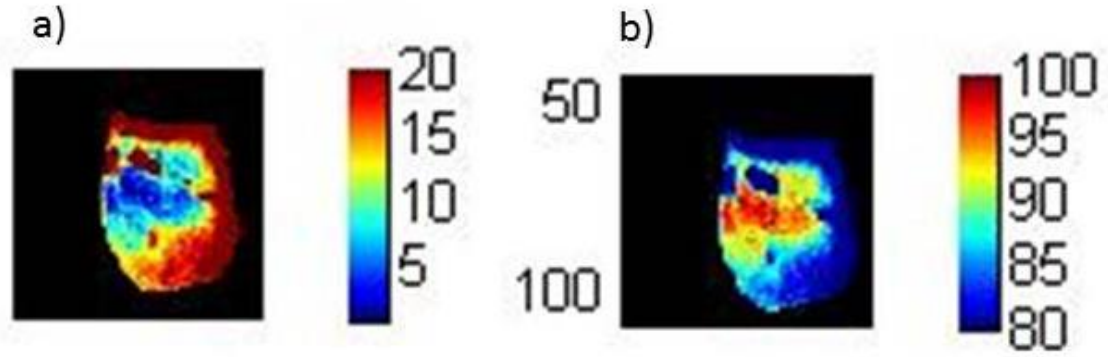

Figure 49. Example of a tooth treated with the remineralising agent where an area of the increased concentration of FA (a) with the simultaneous decrease of the HA concentration (b) in that region could be observed for the samples treated with mixture I.

18.4. Influence of the protein in remineralising treatments of various concentrations of fluoride

18.4.1. Application of the correlation coefficient method and the comparison between two cameras (121 and 256 channels)

For samples acquired with the camera of 121 channels there is an increment in the number of pixels correlated with HA when the protein is applied for mixtures I and II ( ). The observed effect reveals to be the strongest for the mixture III. In case of camera with 256 channels, such behavior could be observed only for mixture II whereas in case of mixture I and III the effect is the opposite one: a drop in the number of pixels correlated with HA was observed when the protein was applied.

When analyzing the position of the peak that represents the biggest amount of pixels classified in the same range of the correlation with HA it could be observed that in case of both cameras mixture I has the highest correlation when the protein is applied (161 channels: 0,6-0,65; 256 channels 0,45-0,5)

Table 35. Position of the maximum peak for the samples treated with mixtures and the protein application with growing concentration of fluoride acquired with the camera with 161 and 256 channels.

	MI + P 161	MII + P 161	MIII + P 161	MI + P 256	MII + P 256	MIII + P 256
Position max. peak	**0,6-0,65**	**0,55-0,6**	**0,55-0,6**	**0,45-0,5**	**0,4-0,45**	**0,4-0,45**

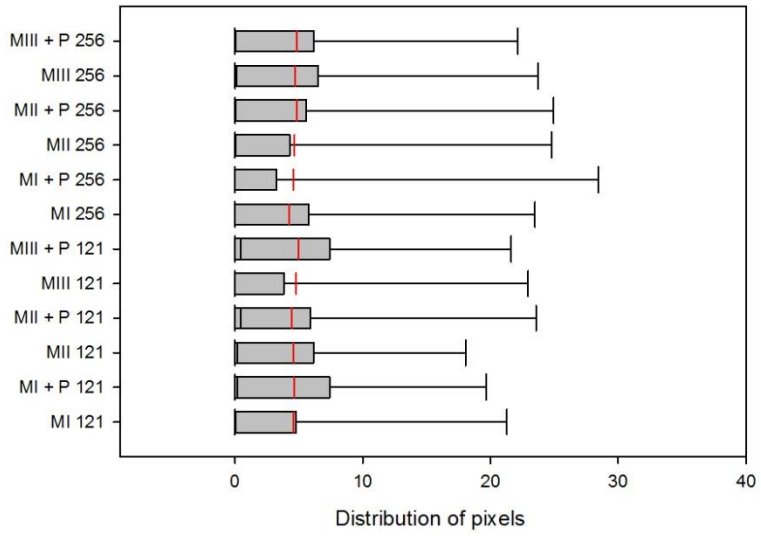

Figure 50. Distribution of pixels obtained for samples treated with mixtures and the protein application with growing concentration of fluoride acquired with both 161 and 256 channel camera.

18.4.2. Application of the MCR method

The distribution of data for samples treated in the presence of the protein reveals the same leptokurtic kurtosis and positive asymmetry as for the samples treated in absence of the protein (
Figure 51). However, in case of samples treated in presence of the protein the detected concentration of FA is much lower than in case of the treatment performed without the protein application (4,3-5,9% and 4,6-16,11% respectively).

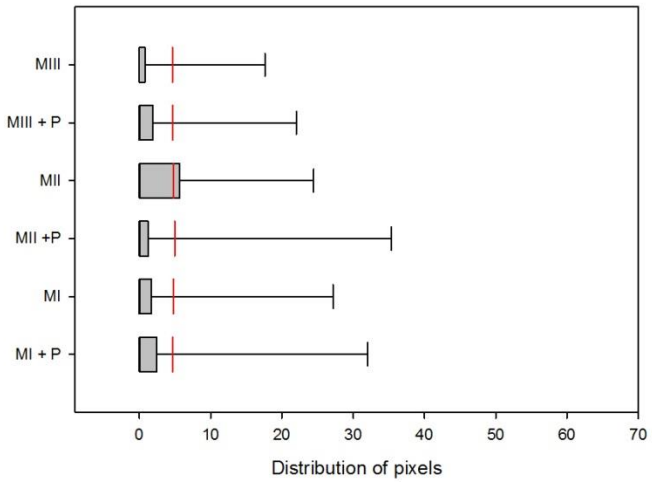

Figure 51. Distribution of pixels obtained for samples treated with remineralising mixtures of the growing concentration of fluoride and the protein

Table 36. Concentration levels detected for samples treated with remineralising mixtures of the growing concentration of fluoride with the simultaneous application of protein

	Concentration of HA				Concentration of FA			
	Blank	MI + P	MII + P	MIII + P	Blank	MI + P	MII + P	MIII + P
Average	95,1%	93,3%	95,7%	94,3%	4,9%	5,9%	4,3%	5,1%
SD	0,01	0,03	0,02	0,02	0,01	0,02	0,02	0,02

Samples treated with mixture I and the protein revealed the higher concentration of the concentration of FA and the lowest of HA. The lowest concentration of FA (even lower than for the blank samples) was detected for samples treated with the mixture II in presence of protein. Observed behavior was not similar to the data obtained for the correlation coefficient method.

18.5. Influence of the prolonged remineralising treatment

18.5.1. Application of the correlation coefficient method and the comparison between two cameras (121 and 256 channels)

There are no significant statistical differences between samples treated during 0,4,8 and 12 days within the confidence interval of 95% when ANOVA was applied. The lack of

difference between the analyzed samples is well seen at the histograms representing the distribution of pixels for the camera with 121 and 256 channels respectively (Figure 52, Figure 53)

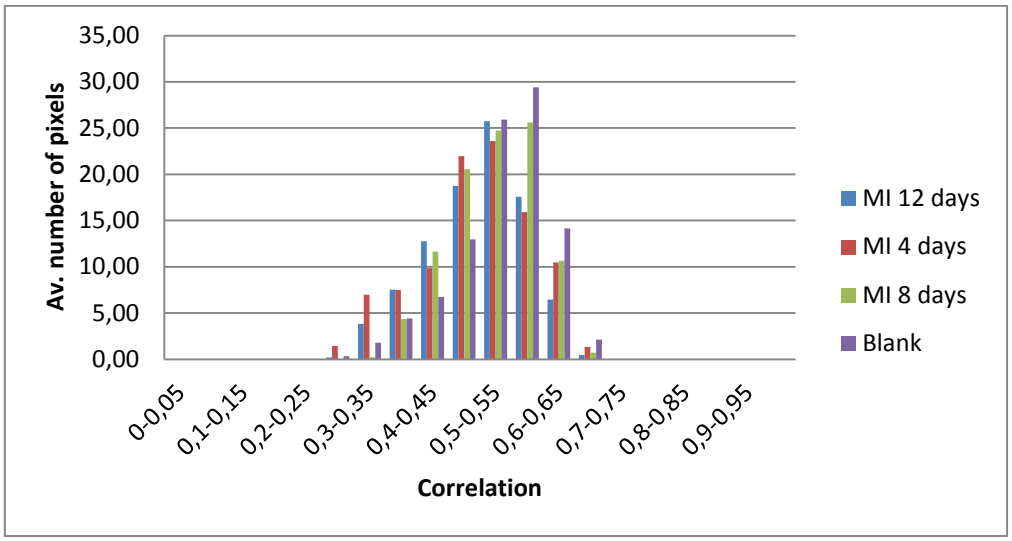

Figure 52. Histograms of the correlation coefficient of HA for samples treated with mixture I during 0,4,8 and 12 days consecutively, acquired with the spectral camera of 121 channels.

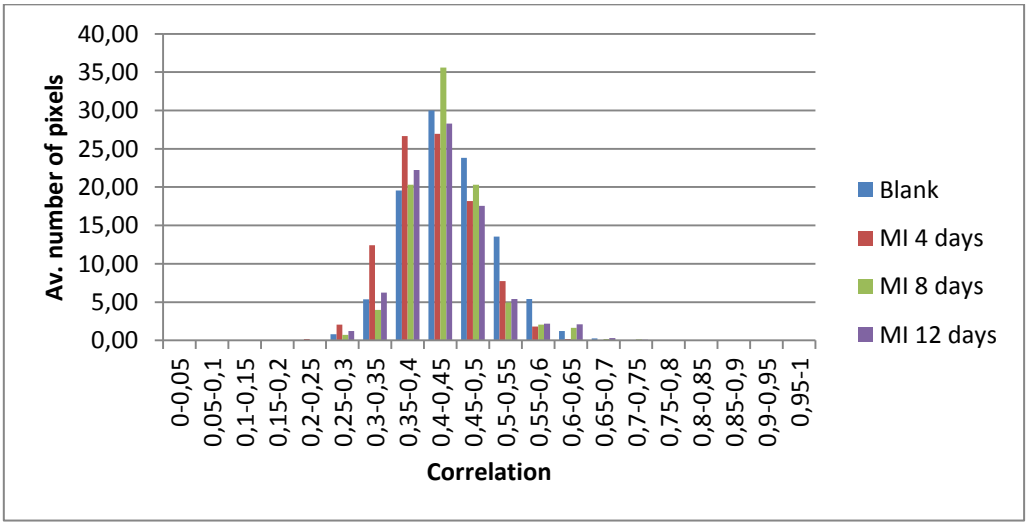

Figure 53. Histograms of the correlation coefficient of HA for samples treated with mixture I during 0,4,8 and 12 days consecutively, acquired with the spectral camera of 256 channels.

18.5.2. Application of the MCR method

The same samples acquired with the 256 channels camera and analyzed with the MCR data treatment reveals differences between the samples (Table 37). Comparing, teeth treated with the remineralising mixture I to the blank samples, the concentration of FA increases and HA decreases with the applied treatment. Once again, as in case of previously discussed treatments, observed fluoridation of teeth was detected in concentrated areas with the simultaneous drop of the HA concentration. In case of blank

samples, there were almost no FA pixels detected (Figure 54). Surprisingly, the highest concentration of FA was detected after 4 days of treatment, whereas the lowest for 12 days.

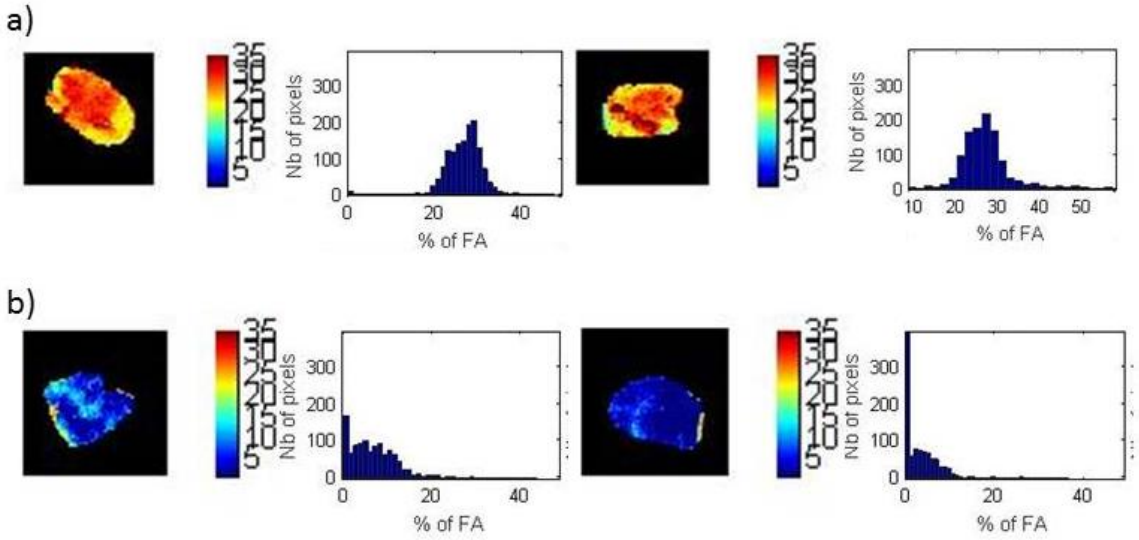

Figure 54. Example of histograms of concentrations of FA for two samples a) treated for 4 days with mixture I b) blank

Although, closer interpretation of the obtained histograms for samples treated during 12 days consecutively (Figure 55) shows that once again the average of the obtained result does not reveal the real characteristics of the obtained results. First five samples reveal low concentrations of the FA whereas another five show much higher (up to 20% of fluoridation degree). It would suggest that maybe there was some experimental error in the treatment performed on those samples and in order to obtain reliable results the experiment should be repeated.

Table 37. Concentration of FA and HA detected for samples treated with mixture I during 0,4,8 and 12 days consecutively, acquired with the spectral camera of 256 channels

	Concentration of HA				Concentration of FA			
	Blank	MI 4 days	MI 8 days	MI 12 days	Blank	MI 4 days	MI 8 days	MI 12 days
Av.	94,7%	80,9%	86,8%	88,1%	5,3%	19,1%	12,7%	11,9%
SD	0,02	0,06	0,01	0,06	0,02	0,06	0,02	0,06

a)

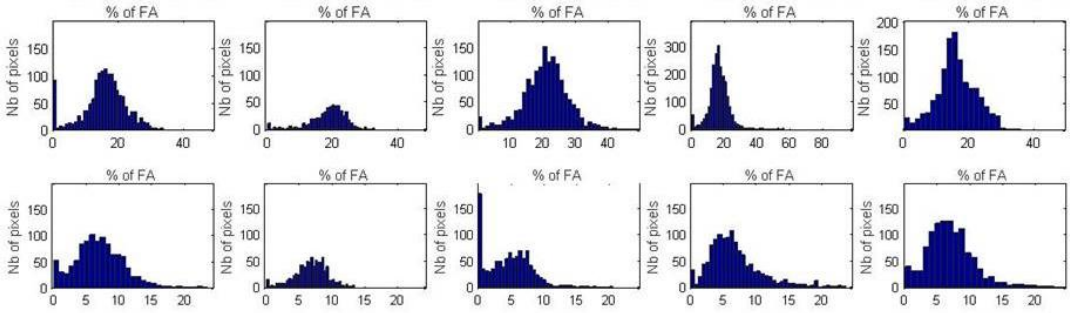

b)

Sample nr	MI 12 days
1	7,07%
2	6,76%
3	4,59%
4	6,68%
5	6,91%
6	15,60%
7	18,39%
8	20,72%
9	16,16%
10	16,14%
Average	11,90%
S.d	0,06

Figure 55. a) Histograms obtained for all samples treated with mixture I for 12 days consecutively b) average percentage concentrations for FA for all 10 samples.

18.6. Daily monitoring of the sample and the durability of the treatment

In order to test how daily treatment is affecting the sample, spectral data of the teeth treated with mixture I,II and III were acquired daily (after performing the entire daily cycle of applications) with the camera of 121 channels.

As a result, it could be observed that for mixture I and III the maximum number of pixels with the same correlation with HA is the lowest before the treatment (at day 0). As a result of the performed applications, this correlation increases and reaches the maximum value of 0,55-0,6 at second day of the treatment. In case of the mixture II, no differences between the blank sample and the treated sample could be observed (Figure 56).

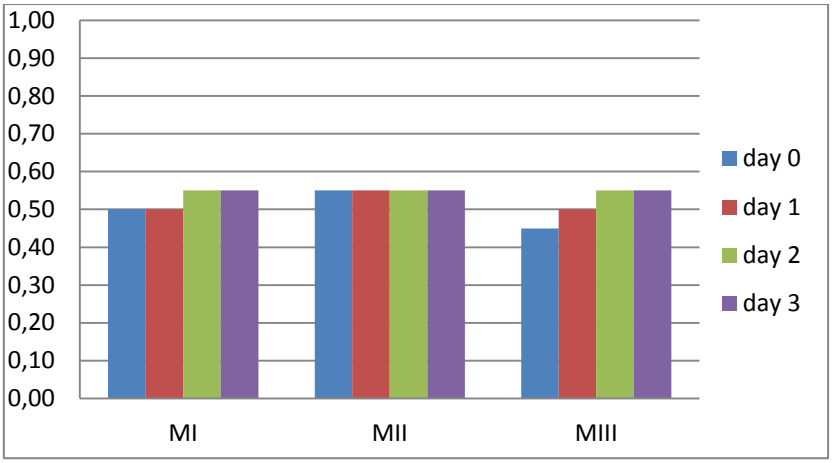

Figure 56. Daily monitoring of the samples treated with mixture I,II and III. Data were gathered at day 0, 1,2 and 3rd with the camera of 121 channels.

Subsequently, the samples were left in the 0,05% chloramine-T solution in the refrigerator for 7 days and again measured. The data revealed a considerable drop in the number of pixels correlated with HA in the measurement delayed in time. The resulting correlations were even smaller than for the sample before the treatment (at day 0) for mixture MI and MII (Figure 57)

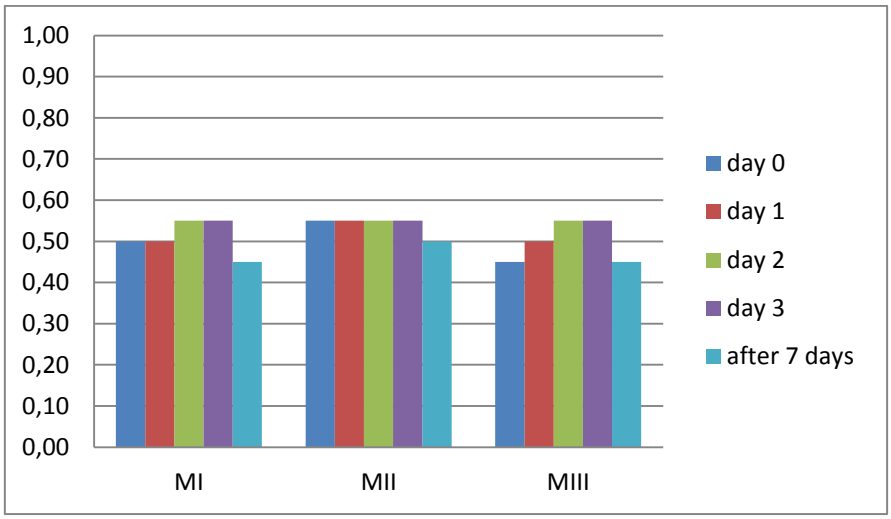

Figure 57.Daily monitoring of the samples treated with mixture I,II and III and the result for the same samples after 7 days without any treatment. Samples were left in the fridge submerged in the solution of antibacterial chloramine-T. Data were gathered with the camera of 161 channels.

18.7. Raman measurements for the evaluation of the fluoridation degree of human enamel

In order to confirm the creation of fluorapatite as a result of the applied treatments, which was detected with NIR Hyper Spectral Imaging, confocal Raman microscopy measurements were performed. Teeth were investigated before and after the treatment followed by a daily monitoring of the treated samples.

18.7.1. Raman measurements of the human enamel

Tooth enamel was successfully detected using Raman microscopy. A spectrum assigned to the etched human enamel, presented in
Figure 58, shows peaks specific for the different stretching and bending vibrations of PO_4 and CO_3 groups of hydroxyapatite. The most prominent peak is represented by the v_1 PO_4^{3-} stretching vibration at 960 cm^{-1}. In addition, further peaks and their spectral assignments are presented in Table 38.

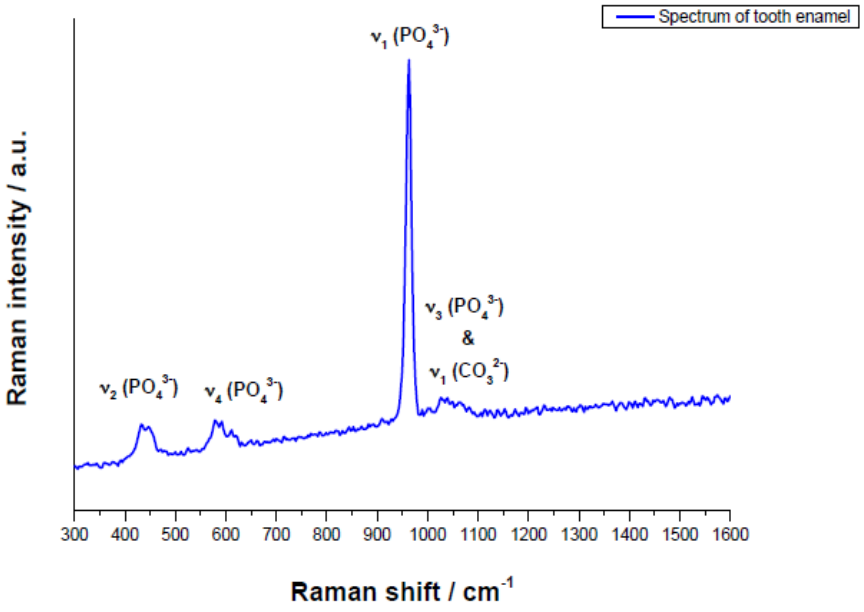

Figure 58 Raman spectrum of the etched human enamel

Table 38. Prominent peaks in the Raman spectrum of the etched human enamel and their spectral assignments

Peak position (cm^{-1})	Assignment
960	v_1 symmetric stretching mode of PO_4^{3-}
431, 446	v_2 symmetric bending mode of PO_4^{3-}
1023, 1043, 1052, 1069	v_3 asymmetric stretching mode of PO_4^{3-}
579, 590, 608, 614	v_4 asymmetric bending mode of PO_4^{3-}
1069	v_1 symmetric stretching mode of type B CO_3^{2-}

18.7.2. HA and FA differentiation

Spectra obtained by recording the etched enamel surface as well as magnified prominent peak region are presented in Figure 59. Differentiation of HA and FA is possible based on a peak shift from 960.14 (HA) to 962.81 (FA).

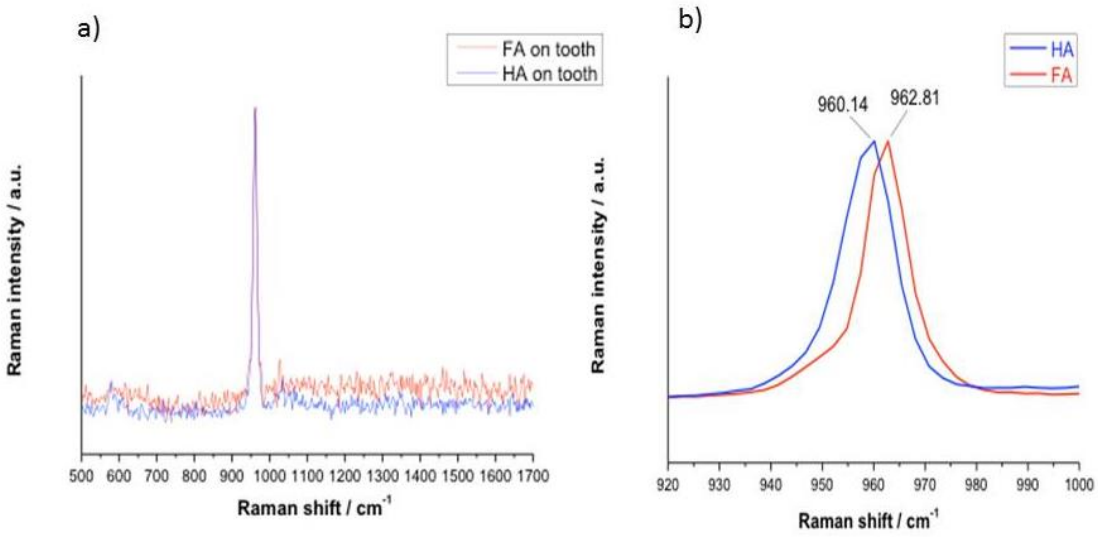

Figure 59. Raman spectra of HA and FA detected on the etched tooth enamel(a) and magnified prominent peak region (b).

18.7.3. Surface topography analysis

Since the tooth enamel has a structured surface, the sampling area needs to be topographically analyzed prior to Raman mapping. One representative topography map which is subsequently used for Raman analysis is presented in
Figure 60.

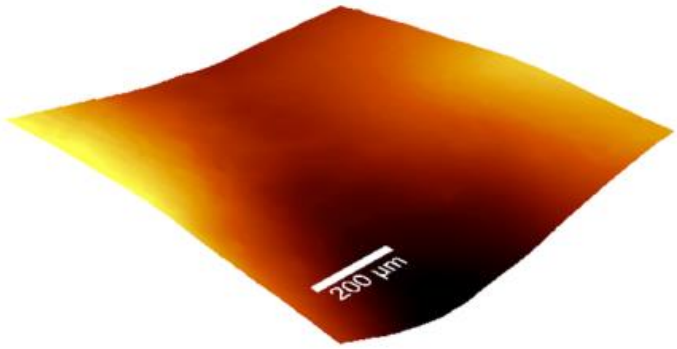

Figure 60. Representative topography map of the tooth surface

18.7.4. Raman analysis of the tooth treated with the commercial toothpaste

Daily monitoring of the samples treated with the commercial toothpaste Sensodyne®, as described in paragraph 17.7, was performed using confocal Raman microscopy. Based on the spectral assignment depicted in

Figure 58, each sampling pixel can be assigned to either HA or FA. Figure 61 visualizes the spatial distribution of HA and FA. Measurement performed before the etching procedure revealed both FA and HA $v_4PO_4^{3-}$ stretching vibrations.

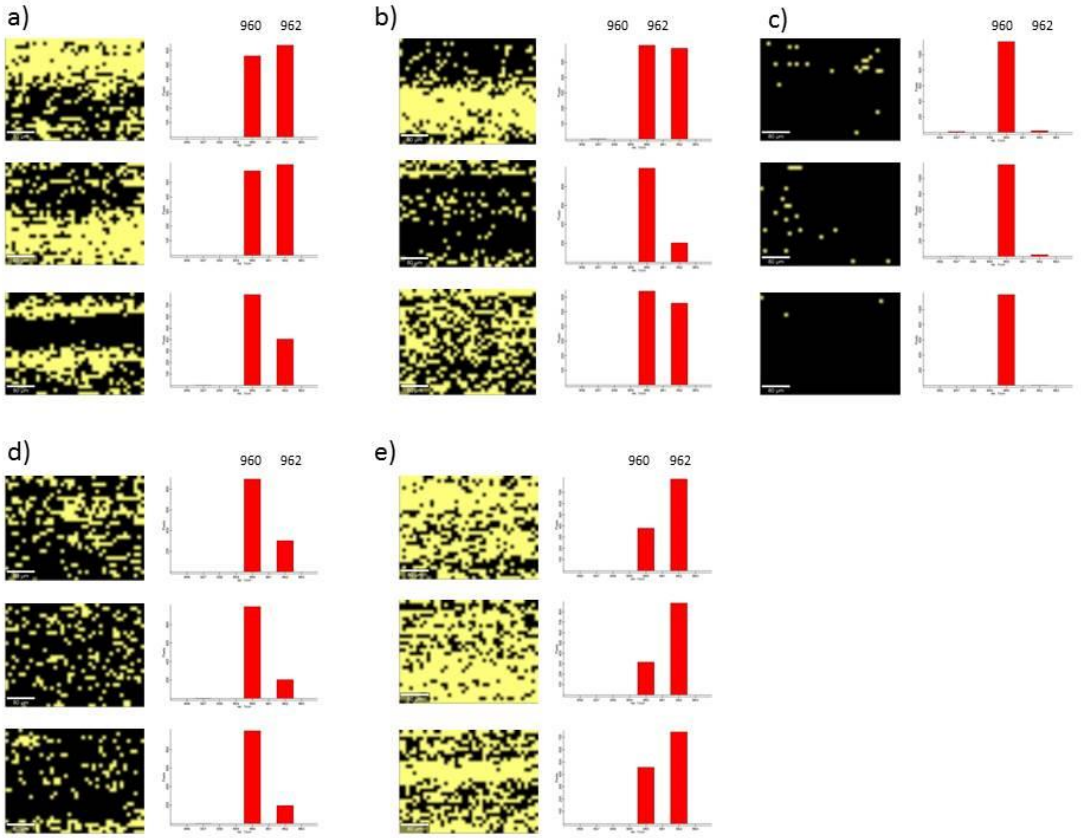

Figure 61. Raman maps of the experimental areas obtained a) before etching, b) after etching procedure and after c) 1 day, d) 2 days and e) 4 days of treatment with Sensodyne.

However, naturally it was not possible to image exactly the same sampling area in the tooth surface after each treatment. Consequently, the degree of fluoridization differs.
This could potentially explain the increased fluoridation degree after the first day of treatment compared to the etched sample. However, the overall trend is evident, as the treatment is followed by increase in fluorapatite, confirming the results obtained with *NIR HSI MCR*.
Based on the distribution maps in Figure 61, the fluoridation degree was calculated applying the following equation:

$$FA_{ratio} = \frac{nr\ of FA\ attributed\ pixels}{total\ number\ of\ pixels} x100\% \quad \text{(Eq.9)}$$

Table 39. Fluoridation degree obtained for all analyzed sampling areas treated with Sensodyne toothpaste (day -1 indicates the tooth before etching, whereas day 0 represents the data after etching).

Day of the treatment	Map	Fluoridation degree [%]
-1	1	53.1
	2	51.8
	3	33.8
0	1	49.1
	2	17.0
	3	46.6
1	1	1.8
	2	1.8
	3	0.3
2	1	25.2
	2	16.9
	3	16.3
4	1	68.3
	2	73.7
	3	61.9

18.7.5. Raman analysis of the tooth treated with the remineralizing mixture III

The same experimental procedure was performed daily on the second half of the same tooth treated with the remineralizing mixture III. Once again, the spatial distribution of HA and FA was visualized (Figure 62) and the fluoridation degree was calculated for all sampling areas (Table 40). Again, as already shown for the treatment with Sensodyne, the overall trend of increase in FA after treatment with the mixture III could be detected. Once again, comparing the data after day 3 and after day 4 of the treatment, the slight decrease in FA concentration could be attributed to sampling slightly different spots on the tooth surface (Figure 62). However, the final fluoridation is comparable to the Sensodyne treatment, indicating the fluorapatite creation as a consequence of the applied treatment.

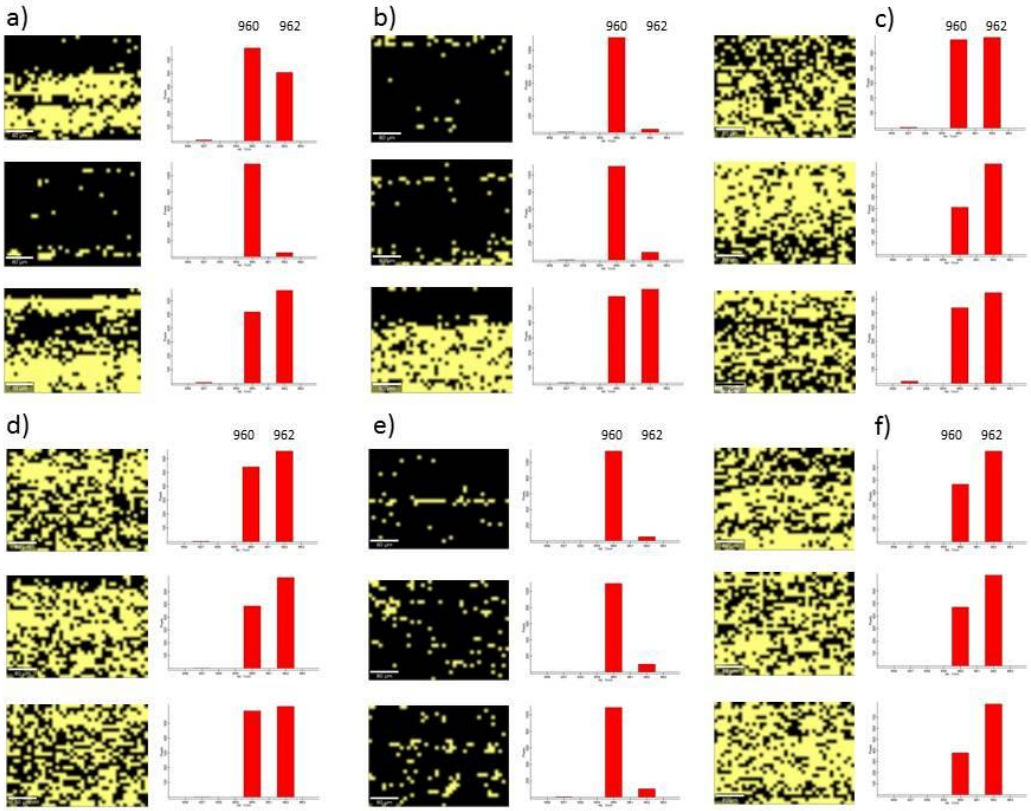

Figure 62. . Raman maps of the experimental areas obtained a) before etching, b) after etching procedure and after c) 1 day, d) 2 days, c) 3 days, d) 4 days of treatment with the remineralizing Mixture III.

Table 40. Fluoridation degree obtained for all analyzed sample areas for sample treated with the mixture III.

Day of the treatment	Map	Fluoridation degree [%]
-1	1	42.2
	2	4.3
	3	56.3
0	1	3.4
	2	7.8
	3	51.9
1	1	50.4
	2	65.8
	3	53.8
2	1	54.6
	2	59.3
	3	51.2
3	1	4.3
	2	8.3
	3	8.7
4	1	61.2
	2	60.7
	3	68.4

18.7.6. Comparison of the commercial Sensodyne toothpaste and the remineralizing mixture III

The comparison of the fluoridation of the tooth enamel after applying Sensodyne and mixture III shows the increment of the fluoridation degree comparing to the etched samples (Figure 63).
Faster fluoridation was achieved with the mixture III, although after 4 days of treatment the fluoridation degrees of both treatments are at almost the same level. Based on these data, the two products can be considered as equivalent.

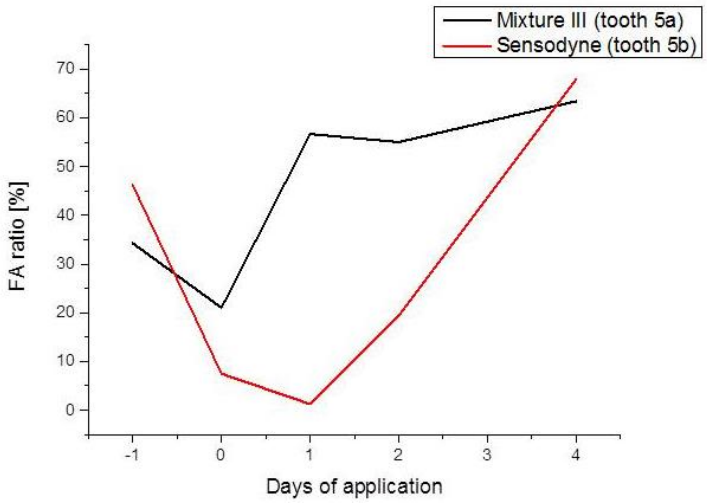

Figure 63. Comparison of the fluoridation degree between two applied treatments

19. Discussion

The main obstacle in the presented work is the differentiation of the fluorpapatite in presence of hydroxyapatite with the NIR methodology. FA is a common substitution of HA. During the creation of the dentine and enamel, fluoride fixes calcium and creates fluorapatite (FA) - a different type of apatite that from the crystallographic point of view differs from hydroxyapatie only in the substitution of the ion OH^- by the F^-. To this structural change, FA can attribute its increased stability that results for example in the bigger resistance to the acid attacks than HA (20). With NIR spectroscopy, the visible vibrations are based on OH^- group; whereas calcium, phosphate or fluoride ions have no relevant signal in NIR region. Thus, the only difference between two apatite species is a change (or a lack) of the OH^- stretching where the group is substituted with the fluoride ion. Consequently, the HA spectra has more intense bands than FA what makes the detection of the FA more difficult.
When it comes to real tooth sample, the differentiation between the etched surface (blank samples) and remineralised one is facilitated due to the favoring scattering effect. The acid treatment changes the enamel structure by dissolving the surface and leads to the mineral loss. As a result, the porosity of the treated surface is greater than in case of

the remineralised one (where the raise in the mineral content occurs). Since the increased porosity increments the scattering effect of the incident light, the reflectivity of the sample changes. Consequently, the detected spectra also change. Described phenomena facilitate the differentiation of the etched surface from the remineralised one (183).

As it was explained, the scattering can have a favorable influence on the detection. However, in this work, also a negative aspect of the phenomena have been encountered. Scattering is the process in which the incident light changes its direction without the loss of the energy. It is deviated from its original straight path as a result of the interaction with irregular surface (183) (Figure 64). In this sense, the negative scattering effect was encountered on the edges of some teeth samples or in other small irregularities (hollows). In those locations, an increase in the fluorapatite detection was encountered what could be cause by a scattering effect. However, it could also be induced by the fact that in the irregularities or at the edges of the sample, a bigger amount of the remineralised agent is gathered and that could result in more efficient remineralization of those zones. Nevertheless, in order to better study the described finding further experiments should be performed.

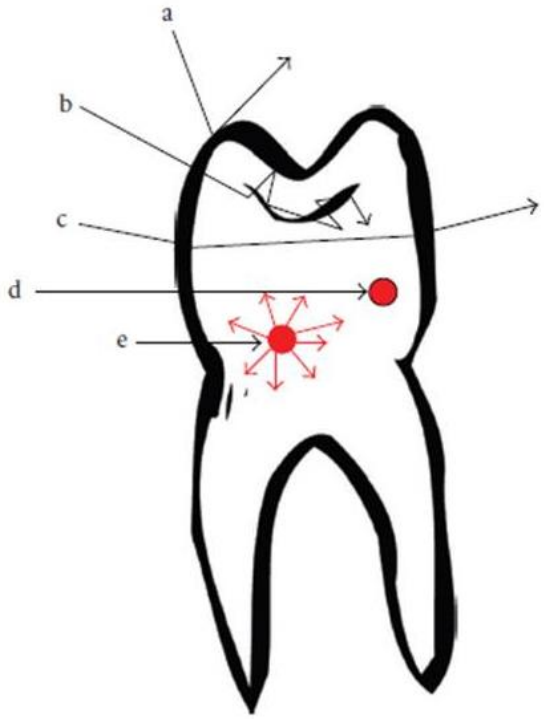

Figure 64. Scheme of some common interactions of the light with the tooth. A) a rebound of the incident light, b)Light enters the tooth and photons are deviated inside of it. Photons then leave the tooth as backscattering (leave from the same surface as it entered) or with another surface (diffused transmission), c) transmission, d) absorption with heat production, e) absorption with fluorescence

Due to the described difficulty, the MCR method appears to be more suitable than correlation coefficient for the FA determination in presence of HA. Correlation method is using the reference spectra (HA and FA apatite powders) and is trying to detect the similarity between the sample spectra and the pure reference spectra (133). Since the spectra of the teeth differ from the pure apatite, due to its additional constituents, this

type of differentiation is more difficult. Moreover, the similarity of FA and HA spectra is not facilitating the differentiation either. With the MCR method, on the other hand, one can find the estimated spectra in the model that is the most similar, but not exactly the same as the reference one. Unlike in the correlation coefficient method the pure spectra are not necessary but can help in the initial estimates (137). With a well selected number of components necessary for the calculation, an MCR analyses can easily be performed. In the presented approach, most of the times, FA is detected indirectly. That means that where the HA could not be found the rest of the detected pixels can be classified as the one proceeding from fluorapatite signal.

Another problem encountered during the data treatment was the influence of the embedding polymer on the spectra classification. The signal that came from the polymer was strong and affected the differentiation of the apatite species making the detection of FA even more difficult (Figure 65). Once again, the MCR method occurred to be more reliable in the separation of the polymer spectra from the sample proceeding signals. The correlation coefficient method is more sensible to the side effects such as scattering or interferences from other spectral species such as structural elements or polymer. Presence of the additional spectra is not so disturbing when the pure spectra are considered but when the sought spectra are not pure the differentiation is once again interrupted.

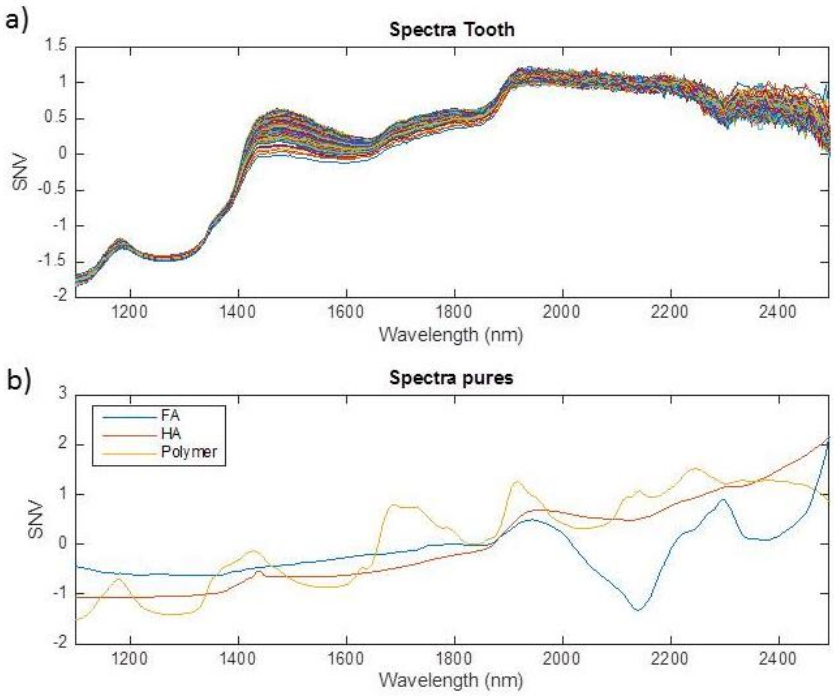

Figure 65. a)An example of spectra extracted from the tooth image b) Comparison of spectra of the pure reference apatites and the embedding polymer

When it comes to the comparison of two spectral cameras used during the measurements, the one that appears to be more suitable for the teeth study is the 256 channel SisuChema Hyperspectral Scanner^{TM} due to its technical characteristics. It has

better spectral resolution and wavelength range than 121 channels camera. As it is demonstrated at Figure 40, the 256 channels camera delivers more information facilitating the differentiation of the two apatite species. Another important aspect is the possibility to control the distance of the camera from the conveyor belt. It is important for small samples such as teeth where the studied region is small, since shorter distance to the detector facilitates acquiring more detailed image. Therefore, the 256 channels is more suitable for the teeth study when detailed analyses needs to be performed. The 121 channels camera can be used for the FA and HA determination although the differentiation becomes more difficult.

When the correlation coefficient was applied for both cameras, a higher correlation with HA for treated samples than for the blank samples was generally observed. On the other hand, for the MCR method it is the opposite: the concentration of HA diminishes for treated samples and concentration of FA increases, whereas there is almost no detection of FA for the correlation method. Such phenomena are possibly caused by the fact that with the correlation method most of the FA stays undetected and is classified as HA pixels due to previously described problems in the FA determination (influence of polymer, additional structural elements, scattering and similarity of the apatite spectra). We suspect that the increase in the HA pixels in the correlation method can be attributed to an increase of the number of FA spectra that were wrongly classified as HA spectra. Nevertheless, this type of classification can lead to misleading results what is a huge weakness of the method.

Another common observation for the correlation coefficient method is a shift in the pixels histograms when the 256 channels camera is applied. These phenomena can be explained with the additional information that is delivered when this camera is applied. Most of all, because of the wider wave range, spectra contains more information what changes the final classification of pixels.

Raman measurements confirmed the creation of fluorapatite in case of samples treated with Sensodyne as well as mixture III as a more accurate approach in high spatial resolution. Here, the complementary aspect of using two analytical techniques is highlighted, as NIR HSI cannot provide the required spatial resolution and chemical selectivity as Raman microscopy, but due to the bigger pixel size can be used to acquire scans of the full tooth surface with minimal time effort, thus minimizing misleading results due to overestimation of local artifacts.

Data obtained from samples treated with the commercial toothpaste revealed less concentration of FA than data of samples treated with the remineralising mixture III. The most effective remineralising product among the commercial toothpastes was Sensodyne that reached an average of 7,8% fluoridation after 4 days of applications. In comparison, the most effective among the remineralising ion exchange resins was mixture II that contained a medium dose of the fluoride applied (16,1% of fluoridation). The less effective was mixture III that did not reveal any changes comparing to blank samples. With Raman measurements, we could observe that although the etching

procedure diminishes the level of the FA present on the tooth surface, FA is not eliminated completely. The same conclusion can be derived from the *NIR HSI MCR* analysis. With this methodology, mixture III is less effective in enhancing the remineralization process, whereas in Raman measurements show an increase in the fluoridation degree. Here, strengths and limitations of the two methods play a role again. *NIR HSI* can sample bigger areas with low spatial resolution, whereas Raman microscopy can sample small areas with high resolution. The experimental spots areas analyzed within Raman spectroscopy are limited in size, due to the applied spatial resolution. As a result, this method cannot be absolutely reliable from the quantitative aspect and performed measurements are not representative for the entire sample. *NIR HSI MCR* measurement, on the other hand, cover the entire sample and the results obtained with this method can be by such considered representative for the applied treatment efficacy, although it is limited by the artifacts proceeding from the complexity of the applied data treatment and surface irregularities.

The fact that the overall fluoridation degree obtained with sample treated with mixture III is even smaller than for the blank sample (etched sample) is possible since the analyzed tooth was not the same one and the obtained data are of approximately the same degree (4,9% for the blank and 4,6% for the mixture III). In the applied mixtures the mass ratios of the phosphate and calcium ion stays the same (3:2 respectively) whereas the concentration of the fluoride raises from mixture I to III (paragraph 17.5). The raise in the fluoridation degree for the mixture I and II is caused by the creation of the fluorapatite on the surface of the teeth as a result of the applied treatment. The small amount of fluorapatite detected for the mixture III could be explained by the possible co-precipitation of the calcium fluoride preventing the formation of fluorapatite. Very interesting conclusion that could be made after performed experiments is that observed changes (increment of the HA correlated pixels for the correlation method and rise of the concentration of FA with the simultaneous drop in the HA concentration for the MCR method) are detected in concentrated areas. Samples that were only treated with acid on the other hand resemble a homogeneous distribution of HA among the observed teeth. We suppose that the remineralization process, understood in here as a creation of fluorapatite, proceeds in zones. The fluoride substitution does not appear to be a homogenous process where fluorapatite is distributed all over the treated sample. It is rather concentrated in small, remineralised areas. It can be confirmed by the Raman measurements, where small dislocation of the experimental spot leaded do detection of different FA or HA concentrations.

In case of the experiment that implemented the application of mixture III (paragraph 18.3.2) and the prolongation of the treatment (paragraph 18.5.2), the analyzed histograms of obtained samples did not coincide with the information extracted from the average fluoridation degree. In our opinion, the average value should be treated as an indicator of the efficacy of the treatment and not as a general conclusion. In order to better represent the information about the changes that causes the application of each

treatment, all images and histograms of samples should be analyzed and compared separately.

The application of the protein revealed a smaller fluoridation degree than in case of samples treated without the protein application. According to Y. Fan (190) et al. the optimal conditions for the fluorapatite growth controlled by the amelogenin are pH 6.8 ± 0.4 Outside this range, crystals are loose nanorods or plate-like shape that because of their porous characteristics would not facilitate the remineralization process of teeth (187), (23), (172). As to the presence of amelogenin, the concentration range was of 40 ± 10 µg/ml and the fluoride concentration of 1.5 ± 0.5 mg/l. In the mentioned study, florapatite is created in solution, whereas in the presented study fluorapatite is growing on the surface of the teeth with artificial saliva as a unique solvent. Although all other conditions (pH and concentration of the protein) were maintained, the fluoride level could not be maintained due to different environment evolution during the experiment. Since the best result was achieved for the lowest concentration of the fluoride, probably, the applied fluoride concentration was too big for proper functioning of the amelogenin. Thus, in our opinion, the experiment should be performed with lover levels of fluoride ions to be delivered during the process to observe the influence of the protein.

The experiment with the treatment prolongation, revealed the highest concentrations of the fluorapatite after 4 days of treatment. Surprisingly, the extension of the treatment interval to 12 days did not result in growth of the remineralised zone. Since a possible experimental error was detected for some samples, additional daily monitoring of the remineralising treatments at the same dental sample should be performed in order to get better knowledge of the characteristics of the process of remineralization.

Daily monitoring of the samples showed an increment of the HA correlated pixels for mixture I and III throughout the days when the treatment was performed. Since for the correlation method the pixels with increased correlation with HA can be identified as a possible FA creation, such an increment would suggest the remineralization of measured samples. The measurement performed on the same samples after 7 days without treatment revealed a drop in the HA correlated pixels. It could be suggested that the created remineralised layer was washed away with time, although further experiments should be performed preferably with the 256 channels camera and the MCR as a data treatment approach in order to confirm such a hypothesis.

20. Conclusions

As a result of the performed study the following conclusions can be presented:

- ✓ NIR HSI is a method that allows differentiating remineralised tissue from the demineralized one
- ✓ NIR HSI with the MCR multivariate data analysis allows comparing the efficacy of various remineralizing treatment and characterization of the enamel surface that

undercame during the remineralization process. It also shows the distribution of the deposited fluorapatite on the tooth surface

- ✓ Correlation coefficient method is not a suitable method for the determination of fluorapatite on the dentinal tissue since it did not differentiate the fluorapatite from the hydroxyapatite and it is influenced by the embedding polymer contribution
- ✓ 256 channels camera delivers more information about the sample due to its wider spectral range and better spectral resolution
- ✓ Raman measurements confirmed the creation of fluorapatite in case of samples treated with Sensodyne as well as mixture III
- ✓ Since Raman microscopy can sample small areas with high resolution it properly detects the fluorapatite. However, it does not give the information about its distribution over the sample. Thus it can be applied as a verifying methodology but it cannot be used for quantitative studies.
- ✓ As a result of the performed NIR HSI MCR study it could be observed that:
    - the most effective remineralising product among the commercial toothpastes was Sensodyne;
    - the most effective among the remineralising ion exchange resins was mixture II that contained a medium dose of the fluoride;
    - the extension of the treatment interval to 12 days did not result in growth of the remineralised zone although there was a probable experimental error encountered in this study;
    - The application of the protein revealed a smaller fluoridation degree than in case of samples treated without the protein. Probably, the fluoride concentration was too high for the proper functioning of the amelogenin
- ✓ The application of the correlation coefficient for the daily monitoring of the remineralising process showed an increment of the HA correlated pixels for mixture I and III throughout the days when the treatment was performed. An experiment repeated after 7 days without treatment suggest that created remineralised layer was washed away with time.

STUDY OF THE REMINERALISED HUMAN DENTAL TISSUES BY THE SYNCHROTRON INFRARED SPECTROSCOPIC ELLIPSOMETRY: OPTICAL CONSTANTS DETERMINATION

Summary of the study

Objectives

Although multiple studies were performed on human dental tissue, still the influence of the remineralization process on the structure and chemical composition of enamel and dentin is not fully discovered. In present study, Infrared Spectroscopic Ellipsometry (IRSE) and synchrotron ellipsometry are proposed for the determination of the optical constants of human dental tissues.

Methodology

Human teeth were treated with the remineralising agent (NMTD) and analyzed with the synchrotron IR ellipsometer. A cross section of the tooth was acquired and analyzed. Reference samples were measures with the laboratory ellipsometer of the internal source of light and FTIR spectrometer at ISAS facility.

Results

Differences in the spectral signature depending on the position of the experimental point in the tooth were observed when synchrotron IRSE was implemented.

In order to construct an experimental model for the synchrotron data interpretation two types of reference samples were measure: pure apatites (hydroxyl and fluorapatite) and etched human teeth.

Optical constants derived from the powder reference apatites could not be applied in order to compare them with the experimental data of the real tooth sample due to spectral differences between reference and experimental samples. However, similarities between spectra of teeth reference samples and synchrotron measurements were encountered. It could be concluded that a sample where traditional demineralisation was performed (acid etching) corresponds to the upper part of the enamel whereas severely demineralized samples correspond to deeper parts of the tooth.

Conclusions

Performed simulations revealed high similarity of the obtained reference spectra to the experimental synchrotron spots. That allows suspecting that once reference samples are analyzed with the synchrotron IRSE method, valuable information about the influence of the remineralising treatment on the dental tissue structure and composition will be revealed.

Introduction

Dental caries are defined as localized damages of the hard tissue caused by the acids produced during the bacterial activity in the buccal plaque. The process begins in the bacterial biofilm by the fermentation of the carbohydrates and starts to be visible on the hard tissue. Dental caries are the most common reason of the oral pain and the tooth loss (7).

The process of demineralisation and remineralisation takes place constantly during the day in the oral cavity. The balance between those two processes stop, reverse or maintains the progress of the creation of caries. Without any doubt the most popular agent that enhances the remineralization is fluoride. Beside the antibacterial properties at low concentrations, fluoride stops the demineralization and favours the opposite-remineralizing process on the tooth surface (section 5).

In order to characterize the tooth surface a big number of methodologies have been applied (section 7).

Although multiple studies were performed on human dental tissue, still the influence of the remineralization process on the structure and chemical composition of enamel and dentin is not fully understood. In present study, Infrared Spectroscopic Ellipsometry (IRSE) and synchrotron ellipsometry are proposed for the determination of the optical constants of human dental tissues.

Ellipsometric studies are getting popular nowadays especially in composition, thickness or roughness determination of organic films and multilayers (191). When determined properties are changing along the probed material, the polarization degree is affected, and very sophisticated models are required to process the obtained data. In order to apply a reasonably defined angle, the spot size of the probed sample has to be limited. Sometimes, it has to be set close to the diffraction limit. It means that IR ellipsometry is limited by the degree of the brightness of the light. In order to improve it, the synchrotron storage rings have been applied (126).

Nowadays there are three instruments that apply the IR synchrotron radiation in ellipsometric measurements: NSLS in Brookhaven (New York), ANKA in Karlsruhe (Germany) and IRIS at BESSY II in Berlin. The last one, constructed as a micro-focus mapping ellipsometer, was applied in present work. The experimental set up allows to scan the area of 50x50mm, has a spectral range of 2,5-30µm (4000-333 cm^{-1}) (126) and lateral resolution below 1 mm^2 whereas the traditional ellipsometers are of around 50 mm^2 (127).

Although there is a big increment of the noise produced by accelerator source, the sensitivity improves enormously thanks to the brilliance provided by the synchrotron light, that is twice the magnitude of the Globar source instrumentation. Its first commissioning was performed in 2003 and since than it has been applied in many investigations but mainly in the area of thin films (126). In the present work the

synchrotron ellipsometry was applied to determine optical constants of the remineralised human dental tissue what would allow to explore the changes in the dental structure caused by such treatment.

In order to extract all necessary data from the synchrotron ellipsometric measurements well matched reference samples are indispensable. In the present study, a series of experiments to evaluate the characteristics of an adequate dental reference sample for the synchrotron ISRE measurements are presented.

Experimental Section

21. Methodology

21.1. Specimen preparation

Human teeth extracted from patients of age between 20-50 years old were extracted and carefully selected to obtain specimens lacking any defects like cementoenamel defects or dental caries that could affect results of the study. After the extraction, specimens were stored in a 0,05% Chloramine-T solution that besides its antibacterial properties also prevents the precipitation of ions.
Subsequently, the teeth were immobilized in a Triplex Cold ® polymer (Ivoclar Vivadent, Liechtenstein) and Epofix™ Cold-Setting Embedding Resin (Struers, USA) once the remineralising treatment was performed. Subsequently, samples were longitudinally cut using the diamond saw (Southbay Technology Inc., USA.) to obtain a cross section of the tooth (excluding the root).

21.2. Reference apatite samples

Reference sample of the hydroxyapatite (HA) were of analytical grade and was used as received without any further purification (>90%, Fluka, Sigma-Aldrich, Germany).
The fluorapatite (FA) reference powder was synthetized in the solid phase reaction (192). Calcium fluoride (95%, Riedel de Haen, Sigma-Aldrich ,Germany) and tricalcium phosphate (35-40% (Ca), Panreac, Spain) were mixed in the agate miller at the ratio of 1.67 Ca/P. Subsequently, the reagents were placed in the electric oven (Selecta 366 PE, Spain) and heated to 1200˚C during 2 hours. The solid FA was then grounded during 15 min. into powder.

21.3. Reference teeth samples

Three different teeth samples were at first etched with 1M HCl for 30 seconds to simulate the early stage caries creation. Another three samples were etched with 1M HCl for 30 seconds with a constant flow of the nitrogen gas through the acid solution.

21.4. Treatment performance

Previously etched teeth were treated with the NMTD remineralising agent (48). Approximately 0.5 g of the product was mixed with few drops of artificial saliva (KCl 0,625 g/l; $CaCl_2 \cdot 2H_2O$ 0,166 g/l, K_2HPO_4 0,804 g/l; pH 6,8 ± 0,4) to obtain the optimal consistence for its further application on the enamel surface. The coating was changed every 12 hours and the treatment lasted 4 days. The NMTD agent was renewed by

carefully washing the specimens with artificial saliva and applying a fresh portion of NMTD. During the time of the experiment, samples were placed in the incubator to maintain it in the natural temperature of the mouth that is in 37°C. Once the treatment was finished the samples were stored under a relative humidity of 100% in a 0,5% chloramine –T solution in the refrigerator.

21.5. Instrumentation

The samples were analyzed by using IR spectroscopic ellipsometry in the laboratory and at the synchrotron BESSY facility in Berlin. In the laboratory, IR spectroscopic ellipsometry measurements were performed on a custom-build ellipsometric set-up in the mid-IR spectral range (4000-400 cm^{-1}) attached to a Bruker Tensor 37® (Germany) Fourier transform spectrometer. Measurements were performed with a spectral resolution of 4 cm^{-1} using a photovoltaic mercury cadmium telluride (MCT) detector cooled by liquid nitrogen. Incidence angles in the range between 50-70° were used.
At the synchrotron facility, a mapping ellipsometer attached to a BRUKER IFS 66/v was used. The mapping system provided a lateral resolution below 500 μm^2 using a photovoltaic mercury-cadmium-telluride (MCT) detector.
The principle of ellipsometry is the following: Incident linearly polarized radiation is reflected from the sample surface as elliptically polarized radiation described via the ellipsometric parameters: $tan\Psi$ and Δ. $tan\Psi$ is the amplitude ratio and Δ for the phase shift difference of the orthogonally p- and s- polarized components of the reflected waves (r_s and r_p). The ellipsometric parameters are defined by the quantity ρ, which is the ratio of the complex reflection coefficients r_p and r_s:

$$\rho = \frac{r_p}{r_s} = \tan\Psi \cdot e^{i\Delta} \quad \text{(Eq.10)}$$

For the reference measurements of bulk samples, the measured ellipsometric parameters could be directly converted to the complex optical constant $\tilde{n}$ defined by the real refractive index n and the absorption index k:

$$\tilde{n} = n + ik \quad \text{(Eq.11)}$$

For these bulk samples (half space samples neglecting any surface contributions), the complex optical constant can be calculated directly at certain angle of incidence φ (193).

$$\tilde{n}^2 = sin^2(\varphi)\left[1 + \left(\frac{1-\rho}{1+\rho}\right)^2 \tan(\varphi)^2\right] \quad \text{(Eq.12)}$$

For all other evaluations, where layered samples need to be considered, the simulations were performed with optical layer models (see 1.7.)
Microscopic measurements were performed with a Bruker Hyperion 3000 FTIR microscope using a Cassegrain objective (15x) with numerical aperture of 0.4 (*f*). In order

to ensure best linearity of the detected signals, the microscope was equipped with a photovoltaic mercury cadmium telluride detector. All spectra were taken with a spectral resolution of 4 cm^{-1}.

21.6. Data processing

The ellipsometry software, SpectraRay/3 from SENTECH Instruments GmbH Germany was used for optical modeling.

22. Results and Discussion

22.1. Measurements of the reference apatite samples

In order to understand the ellipsometric spectra of the measured teeth, reference apatite samples were studied. For this purpose, hydroxyapatite and fluorapatite powders were compressed with the KBr powder in order to obtain the corresponding pellets. Measurements were performed at the laboratory ellipsometer at the incidence angle of 70˚.

By the comparison of the resulting refractive index (n) and absorption index (k) of the two reference apatites it could be observed that the main difference between the two reference samples could be encountered in the 1000-1100 cm^{-1} region (

Figure 66,

Figure 67) where phosphate vibrations are located. For both optical constants, the band around 1080 cm^{-1} is more intense in case of the HA (n=0.82 , k=1) comparing to the FA (n=0.57 , k=0.81) . Moreover, for the absorption index (k) a sharp peak could be differentiated: for the FA powder at 1084 cm^{-1}, whereas a broader one and located at 1088 cm^{-1} for HA spectra.

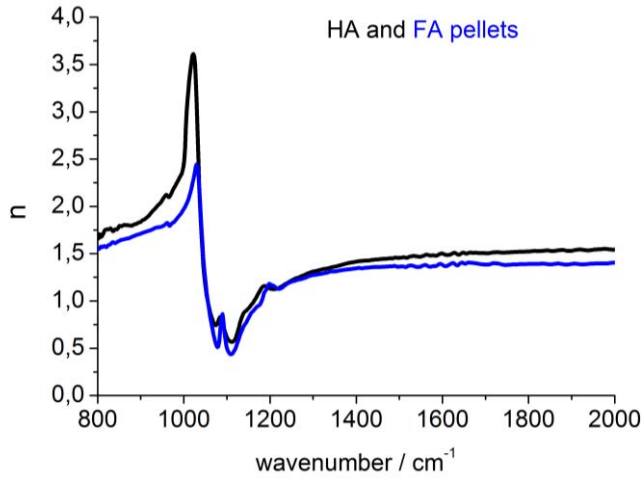

Figure 66. Resulting refractive indexes of the reference HA and FA powders measured at the laboratory ellipsometer.

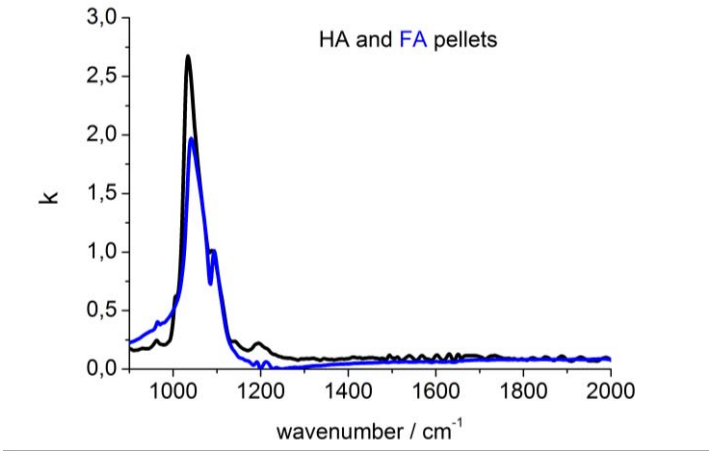

Figure 67. Resulting absorption indexes of the reference HA and FA powders measured at the laboratory ellipsometer.

22.2. Determination of the possible contributions of the embedding polymers

In order to ascertain whether there are spectral contributions of the embedding polymers used during the sample preparation with the apatite reference samples, a comparison of all four spectra was performed. It could be observed that in the region where the two species could be differentiated (1000-1100 cm^{-1}) no important contribution from the embedding polymers could be distinguished for both refractive and absorption index(Figure 68, Figure 69). Larger bands could be encountered around 1400 cm^{-1} and 1750 cm^{-1}, however, since in those regions there are no important bands for neither HA nor FA, discussed contributions could be neglected in case of the differentiation of the reference apatites, in presence of the embedding polymers.

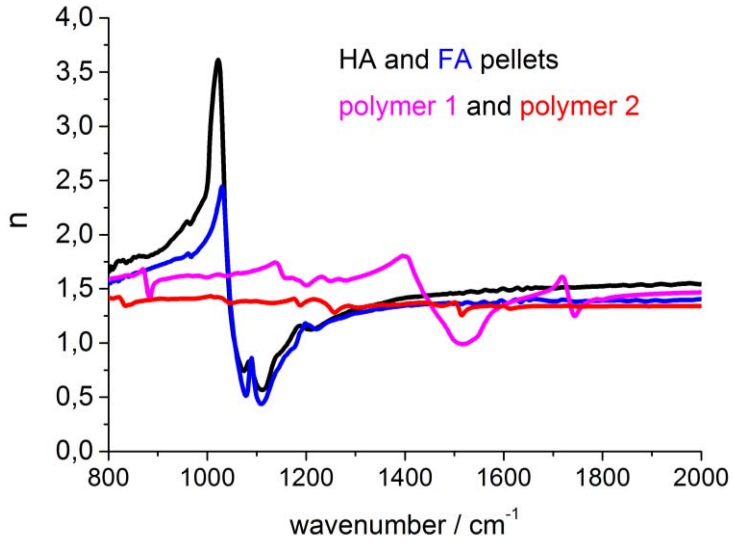

Figure 68. Resulting refractive index of the embedding polymers compared with the reference HA and FA powders measured at the laboratory ellipsometer.

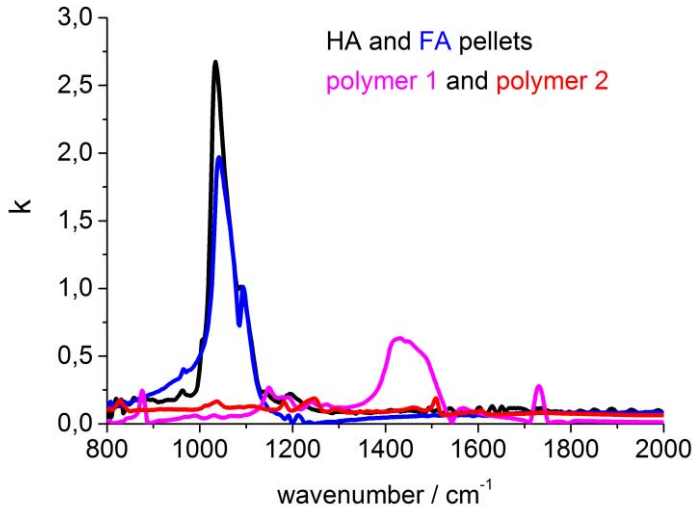

Figure 69. . Resulting absorption index of the embedding polymers compared with the reference HA and FA powders measured at the laboratory ellipsometer.

Comparison of the synchrotron IRSE measurements the previous laboratory experiments In order to obtain a cross – section line of a human tooth a sampling of the longitudinally cut teeth was performed with the synchrotron IR mapping ellipsometer. One spectrum was acquired every 0,5 mm. As a result, 14 spots in a line that included the spectra proceeding from the embedding polymer, enamel and dentin were obtained(Figure 70, Figure 71)

.

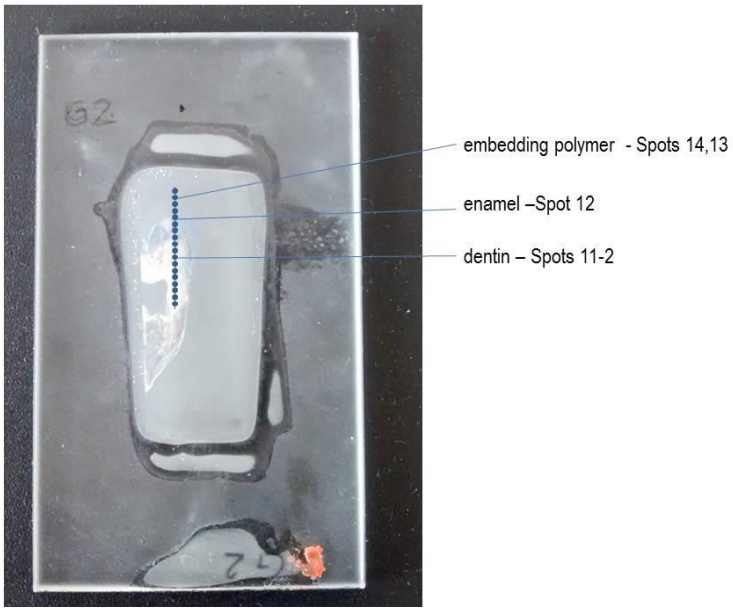

Figure 70. Experimental spots acquired at the synchrotron IRSE experiment on the remineralised tooth sample

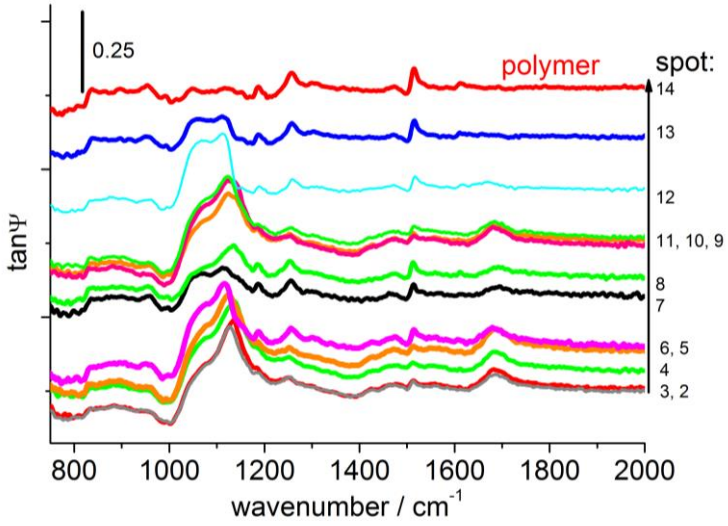

Figure 71. Ellipsometric linescan polymer-enamel-dentin. Baseline shifted for convenience, line scan 0,5 mm steps. Spot 14: polymer, 13: interface, 12:enamel, 11- 2 dentin.

As a result of the calculated tanΨ spectra, on base of the reference optical constants determined for the laboratory samples, it could be observed that the polymer spectra showed similar behavior in both laboratory and synchrotron (Figure 72). Such a coincidence, allows us to claim that the measurements performed at both experimental set-ups coincide and can be further compared.

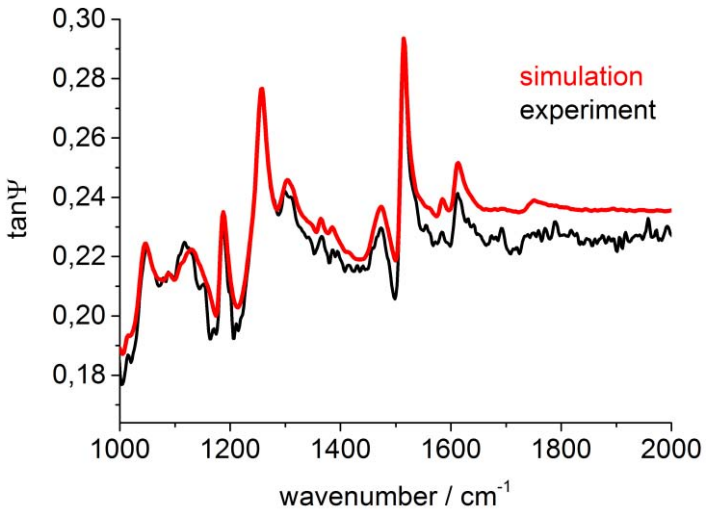

Figure 72. Comparison of the embedding polymer spectra obtained during the synchrotron (black) and laboratory (red) experiments.

For the following spots, four spectra: the synchrotron spectra and the calculated HA, FA and polymer spectra were overlapped in order to compare them. As a result of such a comparison some differences could be encountered.

A clear contribution of the polymer peaks at around 1500 and 1250 cm^{-1} into the tooth spectra was detected. Probably due to the imperfect surfaces, since the probed spot

areas, partially included part of the polymer matrix. Described contribution could be found in all of the resulting spots (Figure 72).

There are differences in the number of bands and its positions when the tooth spot is compared with the reference (Figure 73). A doublet around 1000-1200 cm^{-1} can be differentiated for the HA and FA powders whereas for the tooth spots the spectra vary. In case of the spot 12, that represents the enamel spectra, a similar broad peak in that region could be differentiated, although it is moved into the smaller wavelengths comparing to the spectra of the reference apatites (Figure 73 b)Moreover, it is not as well separated as in case of the reference samples. On the other hand, in case of the spot 11, a completely different shape of the discussed peaks could be observe (Figure 73 a). Such difference confirms that the spot was acquired at the dentin of the tooth. Also, a presence of a band around 1680 cm^{-1}, where the amide I vibrations are detected, indicates the presence of the protein, that has been already encountered in the human dentin. The main protein present in the dentin is collagen type I. It has a form of elongated fibrils that are covered with glycoproteins and proteoglycans (31). Mature enamel, on the other hand, is almost without the protein, its content is up to 1% of weight (17), (30).

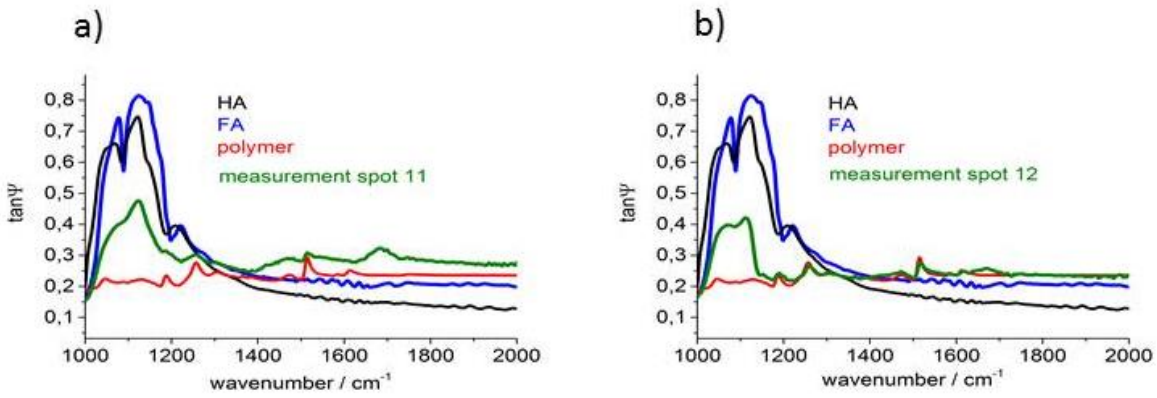

Figure 73. Comparison of the a) dentin and b) enamel spectra obtained at the synchrotron ellipsometer.

Going deeper into the dentin, the main band maintains its previous shape and reveals the similarity to the spot 11 (Figure 74). The protein band is seen also for deeper regions of the dentin at almost constant level.

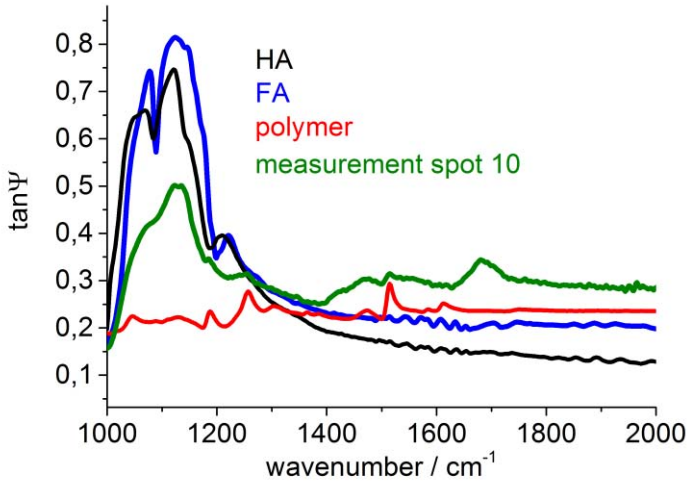

Figure 74. Spectra of the deeper parts of the dentin obtained at the synchrotron ellipsometer.

22.3. Measurements of reference teeth samples with defined treatments

Since there were clear spectral differences encountered between reference apatite samples and the tooth spectra at each experimental spot of the tooth, additional measurements at the laboratory ellipsometer were performed. In order to obtain an adequate reference samples for the synchrotron experiment, two type of teeth samples were prepared: first etched with traditional acid etching procedure and the second one, etched with more aggressive oxidant (acid + nitrogen) (three duplicates of each treatment) (paragraph 21.3). Both treatments were employed to simulate the process of desmineralisation of a dental tissue: first traditional one, second severe one. Described samples were then measured at the 50˚ and 70˚ incidence angle (Figure 75).

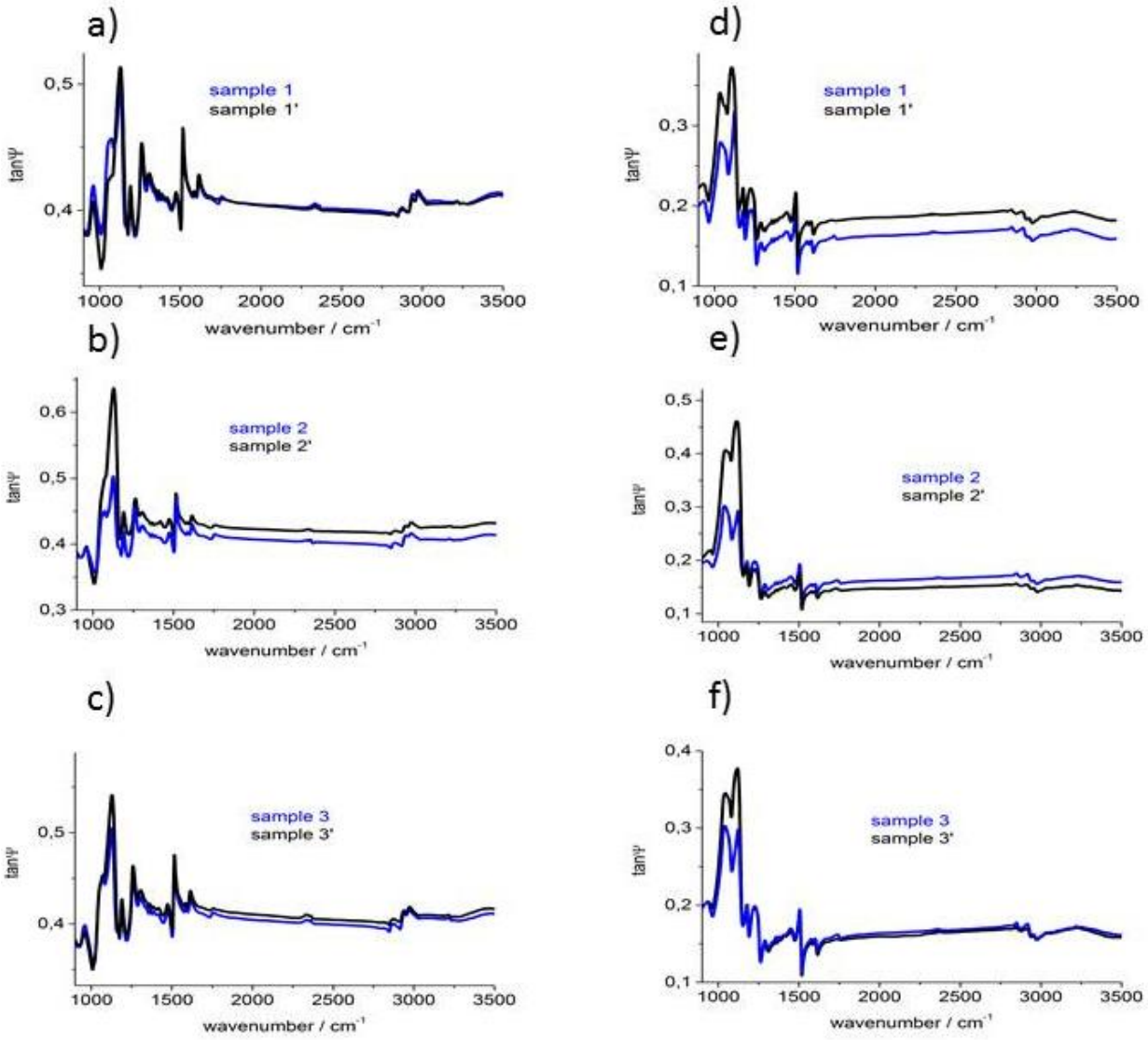

Figure 75. Ellipsometric tanΨ measurements of the traditionally desmineralised (blue) and severely desmineralised (black) reference samples at 50˚ (a), b),c)) and 70˚ (d),e),f)) incidence angle.

As a result of the performed comparison, some similarities between etched samples were encountered. For all analyzed teeth, a clear two bands, first at about 1050 cm^{-1} and second at 1125 cm^{-1} could be differentiated. On the other hand, in case of the severely demineralized samples, the 1125 cm^{-1} band is slightly moved to the lower wavelengths. In case of the 1125 cm^{-1} band, the observed peak is sharper for the etched samples comparing to severely etched teeth. Moreover, for these samples the discussed bands are more intense than for the traditionally etched teeth.

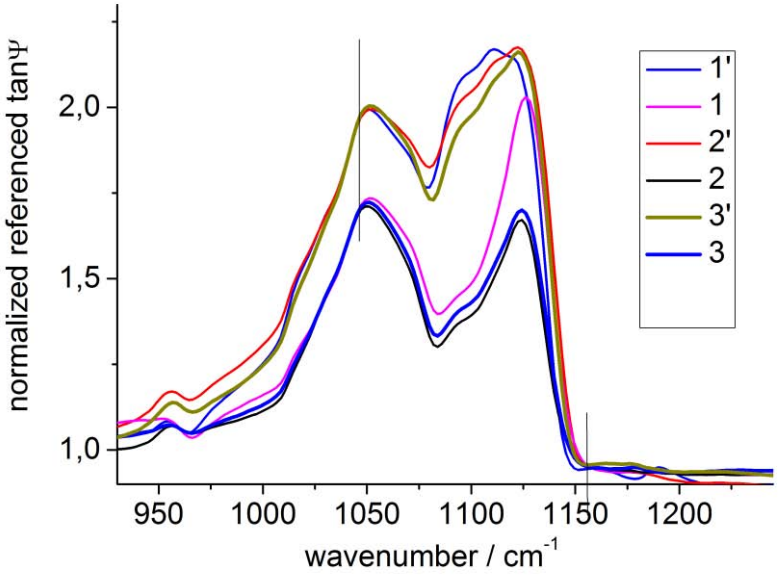

Figure 76. Normalized referenced spectra (the same intensity at 1046 cm^{-1} and 1156 cm^{-1}) for traditionally desmineralised (1,2,3) and severely desmineralised (1',2',3') teeth samples at the 50° incidence angle.

Comparing obtained results with the reference apatite powders, no similarity in the calculated k constants can be observed. The phosphate sharp band, in case of HA and FA, is located around 1080 cm^{-1} (Figure 67)whereas for the teeth samples, the two band are located around 1050 cm^{-1} and 1125 cm^{-1}.

In order to compare better the variations for the three sets of samples, the normalized spectra of the teeth etched only with hydrochloric acid in the previous figure were rationed to the normalized spectra of the (Figure 77).

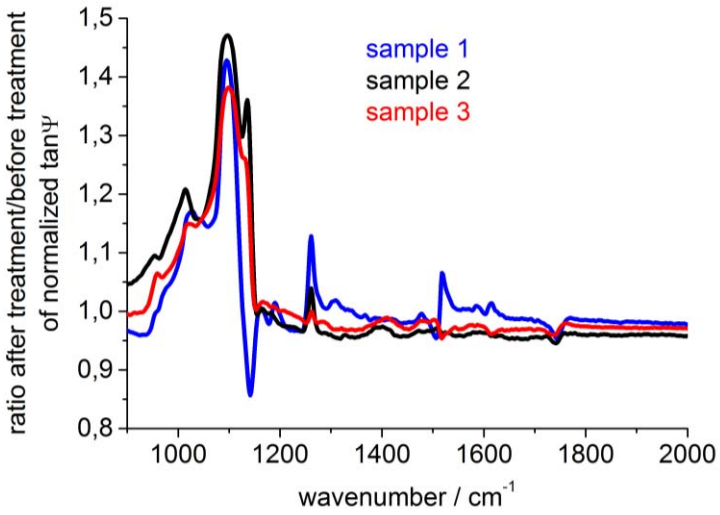

Figure 77. Spectra of the three traditionally etched teeth samples normalized to the polymer spectra

As a result of the performed normalization, obtained spectra are almost the same. The sharp peak at 1125 cm^{-1} is common for all of three samples. Observed differences

among the analyzed spectra come from the contribution of the embedding polymer. These contributions are different in the individual spectra since the spot size of the lab-ellipsometer is slightly larger than the probed sample spot. Thus, the bands around 1300 cm^{-1} and 1500 cm^{-1} are clearly proceeding from the polymer and have contribution in each sample spectra, although contributions are of various intensity. Also, the band around 1000 cm^{-1} can be classified as such. Moreover, negative peak around 1150 for sample number one can also be interpreted as a small overlapping contribution of the polymer. Again, the performed calculation does not reveal similarities between the optical constant obtained for reference apatite powders.

22.4. Modelling of the IR data

In order to reach better lateral resolutions in ellipsometric measurements further synchrotron ellipsometric experiments would be needed. However, having the obtained reference optical constants for the apatites and polymers also a quantitative interpretation of IR microscopic measurements is possible with optical modelling. In order to confirm that the previously discussed teeth samples are suitable references for the obtained synchrotron data further measurement with the IR microscopy were performed. Obtained simulations were then compared and the similarities were discussed.

Figure 78 presents the microscopic measurements obtained for traditionally and severely etched sample number 3. The clear differences in the number and shape of peaks are once again confirmed. Severely demineralized sample presents two well defined bands around 1000-1100 cm^{-1} whereas for the etched sample the peak around 1100 cm^{-1} is less defined, consequently difference in the reflectivity of the two peaks is bigger than for the severely etched sample (Figure 79). For the peak around 1110 cm^{-1} it is of about 0,07.
The obtained spectral differences in the reflectivity between samples have the same characteristics as in case of the optical constants in the ellipsometric (Figure 79) where the difference was of 0,1.

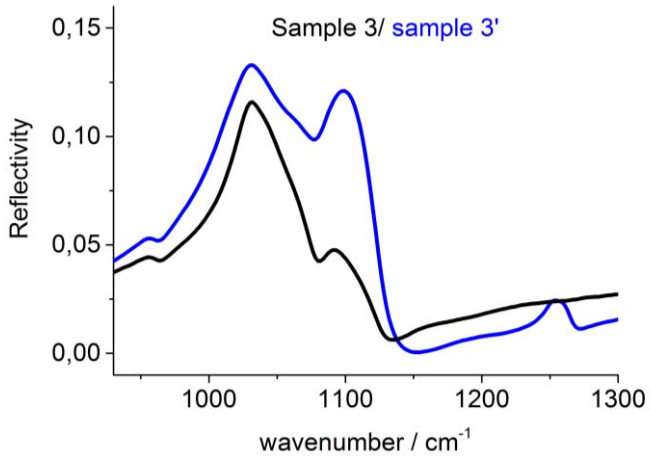

Figure 78. FTIR spectra for sample treated only with acid (black) and decarbonised sample (blue).

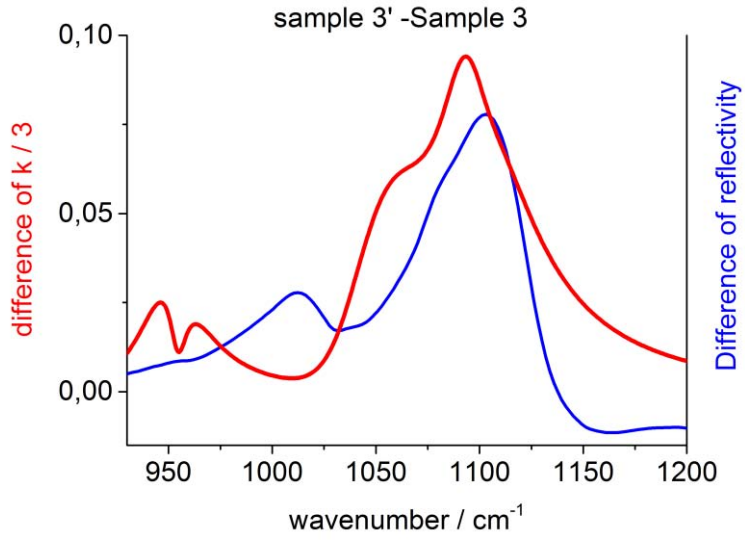

Figure 79. Difference in the reflectivity and optical constants of the two types of etched samples

Subsequently, the microscopic reflection spectra and ellipsometric spectra were modelled with (except a small offset for the baseline of the microscopic spectra) the same simulation parameters applying a harmonic oscillator model. The revealed optical constants are presented in Figure 80

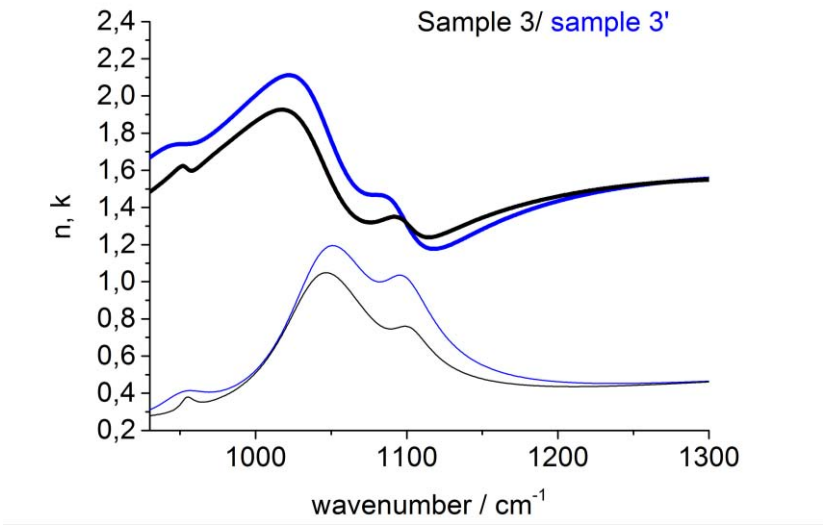

Figure 80. Optical constants applied in the modelling of the reference samples

Figure 81 presents the experimental FTIR data compared with the simulation of the same spectra. There is an overall similarity between experimental and simulated spectra. Moreover, the spot 12 proceeding from the enamel reveals the similarity with the reference sample etched only with acid, whereas spot 11 looks more like severely demineralized sample (Figure 81).

Taking into consideration that samples etched only with acid simulate less invasive procedure of caries creation, consequently, less hydroxyapatite is dissolved during the treatment. It would suggest that measured part of the teeth proceeds from upper (closer to the edge) section of the enamel. The other type of sample (etched with acid and nitrogen) suffered a more severe deterioration since the applied treatment is more oxidative and by dissolving the enamel it goes deeper into its structure (closer to the DEJ) thus the observed part of the teeth proceeds from deeper parts of the enamel.

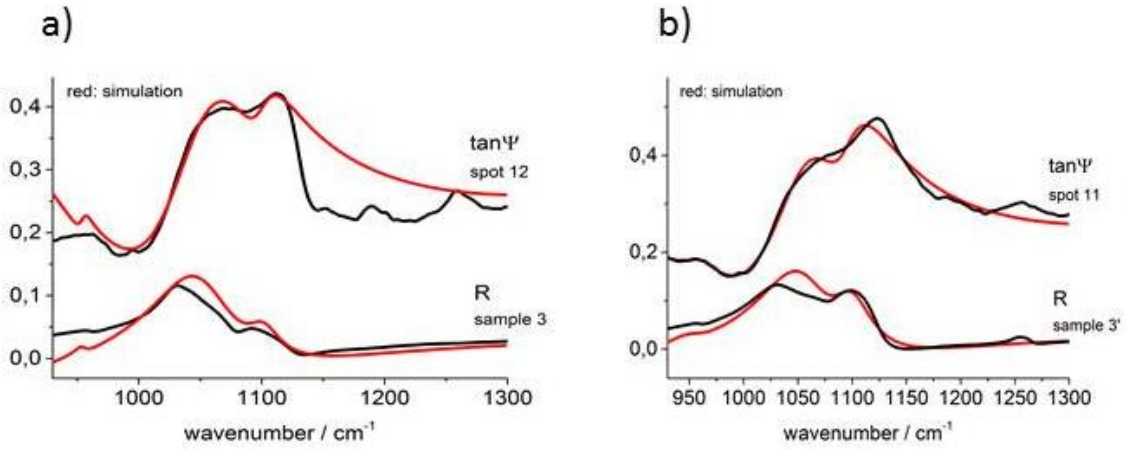

Figure 81. a) Comparison of the measurement of sample etched with acid and the spot number 12 from the synchrotron-ellipsometric measurements b) Sample treated with acid and nitrogen compared with spot number 11 (synchrotron-ellipsometric measurement). With red simulation spectra, with black real measurement are presented.

23. Conclusions

In the present study, synchrotron IRSE was applied to evaluate the structural changes that under come human teeth when treated with the reminearalising agents. Since the influence can vary depending on the zone of the teeth, a cross section line going from the enamel into the pulp chamber was performed. As a result, differences in the spectral signature depending on the position of the experimental point were observed. The spot localized at the enamel, differed in the shape and the position of the bands in the region of the phosphate vibrations from the spots localized in the dentin region of the tooth. Also, the amide I bands revealed to be present in the dentine regions whereas they could not be encountered in the enamel.

The comparison of the resulting IRSE synchrotron measurements with the previously obtained reference HA and FA samples revealed various spectral differences between the samples. Consequently, the optical constants derived from the powder reference apatites could not be applied in order to compare them with the experimental data of the real tooth sample. Dentinal apatite differs from the pure HA and FA. The size of the dentinal crystals is of approximately 5nm×30nm×100nm and they are not as reach in calcium as the synthetic ones. Moreover, the stoichiometric apatite contains around 4-5% less carbonate than the biological apatite. Increase in carbonate and the lower content of calcium of the dentin leads to higher acidic solubility and less resistance to acid conditions (194). We presume that the spectral difference encountered in this experiment proceed from mentioned differences in the chemical composition.

In order to obtain more suitable reference samples, two types of differently etched human teeth were measured and compared with the experimental results. The first type of sample etched only with acid represent more gentle demineralization. The surface of the teeth is dissolved exposing the upper part of the enamel. The second type of the applied demineralization generates the creation of N_2O_4 that is a powerful oxidant. As a consequence, with this type of treatments, the demineralization is more severe and exposes deeper parts of the enamel. The phenomenon was confirmed in present measurements. Samples treated with different demineralization procedure revealed different spectral characteristics. Moreover, when the data were compared to previous synchrotron IRSE measurements, the samples treated only with acid were similar to the enamel spectra whereas samples treated with more oxidative demineralization agent, revealed more similarity to the deeper parts from the analyzed teeth.

In all of the analyzed samples, the contribution of the embedding polymers was studied. It shows bands common for all of the obtained spectra in the 1300 and 1500 cm^{-1}. Luckily, in the phosphate and amid I vibrations that are the key regions in the study, the contributions are very small and do not influence significantly the interpretation of the data.

Selected synchrotron measurement spots can be simulated with reasonable agreement in the same optical model as microscopic measurements of adequate reference samples.

From the similarity of the spectra, it is concluded that a reference sample etched only with acid (gentle demineralization) corresponds to the upper part of the enamel, and a sample more strongly oxidized (severe demineralization), corresponds to lower parts of the enamel. The simulated spectra revealed high similarity to the experimental synchrotron spots what allows to suspect that once both type of samples are analyzed with the synchrotron IRSE method, more detailed information about the influence of the remineralising treatment on the dental tissue will be revealed.

APPLICATION OF FTIR SPECTROSCOPY FOR THE DENTAL TISSUE CHARACTERIZATION: A CURVE FITTING APPROACH

Abstract

Objectives

The aim of the present work is to investigate structural changes in the human enamel and dentin induced by the remineralization process. The spectra from various points proceeding from different locations of the tooth were compared and studied applying Principal Component Analysis (PCA) and curve-fitting. Spectroscopic results presented in this work are based on the deconvolution of the phosphate band. Obtained results were compared to the reference hydroxyl and fluorapatite powders and scientific literature.

Methodology

Deconvolution of the pure apatites was performed on the spectra proceeding from the synchrotron FTIR measurements. Curve fitting and PCA analysis were performed on the spectra acquired with the Nicolet FTIR spectroscope with the Grobal source of light. Deconvolution was carried out by the OMNIC® scientific software whereas for the PCA Uncrambler® was implemented.

Results

Performed curve fitting of the pure apatite sample did not give clear results that could be confirmed in the bibliography. However, curve fitting of the real samples as well as the comparison of the spectra points and PCA analysis showed clear differences between various points proceeding from different locations in the enamel. In general the first point from the edge resembled the FA spectra whereas the rest of the point could be attributed to the HA.

PCA of various remineralising mixtures showed separated populations for different treatments, especially when samples that undercame protein assisted remineralization and commercial agents were compared to the remineralising equivalents of NMTD material.

Conclusions

Scattering effects and the general difficulties connected with the curve fitting performance leads to serious doubts about the interpretation of the obtained calculations and the interpretation of the bands. In order to confirm the statements the experiment should be performed on bigger number of the samples at many experimental points.

Introduction

As it was previously described FTIR spectroscopy is a powerful approach for the characterization of dental tissue. It delivers valuable information about the chemical structure of the dental tissues (97), (90), (98), (99). The careful analysis of the spectra proceeding from the teeth allows observing the nature of the sample and its changes depending on the applied treatment or the stress agent. It allows examining inorganic and organic materials of the sample and has been successfully applied for the quantitative analysis of the mineralized composition and the determination of the physical properties of the dental tissue (98). Moreover it was also applied in order to determine the CI (crystallinity index) of the teeth that delivers the information about the percentage of the crystalline material in the sample (97).

The aim of the present work is to investigate structural changes in the human enamel and dentin induced by the remineralization process. The spectra from various points proceeding from different locations of the tooth were compared and studied applying Principal Component Analysis (PCA) and curve-fitting. Spectroscopic results presented in this work are based on the deconvolution of the phosphate band. Obtained results were compared to the reference hydroxyl and fluorapatite powders and scientific literature.

Spectral curve fitting is a mathematical procedure which generates a series of individual peaks that when added together match the original spectra. The process of curve fitting is called convergence and is performed by the scientific software. In presented work, OMNIC software with the Fletcher-Powell-McCormnik algorithm was implemented. The points are determined by the RMS (root mean square) of the residuals of the sum of the created peaks to the RMS noise (195) .

Curve fitting is performed in three steps: fixing the initial profile where line shapes and baselines has to be chosen. Constant, linear, quadratic or cubic baseline can be applied in order to minimize the residuals. The choice highly affects the final result and has to be made very wisely (195).

Next step is to fix the initial parameters (width, height, location). The user can manually fix the certain peak at expected position and adjust its height and width (195). The selection of the position of the peaks can be guided by the position of the minimums in the second derivative of the spectrum and also by the bibliographic suggestions.

Once all the information is set the minimization procedure is performed in order to reflect the implemented set ups. As a result peaks are generated. The success of the final fit depends on the fixed parameters, the better initial parameters the better final deconvolution is obtained (195).

Since the performed operation is a mathematical equation generated peaks can have no spectral meaning. Sometimes large amount of selected peaks give better peak, although they are meaningless in the interpretation. That is why the entire procedure tends to be a very difficult and highly dependent from the scientists personal judgment.

Experimental Section

24. Methodology

24.1. Instrumentation

Curve fitting experiments of the teeth samples were performed on the spectra acquired with a Thermo Scientific Nicolet iN10 FT-IR Microscope, Spectra were recorded in the reflection mode at spectral resolution of 8 cm^{-1} in the range between 2000-900 cm^{-1}, after recording a background from Au reference sample. The step size applied in the measurement was of 100x100 µm.

Pure apatite reference spectra and specific areas of the enamel and dentin where performed at the synchrotron infrared microscopy at the SMIS beamline (SOLEIL, France). Continuum IR microscope (Thermo Nicolet, USA) coupled to a NEXUS FTIR spectrometer bench Nicolet 5700 (Thermo Nicolet, USA) and a liquid nitrogen cooled mercury cadmium telluride (MCT-A) detector was implemented. The microscope was equipped with a computer-controlled x/y stage allowing acquisition of profiles or maps of the sample. Spectra were collected in reflection mode, at 6 cm^{-1} spectral resolution over the range between 3000-800 cm^{-1} and step size 10x10 µm, using Atlµs software (Thermo Nicolet Instruments).

24.2. Specimen preparation

Specimen preparation was performed as described in Section 21.1 page 141.

24.3. Reference apatite samples

Reference apatite samples were prepared as described in Section 21.2 page 141.

24.4. NMTD (Remineralizing Agent) Preparation (48)

VI types of remineralising mixtures that varied in the ratio of calcium, phosphates and fluoride were prepared. The mass ratio is presented in Table 28

Figure 82. Mixtures applied during the study. The concentration is presented in the mass ratio of atoms of calcium, phosphate and fluoride

	Ca	P	F
Mixture I	2	3	1
Mixture II	2	3	3
Mixture III	2	3	6
Mixture IV	4	3	1
Mixture V	4	3	3
Mixture VI	4	3	6

Apart from above mentioned ions all resins contained of 2% of Zn (186).
In order to confirm the concentration of prepared mixtures the ICP-MS analyze was performed for calcium, phosphor and zinc content. Fluoride concentration was measured by ISE (Ion Selective Electrode). The comparison of the theoretical load and the measured one are presented in Table 29. Remineralising mixtures were prepared taking into consideration the experimental loadings.

24.5. Treatment performance

Treatment performance was as it is described in Section 21.4 page 141

24.6. Data processing

Data acquisition and processing (curve fitting, PCA maps) were performed using Nicolet Omnic software (Version 8.0, Thermo-Nicolet). The raw data was transformed into absorbance values format and the Kramers – Kroning transformation was performed applying Nicolet Omnic software.
The PCA analysis and the MCR, SNV, Savitsky-Goley pre-treatment were performed using the Unscrambler X® CAMO ™ scientific software.

25. Results

25.1. Kramers –Kroning (KK) transformation

In spectroscopy the incident light is partially reflected and shifted in phase at the same time. The resulting reflectance spectra give the information about the reflected wave amplitude but not about the phase shift of the light. In order to obtain it the Kramers-Kronig transformation has to be applied. The Kramers-Kronig are mathematical relationships that connect the real and imaginary part of any physical function. They are commonly used in spectroscopy in order to extract the real part of the spectra from its imaginary one. Since the reflected wave amplitude, as well as the phase shift are known after applying this transformation, further information such as the material refractive index or absorption coefficient can be evaluated (196). Kramers-Kronig is normally

applied on the entire range of the spectra. However in case of the teeth spectra the contribution from the distant wave lengths is insignificant thus in this research all spectra were centered approximately on the spectral range between 2400- 800 cm^{-1} where the most important vibrations occur. Measurements performed on the spectrometer with the internal source of light were performed in order to obtain the general information about the distribution of the most important components; that is why in this case the spectral range considered was 900-2000 cm^{-1}. When it comes to measurements performed with the synchrotron source of light, the aim was to extract all the information possible from the resulting spectra. Since it is important to cover all nearby spectral features 4 ranges of low frequency cut-off at 700, 750, 800 and 850 cm^{-1} were tested (Figure1.) As a result the final cut-off at 800 cm^{-1} was considered the most suitable and subsequently applied in all further data treatments.

Figure 83. FTIR spectra of enamel with low frequency cut-off at 700 (blue), 750 (violet), 800 (green) and 850 (red) cm^{-1}

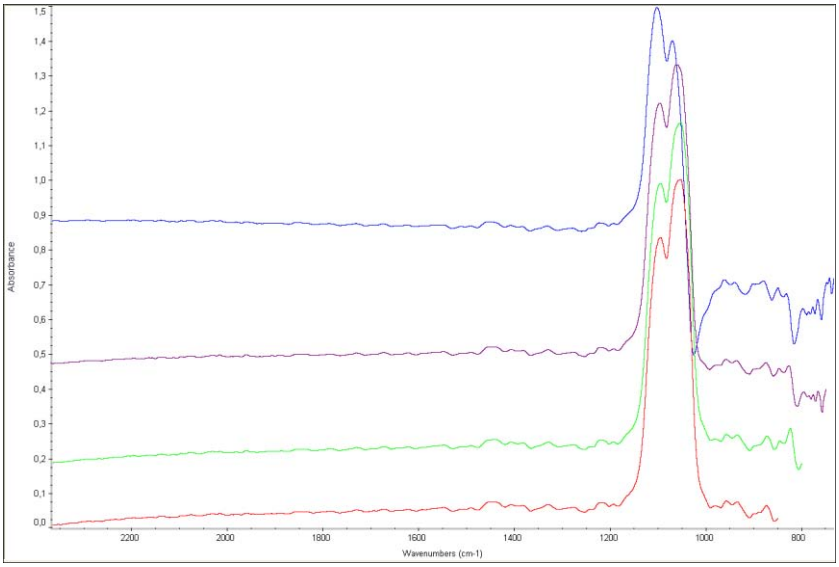

25.2. Description of the typical spectra form the enamel and dentin region

In Figure 84 the typical spectra of enamel (red) and dentine (blue) are presented. In enamel spectra there is a duplet in the region 900-1200 cm^{-1} where the phosphate vibrations are located. In dentine spectra beside the phosphate peak at 1033 cm^{-1} an amide I (1632 cm^{-1}) and II (1511 cm^{-1}) stretching can be differentiated . In the zone 1400-1470 cm^{-1} the $\nu_3 CO_3^{2-}$ vibrations can be found. Carbonate can be found above all in dentine, although there is also a small contribution in the enamel spectra as well (197), (198).

Figure 84 Typical absorbance FTIR spectra of enamel (red) and dentine (blue) with the main bands that are most commonly encountered

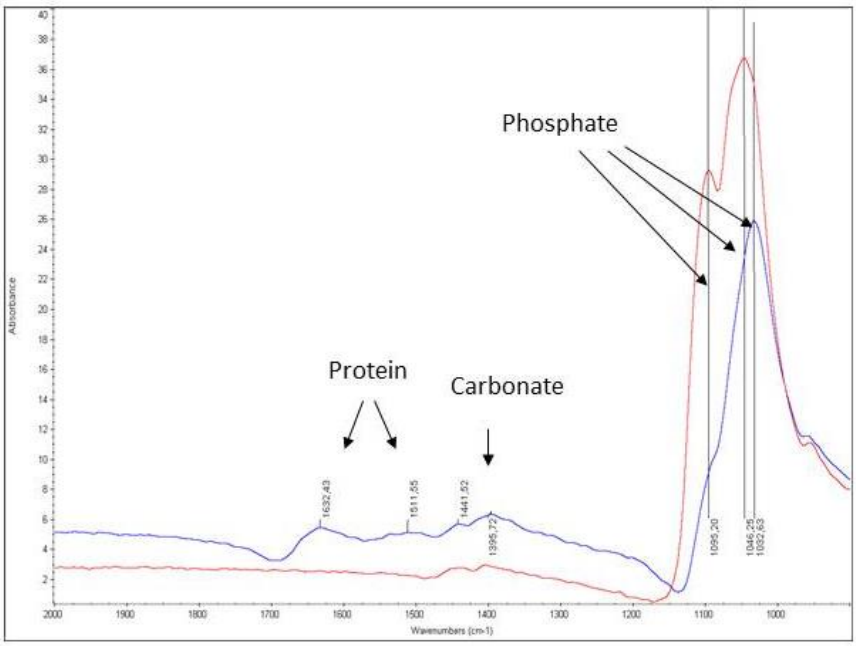

25.3. HA and FA differentiation

In order to differentiate two types of the apatite the P-O stretching vibrations (ν_1 and ν_3) around 900 - 1200 cm $^{-1}$ were taken into consideration (196). In case of the fluorapatite (FA), as it is demonstrated on Figure 1 a doublet can be observed at 1102 cm^{-1} (0,69 Abs) and 1067 cm^{-1} (0,95 Abs), whereas for hydroxyapatite (HA) first peak is present at 1095 cm^{-1} (0,55 Abs) and the second one at 1048 cm^{-1} (0,96 Abs). This small shift in the position of the doublets allows differentiating those two forms of apatite. Also the ratio of the intensities between two peaks in doublets can be helpful since for FA (1.37) it is smaller than for HA (1.75).

Figure 85. FTIR absorbance comparative spectra of the reference samples of HA (green) and FA (red).

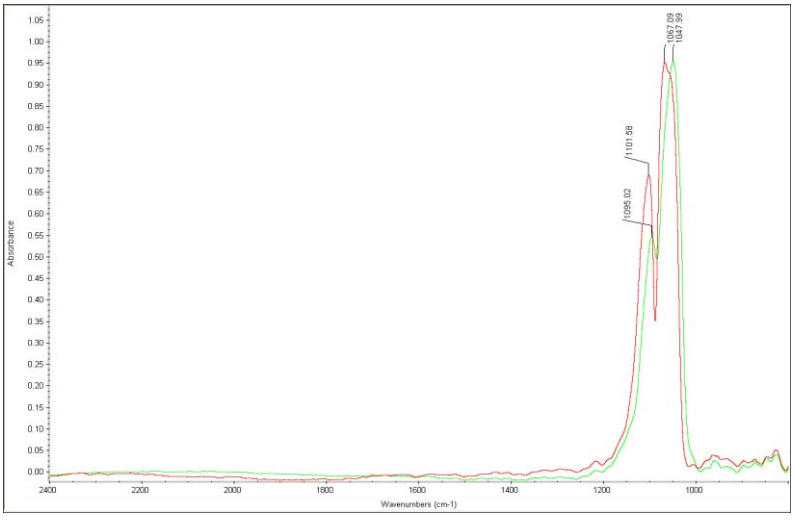

25.3.1. HA and FA differentiation - curve fitting

Further differentiation between the two components considered the P-O stretching vibrations (ν_1 and ν_3) around 900 - 1200 cm $^{-1}$. In order to find detailed information about spectral differences between the two apatite species a curve fitting procedure was performed on spectra obtained at the synchrotron FTIR instrument.
In case of this study spectra of the pure HA required 8 components for the satisfactory fit whereas in case of FA spectra 9 bands where necessary.

Figure 86. Hydroxyapatite curve fitting (F value 1,011; noise 5; Gausian constant base line, baseline for the average-polynolmial)

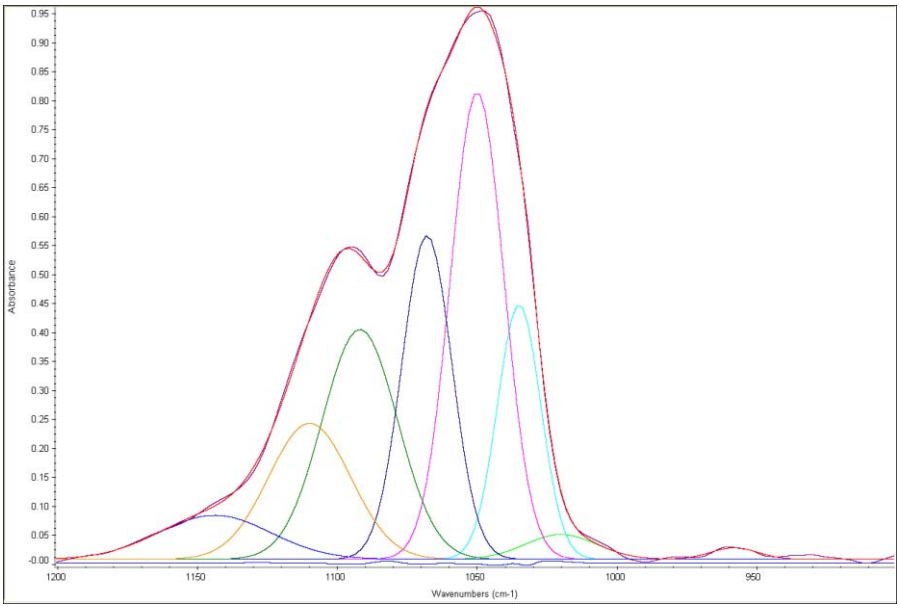

Figure 87. Fluorapatite curve fitting result. (F value 0,93; noise 5; Gausian constant base line, baseline for the average-polynolmial)

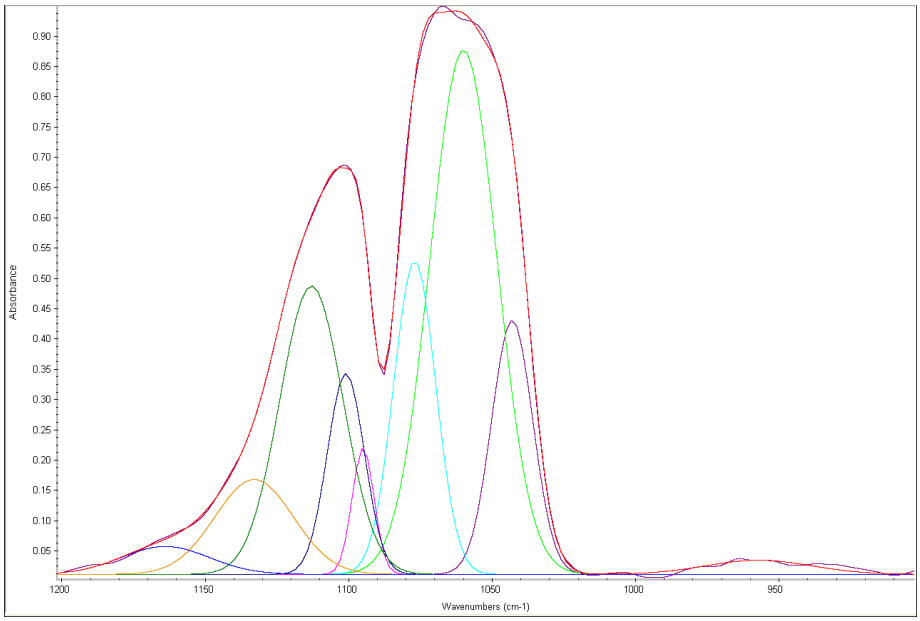

Table 41 presents assignments of the bands generated during the curve fitting procedure.

Theoretically the symetry of the orthophosphate group that is tetrahedral makes the v_1 stretching inactive. Although when the symmetry of the crystal is lowered as is in case of some hydroxyapatite a weak band between 950-970 cm^{-1} can appear (199). There is a correlation found between the percentage area of this peak and the crystal size of the studied apatite. Pleshko et al claims that this component could be a useful indicator of a crystal size since its % area decreases from 1.9 to 0.5 % as the crystal size increases from 200 to 450 Å. What is more in well crystallised apatites the v_1 component is clearly defined.

Table 41 Assignments of the bands of deconvoluted spectra of HA and FA in the v_1 v_3 domain between 900-1200 cm^{-1}

Hydroxyapatite		**Fluorapatite**				
Wavenumbers (cm^{-1})	% area of peak	**Wavenumbers (cm^{-1})**	% area of peak	Assignment	References	Comments
958	0,06	**957**	1,51	$v_1PO_4^{3-}$	(199), (200), (201), (198)	
1020	2,03			$v_3PO_4^{3-}$	(199), (202)	*Poorly crystaline apatite,* nonstoichiometric *with HPO_4^{2-} and CO_3^{2-}*
1035	12,65	**1043**	10,63	$v_3PO_4^{3-}$	(198), (202), (200), (197)	*Stoichiometric apatites*
1050	28,57	**1060**	35,49	$v_3PO_4^{3-}$	(199), (197), (200), (202)	*Poorly crystaline apatite, disordered phosphate phase located outside from the crystal line*
1068	18,49	**1077**	13,40	$v_3PO_4^{3-}$	(198), (202)	*Poorly crystaline apatite*
1092	19,81	**1095**	2,82	$v_3PO_4^{3-}$	(198), (201), (200), (202)	*Stoichiometric apatites*
1110	12,74	**1101**	7,57	$v_3PO_4^{3-}$	(199)	
		1113	18,53	*HPO_4^{2}*	(198), (202)	*In newly precipitated apatites*
1144	5,65	**1133**	7,56	*HPO_4^{2}*	(198), (199), (197), (202)	*HPO_4^{2-} containing apatites*
		1164	2,49			

In the present study in both apatites the band is present, although it is not well defined, in fluorapatite it is in the form of a very wide peak (957 cm^{-1}), whereas in hydroxyapatite it is slightly better defined (958 cm^{-1}). It would lead us to the conclusion that measured apatites are poorly crystallised ones. Since the percentage area of the peak representing the $v_1PO_4^{3-}$ stretching in fluorapatite case represents bigger value than in hydroxyapatite

that would indicate that fluorapatite has smaller crystal size. What would contradict the Pleshko et al who claimes that fluorapatites have slightly larger size of the crystals than the hydroxyapatite or it would suggest that measured samples are poorly crystallised ones and to derived its crystallinity indices peaks around 1020 and 1050 cm^{-1} should be taken into consideration instead of the ν_1 band discussion (199).

On the other hand Uysal (201) et al. that was studying the spectral differences between pure and F doped hydroxyapatites among others didn't observe any differences in discussed peak when the fluoride was introduced into the lattice. Neither A.Antonakos et al. (200) observed such a relation.

When the width of the peak is considered the apatites that are doped with the fluoride atoms had slightly larger value of the width of the peak. That would correlate with the results obtained in this study (958_{HA} cm^{-1}= 19.75 and 957_{FA} cm^{-1}= 43.50). A comparison of the widths shows the higher crystallinty or increased atomic ordering when the width of the peak is smaller (200). In case of this study it is smaller for hydroxyapatite. That would indicate that it has higher crystallinity (or increased atomic ordering) than fluorapatite.

Pleshko et al found the correlation betwen the frequency of the 1020 cm^{-1} component and the crystal size of the apatite. According to that work the frequency is not greater than 1027 cm^{-1} for the crystal sizes smaller than 166 Å. An increase in the frequency from 1028-1032 cm^{-1} was correlated with an increase in the crystal size 160-190 Å. The frequency of the component at 1020 is reduced when the crystallinity is diminished. That parameter right after the percentage area of the band at 1050 cm^{-1} was considered the secondary indicator of the crystal size for poorly crystallized specimens (199).

According to Magne et al. the crystallinity of the biological samples can be established by the value of the intensity of two peaks 1020/1030 cm^{-1}. 1020 cm^{-1} are the stretching arising from the nonstoichiometric apatites with HPO_4^{2-} and CO_3^{2-} with their vacancies and 1030 cm^{-1} come from the stoichiometric apatites.

In the preset study the peak 1020 cm^{-1} was generated only in the hydroxyapatite spectra. Its absence in the fluorapatite spectra could indicate the lack of carbonate ions incorporated into the lattice. Taking into consideration the lack of the bands around 1420 – 1465 cm^{-1} and 1545 cm^{-1} that information could be confirmed with this study.

In case of fluorapatite the peak 1030 cm^{-1} was moved to 1043 cm^{-1}. I have not found bibliographic information whether this shift in the frequency represents some changes in the crystallinity or crystal size of the apatite.

The relationship between the percentage area of the band at 1050 cm^{-1} and crystal size was encountered. The percentage area drops from 45-5 % as the crytal size increases from 135-190 Å. That behavior comes from the disordered phosphate phase that is located outside from the crystal line (199). According to Pleshko et al. this can be a very good indicator of the crystal size of the studied apatite. In case of fluorapatite in the present study this band was found at the 1060 frequency and shown the increase in the percentage area comparing to HA spectra. It would suggest that fluorapatite measured

in this study has a smaller crystal size than HA (the same information was concluded from the band 958 and it was contradicting the Pleshko et al. statements.)
Uysal et al. (201) have discovered that when the Fluor is incorporated into the lattice the shift into the higher wave numbers of the bands at 1090 cm^{-1} and 1045 cm^{-1} could be observed. In case of this study the same tendency was encountered. For fluorapatite the shift of the 1090 cm^{-1} band was of 4 cm^{-1} comparing to hydroxyapatite. When it comes to the band at 1045 cm^{-1} in case of fluorapatite it was present at 1043 cm^{-1} and for hydroxyapatite at 1035 cm^{-1}.
1111 and 1144 cm^{-1} bands indicate the presence of the HPO_4^{3-} in the lattice. In case of a dental sample it can indicate the degree of maturation of the certain point of the teeth since the decrease in its intensity means the loss of HPO_4^{3-} and as a result indicates the maturation of the apatite (202). In case of the present study both band where find in hydroxyapatite as well as fluorapatite sample. Since both apatites are synthetic ones obtained information suggests that analyzed apatites refer to early stage apatites.

25.4. FTIR analysis of the human teeth

25.4.1. Reference sample (etched with acid)

25.4.1.1. Spectra comparison

Four points varying in the distance from the edge of the enamel were carefully studied and compared. 10 spectra located at the same distance were chosen and further the average spectrum was generated in order to create the representative spectra for each point. The first one was taken exactly from the edge of the enamel, second and third one at 150 µm and 900 µm respectively. The fourth one was located 300 µm from the DEJ (dentine enamel junction). Figure 6 shows the general comparison of the four spectra.
Bands that could be differentiated in all spectra come from phosphate and carbonate groups. The comparison of the intensities of those bands in various locations of the enamel is presented in Table 2. Phosphate v_3A represents the peak between 1050 and 1070 cm^{-1} whereas v_3B the one at 1090-1110 cm^{-1}.

Figure 88. Resulting average spectra from 4 different locations in the enamel: violet - 1 point (the edge of the enamel), blue - 2nd point (150 µm from the edge), green - 3rd point (900 µm from the edge), red – 4th point (300 µm from DEJ).

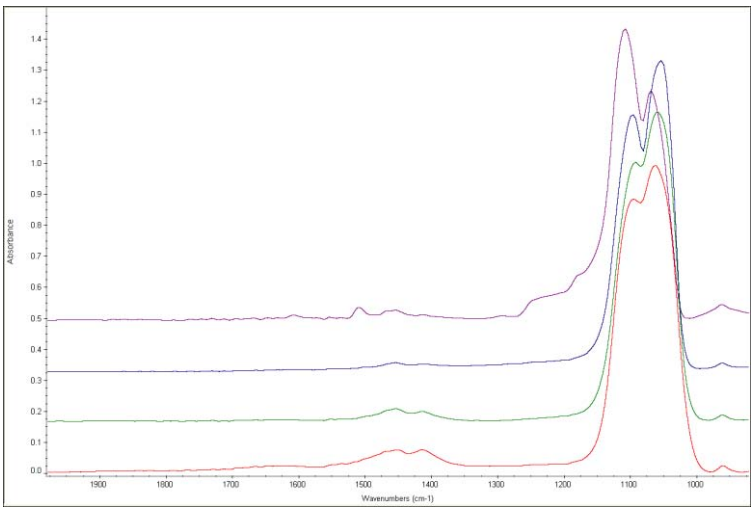

Table 42. Comparison of the intensities of the carbonate and phosphate bands of all 4 points of interest proceeding from the enamel

Position of the peak	Intensity						
	Carbonate				Phosphate		
	$\nu_3CO_3^{2-}$ type A (aprox.1545 cm^{-1})	$\nu_3CO_3^{2-}$ type B (aprox.1465 cm^{-1})	$\nu_3CO_3^{2-}$ type A (aprox.1450 cm^{-1})	$\nu_3CO_3^{2-}$ type B (aprox.1420 cm^{-1})	$\nu_3PO_4^{3-}$ ν_3A	$\nu_3PO_4^{3-}$ ν_3B	$\nu_1PO_4^{3-}$ (aprox.950-970cm^{-1})
At the edge	0,03	0,02	0,03		0,73	0,93	0,04
150 µm			0,02	0,02	1,00	0,82	0,02
900 µm			0,04	0,03	1,00	0,84	0,02
300 from DEJ			0,07	0,07	0,99	0,88	0,02

As a result of the comparison of 4 selected points it could be concluded that in the spectra from the edge of the enamel, among others, the bands with the maxima at 1509, 1564 and 1554 cm^{-1} could be resolved. All bands represent the stretching proceeding from the both A and B type carbonate. Respect to the rest of the spectra only in this one well defined bands at 1509 cm^{-1} and 1564 cm^{-1} could be observed. In the rest of the points carbonate bands were present around 1450 cm^{-1} and 1420 cm^{-1} with the intensities of the peaks increasing in the direction from the edge of the enamel toward the DEJ.

When it comes to the comparison of the $\nu_3PO_4^{3-}$ bands there is a big difference in the intensity ratio of the peak ν_3A/ ν_3B (Table 3). The point at the edge of the enamel has

the smallest value of the intensity ratio comparing to the rest of the points. In this case peak ν_3A has bigger intensity than ν_3B band whereas in the rest of the points this relation is the opposite one: ν_3B band represent higher absorbance. Beginning from the 2 point (150 µm from the edge) the ratio is diminishing toward the dentine enamel junction (Absorbance: 2nd point>3rd point >4th point).

Table 43. $\nu_3PO_4^{3-}$ band : comparison of the frequencies of peaks ν_3A and ν_3B and its intensities ratio for all 4 analyzed point.

Position of the peak	Wave numbers [cm^{-1}]		Intensity ratio ν_3A / ν_3B
	ν_3A	ν_3B	
At the edge	1069	1108	0,79
150 µm	1054	1096	1,21
900 µm	1059	1092	1,19
300 µm from DEJ	1062	1094	1,12
Fluorapatite	1067	1102	1,37
Hydroxyapatite	1092	1047	1,75

Also the positions of the bands are worth mentioning. The frequency of the $\nu_3PO_4^{3-}$ bands in the point located at the edge of the enamel are moved towards higher wavelengths comparing to the rest of the points (Table 3). Referring this information to the position of the peaks in the FA and HA the point from the edge of the enamel shows an incredibly strong resemblance to the FA spectra considering the position of the ν_3A and ν_3B bands whereas the rest of the point are similar to the HA spectra. Since the intensity ratio of those two bands is smaller for the FA than for the HA spectra a resemblance can also be considered in this aspect.

This clear difference that was encountered when the $\nu_3PO_4^{3-}$ was considered is well illustrated by the map resulting from the Principal Component Analysis (Figure7). In the analysis the area between 900-1200 cm^{-1} was applied. As a result it can be concluded that the biggest variance proceeds from the points located at the edge of the enamel.

Figure 89. a) map resulting from the PCA analysis (second component) b) 3D map resulting from the PCA analysis

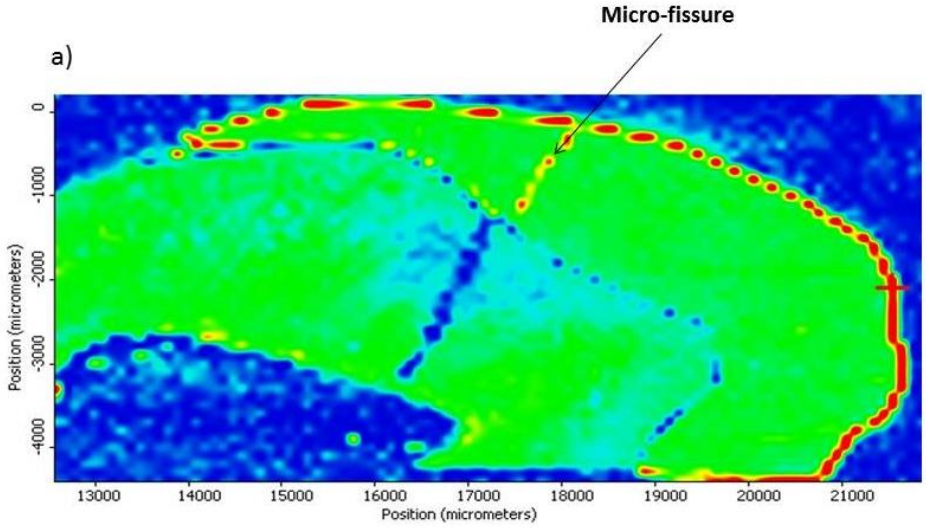

b)

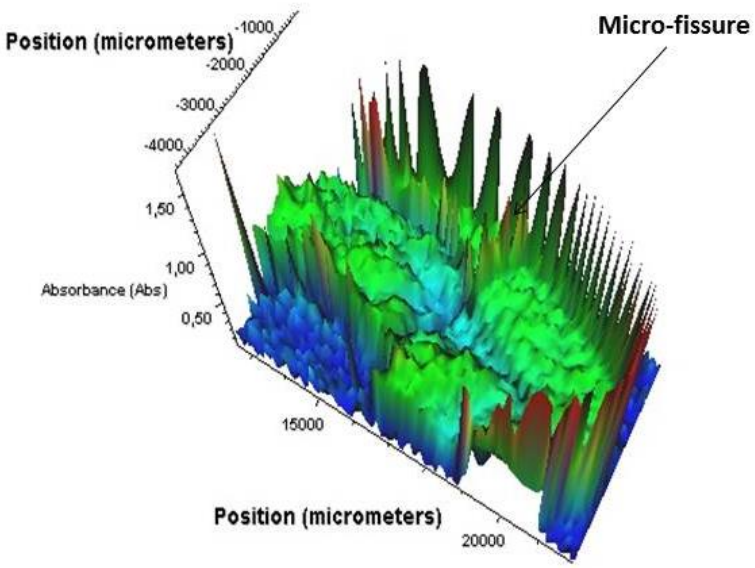

Considering the $v_1PO_4^{3-}$ band all the points beside the point proceeding form the edge of the enamel has the same intensity of the peak. First point has higher intensity of the v_1 band but it could be caused by the Kramers-Kroning transformation (spectra has a bit derivative shape after the KK what has been corrected with the baseline correction). Another factor that can have a huge influence on the shape of the peak and its further transformation with the Kramers –Kroning algorithm are the characteristics of the surface. Although sample was very carefully prepared in order to prepare a flat surface, it is possible that at the edge of the sample where tooth meets with the embedding polymer the area is not perfectly flat. Local micro slops and imperfections of this area may cause a scattering effect that lead into the misleading results. It is worth noticing that the same type of spectra was encountered in a place where a micro fissure is crossing the sample (Figure 89). This kind of fissure can be created during the preparation of the sample but also during patience live. Whatever the cause, the spectra coming from this location resemble the spectra from the edges of the tooth.

25.4.1.2. Curve fitting of tooth spectra

Points described in paragraph 4.1.1 of this work have been subsequently deconvoluted. Figure 8 shows the results of the curve fitting of all 4 points and Table 4 includes the resulting bands and its percentage areas of the peaks.

In general for the point at the edge of the enamel 7 peaks were necessary for the satisfactory fit, 2nd point needed 6 peaks whereas 3rd and 4th points were both deconvoluted into 8 peaks.

Figure 90. Curve fitting of a) 1st point b) 2nd point c) 3rd point d) 4th point

a)

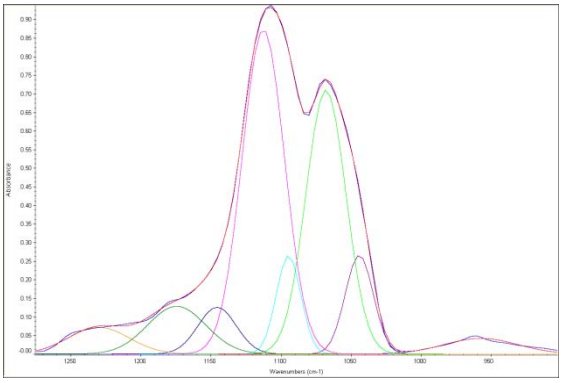

b)

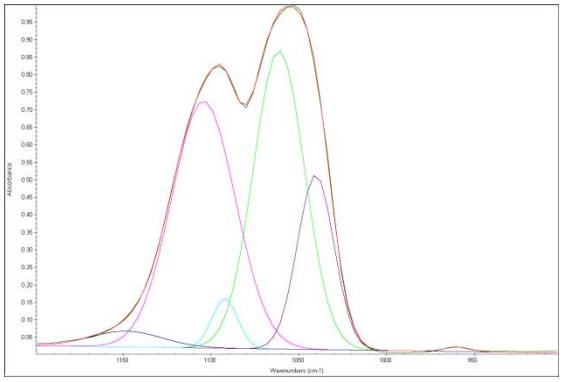

c)

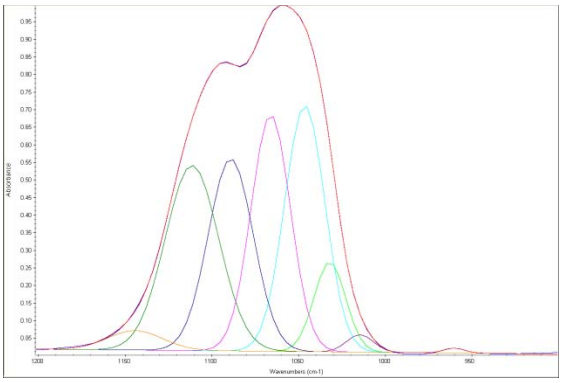

d)

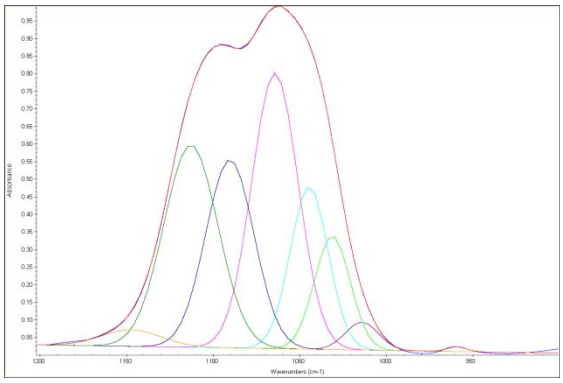

Table 44. Bands resulting from the curve fitting of spectra proceeding from 4 different locations in the enamel

1st point		2nd point		3rd point		4th point	
position (cm^{-1})	ar.peak[%]	position (cm^{-1})	ar.peak[%]	position (cm^{-1})	ar.peak[%]	position (cm^{-1})	ar.peak[%]
957	3,27	**960**	0,28	**960**	0,23	**959**	0,20
				1015	1,10	**1014**	2,05
				1032	6,72	**1031**	9,01
1044	9,25	**1040**	16,00	**1046**	23,50	**1045**	13,67
1068	25,18	**1061**	38,24	**1066**	21,99	**1064**	28,40
1095	17,00	**1092**	3,18	**1089**	20,49	**1090**	20,17
1113	25,33	**1104**	39,47	**1111**	23,46	**1113**	24,31
1146	7,45	**1149**	2,83	**1144**	2,51	**1147**	2,19
1175	7,11						
1230	5,41						

Accoring to Pleshko et al. theory the presence of the v_1 band in not well definded form is caracteristic for poorly crystalised apatites and is commonly encountered in this form in biological samples such as bone or teeth (199). The percentage area of the peak is diminishing for the points located farther from the edge. Only the first point represents a high value of this peak ,but again it can be due to the scattering effect.

Since the width of the peak at 958 cm^{-1} is growing in the dirrection 4th (12,2)< 3rd (13,4) <2nd (17,6) < 1st (61,6) point it would suggest that there is more fluoride - dopped type of crystals for the points that are closer to the edge of the enamel (200). What is more the crystallinity would grow from edge to DEJ (200).

1015 and 1035 cm^{-1} bands were encoutered only for the points located in deeper enamel (3rd and 5th). What would indicate that the size of the crystals in this parts are less than 166 Å (199).

The percentage area of 1050 cm^{-1} band clearly grows from the edge of the enamel toward the deeper enamel, than again drops to smaller value in the DEJ zone. According to Pleshko et al. (199) the percentage area drops from 45-5 % as the crystal size increases from 135-190 Å. It would indicate that the crystal size of the points closer to the edge is bigger than in deeper enamel and that there is a change when approaching the DEJ zone.

Uysal et al. have discovered that when the Fluor is incorporated into the lattice the shift into the higher wave numbers of the bands at 1090 cm^{-1} and 1045 cm^{-1} could be observed. In case of this study the point at the edge of the enamel represents the higher frequencies for the peak at 1090 cm^{-1} (1095 cm^{-1}) comparing to the deeper in the enamel located points. This tendency on the other hand could not be attributed for the band at 1045 cm^{-1}.

1145 cm^{-1} bands indicate the presence of the HPO_4^{3-} in the lattice. In case of a dental sample it can indicate the degree of maturation of the certain point of the teeth since the decrease in its intensity means the loss of HPO_4^{3-} and as a result indicates the maturation of the apatite (202). That can be confirmed in this study since the point at the edge of the enamel represents the highest intensity for this band comparing to the points in deeper enamel. Since enamel starts to grow from the DEJ the less matured point should be the one at the edge.

25.4.2. Principal Component Analysis

In order to see whether there are spectral differences between the groups of specimens that undercame different treatments a PCA analysis was performed on prepared samples (section 24.5). In all cases experimental spots where extracted from the point being the closest to the enamel external edge. Localization was carefully chosen since, as it was previously demonstrated, the inequalities in the sample surface that were observed at the edges of the teeth may give confusing results.

25.4.2.1. PCA analysis of remineralising mixture III

In order to find differences between samples treated with remineralising mixture III obtained FTIR spectra were organised into four groups:

1. Spectra proceeding from sample treated with remineralising mixture III

2. Spectra proceeding from sample treated with protein assisted remineralising mixture III
3. Spectra proceeding from sample treated with commercial remineralising product
4. Spectra proceeding from sample etched with acid (Blank sample)

All compared spectra undercame the same pre-treatment. In order to diminish the scattering effect a MCR (*Multiplicative Scatter Correction*) analysis was applied. MCR transformation was designed to eliminate the multiplicative effect of the scattering. It bases its calculations on the mean spectrum of all analyse spectra: offset (displacement) (*a*) and the slope (*b*) are calculated. Subsequently the original spectra are corrected with the calculated correction coefficient (*a* and *b*) (203).

Subsequently Savitsky-Goley (SG) derivative was applied on the compared data. In general derivatives are used in order to correct the baseline and remove effects that come from nonchemical sources. They also resolve overlapped bands in the analysed raw data. SG derivative applies the information from a certain spectra region in order to calculate the derivative at the certain wavelength. It avoids the influence of the noise and smooths the data (203).

The PCA analysis performed on the pre-treated spectra is presented in Figure 91.

Figure 91. PCA analysis on spectra proceeding from the first point close to the edge of the enamel of four types of samples: treated with mixture III, protein assisted remineralization with mixture III, commercial remineraliser, blank sample.

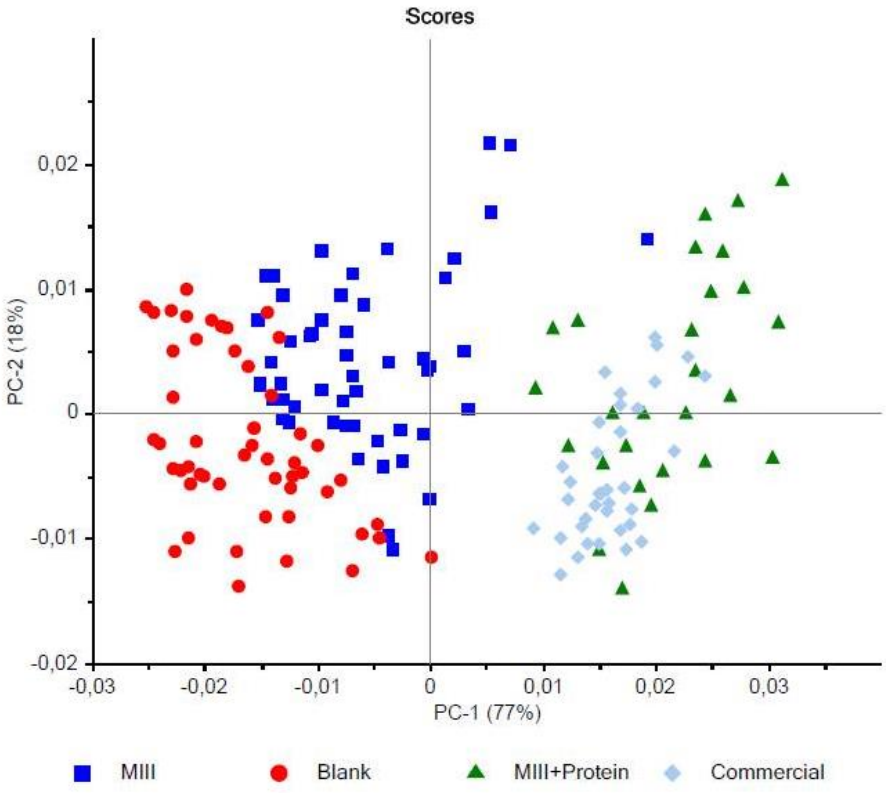

It could be observed that spectra proceeding from samples treated with commercial product and with protein assisted treatment with mixture III represent the similar spectral characteristics and as a result were grouped together. They were separated from the blank samples and mixture III. The last ones also formed two different populations, although resembling more similarities than with the first two groups (commercial and MIII + protein).

25.4.2.2. PCA analysis of various remineralising mixtures

Principal Component Analysis was also performed on spectra proceeding from six different remineralising mixtures that varied in the concentration of the fluoride and calcium ion (section 24.5).

As a pre-treatment of the data the SNV (*Standard Normal Variate*) was applied in order to eliminate the scattering effect. This transformation centres and scales each individual spectrum. Practically it gives the same effect as the MCR transformation. In SNV each spectrum is standardised basing on the data from that spectrum whereas the MCR uses the mean spectrum values. This time the SNV transformation was applied since it separated more efficiently the data.

Subsequently the SG derivative was used and the PCA analysis was performed. The result is shown in Figure 92. As it can be observed almost all of the spectra have the same spectral characteristics beside the mixture I that formed separated spectral group.

Figure 92. PCA analysis on spectra proceeding from the first point close to the edge of the enamel of six types of samples treated with remineralising mixtures varying in the concentration of fluoride and calcium ions.

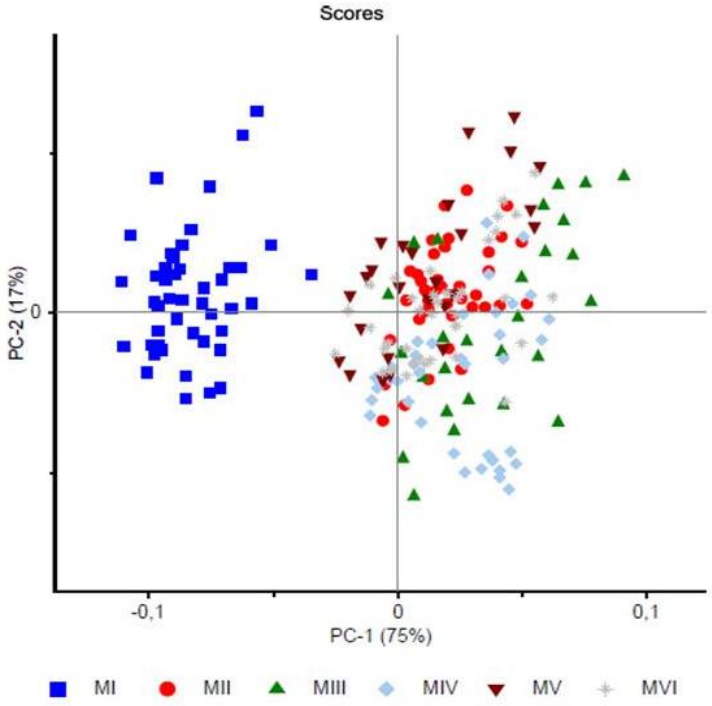

26. Conclusions

Performed curve fitting of the pure apatite sample did not give clear results that could be confirmed in the bibliography. Some of the encountered information are contradictory. For example the comparison of the 958 cm^{-1} band in both apatites indicates that FA had smaller crystals than HA apatite, what contradict the biblioghaphical information (199) that FA has bigger crystals than HA. The analysis of the 1050 cm^{-1} band on the other hand revealed that fluorapatite measured in this study had smaller crystal size than HA.

Curve fitting of the real samples as well as the comparison of the spectra points and PCA analysis showed clear differences between various points proceeding from different locations in the enamel. In general the first point from the edge resembled the FA spectra whereas the rest of the point could be attributed to the HA. However, the possible scattering effects allow me to have serious doubts about the interpretation of the obtained calculations and the interpretation of the bands. In order to confirm the statements the experiment should be performed on bigger number of the samples in many experimental points. Moreover, I have observed that curve fitting procedure is very difficult to perform and can be easily influence by the technician. The treatment performed on the spectra depends from the personal judgment of the scientist and can be easily manipulated. That also makes me uncertain whether this type of the data analysis is suitable for the analyzed type of samples. Performed calculations can be taken into consideration however should be confirmed with further experiments. One of the possible approach is the comparison of the CI (crystallinity index) obtained with the FTIR measurements with the CI derived from the ellipsometric measurements. If the obtained data coincide the continuation of the performed approach can be performed.

The Principal Component Analysis performed on samples with various treatments shows spectral differences between the analyzed populations. The future investigation should be centered on the samples treated with the remineralising mixture and the protein assisted remineralization since clear differences between those groups were encountered. The curve fitting procedure could be a choice in order to investigate the source of the encountered spectral differences. However, since the deconvoluted spectrum is the average one, all analyzed spectra proceeding from the same samples should represent close and compact populations. Since it is not the case, in future, better polishing of the sample should be performed and the resulting spectra should proceed from a bigger number of samples in order to obtain a representative average spectrum. Once again the IR ellipsometry is suggested as another approach in order to investigate the source of the encountered differences.

There were no clear spectral differences between various remineralising mixtures. It could suggest that the concentration of fluoride and ion did not change the dental tissue. The only difference encountered for the mixture I could indicate that the fluoride concentration was too small to initiate the remineralization process.

Supplemental material

Supplemental material 1 Test ANOVA within a confidence interval of 95% between zone 1 and zone 2 of three analyzed teeth

Table 45. Test ANOVA performed on zone 1 and zone 2 when the average percentage of the area occupied by open tubules is considered.

Tooth	*F*	*P-value*
1	168,27	1,27E-35
2	22,56	2,65E-06
3	28,12	1,48E-07
	F crit **3,85**	

Table 46. Test ANOVA performed on zone 1 and zone 2 when the average number of open tubules is considered.

Tooth	*F*	*P-value*
1	187,09	4,25E-39
2	24,33	1,1E-06
3	20,86	5,72E-06
	F crit **3,85**	

Supplemental material 2 Evaluation of the statistical differences of variances derived from the results obtained in automatically computed analysis and semi-automatic ones performed by three independent technician on 120 pictures randomly chosen (60 images after the demineralization and 60 images after the remineralising treatment), proceeding from the zone 1 of the teeth.

Table 47. Analysis of variance automatically computed analysis vs semi-automatic performed by three independent technicians when the percentage of area of open tubules after the demineralizing treatment is concerned.

ANOVA						
Source of Variation	*SS*	*df*	*MS*	*F*	*P-value*	*F crit*
Between Groups	2,372485	3	0,790828	0,049796	0,985275	2,642851
Within Groups	3748,035	236	15,8815			
Total	3750,408	239				

Table 48. Technician / Tukey (HSD) / Analysis of the differences between the categories with a confidence interval of 95% for the percentage area of open tubules after the demineralizing treatment

Contrast	Difference	Standardized difference	Critical value	Pr > Diff	Significant
Software vs Technician 1	0,263	0,362	2,587	0,984	No
Software vs Technician 3	0,188	0,258	2,587	0,994	No
Software vs Technician 2	0,089	0,123	2,587	0,999	No
Technician 2 vs Technician 1	0,174	0,239	2,587	0,995	No
Technician 2 vs Technician 3	0,098	0,135	2,587	0,999	No
Technician 3 vs Technician 1	0,076	0,104	2,587	1,000	No
Tukey's d critical value:			3,659		

Table 49. Technician / Dunnett (two sided) / Analysis of the differences between the control category: software and the other categories with a confidence interval of 95% for the percentage area of open tubules after the demineralizing treatment

Category	Difference	Standardized difference	Critical value	Critical difference	Pr > Diff	Significant
Software vs Technician 1	0,263	0,362	2,364	1,720	0,969	No
Software vs Technician 3	0,188	0,258	2,364	1,720	0,988	No
Software vs Technician 2	0,089	0,123	2,364	1,720	0,999	No

Table 50. Analysis of variance automatically computed analysis vs semi-automatic performed by three independent technicians when the number of tubules is concerned after the demineralizing treatment

Source of Variation	*SS*	*df*	*MS*	*F*	*P-value*	*F crit*
Between Groups	510,4333	3	170,1444	0,109202	0,954665	2,642851
Within Groups	367703,3	236	1558,065			
Total	368213,7	239				

Table 51. Technician / Tukey (HSD) / Analysis of the differences between the categories with a confidence interval of 95% for the number of tubules after the demineralizing treatment

Contrast	Difference	Standardized difference	Critical value	Pr > Diff	Significant
Software vs Technician 1	3,817	0,530	2,587	0,952	No
Software vs Technician 3	0,983	0,136	2,587	0,999	No
Software vs Technician 2	0,667	0,093	2,587	1,000	No

Technician 2 vs Technician 1	3,150	0,437	2,587	0,972	No
Technician 2 vs Technician 3	0,317	0,044	2,587	1,000	No
Technician 3 vs Technician 1	2,833	0,393	2,587	0,979	No
Tukey's d critical value:			3,659		

Table 52. Technician / Dunnett (two sided) / Analysis of the differences between the control category: software and the other categories with a confidence interval of 95% for the number of tubules after the demineralizing treatment

Category	Difference	Standardized difference	Critical value	Critical difference	Pr > Diff	Significant
Software vs Technician 1	3,817	0,530	2,364	17,039	0,913	No
Software vs Technician 3	0,983	0,136	2,364	17,039	0,998	No
Software vs Technician 2	0,667	0,093	2,364	17,039	0,999	No

Table 53. Analysis of variance automatically computed analysis vs semi-automatic performed by three independent technicians when the percentage of area of open tubules after the remineralising treatment is concerned.

ANOVA						
Source of Variation	*SS*	*df*	*MS*	*F*	*P-value*	*F crit*
Between Groups	1,07901	3	0,35967	0,107329	0,955753	2,642851
Within Groups	790,8566	236	3,351087			
Total	791,9357	239				

Table 54. Technician / Tukey (HSD) / Analysis of the differences between the categories with a confidence interval of 95% for the percentage area of open tubules after the remineralizing treatment

Contrast	Difference	Standardized difference	Critical value	Pr > Diff	Significant
Software vs Technician 3	0,180	0,540	2,587	0,949	No
Software vs Technician 1	0,106	0,317	2,587	0,989	No
Software vs Technician 2	0,050	0,150	2,587	0,999	No
Technician 2 vs Technician 3	0,130	0,390	2,587	0,980	No
Technician 2 vs Technician 1	0,056	0,166	2,587	0,998	No
Technician 1 vs Technician 3	0,075	0,223	2,587	0,996	No
Tukey's d critical value:			3,659		

Table 55. Technician / Dunnett (two sided) / Analysis of the differences between the control category: software and the other categories with a confidence interval of 95% for the percentage area of open tubules after the remineralizing treatment

Category	Difference	Standardized difference	Critical value	Critical difference	Pr > Diff	Significant
Software vs Technician 3	0,180	0,540	2,364	0,790	0,908	No
Software vs Technician 1	0,106	0,317	2,364	0,790	0,979	No
Software vs Technician 2	0,050	0,150	2,364	0,790	0,998	No

Table 56. Analysis of variance automatically computed analysis vs semi-automatic performed by three independent technicians when the number of open tubules after the remineralising treatment is concerned.

ANOVA						
Source of Variation	*SS*	*df*	*MS*	*F*	*P-value*	*F crit*
Between Groups	205,3	3	68,43333	0,024171	0,994903	2,642851
Within Groups	668162,6	236	2831,198			
Total	668367,9	239				

Table 57. Technician / Tukey (HSD) / Analysis of the differences between the categories with a confidence interval of 95% for the number of open tubules after the remineralizing treatment

Contrast	Difference	Standardized difference	Critical value	Pr > Diff	Significant
Software vs Technician 3	2,283	0,235	2,587	0,995	No
Software vs Technician 1	1,950	0,201	2,587	0,997	No
Software vs Technician 2	0,700	0,072	2,587	1,000	No
Technician 2 vs Technician 3	1,583	0,163	2,587	0,998	No
Technician 2 vs Technician 1	1,250	0,129	2,587	0,999	No
Technician 1 vs Technician 3	0,333	0,034	2,587	1,000	No
Tukey's d critical value:			3,659		

Table 58. Technician / Dunnett (two sided) / Analysis of the differences between the control category: software and the other categories with a confidence interval of 95% for the number of open tubules after the remineralizing treatment

Category	Difference	Standardized difference	Critical value	Critical difference	Pr > Diff	Significant
Software vs Technician 3	2,283	0,235	2,364	22,968	0,991	No
Software vs Technician 1	1,950	0,201	2,364	22,968	0,994	No

Software vs Technician 2	0,700	0,072	2,364	22,968	1,000	No

Supplemental material 3 Evaluation of the representation of the data analysed by 3 skilled technicians derived from the results obtained in semi-automatic analysis performed on 120 pictures randomly chosen (60 images after the demineralization and 60 images after the remineralising treatment), proceeding from the zone 1 of the teeth.

Table 59. Results obtained after the desmineralising treatment

After the desmineralising treatment								
	number of open tubules				area of open tubules			
	Software	Tech. 1	Tech. 2	Tech. 3	Software	Tech. 1	Tech. 2	Tech. 3
Median	161,0	155,5	161,0	161,0	10,6	9,8	10,3	10,2
Mode	131	131	131	131				
Standard Deviation	39,8	39,4	39,0	39,7	4,0	4,1	3,9	3,9
Variance	1586,8	1551,2	1517,6	1576,6	15,9	16,8	15,4	15,4
Kurtosis	-0,97	-0,86	-0,86	-1,04	-0,66	-0,72	-0,59	-0,95
Asymmetry coefficient	0,26	0,32	0,33	0,24	0,39	0,46	0,42	0,31
Range	146	154	146	146	16,59	16,59	16,59	15,32
Minimum	100	92	100	100	4,40	4,40	4,40	4,40
Maximum	246	246	246	246	20,99	20,99	20,99	19,72
Sum	9944	9715	9904	9885	671,22	655,41	665,85	659,97
Asymmetry coefficient	+	+	+	+	+	+	+	+
Curtosis	Platyk.	Platyk.	Platyk.	Platyk.	Platyk.	Platyk.	Platyk.	Platyk.

Table 60. Results obtained after the resmineralising treatment

After the desmineralising treatment								
	number of open tubules				area of open tubules			
	Software	Tech. 1	Tech. 2	Tech. 3	Software	Tech. 1	Tech. 2	Tech. 3
Median	79,5	71,5	79,5	73,0	2,3	2,0	2,1	2,0
Mode	22	15	22	22		1,56		
Standard Deviation	53,4	53,8	53,4	52,3	1,9	1,8	1,8	1,8
Variance	2847,7	2894,2	2848,0	2734,8	3,5	3,4	3,4	3,1
Kurtosis	-1,28	-1,29	-1,32	-1,29	-0,15	-0,18	-0,30	0,19
Asymmetry coefficient	0,22	0,22	0,19	0,23	0,72	0,73	0,67	0,82
Range	185	181	177	175	7,12	7,21	7,12	7,12
Minimum	2	0	2	2	0,09	0,00	0,09	0,09
Maximum	187	181	179	177	7,21	7,21	7,21	7,21
Sum	4533	4416	4491	4396	153,34	146,99	150,32	142,51
Asymmetry coefficient	+	+	+	+	+	+	+	+
Curtosis	Platyk.	Platyk.	Platyk.	Platyk.	Platyk.	Platyk.	Platyk.	Leptok.

Conclusions

Presented doctoral dissertation brings up two vital topics of the oral health: hypersensitivity and remineralization of teeth. It includes a wide number of analytical methods such SEM, NIR/IR spectroscopy and ellipsometry and Raman. It also involves IR synchrotron techniques. The presented work extends the knowledge about the human dental tissue and deveopled new analytical methodologies attractive for both scientific as well as private dental market.

Presented thesis is organized in four topics. Detailed conclusions were included in each part and the general outcomes are furtherly enlisted.

In the first part of the dissertation a robust methodology based on the dentin disc model that applies a novel automatic segmentation algorithm for the data analysis has been developed and optimized. The determination of the region of interest was established by analyzing images that covered the entire surface of teeth. As a result of the performed studies it was proved that developed routine facilitates the observation and characterization of the dentin surface treated with the occluding agents. The present method can be a suitable scientific tool that will allow scientists and private companies the *in vivo* monitoring and assist on the development of new remineralising agents. It is operator independent and can be successfully applied in order to evaluate the obliterating capacity of the given agent as well as to perform comparative studies.

The second part presents a novel complementary analytical approach based on Hyper Spectral Imaging (HSI) with two types of NIR cameras (161 and 256 channels) and confocal Raman microscopy (CRM) was applied for analysis of teeth before and after application of different remineralizing agents. Obtained results were carefully analyzed and compared by the implementation of a Matlab routine that applies the correlation coefficient or MCR multivariate data analysis in order to obtain necessary information from the acquired spectra of dental samples.

As a result, a novel NIR HSI MCR method that allows differentiating remineralised tissue from the demineralized one was developed. It allows comparing the efficacy of various remineralizing treatment and characterization of the enamel surface that undercame the remineralization process. It also shows the distribution of the deposited fluorapatite on the tooth surface. Raman measurements confirmed the creation of fluorapatite detected by the NIR HSI MCR method and by such its suitability on the human enamel characterization.

The third topic shows the application of the synchrotron IRSE in order to evaluate the structural changes that undercome human teeth when treated with the reminearalising agents. Since the influence can vary depending on the zone of the teeth a cross section line going from the enamel into the pulp chamber was measured. As a result differences in the spectral signature depending on the position of the experimental point were observed.

In order to find a suitable reference sample for the interpretation of the obtained synchrotron data a serious of experiments and simulations were performed. Due to spectral differences the pure apatites could not be used for that purpose. In order to obtain more suitable reference samples, two types of etched human teeth (severe and gentle demineralization) were measured and compared with the experimental results. The simulated spectra revealed high similarity to the synchrotron data what allows to suspect that once both type of samples are analyzed with the synchrotron IRSE method more detailed information about the influence of the remineralising treatment on the dental tissue will be revealed.

The aim of the last part was to investigate structural changes in the human enamel and dentin induced by the remineralization process. The IR spectra from various points proceeding from different locations of the tooth were compared and studied applying Principal Component Analysis (PCA) and curve-fitting procedure.

Performed curve fitting of the pure apatite sample did not give clear results that could be confirmed in the bibliography. However, curve fitting of the real samples as well as the comparison of the spectra points and PCA analysis showed clear differences between various points proceeding from different locations in the enamel. Scattering effects and the general difficulties connected with the curve fitting performance leads to serious doubts about the interpretation of the obtained calculations and the interpretation of the bands. Performed calculations can be taken into consideration however should be confirmed with further experiments. One of the possible approach is the comparison of the CI (crystallinity index) obtained with the FTIR measurements with the CI derived from the ellipsometric measurements. If the obtained data coincide the continuation of the performed approach can be performed.

Bibliography

1. **Jalalian E, Meraji N, Mirzaei M. A.** A comparisson of the efficacy of potassium nitrate and Gluma desensitizerin the reduction of hypersensitivity in teeth with Full -crown preparations. *Journal of Contemporary Dental Practice.* 2009, Vol. 10, pp. 066-073.

2. **Schwarz F, Arweiler N, Georg T, Reich E.** Desensitizing effects of an Er:YAG laser on hypersensitive dentine. A controlled, prospective clinical study. *Journal of Clinical Periodontology.* 2002, Vol. 29, pp. 211–215.

3. **Thrash WJ, Jones DL, Dodds WJ.** Effect of a fluoride solution on dentinal hypersensitivity. *American Journal of Dentistry.* 1992, Vol. 5, pp. 299-302.

4. **Walters, P.A.** Dentinal Hypersensitivity: A Review. *The Journal of Contemporary Dental Practice.* 2005, Vol. 6, pp. 1-10.

5. **N. West a, R.G. Newcombe , N. Hughes , S. Mason , B. Maggio , F. Sufi , N. Claydon.** A 3-day randomised clinical study investigating the efficacy of two toothpastes, designed to occlude dentine tubules, for the treatment of dentine hypersensitivity. *Journal of Dentistry.* 2013, Vol. 41, pp. 187 – 194.

6. **Eilis Lynch, Delia S. Brauer,Natalia Karpukhina, David G. Gillam, Robert G. Hill.** Multi-component bioactive glasses of varying fluoride content for treating dentin hypersensitivity. *Dental Materials.* 2012, Vol. 28, pp. 168–178.

7. **Robert H Selwitz, Amid I Ismail, Nigel B Pitts.** Dental caries. *Lancet.* 2007, Vol. 369, pp. 51–59.

8. **Hannig C, Hamkens A, Becker K,.** Erosive effects of different acids on bovine enamel: release of calcium and phosphate in vitro. *Archives of Oral Biology.* 2005, Vol. 50 (6), pp. 541-552.

9. **Walsh, L.J.** Contemporary technologies for remineralization therapies: A review. *International Dentistry SA.* 2009, Vol. 11.

10. **Reynolds, EC.** Calcium phosphate-based remineralization systems: scientific evidence? *Australian Dental Journal.* 2008, Vol. 53, pp. 268–273.

11. **Walsh, L.J.** Contemporary technologies for remineralization therapies: A review. *International Dentistry SA.* 2009, Vol. 11, pp. 6-16.

12. **Attin, T; Kielbassa, A.M; Schwanenberg , M; Helwig, E.** Effect of fluoride treatment on remineralization of bleached enamel. *Journal of Oral Rehabilitation.* 1997, Vol. 24, pp. 282–286.

13. **Jones, F.H.** Teeth and bones: application of surface science to dental materials and related biomaterials. *Surface Science Report.* 2001, Vol. 42, pp. 75-205.

14. **Thomas Attin, Patrick R. Schmidlin, Florian Wegehaupt, Annette Wiegand.** Influence of study design on the impact of bleaching agents on dental enamel microhardness: A review. *Dental Materials.* 2009, Vol. 25, pp. 143–157.

15. **Alías, Pilar Ortiz.** *Aplicacción de Microscopia Electrónica y Radiación Sincrotrón al Estudio de Materiales y Procesos Avanzados para la Salud y la Estética Dental.* 2012.

16. **Sonica Singhal, Rejane Correa, Carlos Quinonez.** The impact of dental treatment on employment outcomes: A systematic review. *Health Policy.* 2013, Vol. 109, pp. 88– 96.

17. **Paola Fattibene, Freddy Callens.** EPR dosimetry with tooth enamel: A review. 2010, Vol. 68, pp. 2033-2116.

18. **Michael L. Painea, Shane N. White, Wen Luo, Hanson Fong,Mehmet Sarikaya, Malcolm L. Snead.** Regulated gene expression dictates enamel structure and tooth function. . *Matrix Biology.* 2001, Vol. 20, pp. 273-292.

19. **Yuwei Fan, Zhi Sun, Janet Moradian-Oldak.** Controlled remineralization of enamel in the presence of amelogenin and fluoride. *Biomaterials.* 2009, Vol. 30, pp. 478–483.

20. **N. Leroy, E. Bres.** Structure and substitutions in fluorapatite. *European Cells and Materials.* 2001, Vol. 2, pp. 36-48.

21. **St, Naray-Szabo.** The structure of apatite (CaF)Ca4(PO4)3. *Z für Kristallographie.* 1930, Vol. 75, pp. 387-398.

22. **J. Moradian-Oldak, J. Tan, A. G. Fincham.** Interaction of Amelogenin with Hydroxyapatite Crystals:An Adherence Effect Through Amelogenin Molecular Self-Association. *Biopolymers.* 1998, Vol. 46, pp. 225–238.

23. **Kun Tian, Min Peng, Xiaohua Ren, Chuhang Liao, Wei Fei.** Regeneration of tooth-like hydroxyapatite depended on amelogenin functional section monolayer: A new approach for tooth repair. *Medical Hypotheses.* 2012, Vol. 79, pp. 143–146.

24. **Gibson, Carolyn W.** The Amelogenin Proteins and Enamel Development in Humans and Mice. *J. Oral Biosci.* 2011, Vol. 53, pp. 248-256.

25. **Daming Fan, Rajamani lakshminarayanan, Janet Moradian-Oldak.** The 32 kDa enamelin undergoes conformational transitions upon calcium binding. *Journal of Structural Biology.* 2008, Vol. 163, pp. 109-115.

26. **Jan C.-C. Hu, Yuanyuan Hu, Charles E. Smith,Marc D. McKe, J. Timothy Wright, Yasuo Yamakoshi.** Enamel Defects and Ameloblast-specific Expression in Enam Knock-out/lacZ Knock-in Mice. . *Journal of Bilogical CHemistry.* 2008, Vol. 283, pp. 10858–10871.

27. **Bouropoulos, N., Moradian-Oldak, J.** Induction of apatite by the cooperative effect of amelogenin and the 32-kDa enamelin. *Journal of Dental Research.* 2004, Vol. 83, pp. 278–282.

28. **Daming Fan, Chang Du, Zhi Sun, Rajamani Lakshminarayanan, Janet Moradian-Oldak.** In vitro study on the interaction between the 32 kDa enamelin and amelogenin. . *Journal of Structural Biology.* 2009, Vol. 166, pp. 88–94.

29. **Caroline T. Paine, Michael L. Paine, Wen Luo, Curtis T. Okamoto, S. Petter Lyngstadaas, Malcolm L. Snead.** A Tuftelin-interacting Protein (TIP39) Localizes to the Apical Secretory Pole of Mouse Ameloblasts. *The Journal of Biological Chemistry.* 2000, Vol. 275, pp. 22284–22292.

30. **Cate, Ten.** *Oral histology: Development, Structure, and Function.* s.l. : Mosby-Year Book, 1994.

31. **Stefan Habelitz, Mehdi Balooch, Sally J. Marshall, Guive Balooch, Grayson W. Marshall Jr.** In situ atomic force microscopy of partially demineralized human dentin collagen fibrils. *Journal of Structural Biology.* 2002, Vol. 138, pp. 227–236.

32. **Linde A, Goldberg M.** Dentinogenesis. *Critical Reviews in Oral Biology and Medicine.* 1993, Vols. 4(5),, pp. 679-728.

33. **Pashley, D. H.** Clinical correlations of dentin structure and function. *The Journal of Prosthetic Dentistry.* 1991, Vol. 66, pp. 777-81.

34. **Lopez M.B, Sinhoreti M.A.C, Gonini Jr A, Consani S, Mccabe J.F.** Comparative Study of Tubular Diameter and Quantity for Human and Bovine Dentin at Different Depths. *Brazilian Dental Journal.* 2009, Vol. 20, pp. 279-283.

35. **R H Selwitz, A I Ismail, N B Pitts.** Dental Caries. *Lancet.* 2007, Vol. 369, pp. 51–59.

36. **Attin, T; Schmidlin , P.R; Wegehaupt, F; Wiegand, A.** Influence of study design on the impact of bleaching agents on dental enamel microhardness: A review. *Denatl Materials.* 2009, Vol. 25, pp. 143-157.

37. **Gladwell, J; Simmons , D; Wright, J.T.** Remineralization potential of a fluoridated carbamide peroxide whitening gel. *Journal of Esthetic and Restorative Dentistry.* 2006, Vol. 4, pp. 206-213.

38. **Moreno , E.C; Zahradnik, R.T.** Demineralization and remineralization of dental enamel. *Journal of Dental Research.* 1979, Vol. 58b, pp. 896-902.

39. **Karlinsey, R.L and Mackey, A.C.** Solid-state preparation and dental application of an organically modified calcium phosphate. *Journal of Material Sciences.* 2009, Vol. 44, pp. 346–349.

40. **Athena Papas, David Russell, Mabi Singh, Ralph Kent, Cal Triol,Anthony Winston.** Caries clinical trial of a remineralising toothpaste in radiation patients. *Gerodontology.* 2008, Vol. 25, pp. 76-88.

41. **Skrtic, D, et al., et al.** Silica- and zirconia-hybridized amorphous calcium phosphate: Effect on transformation to hydroxyapatite. *Journal of Biomedical Materials Research.* 2002, Vol. 59, pp. 597-604.

42. **Reynolds, E.C.** Casein phosphopeptide-amorphous calcium phosphate and the remineralization of enamel. *US Dentistry.* 2006, pp. 51-54.

43. **Jeremy Rees, Theresa Loyn, Barbara Chadwick.** Pronamel and tooth mousse: An initial assessment of erosion prevention in vitro. *Journal of Dentistry,.* 2 0 0 7, Vol. 3 5, pp. 35 5 – 35 7.

44. **EC, Reynolds.** Anticariogenic complexes of amorphous calcium phosphate stabilized by casein phosphopeptides: a review. *Spec CareDentist.* 1998, Vol. 18(1), pp. 8-16.

45. **Shannon M, Bohn PW, Elemelech M et al.** Science and technology for water purification in the coming decades. *Nature.* 2008, Vol. 452, pp. 301-310.

46. **O, Samuelson.** *Ion Exchange separation in analytical chemistry.* s.l. : Alquist & Wiksell, 1963.

47. **Reeves JP, Sutko JL.** Sodium-calcium ion exchange in cardiac membrane vesicles. . *Proc Natl Acad Sci.* 1979, Vol. 76.

48. **Valiente M.** *Remineralizing material for organomineral tisues. 6,413,498 B1* USA, 1999.

49. **W, Dorfner.** *Ion exchangers.* s.l. : Walter de Gruyter & Co, 1991.

50. **Attin, T, et al., et al.** Effect of fluoride treatment on remineralization of bleached enamel. *Journal of Oral Rehabilitation.* 1997, Vol. 24, pp. 282–286.

51. **JDB, Featherstone.** Prevention and reversal of dental caries: role of low level fluoride. *Community Dentistry and Oral Epidemiology.* 1999, Vol. 27(1), pp. 31–40.

52. **EH, Lukomsky.** Fluorine therapy for exposed dentin and alveolar antrophy. *Journal of Dental Research.* 1941, Vol. 20(6), pp. 649–59.

53. **Akiniwa, K.** Re-examination of acute toxicity of fluoride. *Fluoride.* 1997, Vol. 30, pp. 89-104.

54. **Levy SM, Guha-Chowdhury N.** Total Fluoride Intake and Implications for Dietary Fluoride Supplementation. *Journal of Public Health Dentistry.* 1999, Vol. 59, pp. 211-23.

55. **Athena Papas, David Russell, Mabi Singh, Ralph Kent, Cal Triol,Anthony Winston.** Caries clinical trial of a remineralising toothpaste in radiation patients. . *Gerodontology.* 2008, Vol. 25, pp. 76-88.

56. **Eilis Lynch, Delia S. Brauer,Natalia Karpukhina, David G. Gillam, Robert G. Hill.** Multi-component bioactive glasses of varying fluoride content for treating dentin hypersensitivity. *Dental Materials.* 2012, Vol. 28, pp. 168-178.

57. **Jones, Julian R.** Review of bioactive glass: From Hench to hybrids. *Acta Biomaterialia.* 2013, Vol. 9, pp. 4457–4486.

58. **Cummins, D.** The Efficacy of a New Dentifrice Containing 8.0% Arginine,Calcium Carbonate, and 1450 ppm Fluoride in Delivering Instant and Lasting Relief of Dentin Hypersensitivity. *The Journal of Clinical Dentistry.* 2009, Vol. 20, pp. 109–114.

59. **N. West a, R.G. Newcombe , N. Hughes , S. Mason , B. Maggio , F. Sufi , N. Claydon.** A 3-day randomised clinical study investigating the efficacy of two toothpastes, designed to occlude

dentine tubules, for the treatment of dentine hypersensitivity. *Journal of Dentistry.* 2013, Vol. 41, pp. 187 – 194.

60. **Petrou I, Heu R, Stranick M, Lavender S, Zaidel L, Cummins D, Sullivan RJ, Hsueh C, Gimzewski JK.** A Breakthrough Terapy for Dentin Hypersensitivity: How dental Product Containing 8% of Arginine and Calcium Carbonate Work to Deliver Effective Relief of Sensitive Teeth. *Journal of Clinical Dentistry.* 2009, Vol. 20, pp. 23-31.

61. **Hui-Chieh Hsu, Shiuan-Shinn Lee, Yu-Chao Chang.** Clinical efficacy of toothpaste containing 8.0% arginine and calcium carbonate for teeth hypersensitivity. *Journal of Dental Sciences.* 2013, Vol. 8, pp. 444-447.

62. **Ayad F, Berta R, De Vizio W, McCool J, Petrone ME, Volpe AR.** Comparative efficacy of two dentifrices containing 5% potassium nitrate on dentinal sensitivity: a twelve-week clinical study. *The Journal of Clinical Dentistry.* 1994, Vol. 5, pp. 97-101.

63. **Peter Tschoppe, Daniela L. Zandim, Peter Martus, Andrej M. Kielbassa.** Enamel and dentine remineralization by nano-hydroxyapatite toothpastes. *Journal of Dentistry.* 2011, Vol. 39, pp. 430–437.

64. **S B Huang, S S Gao and H Y Yu.** Effect of nano-hydroxyapatite concentration on remineralization of initial enamel lesion in vitro. *Biomedical materials.* 2009, Vol. 4, p. 034104 (6pp).

65. **K. Najibfard, K. Ramalingam, MPhil, I. Chedjieu, B.T. Amaechi.** Remineralization of Early Caries by a Nano-Hydroxyapatite Dentifrice. *The Journal of Clinical Dentistry.* 2011, Vol. 22, pp. 22:000–000.

66. **Christian H. Splieth, Aikaterini Tachou.** Epidemiology of dentin hypersensitivity. *Clinical Oral Investigations.* 2013, Vol. 17, pp. S3–S8.

67. **Hongchun Liu, Deyu Hu,.** Efficacy of a Commercial Dentifrice Containing 2% Strontium Chloride and 5% Potassium Nitrate for Dentin Hypersensitivity: A 3-Day Clinical Study in Adults in China. *Clinical Therapeutics.* 2012, Vol. 34, pp. 614-622.

68. **P.L Jacobsen, G.Bruce.** Clinical Dentin Hypersensitivity: Understanding the Causes and Prescribing a Treatment. *The Journal of Contemporary Dental Practice.* 2001, Vol. 2, pp. 1-8.

69. **Pashley, David H.** How can sensitive dentine become hypersensitive and can it be reversed? *Jornal of Dentistry.* 2013, Vol. 41s4, pp. s49–s55.

70. **Cummins, D.** Dentin Hypersensitivity: From Diagnosis to a Breakthrough Therapy for Everyday Sensitivity Relief. *The Journal of Clinical Dentistry.* 2009, Vol. 20, pp. 1–9.

71. **J. Cunha-Cruz, J.R. Stout, L.J. Heaton, and J.C. Wataha.** Dentin Hypersensitivity and Oxalates: a Systematic Review. *Journal of Dental Research.* 2011, Vol. 90, pp. 304-310.

72. **D. G. Gillam, N. J. Mordan, A. D. Sinodinou, J. Y. Tang, J. C. Knowles.** The effects of oxalate-containing products on the exposed dentine surface: an SEM investigation. *Journal of Oral Rehabilitation.* 2001, Vol. 28, pp. 1037-1044.

73. **Petrou I, Heu R, Stranick M, Lavender S, Zaidel L, Cummins D, Sullivan RJ, Hsueh C, Gimzewski JK.** A Breakthrough Terapy for Dentin Hypersensitivity: How dental Product Containing 8% of Arginine and Calcium Carbonate Work to Deliver Effective Relief of Sensitive Teeth. *Journal of Clinical Dentistry.* 2009, Vol. 20, pp. 23-31.

74. **Hui-Chieh Hsu, Shiuan-Shinn Lee, Yu-Chao Chang.** Clinical efficacy of toothpaste containing 8.0% arginine and calcium carbonate for teeth hypersensitivity. *Journal of Dental Sciences.* 2013, Vol. 8, pp. 444-447.

75. **Ayad F, Berta R, De Vizio W, McCool J, Petrone ME, Volpe AR.** Comparative efficacy of two dentifrices containing 5% potassium nitrate on dentinal sensitivity: a twelve-week clinical study. *The Journal of Clinical Dentistry.* 1994, Vol. 5, pp. 97-101.

76. **Cummins, D.** The Efficacy of a New Dentifrice Containing 8.0% Arginine,Calcium Carbonate, and 1450 ppm Fluoride in Delivering Instant and Lasting Relief of Dentin Hypersensitivity. *The Journal of Clinical Dentistry.* 2009, Vol. 20, pp. 109–114.

77. **Sigee, David C.** Environmental SEM and X-Ray Microanalysis of Biological Materials. *Mikrochimica Acta Supplement.* 1998, Vol. 15, pp. 283-293.

78. **Toshiaki USHIGOME, Shinji TAKEMOTO, Masayuki HATTORI, Masao YOSHINARI, Eiji KAWADA, Yutaka ODA.** Influence of peroxide treatment on bovine enamel surface —Cross-sectional analysis. *Dental Materials Journal .* 2009, Vol. 28(3), pp. 315–323.

79. **Laise Daniela Carrasco-Guerisoli, Renato Jonas dos Santos Schiavoni, Juliana Machado Barroso, Danilo Mathias Zanello Guerisoli, Jesus Djalma Pecora, Izabel Cristina Froner.** Effect of different bleaching systems on the ultrastructure of bovine dentin. *Dental Traumatology .* 2009, Vol. 25, pp. 176–180.

80. **Hermann Gotz, Heinz Duschner, Donald J. White , Malgorzata A. Klukowska.** Effects of elevated hydrogen peroxide ‘strip’ bleaching on surface and subsurface enamel including subsurface histomorphology, micro-chemical composition and fluorescence changes. *Journal of Dentistry .* 2007, Vol. 35, pp. 457-466.

81. **Alexander V. Zavgorodniy, Ramin Rohanizadeh, Michael V. Swain.** Ultrastructure of dentine carious lesions. *Archives of Oral Biology .* 2008, Vol. 53, pp. 124-132.

82. **L.Ciocca, I.Gallina, E.Navacchia,P.Baldissara, R. Scotti.** A new method for quantitative analysis of dentinal tubules. *Computers in Biology and Medicine.* 2007, Vol. 37, pp. 277-286.

83. **M. Farina, A. Schemmel, G. Weissmuller,R. Cruz,B. Kachar, P. M. Bisch.** Atomic Force Microscopy Study of Tooth Surface. *Journal of Structural Biology.* 1999, Vol. 125, pp. 39–49.

84. **Salah Hasab Mahmoud, Abeer El Sayed Elembaby, Ahmed Ragheb Zaher, Mohammed El-Awady Grawish,Heba M Elsabaa, Salwa Abd El-Raof El- Negoly, Mohamed Abdel Kader Sobh,.**

Effect of 16% Carbamide Peroxide Bleaching Gel on Enamel and Dentin Surface Micromorphology and Roughness of Uremic Patients: An Atomic Force Microscopic Study. *European Journal of Dentistry.* 2010, Vol. 4.

85. **C. Hegedus, T. Bistey, E. Flora-Nagy, G. Keszthelyi, A. Jenei.** An atomic force microscopy study on the effect of bleaching agents on enamel surface. *Journal of Dentistry.* 1999, Vol. 27, pp. 509–515.

86. **Charles R. Parkinson, Atif Shahzad, Gareth D. Rees.** Initial stages of enamel erosion: An in situ atomic force microscopy study. *Journal of Structural Biology.* 2010, Vol. 171, pp. 298–302.

87. **Samjin Choi, Yeri Rhee, Jeong-Hoon Park, Gi-Ja Lee, Kyung-Sook Kim, Jae-Hong Park, Young-Guk Park, Hun-Kuk Park.** Effects of fluoride treatment on phosphoric acid-etching in primary teeth: An AFM observation. *Micron.* 2010, Vol. 41, pp. 498–506.

88. **Yeau-Ren Jeng, Tsung-Ting Lin, Hsiu-Ming Hsu, Hsin-Ju Chang, Dar-Bin Shieh,.** Human enamel rod presents anisotropic nanotribological properties. *Journal of Mechanical Behaviour of Biomedical Materials.* 2011, Vol. 4, pp. 515-522.

89. **Leo Lou, Alan E. Nelson, Giseon Heo, Paul W. Major.** Surface chemical composition of human maxillary first premolar as assessed by X-ray photoelectron spectroscopy (XPS). *Applied Surface Science.* 2008, Vol. 254, pp. 6706–6709.

90. **F. Taube, R. Ylmen, A. Shchukarev, S. Nietzsche, J.G. Noren.** Morphological and chemical characterization of tooth enamel exposed to alkaline agents. *Journal of Dentistry.* 2010, Vol. 38, pp. 72-81.

91. **Bat-Ami Gotliv, Joshua S. Robach, Arthur Veis.** The composition and structure of bovine peritubular dentin: Mapping by time of flight secondary ion mass spectroscopy. *Journal of Structural Biology .* 2006, Vol. 156, pp. 320–333.

92. **Birgitta Jalevik, Hans Odelius, Wolfram Dietz, Jorgen G. Noren.** Secondary ion mass spectrometry and X-ray microanalysis of hypomineralized enamel in human permanent first molars. *Archives of Oral Biology .* 2001, Vol. 46, pp. 239–247.

93. **Tobias Nilsson, Ted Lundgren, Hans Odelius, Rudolf Sillen, Jorgen G. Noren.** A computerized induction analysis of possible co-variations among different elements in human tooth enamel. *Artificial Intelligence in Medicine.* 1996, Vol. 8, pp. 515 -526.

94. **T. Lundgren, L.G. Persson, E.U. Engstrom, J. Chabala, R. Levi-Setti,J.G. Noren.** A secondary ion mass spectroscopic study of the elemental composition pattern in rat incisor dental enamel during diferent stages of ameloblast differentiation. *Archives of Oral Biology.* 1998, Vol. 43, pp. 841-848.

95. **Y.L. Chan, A.H.W. Ngan, N.M. King.** Nano-scale structure and mechanical properties of the human dentine–enamel junction. *Journal Of The Mechanical Behavior OF Biomedical Materials.* 2011, Vol. 4, pp. 785-795.

96. **S. Wongkhantee, V. Patanapiradej C. Maneenut, D. Tantbirojn.** Effect of acidic food and drinks on surface hardness of enamel, dentine, and tooth-coloured filling materials. *Journal of Dentistry.* 2006, Vol. 34, pp. 214–220.

97. **José Reyes-Gasga, Esmeralda L. Martínez-Piñeiro, Galois Rodríguez-Álvarez, Gaby E. Tiznado-Orozco,Ramiro García-García, Etienne F. Brès.** XRD and FTIR crystallinity indices in sound human tooth enamel and synthetic hydroxyapatite. *Materials Science and Engineering C.* 2013, Vol. 33, pp. 4568–4574.

98. **Alessandra Marques Correa-Afonso, Luciano Bachmann, Cıntia Guimaraes de Almeida, Silmara Aparecida Milori Corona, Maria Cristina Borsatto.** FTIR and SEM analysis of CO2 laser irradiated human enamel. *Archives Of Oral Biology* . 2012, Vol. 57, pp. 1153-1158.

99. **Isabel Maria Porto, Regina Aparecida Saiani, K.L. Andrew Chan, Sergei G. Kazarian, Raquel Fernanda Gerlach, Luciano Bachmann.** Organic and inorganic content of fluorotic rat incisors measured by FTIR spectroscopy. *Spectrochimica Acta Part A.* 2010, Vol. 77, pp. 59–63.

100. **P.L Jacobsen, G.Bruce.** Clinical Dentin Hypersensitivity: Understanding the Causes and Prescribing a Treatment. *The Journal of Contemporary Dental Practice.* 2001, Vol. 2, pp. 1-8.

101. **L., Camps Giménez, F., Alpiste Illueca and FJ, Gil Loscos.** *Hipersensibilidad dentiaria: comparativa "in vitro" de tres dentífricos comerciales específicos para su tratamiento.* s.l. : Máster de periodoncia e implantes. Facultad de medicina y odontología. Universidad de Valencia., 2012.

102. **Oberg, C., et al., et al.** Evaluation of desensitizing agents on dentin permeability and dentinal tubule occlusion: an in vitro study. *General dentistry.* 2009, Vol. 57, pp. 496-5016.

103. **Camilleri, J., et al., et al.** Porosity and root dentine to material interface assessment of calcium silicate-based root-end filling materials. *Clinical Oral Investigations.* 2014, Vol. 18, pp. 1437-1446.

104. **De-Deus, G., et al., et al.** Co-site digital optical microscopy and image analysis: an approach to evaluate the process of dentine demineralization. *International Endodontic Journal.* 2006, Vol. 40, pp. 683-692.

105. **Arends J, Stokroos I, Jongebloed WG, Ruben J.** The diameter of dentinal tubules in human coronal dentine after demineralization and air drying. A combined light microscopy and SEM study. *Caries Research.* 1995, Vol. 29, pp. 118–121.

106. **D.G. Gillam, N.J. Mordan, H.N. Newman.** The Dentin Disc Surface: A Plausible Model for Dentin Physiology and Dentin Sensitivity Evaluation. *Advances in Dental Research.* 1997, Vol. 11(4), pp. 487-501.

107. **Gillam DG, Khan N, Mordan NJ, Barber PM.** Scanning electron microscopy (SEM) investigation of selected desensitizing agents in the dentine disc model. *Endodontics & Dental Traumatology.* 1999, Vol. 15, pp. 198-204.

108. **H. C. Ruschel, O. Chevitarese.** Density and diameter of dentinal tubules of first and second primary human molars - comparative scanning electron microscopy study. *Journal of Clinical Pediatric Dentistry.* 2002, Vol. 26, pp. 297–304.

109. **Isik AG, Tarim B, Hafez AA, Yalçin FS, Onan U, Cox CF.** A comparative scanning electron microscopic study on the characteristics of demineralized dentin root surface using different tetracycline HCl concentrations and application times. *Journal of Periodontology.* 2000, Vol. 71, pp. 219-25.

110. **McAndrew R, Kourkouta S.** Effects of toothbrushing prior and/or subsequent to dietary acid application on smear layer formation and the patency of dentinal tubules: an SEM study. *Journal of Periodontology.* 1995, Vol. 66, pp. 443–448.

111. **T.Y.Y. Ling, D . G . G illam, P . M . B arber , N . J . Mordan, J . Critchell.** An investigation of potential desensitizing agents in the dentine disc model: a scanning electron microscopy study. *Journal of Oral Rehabilitation.* 1997, Vol. 24, pp. 191-203.

112. **C L Chen, A Parolia, A Pau, I C Celerino de Moraes Porto.** Comparative evaluation of the effectiveness of desensitizing agents in dentine tubule occlusion using scanning electron microscopy. *Australian Dental Journal.* 20015, Vol. 60, pp. 65-72.

113. **De-Deus, G., et al., et al.** Real-time atomic force microscopy of root dentine during demineralization when subjected to chelating agents. *International Endodontic Journal.* 2006, Vol. 39, pp. 683-692.

114. **C.R. Wen, R.G. Caffesse, E.C. Morrison, C.E. Nasjleti, U.K. Parikh,.** In vitro effects of citric acid application techniques on dentin surfaces. *Journal of Periodontology.* 1992, Vol. 63, pp. 883–889.

115. **S. Olsson, G. Öilo,E. Adamczak.** The structure of dentin surfaces exposed for bond strength measurements. *European Journal of Oral Sciences.* 1993, Vol. 101, pp. 180–184.

116. **T. R. AHMED, N. J. MORDAN, M. S. GILTHORPE, D. G. GILLAM.** In vitro quantification of changes in human dentine tubule parameters using SEM and digital analysis. *Journal of Oral Rehabilitation.* 2005, Vol. 32, pp. 589–597.

117. **Wells, OC.** *Scanning electron microscopy.* Oxford : Elsevier, 2001.

118. **Das RS, Agrawal YK.** Raman spectroscopy: Recent advancements, techniques and applications. *Vibrational Spectroscopy.* 2011, Vol. 57, pp. 163-176.

119. **GC., Baldwin.** Origin of Synchrotron Radiation. *Physics Today.* 1975, Vol. 28, p. 9.

120. **RP, Madden.** *Synchrotron Radiation and Applications. .* New York : McGraw-Hill Book Company, 1974.

121. **K., Codling.** Atomic and Molecular Physics Using Synchrotron Radiation—the Early Years. *Jornal of Synchrotron Radiation.* 1997.

122. **Pelletier MJ, Pelletier CC.** *Spectroscopic theory for Chemicals Imaging.* New Yersey : John Wiley & Sons, 2010.

123. **Stuart, B.** *Infrared Spectroscopy.* s.l. : Willey & Sons, 2005.

124. **H.Fujiwara.** *Spectroscopic Ellipsometry Principles and Applications.* Tokyo : John Wiley & Sons Ltd, 2007.

125. **Arwin, H.** Application of ellipsometry techniques to biological materials. *Thin Solid Films.* 2011, Vol. 519, pp. 2589–2592.

126. **Karsten Hinrichs, Klaus-Jochen Eichhorn.** *Ellipsometry of Functional Organic Surfaces and Films.* s.l. : Springer, 2014.

127. **M. Gensch, E.H. Korte, N. Esser, U. Schade , K. Hinrichs.** Microfocus-infrared synchrotron ellipsometer for mapping of ultra thin films. *Infrared Physics & Technology.* 2006, Vol. 49, pp. 74–77.

128. **M. Blanco, I. Villarroya.** NIR spectroscopy: a rapid-response analytical tool. *Trends in analytical chemistry.* 2002, Vol. 21.

129. *Multi- and hyperspectral geologic remote sensing: A review.* **Van der Meer, F D, et al., et al.** 2012, International Journal of Applied Earth Observation and Geoinformation, Vol. 14, pp. 112-128.

130. *Multivariate image analysis: A review with applications.* **Prats-Montalban, J M, de Juan, A and Ferrer, A.** 2011, Chemometrics and Intelligent Laboratory Systems, Vol. 107, pp. 1-23.

131. **Lucena, F.B.** *Chemical Speciation on Urinary Lithiasis. Image Analysis and Separation Techniques for the study of Lithogenesis. Doctoral Thesis.* 2014.

132. *Data processing of vibrational chemical imaging for pharmaceutical applications.* **Sacre, P Y, et al., et al.** 2014, Journal of Pharmaceutical and Biomedical Analysis, Vol. Article in Press, p. DOI: 10.1016/j.jpba.2014.04.012.

133. **Juan G. Rosas, Marcelo Blanco.** A criterion for assesing homogenity distribution in spectral images. Part 2: Application of homogeneity indices to solid pharmaceutical dosage forms. *Journal fo Pharmaceutical and Biomedical Analysis.* 2012, Vol. 70, pp. 691-699.

134. **H. Ma, C.A. Anderson.** Characterization of pharmaceutical powder blends by NIR chemical imaging. *J. Pharm. Sci.* 2008, Vol. 97, pp. 3305–3320.

135. **Y. Roggo, A. Edmond, P. Chalus, M. Ulmschneider.** Infrared hyperspectral imaging for qualitative analysis of pharmaceutical solid forms. *Analytica Chimica Acta.* 2005, Vol. 535, pp. 79–87.

136. **Clarke, F.** Extracting process-related information from pharmaceutical dosage forms using near infrared microscopy. *Vib. Spectrosc.* 2004, Vol. 34, pp. 25–35.

137. **J.M. Amigo, J. Cruz, M. Bautista, S. Maspoch, J. Coello, M. Blanco.** Study of pharmaceutical samples by NIR chemical-image and multivariate analysis,. *Trends in Analytical Chemistry.* 2008, Vol. 27, pp. 696–713.

138. **R.C. Lyon, D.S. Lester, E.N. Lewis, E. Lee, L.X. Yu, E.H. Jefferson, A.S. Hussain.** Nearinfrared spectral imaging for quality assurance of pharmaceutical products:analysis of tablets to assess powder blend homogeneity. *AAPS PharmSciTech.* 2002, Vol. 3, pp. 1–15.

139. **B.J. Westenberger, C.D. Ellison, A.S. Fussner, S. Jenney, R.E. Kolinski, T.G. Lipe, R.C. Lyon, T.W. Moore, L.K. Revelle, A.P. Smith, J.A. Spencer, K.D. Story, D.Y.Toler, A.M. Wokovich, L.F. Buhse,.** Quality assessment of internet pharmaceutical products using traditional and non-traditional analytical techniques. *Int. J. Pharm. .* 2005, Vol. 306, pp. 56–70.

140. **A. Palou, J. Cruz, M. Blanco, J. Tomas, J. De los Rios, M. Alcala.** Determination of drug, excipients and coating distribution in pharmaceutical tablets using NIR-CI. *J. Pharm. Anal.* 2012, Vol. 2, pp. 90–97.

141. **Tauler, R.** Multivariate curve resolution applied to second order data. *Chemometrics and Intelligent Laboratory Systems.* 1995, Vol. 30, pp. 133-146.

142. **al., N.Jovanovic et.** Near-Infrared Imaging for Studying Homogeneity of Protein-Sugar Mixtures. *Pharmaceutical Research.* 2006, Vol. 23, pp. 2002-2013.

143. **Blanco, J.G. Rosas and M.** Criterion to assess homogeneity distribution on hyperspectral images. Part 2: Application of homogeneity indices to solid pharmaceutical dosage forms. *Journal of Pharmaceutical and Biomedical Analysis.* 2012, Vol. 70, pp. 691–699.

144. **Joaquim Jaumot, Raimundo Gargallo, Anna de Juan, Roma` Tauler.** A graphical user-friendly interface for MCR-ALS: a new tool for multivariate curve resolution in MATLAB. *Chemometrics and Intelligent Laboratory Systems.* 2005, Vol. 76, pp. 101–110.

145. *Study of pharmaceutical samples by NIR chemical-image and multivariate analysis.* **Amigo, J, et al., et al.** 2008, Trends in Analytical Chemistry, Vol. 27, pp. 696-713.

146. **Moreno, E.C and Zahradnik, R.T.** Demineralization and remineralization of dental enamel. *Journal of Dental Research.* 1979, Vol. 58b, pp. 896-902.

147. **JDB, Featherstone.** Prevention and reversal of dental caries: role of low level fluoride. *Community Dentistry and Oral Epidemiology.* 1999, Vol. 27(1), pp. 31–40.

148. **EH, Lukomsky.** Fluorine therapy for exposed dentin and alveolar antrophy. . *Journal of Dental Research.* 1941, Vol. 20(6), pp. 649–59.

149. **EC, Reynolds.** Anticariogenic complexes of amorphous calcium phosphate stabilized by casein phosphopeptides: a review. *Spec CareDentist.* 1998, Vol. 18(1), pp. 8-16.

150. **Reynolds, E.C.** Casein phosphopeptide-amorphous calcium phosphate and the remineralization of enamel. *US Dentistry.* 2006, pp. 51-54.

151. **Skrtic, D, et al., et al.** Silica- and zirconia-hybridized amorphous calcium phosphate: Effect on transformation to hydroxyapatite. . *Journal of Biomedical Materials Research. .* 2002, Vol. 59, pp. 597-604.

152. **Eilis Lynch, Delia S. Brauer,Natalia Karpukhina, David G. Gillam, Robert G. Hill.** Multi-component bioactive glasses of varying fluoride content for treating dentin hypersensitivity. *Dental Materials.* 2012, Vol. 28, pp. 168-178.

153. **Jones, Julian R.** Review of bioactive glass: From Hench to hybrids. *Acta Biomaterialia.* 2013, Vol. 9, pp. 4457–4486.

154. **Cummins, D.** The Efficacy of a New Dentifrice Containing 8.0% Arginine,Calcium Carbonate, and 1450 ppm Fluoride in Delivering Instant and Lasting Relief of Dentin Hypersensitivity. . *The Journal of Clinical Dentistry.* 2009, Vol. 20, pp. 109–114.

155. **N. West a, R.G. Newcombe , N. Hughes , S. Mason , B. Maggio , F. Sufi , N. Claydon.** A 3-day randomised clinical study investigating the efficacy of two toothpastes, designed to occlude dentine tubules, for the treatment of dentine hypersensitivity. *Journal of Dentistry.* 2013, Vol. 41, pp. 187 – 194.

156. **Petrou I, Heu R, Stranick M, Lavender S, Zaidel L, Cummins D, Sullivan RJ, Hsueh C, Gimzewski JK. A.** Breakthrough Terapy for Dentin Hypersensitivity: How dental Product Containing 8% of Arginine and Calcium Carbonate Work to Deliver Effective Relief of Sen.

157. **D.J., White.** Use of Synthetic Polymer Gels for Artificial Carious Lesion Preparation. *Caries Research.* 1987, Vol. 21, pp. 228–242 .

158. **A.Torrado, M.Valiente, W. Zhang,Y.Li, C.Munoz.** Remineralization Potential of a New Toothpaste Formulation: An In-Vitro Study. *Journal of Contemporary Dental Practice.* 2004, Vol. 5.

159. **Ten Cate JM, Duijsters PPE,.** Alternating demineralisation and remineralisation of artificial enamel lesions. *Caries Research.* 1982, Vol. 16, pp. 201-210.

160. **Bonals, Anna Torrado.** *Estudi de processos de bescanvi iònic per a l'alliberació controlada en sistemes aplicats al tractaments de teixits organomaterials. Desenvolupament u caracterització d'una pasta dental.* Barcelona : s.n., 2003.

161. **Hongye Yanga, Dandan Peia, Zhiyong Chena, Jinmei Leia, Liqun Zhoua, Cui Huanga.** Effects of the application sequence of calcium-containing desensitising pastes during etch-and-rinse adhesive restoration. *journal of Dentistry.* 2014, Vol. 42, pp. 1115–1123.

162. **N. Erdman, N. Kikuchi, A. Laudate,V. Robertson.** Multispectral Imaging in an FEG-SEM. *Advanced Materials and Processes.* September 2009.

163. **Reinhard Schilke, JoÈ rg A. Lisson, Oskar Bauss, Werner Geurtsen.** Comparison of the number and diameter of dentinal tubules in human and bovine dentine by scanning electron microscopic investigation. *Archives of Oral Biology.* 2000, Vol. 45, pp. 355-361.

164. **K., Dorfner.** *Introduction to ion exchange and ion exchangers.* s.l. : Walter de Gruyter , 1991.

165. **S Rengaraj, Kyeong-Ho Yeon, Seung-Hyeon Moon.** Removal of chromium from water and wastewater by ion exchange resins. *Journal of Hazardous Materials.* 2001, Vol. 87, pp. 273–287.

166. **S. Chiarle, M. Ratto, M. Rovatti.** Mercury removal from water by ion exchange resins adsorption. *Water Research.* 2000, Vol. 34, pp. 2971–2978.

167. **Sema B. Erdemoğlua, Krystyna Pyrzyniska, Şeref Güçer.** Speciation of aluminum in tea infusion by ion-exchange resins and flame AAS detection. *Analytica Chimica Acta.* 2000, Vol. 411, pp. 81–89.

168. **Vikas Anand, Raghupathi Kandarapu, Sanjay Garg.** Ion-exchange resins: carrying drug delivery forward. *Drug Discovery Today.* 2001, Vol. 6, pp. 905–914.

169. **Richard H. Sterns, Maria Rojas, Paul Bernstein and Sreedevi Chennupati.** Ion-Exchange Resins for the Treatment of Hyperkalemia: Are They Safe and Effective? *Journal of American Society of Nephrology.* 2010, Vol. 21, pp. 733-735.

170. **J. Kirkham, J. Zhang, S.J. Brookes, R.C. Shore, S.R. Wood, D.A. Smith, M.L. Wallwork, O.H. Ryu and C. Robinson.** Evidence for Charge Domains on Developing Enamel Crystal Surfaces. *Journal of Dental Research.* 2000, Vol. 79, pp. 943-1 947.

171. **Yuwei Fan, Zhi Sun, Rizhi Wang, Christopher Abbott, Janet Moradian-Oldak.** Enamel inspired nanocomposite fabrication through amelogenin supramolecular assembly. *Biomaterials.* 2007, Vol. 28, pp. 3034–3042.

172. **Rachel E. Grayson, Y. Yamakoshi, Edward J. Wood, Magnus S. Agrenc.** The effect of the amelogenin fraction of enamel matrix proteins on fibroblast-mediated collagen matrix reorganization. *Biomaterials.* 2006, Vol. 27, pp. 2926–2933.

173. **Isabel Maria Porto, Helen Julie Laure, Frederico Barbosa de Sousa,Jose Cesar Rosa, Raquel Fernanda Gerlach.** New techniques for the recovery of small amounts of mature enamel proteins. *Journal of Archaeological Science.* 2011, Vol. 38, pp. 3596-3604.

174. **Wiedemann-Bidlack FB, Beniash E, Yamakoshi Y, Simmer JP, Margolis HC.** pH triggered self-assembly of native and recombinant amelogenins under physiological pH and temperature in vitro. *J Struct Biol.* 2007, Vol. 160, pp. 57–69.

175. **Ario Santini, Colin R. Pulham,Ahmed Rajab, Richard Ibbetson.** The effect of a 10% carbamide peroxide bleaching agent on the phosphate concentration of tooth enamel assessed by Raman spectroscopy. *Dental Traumatology.* 2008, Vol. 24, pp. 220–223.

176. **Anastasios Antonakos, Efthymios Liarokapis, Theodora Leventouri.** Micro-Raman and FTIR studies of synthetic and natural apatites. *Biomaterials.* 2007, Vol. 28, pp. 3043–3054.

177. **F.Blanco, M. López Mesas, S.Serranti, G. Bonifazi, J.Havel, M.Valiente.** Hyperspectral imaging based method for fast characterization of kidney stone types. *Journal of Biomedical Optics.* 2012, Vol. 17(7).

178. **E.N. Lewis, L.H. Kidder, E. Lee.** NIR chemical imaging as a process analytical tool. *Innov. Pharm. Technol.* 2005, pp. 107–111.

179. **J. Cruz, M. Blanco.** Nir-chemical imaging study of acetylsalicylic acid in commercial tablets. *Talanta.* 2009, Vol. 80, pp. 473–478.

180. **J.M. Amigo, C. Ravn.** Direct quantification and distribution assessment of major and minor components in pharmaceutical tablets by NIR-chemical imaging. *Eur. J. Pharm. Sci.* 2009, Vol. 37, pp. 76–82.

181. **Soojeong Chung, Daniel Fried, Michal Staninec, Cynthia L. Darling.** ear infrared imaging of teeth at wavelengths between 1200 and 1600 nm. . *The international society for optics and photonics.* January, 2011.

182. **Miran Bürmen, Peter Usenik, Aleš Fidler, Franjo Pernuš, Boštjan Likar.** A construction of standardized near infrared hyper-spectral teeth database - A first step in the development of reliable diagnostic tool for quantification and early detection of caries. *The international society for optics and photonics.* February 17, 2011.

183. **Karlsson, Lena.** Caries Detection Methods Based on Changes in Optical Properties between Healthy and Carious Tissue. *International Journal of Dentistry.* 2010, Vol. 10.

184. **Robert C. Lee, Cynthia L. Darling, Daniel Fried.** Assessment of remineralization in simulated enamel lesions via dehydration with near-IR reflectance imaging. *The International Society for Optics and Photonics.* February 24, 20015.

185. **Joiner, A.** The bleaching of teeth: A review of literature. *Journal of Dentistry.* 2006, Vol. 34, pp. 412-419.

186. **Godos, Jordi Margineda de.** *Doctoral thesis: Estudios de procesos de adsorción/desorción de iones en resinas encapsuladas. Aplicaciones a la remineralización de tejidos dentales. .* s.l. : Universidad Autónoma de Barcelona, 2004.

187. **Yuwei Fan, James R. Nelson,Jason R. Alvarez, Joseph Hagan, Allison Berrier, Xiaoming Xu.** Amelogenin-assisted ex vivo remineralization of human enamel: Effects of supersaturation degree and fluoride concentration. *Acta Biomaterialia.* 2011, Vol. 7, pp. 2293–2302.

188. **J. M.l Amigo, J.i Cruz, M. Bautista, S. Maspoch, J.i Coello, M. Blanco.** Study of pharmaceutical samples by NIR chemical-image and multivariate analysis. *Trends in Analytical Chemistry.* 2008, Vol. 27, pp. 696-713.

189. **al, A.M. Pimienta et.** Determination of hydrogen peroxide by near infrared spectroscopy. *Journal of Near Infrared Spectroscopy.* 2003, Vol. 11, pp. 49-53.

190. **Fan Y, Suz Z, Moradian-Oldak J.** Controlled remineralization of enamel in the presence of amelogenin and fluoride. *Biomaterials.* 2009, Vol. 30, pp. 478-483.

191. **Rorseler, A.** IR spectroscopic ellipsometry: instrumentation and results. *Thin Solid Films.* 1993, Vol. 234, pp. 307-313.

192. **Wei M, Evans JH, Bostrom T, Grondahl L.** Synthesis and characterization of hydroxyapatite, fluoride-substituted hydroxyapatite and fluorapatite. *Journal of Materials Science: Materials in Medicine.* 2003, Vol. 14 (4), pp. 191-194.

193. **G. E. Jellison, H. G. Tompkins, E. A. Irene.** *Handbook of Ellipsometry .* s.l. : William Andrew publishing - Springer , 2005.

194. **A.V Zavgorodniy, R. Rohanizadeh, M.V. Swain.** Ultrastucture of dentine carious lesions. *Archives of Oral Bilogy.* 2008, Vol. 53, pp. 124-132.

195. **Bradley, Michael.** *Curve Fitting in Raman and IR Spectroscopy: Basic Theory of Line Shapes and Applications.* s.l. : Thermo Fisher Scientific.

196. **Alvin S. Acerbo, G. Lawrence Carr, Stefan Judex, and Lisa M. Miller.** Imaging the Material Properties of Bone Specimens Using Reflection-Based Infrared Microspectroscopy. *Analytical Chemistry.* 2012, Vol. 84, p. 3607−3613.

197. **Joanna Kolmas, Emil Kalinowski, Andrzej Wojtowicz, Waclaw Kolodziejski.** Mid-infrared reflectance microspectroscopy of human molars: chemical comparison of the dentin-enamel junction with the adjacent tissues. *Journal of Molecular Structure.* 2010, Vol. 966, pp. 113-121.

198. **Simona-Liliana Iconaru, Mikael Motelica-Heino, and Daniela Predoi.** Study on Europium-Doped Hydroxyapatite Nanoparticles by Fourier Transform Infrared Spectroscopy and Their Antimicrobial Properties. *Journal of Spectroscopy .* 2013.

199. **Nancy Pleshko, Adele Boskey and Richard Mendelsohn.** Novel infrared spectroscopic method for the determination of crystallinity of hydroxyapatite minerals. *Biophysical Journal.* 1991, Vol. 60, pp. 786-793.

200. **A.Antonakos, E.Liarokapis, T. Leventouri.** Micro-Raman and FTIR studies of synthetic and natural apatites. *Biomaterials.* 2007, Vol. 28, pp. 3043-3054.

201. **Uysal I, Severcan F, Evis Z.** Characterization by Fourier Transform infrared spectroscopy of hydroxyapatite co-doped with zinc and fluoride. *Ceramics International.* 39, 2013, pp. 7727-7733.

202. **D.Magne, P. Weiss, J-M. Bouler, O. Laboux, G. Daculsi.** Study of the maturation of the organic (type I collagen) and mineral (nonstoichiometric apatite) constituents of a calcified tissue (dentin) as a function of location: A Fourier Transformed Infrared Microspectroscopic Investigation. *Journal of Bone and Mineral Research.* 2001, Vol. 16, pp. 750-757.

203. **AS, CAMO Process.** The Unscrambler X Tutorials .

204. **Leo Lou, Alan E.Nelson, Giseon Heo, Paul W. Major.** Surface chemical composition of human maxillary first premolar as assessed by X-ray photoelectron spectroscopy (XPS). *Applied Surface Science.* 2008, Vol. 254, pp. 6706-6709.

205. **A. G. Fincham, J. Moradian-Oldak, J. P. Simmer.** The Structural Biology of the Developing Dental Enamel Matrix. *Journal of Structural Biology.* 1999, Vol. 126, pp. 270–299 .

206. **Gotz, H; Duschner, H; White, D. J; Klukowska, M. A.** Effects of elevated hydrogen peroxide 'strip' bleaching on surface and subsurface enamel including subsurface histomorphology, micro-chemical composition and fluorescence changes. *Journal of Dentistry.* 2007, Vol. 35, pp. 457-466.

207. **Joiner, A; Thakker, G; Cooper , Y.** Evaluation of a 6% hydrogen peroxide tooth whitening gel on enamel and dentine microhardness in vitro. *Journal of Dentistry.* 2004, Vol. 32, pp. 27–34.

208. **Justino, L.M; Tames, D.R; Demarco, F.F.** In situ and in vitro effects of bleaching with carbamide peroxide on human enamel. *Operative Dentistry.* 2004, Vol. 29, pp. 219-225.

209. *Recent developments on hyperspectral imaging systems and their applications in detecting quality attributes of red meats: A review.* **Xiong, Z, et al., et al.** 2014, Journal of Food Engineering, Vol. 132, pp. 1-23.

210. *Characterization of post-consumer polyolefin wastes by hyperspectral imaging for quality control in recycling processes.* **Serranti, S, Gargiulo, A and Bonifazi, G.** 2011, Waste Management, Vol. 31, pp. 2217-2227.

211. *Monitoring galenical process development by near infrared chemical imaging: One case study.* **Gendrin, C, et al., et al.** 2008, European Journal of Pharmaceutics and Biopharmaceutics, Vol. 68, pp. 828-837.

212. *Near- versus mid-infrared diffuse reflectance spectroscopy for soil analysis emphasizing carbon and laboratory versus on-site analysis: Where are we and what needs to be done?* **Reeves, J B.** 2010, Geoderma, Vol. 158, pp. 3-14.

213. *Line-scan hyperspectral imaging system for real-time inspection of poultry carcasses with fecal material and ingesta.* **Yoon, S, et al., et al.** 2011, Computer and Electronics in Agriculture, Vol. 79, pp. 159-168.

214. **Lisa M. Miller, Vidyasagar Vairavamurthy, Mark R. Chance,Richard Mendelsohn, Eleftherios P. Paschalis, Foster Betts, Adele L. Boskey.** In situ analysis of mineral content and crystallinity in bone using infrared micro-spectroscopy of the v4 PO4 3-. . *Biochimica et Biophysica Acta .* 2001, Vol. 1527, pp. 11-19.

215. **Isabel Maria Porto, Regina Aparecida Saiani, K.L. Andrew Chan, Sergei G. Kazarian,Raquel Fernanda Gerlach, Luciano Bachmann,.** Organic and inorganic content of fluorotic rat incisors measured by FTIR spectroscopy. *Spectrochimica Acta Part A .* 2010, Vol. 77, pp. 59–63.

216. **Bayari, Sevgi Haman.** Application of Vibrational Spectroscopy in Diagnosis and Screening of Dental Tissues. [book auth.] Parvez I. Feride Severcan. *Vibrational Spectroscopy in Diagnosis and Screening .* s.l. : Advances in Biomedical Spectroscopy , 2012.

217. **J. Reyes-Gasga, E.L Martínez-Piñeiro, G. Rodríguez-Alvarez, G.E Tiznado-Orozco, R. García-García, W.F Brès.** XRD and FTIR crystallinity indices in sound human tooth enamel and synthetic hydroxyapatite. *Materials Science and Engineering C.* 2013, Vol. 33, pp. 4568-4574.

218. **J.D. Termine, A.S. Posner.** Infrared Analysis of Rat Bone: Age Dependency of Amorphous and Crystalline Mineral Fractions. *Science.* 1966, Vol. 153, pp. 1523-1525 .

219. **Shemesh, Aldo.** Crystallinity and diagenesis of sedimentary apatites. *Geochimica et Cosmochimica Acta.* 1990, Vol. 54, pp. 2433-2438.

220. **S.Weiner, O. Bar-Yosef.** States of preservation of bones from prehistoric sites in the Near East: A survey. *Journal of Archaeological Science.* 1990, Vol. 17, pp. 187-196.

221. **Christian Rey, M. Shimizu, B. Collins, and Melvin J. Glimcher.** Resolution-Enhanced Fourier Transform Infrared Spectroscopy Study of the Environment of Phosphate Ions in the Early Deposits of a Solid Phase of Calcium-Phosphate in Bone and Enamel, and their Evolution with Age. I: Investigations in the v4 PO4 Domain. *Calcified Tissue International.* 1990, Vol. 46, pp. 384--394.

222. **L.M. Miller, V. Vairavamurthy, M.R. Chance, R. Mendelsohn, E.P. Paschalis, F. Betts and A.L. Boskey.** In situ analysis of mineral content and crystallinity in bone using infrared micro-spectroscopy of the v4 PO3 vibration. *Biochimica Biophysica Acta.* 2001, Vol. 1527, pp. 11–19.

223. **E. Puceat, B. Reynard , C. Lecuyer.** Can crystallinity be used to determine the degree of chemical alteration of biogenic apatites? *Chemical Geology.* 2004, Vol. 205, pp. 83–97.